THE DEVELOPMENT OF A PROTON INDUCED X RAY
EMISSION SYSTEM FOR BIOMEDICAL ANALYSES.

BY

SAYAH OTHMAN SAIED, B.Sc. M.Sc.

A thesis submitted to The University Of Aston,
In Birmingham for the degree of Doctor of Philosophy.

To My Husband,
    December 1981.

THE UNIVERSITY OF ASTON IN BIRMINGHAM

THE DEVELOPMENT OF A PROTON INDUCED X RAY
EMISSION SYSTEM FOR BIOMEDICAL ANALYSES

Submitted for the Degree of PhD

Sayah O. Saied   December, 1981

SUMMARY

This dissertation is concerned with development work carried out on a Proton Induced X-ray Emission (PIXE) analysis system and its application to trace elements analysis of biomedical samples. Samples were bombarded with proton beams of 2.5 MeV, and the characteristic X-rays which were emitted were measured using a high resolution Si(Li) detector coupled to a multi-channel analyzer. The system as developed in this work has a low detection limit of typically $(10^{-7} - 10^{-9})$g for elements with Z numbers between 15 and 42 for irradiations of 20 minutes.

Calibration factors for the system were determined by measuring the proton induced X-ray yields from the K shells of elements contained in thin standard foils of KCl, Ti, Mn, Co, Cu, Ga, Ge, Y, Rb and Mo. The long term stability and reproducibility of the system were checked by repeated measurements of the X-ray yield from these standard foils over the whole period of the experimental work.

The experimental precision and accuracy for biological sample analysis were estimated from the results obtained from at least 60 thin targets made from different solutions of digested NBS standard bovine liver material. A precision of 2-8% was achieved. Comparison of these results with those of NBS recommended values and results obtained from Atomic Absorption Spectroscopy showed that for medium weight element an accuracy of better than 6% had been obtained.

Techniques available for sample preparation are critically reviewed. The use of thin targets is generally recommended for best quantitative results. Several backing materials onto which samples can be mounted, are evaluated.

This work also demonstrates the applicability of PIXE for multi-elemental analysis of a wide variety of biomedical samples. The trace element content of hair for a group of mentally defective females was determined and studied. Quantitative analysis of heart and brain tissue sections were also performed and the homogeneity level of trace element distributions were investigated. Results of these studies indicate the need for a large set of samples due to the natural non-homogeneity of these tissues.

Bladder and kidney stones were also analyzed, to investigate the existance of various elements at different zones of the stones.

Applications of the findings of this study are discussed. Further improvements are suggested for optimizing and extending the analytical capabilities of the present PIXE system.

Key words: PIXE, Proton induced X-rays, Trace element analysis, PIXE applications, X-ray spectrometry.

ACKNOWLEDGEMENTS

TABLE OF CONTENT

Page

LIST OF FIGURES

Page

ix

LIST OF TABLES

xiii

CHAPTER ONE

INTRODUCTION

Over the past century considerable interest has been generated in
the investigation of elements occurring only in trace amounts in living
organisms. This interest has increased significantly since the discov-
ery that many of these elements are essential for life, Bowen (1966),
Underwood (1971), and Prasad (1976).

Ninety two different elements from hydrogen to uranium occur in na-
ture; how many of these are essential and how many are not, is a question
which has attracted and continues to attract major attention from research
workers, Morrison (1965), and Valkovic (1975, 1977). Trace elements can
be divided into two groups; essential, for which physiological functions
are already known, and non-essential, for which no function has yet been
discovered, Tipton (1963). The biochemical function of trace elements as
well as the concentration level in which essential and non-essential
trace elements may become toxic are of significant concern. A comprehen-
sive discussion of essential trace elements and their metabolic roles
have been presented by Schroeder et al (1971) and Frieden (1972). More-
over, in the past decade research workers from various disciplines have
begun to focus their attention on the relationship between the environ-
ment and living organisms. The normal concentration of elements in the
environment is of particular interest; since it is found that the intro-
duction of abnormal quantities of heavy metals into the environment can
have adverse effects on living organisms, Freedman, (1975).

This continuing interest in trace elements and concern over the
quality of environment have stimulated the development of several power-
ful analytical techniques for detecting trace quantities of elements.
To draw meaningful conclusions about changes in trace element concen-

trations, the first step is to find an analytical method capable of determining concentration levels with a high degree of accuracy and precision. High sensitivity, simultaneous multi-element capability and non-destructive analysis are desirable requirements for any analytical technique.

Many techniques have been used in different laboratories to determine the composition of samples of unidentified constituents, several of these methods have been used for many years with good success. A new analytical technique was described by Johansson et al in 1970. They demonstrated experimentally that utilizing characteristic X-ray emissions induced by proton irradiation is an extremely sensitive means for multi-element analysis. They reported that many elements could be detected simultaneously at 10^{-12} gram level and predicted the possibility of analysis at 10^{-15} gram level.

This new analytical technique is a valuable addition to the existing methods and fulfils the majority of all the analytical requirements mentioned above, depending on the target form.

The analysis is based on the bombardment of samples with protons from an accelerator. When protons transverse matter, electrons are ejected from inner electron shells of the atoms present in the sample. The energies of the X-rays emitted when the vacancies are filled by electrons from higher atomic levels are characteristic of the element and the particular transition. The number of X-rays of a certain energy is proportional to the number of atoms of the corresponding element in the sample.

This method, generally referred to as PIXE-proton induced X-ray emission - has been developed further by many researchers, Johansson (1977, 1981) and is now regarded as a reliable technique for trace element analysis.

- 2 -

Excellent reviews of the application of PIXE and the capabilities as well as the limitations of it are provided in articles by Walter et al (1974), Folkmann (1975), Deconnink et al (1975) and Johansson et al (1976), Crumpton et al (1981).

PIXE analysis is the latest in a long line of techniques that has the ability to detect the presence of an element via its characteristic X-ray emission.

In 1895 X-rays were discovered by W.C. Rontgen. Following this discovery, many other scientists began to study their properties. In 1901 C.G. Barkla and his co-workers showed that the characteristic X-rays from a sample have several different wave lengths. They identified and named K and L X-rays. J. Chadwick in 1912 detected characteristic X-rays induced by alpha particles. Later in 1913, W.L. Bragg and W.H. Bragg detected the first X-ray spectrum by crystal diffraction using the Bragg X-ray spectrometer. Following Bragg's work and from systematically studying the X-ray spectra of Ca through to Zn. Mosley established the relationship between the wave length of X-ray lines and atomic number. A. Hadding in 1920 applied X-ray spectra to chemical analysis of minerals. The significance of using X-ray spectra for this kind of analysis was definitely established in 1923, when Van Hevesy proved the existance of the element 72, hafnium from X-ray spectra studies. Glocker and Schreiber introduced X-ray fluorescence analysis in 1928. By the 1930's using X-ray induced characteristic X-rays one could measure concentrations of 100 to 10 parts per million. Thus the use of X-rays, γ-rays and electrons as an excitation source together with wavelength dispersive techniques played a dominant role in X-ray spectrometry, providing good sensitivity and resolution. However, before the advent of efficient multi-crystal spectrometers, Birk and Gilfrich 1976, the use of wavelength dispersive techniques for the analysis of biomedical and

environmental samples was impractical.

In spite of the discovery by Chadwick that characteristic X-ray could be produced by heavy particles which was followed by the reports from Livingston in 1937 on the variation of intensity of X-ray with proton energy and atomic number and from Birks et al (1964) that proton excitation would have considerable advantages over electron excitation because of the reduction of background, this method of analysis was not employed until recently.

Khan et al (1966) appear to be the first group to apply ion induced X-ray emission. Unfortunately, due to the poor resolution of the gas proportional counter used, this technique was not applicable to multi-elemental analysis.

Particle induced X-ray emission has been extensively developed as an analytical technique by employing high resolution semi-conductor lithium drifted silicon Si(Li) detectors for the characteristic X-ray detection.

The rapid advances in the development of high resolution Si(Li) occurred in the 1960's and it became commercially available in the late 1960's. It was pointed out then by Johansson et al (1970) that the combination of X-ray excitation by protons with Si(Li) spectrometer constitute a powerful multi-elemental analytical technique of high sensitivity.

The high resolution of the new solid state detectors permit X-ray lines from adjacent elements of the periodic table (following sodium) to be resolved and up to thirty elements can be detected simultaneously.

Numerous authors have subsequently reported the use of charged particle X-ray fluorescence spectrometry as a mean of observing trace metals in various biological and environmental specimens.

Significantly a large number of applications have appeared in recent years, most of them, of an illustrative nature, concerned with demonstrating the capabilities of PIXE analysis. Discussions on the precision and

accuracy have not been presented in most of these reports, and relatively few investigations in these fields have been reported.

This lack of information on precision of PIXE analysis relating to biomedical applications has been noted by Campbell (1975), Johansson (1976) and Mitchell (1979) and also the fact that particle excitation cannot yet be regarded unreservedly as an accurate quantitative analytical technique. Consequently, the emphasis of the present study was placed on the development of a PIXE system so that the quantitative trace element analysis is obtained with a required degree of precision and accuracy. In the initial period of the work the emphasis of the research was on the development, modification and calibration of a PIXE system and the establishment of its accuracy and precision. Finally, the analytical capabilities of PIXE technique applied to analysis of targets prepared from samples of biomedical interest was studied. The PIXE analysis method used for the work reported here involved sample excitation through 2.37 MeV proton bombardment and X-ray analysis with a Si(Li) energy dispersive detector. Optimum sensitivities for the elements analyzed by PIXE were obtained by employing samples in the form of very thin targets.

The theoretical basis for analysis by PIXE is presented in chapter two including fundamentals of X-ray emission, background production process and system optimization with some other topics.

Also in this chapter, PIXE is compared to electron and X-ray induced X-ray emission spectrometry. The experimental set up is described in chapter three. Since there is a lack of quantitative information regarding the reproducibility and accuracy of this technique, chapter four treats long term reproducibility and precision. The overall accuracy of the technique was assessed by comparison of the results with those obtained by an established technique. Special attention was paid to sources of uncertainty.

Since many elements are present in trace amounts therefore much effort has gone into lowering the detectability limit. The detailed discussion of this subject and backing materials are presented in chapter five. Methods of sample preparation are discussed in chapter six. The results for PIXE analysis for the general survey of applications to the analysis of biomedical specimens are presented in chapter seven. Chapter eight discusses the strength and weakness of PIXE and presents suggestions for future improvements.

THEORY OF CHARGED PARTICLE INDUCED X-RAY ANALYSIS

2.1   INTRODUCTION TO PARTICLE INDUCED X-RAY ANALYSIS

The production of characteristic X-ray lines follows the excitation of target atoms as a result of removal of one or more electrons from the inner atomic shells.   The formation of inner-shell electron vacancies is achieved either by charged particle bombardment, using electrons, protons or heavier ions; or by energetic photons, X-rays or gamma rays.

The mechanism of electron removal by charged particles is simply the Coulomb interaction between the incoming particles and atomic electrons while electro-magnetic radiation causes electron emission by the photo-electric effect.   In both of these cases there is a high probability for inner shell vacancy production.   In the process of de-excitation that is when the resulting vacancy is filled by an outer shell electron , X-rays whose energy is characteristic of the particular atom, may be emitted.   Detection of such X-rays is the basis of a variety of micro-analytical techniques including PIXE analysis.   The energy of the X-ray photons is given by $E_x = h\nu$ and is equal to the energy difference between the level of the vacancy and that of the electron filling that vacancy. This can be expressed as:

$$E_x = E_2 - E_1 \qquad\qquad\qquad ..... (2.1)$$

The electron transition which is subject to transition rules, leaves a vacancy in the outer-shell and is subsequently filled by a second electron transition and so forth until the electron configuration of the ground state atom is reproduced.   Consequently, the X-ray emission consists of K, L, M lines produced by electron transition to the K, L, M

shells of the target atom. A complete energy diagram, showing origin of X-ray lines and all possible transitions for all elements up to Z = 92 is shown schematically in Figure 2.1.

2.2 FUNDAMENTALS OF X-RAY EMISSION

An important feature of characteristic X-ray spectra is the occurrence of several X-ray emission lines from every element present in a sample, except the light elements. These elements possess a unique set of X-ray lines characterized by their energies and relative intensities.

The relative intensities of the emission lines observed for different elements are governed by the transition probabilities, which is an intrinsic feature of each element.

The intensity ratios as well as the characteristic X-ray energies serve as an element's "finger print" which uniquely identifies the specific atoms giving rise to them. The significance of the intensity ratios is particularly obvious when multi-elemental samples are analyzed. Thus interference between different X-ray lines emitted from different elements in the sample may occur. The utilization of the intensity ratios for the present analytical work will be discussed later.

The characteristic nature of X-ray emission was first observed by Moseley who demonstrated that the characteristic X-ray energy is a smooth function of the atomic number Z, according to the following empirical rule.

$$E_i = a_i(Z - b_i)^2 \qquad\qquad \dots\dots (2.2)$$

where a_i and b_i depend on the particular line.

Mosley's result can be verified by the simple Bohr model of the atom in which each atomic energy level is quantized and has a discrete energy according to the well known expression:

- 8 -
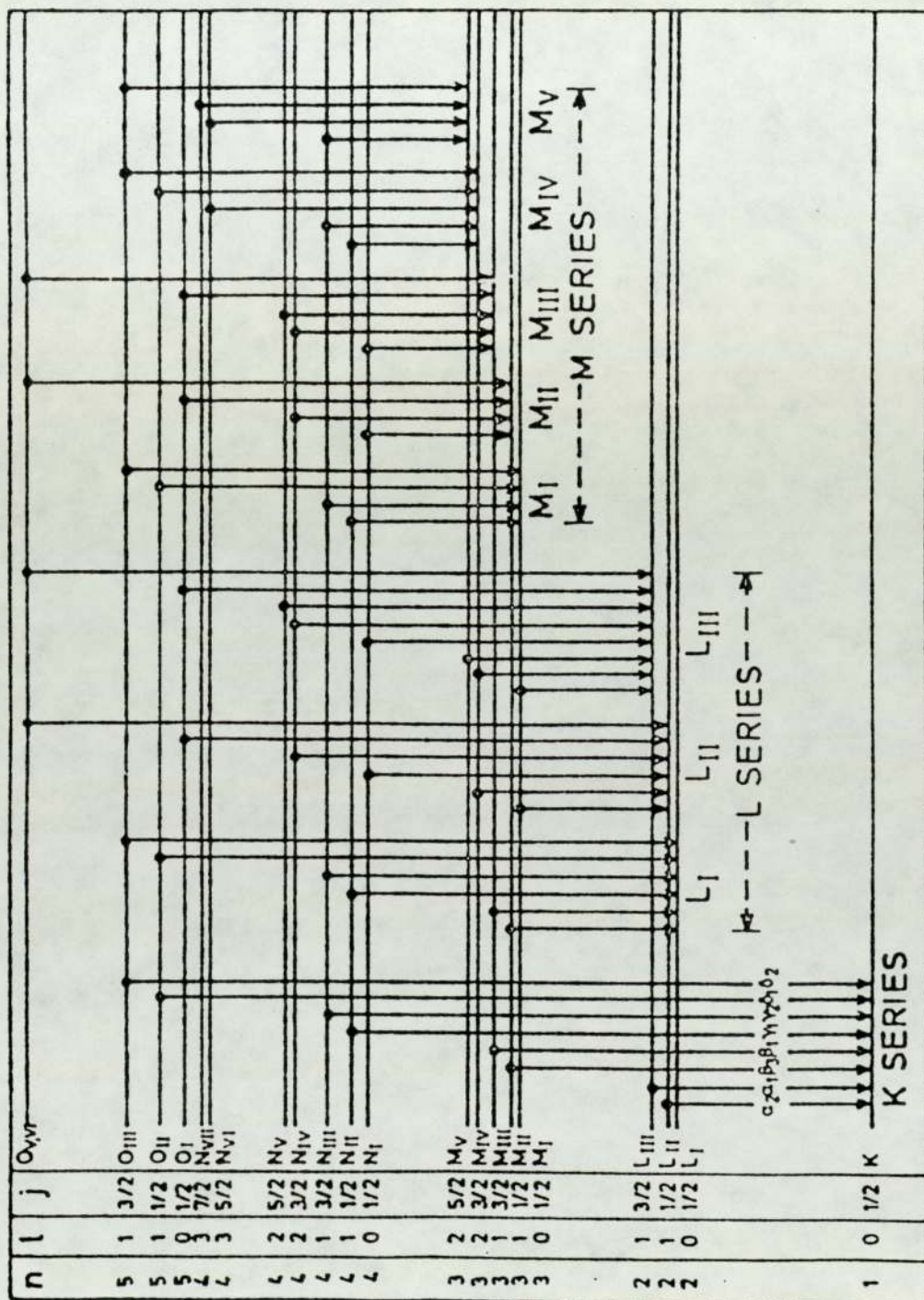
Figure 2.1   Complete energy-level diagram and possible transitions up to the element Z = 92 (from Valkovic, 1975)

$$E_n = -\frac{me^4}{8\,h^2\,\varepsilon_o} \cdot \frac{1}{n^2} \cdot Z^2 \qquad \ldots\ldots (2.3)$$

where ε_o is the permitivity of free space, h is Planck's constant, n represents the principal quantum number of the atomic shell and n = 1 and 2 for K and L-shell respectively.

Since $E_x = E_2 - E_1$

Therefore $\quad E_x = \frac{me^4}{8\,h^2\,\varepsilon_o^2}\left(\frac{1}{n^2} - \frac{1}{m^2}\right)Z^2 \qquad \ldots\ldots (2.4)$

where m = n + 1

The screening of the nuclear charge due to electrons in the inner shell must be accounted for in the previous Bohr's formula. That is achieved by replacing Z with an effective nuclear charge Z_{eff}.

Since the b_i term of Mosley's law is an appropriate screening constant, therefore

$$Z_{eff} = Z - b_i$$

and $\quad E_x = \frac{me^4}{8\,h^2\,\varepsilon_o^2}\left(\frac{1}{n^2} - \frac{1}{m^2}\right)(Z - b)^2 \qquad \ldots\ldots (2.5)$

The agreement between this and the functional form of Mosley law could be observed.

2.3 INNER SHELL VACANCY PRODUCTION

The potential of PIXE for spectro-chemical analysis depends on the method's ability to detect trace amounts of elements in a low level of picogram. This arises from the fact that the cross-section or the probability for characteristic X-ray production is quite large using proton excitation. The production of inner shell vacancies in atoms by ion impact and the subsequent emission of X-rays is well known for light ion projectiles (i.e. protons and alpha particles) and the behaviour of the

- 10 -

ionization cross-section as a function of projectile energy and target atomic number is well understood.

The three theories generally used for predicting X-ray production cross-section and which have been used with considerable success in understanding the main features of inner-shell vacancy are the quantum-mechanical plane wave Born Approximation (PWBA) of Merzbacher and Lewis (1958), and the Garcia's semi - classical Binary Encounter Approximation (BEA), Garcia (1970a, b) and the semi-classical approximation (SCA) Bang et al(1959). Both of the first two formulae are strictly valid only in the limit where the incident proton velocity is much larger than the orbital velocity of the bound electron. Mott et al (1965) reported that the PWBA is only valid for the condition.

$$Z_1 \; Z \; e^2/\hbar \; v \ll 1$$

where Z_1 is the projectile nuclear charge, Z the target nuclear charge and v the relative velocity. However, the SCA holds for low velocity projectiles.

The starting point for each of these models is the assumption that the production of an inner shell vacancy occurs as a result of an inter-action of the nucleus of the charged particle with the bound electron.

In the (PWBA) the incident and the inelastically scattered parti-cles are described by a plane wave. The Coulomb interaction between the bound electron and the incident proton is responsible for vacancy prod-uction.

The BEA theory considers the dominant interaction producing the transition as a direct energy exchange between the incident charged particle and the bound electron. The electron is treated as being free and possessing a momentum distribution determined by the presence of other charged particles in the system. It was pointed out by Garcia et

al (1973) that the binary encounter model offers a scaling law for the cross-section which is composed of only electron binding energy and particle energy. A universal curve is thus derived when:

$$\frac{U_i^2(z)\sigma_i}{z^2} \qquad (i = K \text{ or } L)$$

is plotted against:

$$\frac{E_p}{\lambda U_i(z)}$$

where U_i is the electron binding energy, E_p the particle energy and σ_i the ionization cross-section for K and L shell and λ the ratio of the particle mass to the electron mass. The (SCA) makes use of impact parameter to treat the Coulomb deflection of the incident projectile, which becomes important at low projectile velocities. Appropriate deflection correction are thus inserted. It should be noted that PWBA and SCA are not open to universal scaling similar to BEA theory but also provide for a limited scaling.

In principle, the experimental determination of cross-section could be used to test the validity of a given theory. Ionization cross-sections must be corrected by fluorescence yield factors when compared with X-ray production data. Later experimental work on cross-sections in the MeV range is summarized and presented by Johansson (1976). However, both of (BEA) and (PWBA) theories have been found to fit experimental data for proton energy greater than about 1 MeV reasonably well. Hence, it can be concluded that either of the two theories could be employed for justifying the systematic behaviour of the cross-section. The SCA describes the total cross-section quite well, but has not yet been experimentally tested in detail. Garcia et al (1973), Madison et al (1975) and Hansteen et al (1973, 1975) have discussed these various models in detail. All

the theories, however, describe the cross-section as varying slowly with the energy of bombarding particles in the 1-4 MeV energy range, as reported by Bears et al (1973), Garcia (1970a) and Khandelwal (1969). Small changes in the energy of the bombarding particle of << 1% produce very small changes in the X-ray production cross-section. This is important because beam energy instability becomes insignificant.

However, calculation in PWBA predict that for a given target atom Z ionization cross-section or the production cross-section will increase with the energy E_p of the projectile and reaches for i X-ray, a maximum near the energy:

$$E_p \simeq \frac{M}{m} U_i(z)$$

where the velocity of the projectile equals the mean velocity of the i-shell electrons of binding energy $U_i(z)$, M is the mass of the projectile and m is the electron mass. For higher energies, the cross-sections decrease slowly.

The K-shell ionization cross-section is proportional to the fourth power of the proton energy and is inversely proportional to U_k^6 where $U_k(z)$ is proportional to Z_k^2, the effective atomic number of K-shell electron, thus the ionization cross-section is proportional to $Z_{(k)}^{-12}$. Hence:

$$\sigma_k \alpha \frac{E_p^4}{Z^{12}} \quad \text{(Merzbacher 1958)}$$

$$\text{or} \quad \sigma_k \alpha \frac{E_p^4}{U_k^6}$$

$$\text{therefore} \quad \sigma_k U_k^2 \alpha \left(\frac{E_p}{U_k}\right)^4$$

This suggests that the product of the K-shell ionization cross-section and square of the electron binding energy is a function of $\left(\frac{E_p}{U_k}\right)$ and

not E_p or U_k alone. Therefore $\sigma_k \, U_k^2$ is usually plotted as a function of $(\frac{E_p}{U_k})^4$ and these should define a universal function.

On the other hand, for a given proton energy, the cross-section for X-ray production is a continuous and smoothly varying function of atomic number and does not show significant variation in sensitivity from one element to the other.

2.4 RADIATIONLESS TRANSITIONS

Although there is a high probability for inner shell vacancy production, not every transitions of an outer electron from the atom to the inner shell vacancy results in a radiative emission (X-rays). There is a large probability for a certain region of the periodic table that radiationless transitions known as Auger and Coster Kronig take place.

The physical quantity of interest for trace element analysis is the X-ray production cross-section which is the probability that exposure of a target atom to the excitation source will result in the emission of a radiative characteristic X-rays. The fluoresence yield factor is a measure of the probabilities for radiation and radiationless transitions which could be defined as the number of vacancies filled giving rise to X-ray emission to the number of initial vacancies created. The defining equation is simply $W = \dfrac{n_k}{n_i}$ where primary vacancies are created in n_i atom and n_k of these atoms emit X-ray radiation. Conveniently, W can be expressed as the ratio of the X-ray production cross-section to ionization cross-section and is given by $W = \dfrac{\sigma_k}{\sigma_i}$ where σ_k and σ_i are the X-ray production and ionization cross-sections respectively.

The fluoresence yield is an increasing function of atomic number Z.

In an Auger transition, the inner shell vacancy is filled by an electron from an outer shell accompanied by the ejection of an outer electron from the atom of energy E_A; such that $E_A = (E_1 - E_2) - U_k$,

- 14 -

where U_k is the binding energy of the electron, such an electron is called Auger electron and is emitted from L to higher shells.

In Coster-Kronig transition for the L and higher shells, primary inner-shell vacancy is filled by a transition from a subshell within the same atomic shell. The net effect of these subshell transitions is a change in the primary vacancy distribution of the subshells. Thus, due to these effects, the X-ray yield is not the same as the vacancy production of ionization process.

X-ray fluorescence yields and Coster-Kronig transition are reviewed thoroughly by Bambynek et al (1972), consequently they present useful tables. More recently Krause (1979) has calculated K and L shell fluorescent yield and covered the range $5 \leqslant Z \leqslant 110$ for K shell and $10 \leqslant Z \leqslant 110$ for the L subshells. These values are presented in tables and graphs. Figure 2.2 from his work shows K shell fluorescence and Auger yield versus atomic number.

2.5 BACKGROUND PRODUCTION PROCESS

In PIXE analysis, the peaks in a characteristic X-ray spectrum are always superimposed on a continuous background of electro-magnetic radiation, decreasing with increasing energy. This background is produced by the impact of the ions on the bulk material of the sample, in which the trace elements are always present. Clearly, this background could prevent the observation of a specific element if its characteristic X-ray line does not significantly emerge from the background. Hence, this would be the major factor in determining the detection limit of the measuring system. However, the level of background radiation depends on the target composition and thickness, in addition to the projectiles and their energies. The sources of this background radiation exist primarily in physical processes that are intimately related to the production of

- 15 -
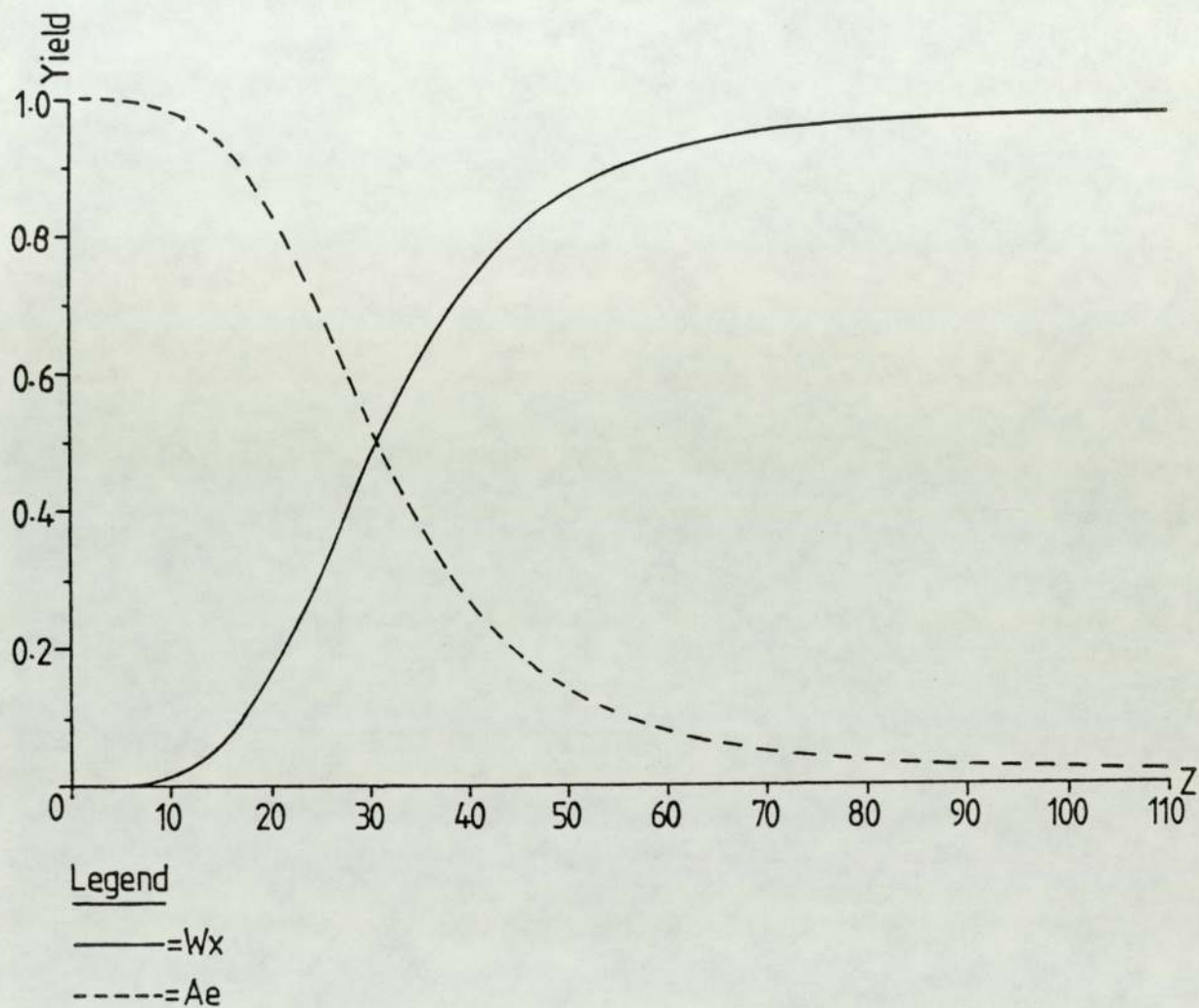
Figure 2.2   K-shell fluorescence and Auger yield versus atomic number.
               The values are calculated value by Krause (1979)

- 16 -

characteristic X-rays. Thus the background contribution can be mini-mized but never eliminated and constitute a fundamental limitation to PIXE sensitivity.

The background could be attributed to several processes. These are bremsstrahlung from the secondary electrons ejected from target atoms by the primary ion beam, bremsstrahlung from the primary ion beam as slowed down in close collision with the matrix nuclei and in case of higher bombarding energy also Compton scattering of γ-rays from nuclear reaction between projectile and matrix nuclei.

Bremsstrahlung is a continuous electro-magnetic radiation and re-sults from acceleration or deceleration of charged particles in the pre-sence of electric fields. Bremsstrahlung from secondary electrons is dominant at low energies while the other processes dominate at higher energies.

These background sources are discussed in more detail in the follow-ing sections:

2.5.1 Electron Bremsstrahlung

At low energies it could be observed experimentally that the con-tinuous background radiation is quite intense. Folkmann et al (1974a) gave detailed calculations which confirmed that the background radiation at low energies does result from secondary electron bremsstrahlung which is a consequence of the radiative collision between the target nuclei and electrons which have been ejected from target atoms by the primary ion beam. This bremsstrahlung radiation has a maximum energy of T_m and decreases rapidly above this, where T_m represents the maximum energy that can be transferred from a projectile to a free electron. For proton excitation T_m is given by:

$$T_m = 4 \frac{m_e}{m_p} E_p$$

- 17 -

where m_e and m_p are the masses of electron and proton, E_p is the energy of the proton. However, most of the electrons do not give up their energy in a single step but rather in numerous unequal portions each resulting in an X-ray photon of a different energy. The result of this stepwise deceleration of a large number of electrons is a continuous spectrum in which the highest energy in it corresponds to electron deceleration to zero velocity in one step.

Production of bremsstrahlung by secondary electrons is a two step process, consisting first of the ejection of electrons from target atoms by the incident projectile and secondly of radiative collision of these electrons with the nuclei of matrix atom resulting in bremsstrahlung. This production process offers the possibility of reducing the background cross-section for extremely thin samples.

Folkmann et al (1974a) estimated the intensity of this bremsstrahlung radiation and reported that the probability of the initial ion ejecting an electron of energy E_e decreases slightly with increasing E_e until $E_e \simeq T_m$. The probability for ejection of a secondary electron with $E_e > T_m$ decreases dramatically, approximately as E_e^{-10}. Folkmann also pointed out that the dominant contribution to secondary electron bremsstrahlung produced in the energy interval E_x to $(E_x + dE_x)$ can be traced to secondary electrons having energies in the range 0% to 20% above E_x. Therefore, it is advantageous in terms of minimizing this source of background to make T_m, hence the projectile energy as small as possible.

Folkmann et al (1974a) did not predict any anisotropy in the secondary electron bremsstrahlung such as observed by Tawara (1976), Ishii (1977) and Renan (1980). According to these workers some reduction in the background intensity at low energies can be achieved by exploiting the angular distribution of the secondary electron bremsstrahlung.

2.5.2   Incident Particle Bremsstrahlung

The bremsstrahlung from the incident particle is a direct conse-
quence of the large deceleration encountered when the projectile inter-
acts with the Coulomb field produced by target nuclei. The importance
of this is obvious for high X-ray energy.

For a projectile (Z_1, M_1, E_1) incident on a target matrix (Z, M) the
cross-section for the production of projectile bremsstrahlung of energy
E_r is given as:

$$\frac{d\sigma}{dE_r} = C \frac{M_1 Z_1^2 Z}{E_1 E_r} (\frac{Z_1}{M_1} - \frac{Z}{M})^2 \qquad \ldots\ldots \text{(2.6)}$$

where C is approximately constant Alder(1956). It is to be noted from
the charge to mass dependence in this formula, the advantage of using
proton or alpha particles rather than electron is obvious. In addition
it could be deduced that contrary to the trend for the secondary electron
the intensity of the projectile bremsstrahlung decreases for higher pro-
jectile energy and higher bremsstrahlung energy.

The dependence of the production cross-section on the Z_1^2 would pre-
dict the more intense primary background for heavier particles.

The term $(\frac{Z_1}{M_1} - \frac{Z}{M})$ arises from interference between the radiation of
the projectile and of the recoiling nucleus. By employing projectiles
of the same charge-to-mass ratio as that of nuclei in matrix, i.e.
$\frac{Z_1}{M_1} = \frac{Z}{M}$, then the bremsstrahlung should vanish. This was verified experi-
mentally for low velocities by Folkmann et al (1974a) by using equal
energy per nucleon alpha particles and protons on the same carbon target,
so that for this matrix $\frac{Z}{M} = \frac{1}{2}$. Meanwhile, attempts to use this cancel-
lation for higher velocities also have as yet failed Folkmann et al(1974b).

Since many trace elements are typically present in a carbon matrix,
Watson et al (1975), therefore, investigated background levels in the

matrix also by bombardment with 1.7 MeV/amu $_1^1$H, $_2^4$He, $_6^{12}$C and $_{10}^{20}$N ions.
They found that the background due to projectile bremsstrahlung was much
less intense for C, He and Ne than for protons.

2.5.3 Compton Scattering

When the incident projectile have a sufficiently high energy to
excite the nuclei in the target, γ-radiation resulting from the decay of
nuclear excited states will be emitted giving rise to a high energy cont-
inuum in the spectrum due to Compton scattering in the detector. Back-
ground contribution from Compton scattered γ-rays can be as important as
the projectile bremsstrahlung or even more. Folkmann et al (1974b)
showed that for 3 and 5 MeV the background due to Compton scattering of
γ-rays was much more important than the background due to proton brems-
strahlung. The production of γ-rays, however, depends on the projectile
species in addition to the elemental composition of the target. Some
nuclei have a high cross-section for γ-emission. For example, nuclei
such as ^{19}F and ^{23}Na provide low energy γ-rays [1.64 MeV γ via the
reaction ^{22}Na (P, P'γ); 1.35 and 1.46 MeV γ's from ^{19}F(P, P'γ); and 6-7
MeV γ's for ^{19}F(P, $\alpha\gamma$)^{16}O and even 1 MeV protons give a substantial
yield]. Generally, the production of γ-rays increases with increasing
bombarding ion energy. Therefore, to minimize the γ-ray background the
energy of the bombarding ion should be as low as possible while still
giving sufficient characteristic X-rays. However, the background from
Compton scattered γ-rays is less pronounced when working with biological
samples, since tissue from higher animal contains essentially no F and
only about 0.1% Na by weight Schutte(1964).

On the other hand, the cross-section for production of nuclear γ-
rays for protons with ^{12}C and ^{14}N, the main constituent of organic
matrix, are extremely small typically 6 μb/sr and 2.4 μb/sr respectively.
Finally, it should be noted that the structural composition and

geometrical design of the target chamber with its contents and the colli-
mators will also affect this background by causing γ-ray back scattering
Folkmann et al (1974b)

2.6   SYSTEM OPTIMIZATION; SELECTION OF EXCITING IONS AND ENERGY

The analytical capabilities of ion induced X-ray spectrometry system
are determined by a number of experimental considerations such as the
choice of ion species, ion energy, sample type and preparation, particu-
lar experimental arrangement including beam current and absorber filters.
The optimum choice of these parameters yields the best sensitivity of
the system which is expressed in terms of a "detection limit" for the
elements of interest, where the minimum detection limit is defined as the
minimum amount of that element that can be reliably detected.

The following paragraph discusses a number of considerations relat-
ing to the optimum choice of ion and energy while the optimization of
experimental set up for achieving maximum sensitivity and other related
factors will be discussed in turn in later chapters.

The selection of bombarding energy and particle species will direct-
ly affect the sensitivity obtained. This is based on the behaviour of
X-ray production cross-section σ_Z^{Prod} which is a function of excitation
source (photons, electrons or heavy ions) and excitation energy E_p.
This has important consequences in optimizing the experimental parameter
for maximum sensitivity in the elemental region of interest.

Due to the fact that the background radiation is the major factor
limiting the sensitivity, the close relation of background radiation to
the excitation particle and energy has also to be considered.

The major feature of the production cross-section of different ex-
citation sources could be understood through studying Figure 2.3 from
Folkmann (1977) in which K-shell X-ray production cross-section versus Z

- 21 -

K x-ray production for
protons(p), electrons(e), and photons(γ)
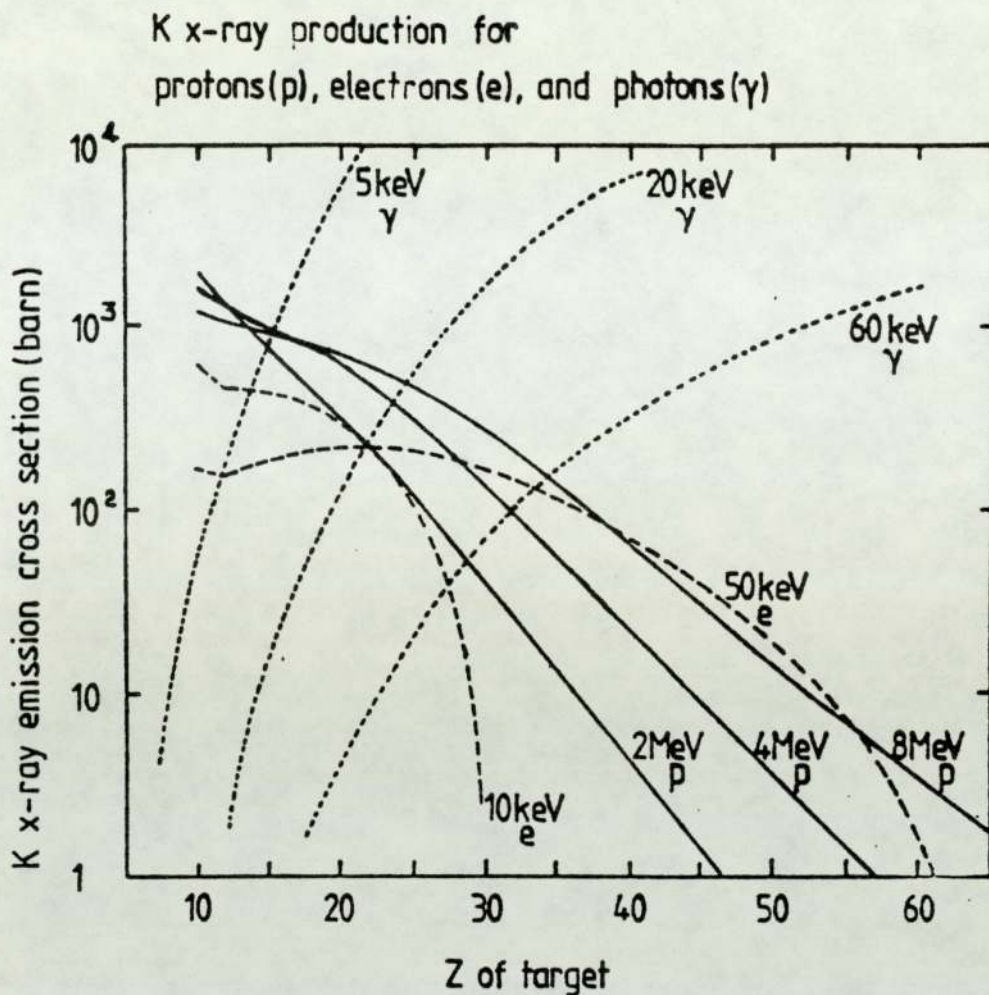
Figure 2.3   K X-ray production cross-section for protons
                  electrons and photons versus target atomic
                  number. The difference in the behaviour of
                  the emission cross-section for particle
                  excitation and photon excitation is illu-
                  strated (from Folkmann, 1977)

via proton, electron and photon excitation at several different energies is shown. The main interesting point to note is that the photon cross-section is a sharply increasing function of Z, contrary to the particle cross-section which is a sharply decreasing function. This trend suggests advantages in using photon exicitation for the analysis of high Z elements and particles for medium to light elements. The background continuum accompanying characteristic X-rays induced by particles has a similar behaviour to that of characteristic X-rays, while for photon excitation the background reaches its maximum intensity at X-ray energies immediately below the photon energy of the excitation source.

Since the elements of interest in most of biological and environmental samples are medium to light elements, particles will be considered in this discussion that follows and in particular, heavy particles rather than electrons.

For all elements, the cross-section for ionization increases with particle energy up to an energy of several MeV in the case of light elements and increasingly higher to the medium and heavy elements (Folkmann 1974a). Since the bremsstrahlung and primary production of characteristic X-ray of interest are closely connected to each other, their production cross-sections also depend similarly on the projectile parameters. Therefore, any increase in characteristic X-ray due to increase in projectile energy will be accompanied by an increased bremsstrahlung. Moreover, Herman et al (1973b) reported that the background intensity for medium to low Z element increases at a somewhat faster rate resulting in degraded signal-to-noise ratios. The fact that the maximum energy of the secondary electron bremsstrahlung T_m increases linearly with projectile energy has also to be considered. In addition, at higher energies, the background due to γ-radiation from nuclear excitation also increases with increasing projectile energy. Therefore increasing the projectile energy

hence obtaining higher inner shell ionization cross-section is not followed by proportional increase in sensitivity. These factors combined with the added problems of beam heating makes the use of more energetic beams undesirable. Numerous studies have been conducted to investigate the relation of ion energy with detectability limit. Proton beams with a wide range of energies have been used for these studies. Raith et al (1977) have examined elements in the range $16 < Z < 83$ for protons of 1.5, 2.0, 3.0 and 4.0 MeV energy. They found that the detectabilities of trace elements improved from 1.5 to 3.0 MeV while they did not observe any improvement at 4.0 MeV. Bearse et al (1977) reported an improvement by a factor of 2-3 in detectabilities of 21 trace elements spanning the periodic table from 1 to 3 MeV protons but their experiments were not carried out for higher energies. The projectile dependence of the signal-to-background ratio has been surveyed by Folkmann et al (1974a), Figure 2.4 shows their theoretical curves for the minimum detectable concentration as a function of atomic number for different bombarding energies. It is evident that for each part of the periodic table there exists an optimum energy. Johansson et al (1976) have calculated the variation of the "minimum detectable concentration" as a function of proton energy and atomic number. Their results indicate that as proton energy increases, the minima in the sensitivity curves shift to higher values of Z. Thus from the theoretical aspect of the subject and experimental investigation of these investigations, we conclude that the optimal choice for the bombarding energy is determined by the elemental region of interest. But in practice one has to choose the bombarding energy for the best overall sensitivity. Since the main elements of interest in biological and enviromental samples fall in the two regions, $20 < Z < 40$ and $75 < Z < 92$ the optimum energy for protons is about 2-3 MeV. As it is seen, only proton excitation has been discussed in the previous experiments, it is of
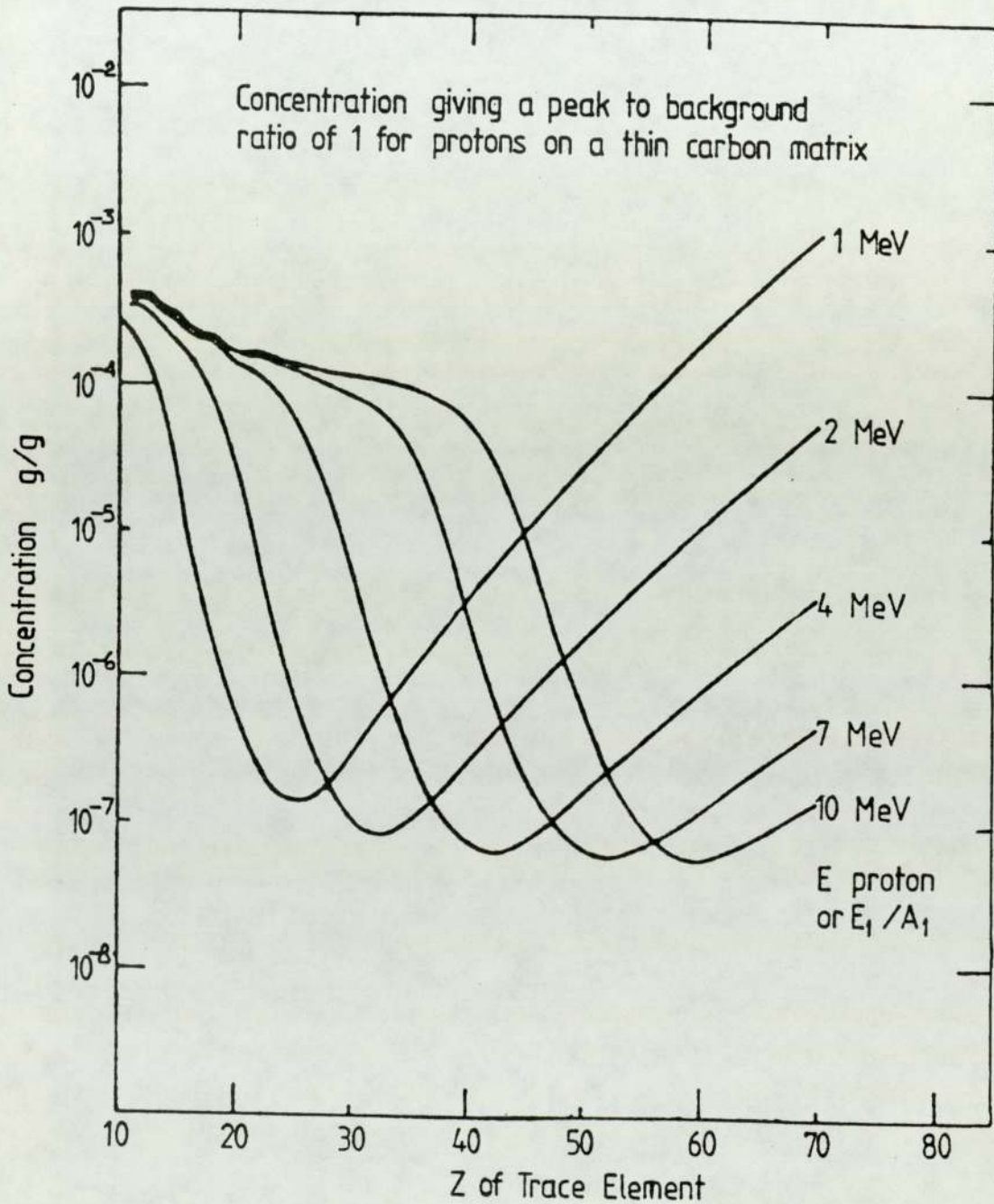
Figure 2.4   Calculated minimum detectable concentration as a function of atomic number for 1 - 10 MeV protons on a thin carbon matrix utilizing the criterion (peak to background ratio of 1). The variation of minimum detection concentration with atomic number is demonstrated (from Folkmann, 1974a)

interest to investigate whether excitation by α-particles or heavier ions can yield higher sensitivities and follow similar trend as that of protons.

It is worthwhile noticing that by using proton cross-section for X-ray production, the cross-section for higher projectiles can be estimated by the scaling law given below for a projectile of A_1 nucleus, charge Z_1 and energy E_1

$$\sigma^{Prod}_{z_1 A_1} (E_1) = Z_1^2 \; \sigma^{Prod}_{proton} (\frac{E_1}{A_1})$$

that is the cross-section equals that of a proton of the same velocity or energy per nucleus multiplied by the charge of the projectile squared (Folkmann et al 1974b). Thus heavier ions have higher inner shell ionization cross-section than light ions but in fact the bremsstrahlung cross-section is also proportional to Z_1^2. Hence, the ratio between the yields of the two processes does not depend on the choice of particle. These scaling factors for the peak-to-background ratio are applicable only in the X-ray region below T_m and apply to targets that are very thin.

Heavy ions having greater energies than equal velocity protons have a greater probablity for inducing gamma radiation via nuclear excitation. This has been verified experimentally by Herman et al (1973b), Folkmann (1974b) and Cahill et al (1974). Thus the resulting Compton tail at higher X-ray energies associated with inelastic scattering of nuclear gamma rays may be a serious limitation for heavy ions.

Many workers have investigated the detection limits as a function of projectile and projectile energy in an effort to determine optimum radiation conditions.

Careful studies by Folkmann et al, to illustrate the effect of projectile species on the sensitivity with atomic number of elements, have been carried out. Their results for an energy of 3 MeV/amu are shown in

Figure 2.5. It will be noted that for light elements all particles give the same sensitivity, which confirms the discussion presented above, and protons are far the better choice where the characteristic X-ray energies are greater than T_m. This is due to a strong γ-ray background which gives an inferior sensitivity for heavy ions. For lower energy region the choice of particle was more often dictated by target damage consideration. However, according to Folkmann et al protons provide better results over the whole periodic table than heavier projectiles of the same energy per nucleon.

Cahill et al (1974) compared 4 MeV/amu ^{1}H and [4]He ion beams. The results obtained were in agreement with predicted scaling property for both characteristic X-ray and secondary electron bremsstrahlung while above 15 keV, the detection limits were approximately 40% higher for [4]He ions because of the more intense Compton background.

Barrette et al (1976) investigated 2.25, 3.0, 6.0 MeV protons and 6.0. 9.0, 12, and 16 MeV [4]He ions and concluded that 3.0 MeV protons provided the best overall sensitivity, generated lower background and proved less damaging to the sample than equal velocity [4]He ions.

Raith et al (1977) in their experiments producing sensitivity curves for 37 elements using protons and ^{16}O-ion found that for ^{16}O-ion of 24 MeV, the minimum detection limit is much higher than for bombarding with protons of the same velocity.

According to all the previous discussion, we conclude that protons rather than heavier ions yield maximum sensitivity for the detection of characteristic X-rays for the elemental range of interest. The above argument also show the optimal proton energy to be between 2 and 4 MeV.
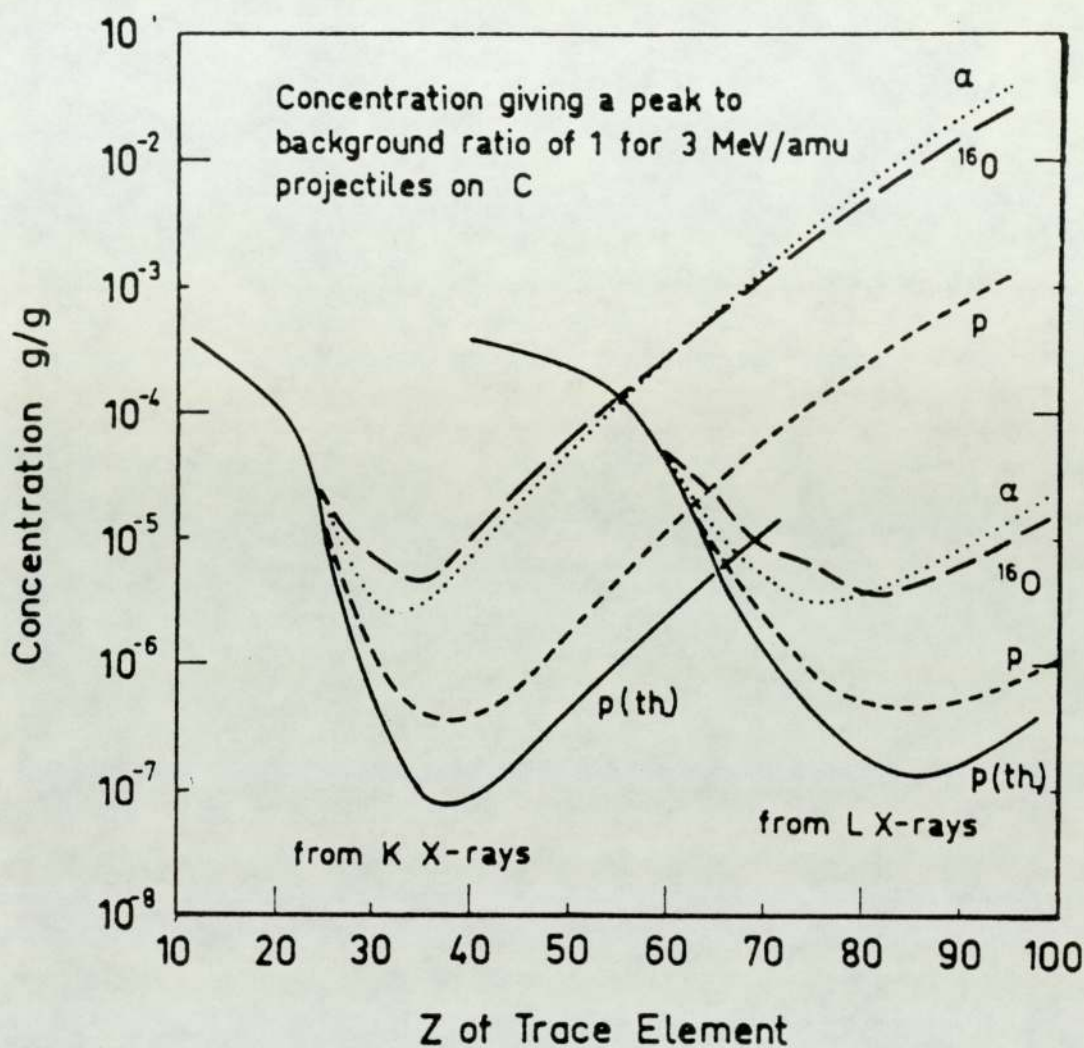
Figure 2.5   Minimum detectable concentration as a function of
               atomic number for protons α-particles and heavy
               ions with an energy of 3 MeV/amu. Solid curves
               represent theoretical values, the broken curves
               represent experimental values (from Folkmann, 1974b)

- 28 -

CHAPTER THREE

APPARATUS AND EXPERIMENTAL TECHNIQUE

3.1   PROTON GENERATION AND BEAM HANDLING

Samples to be analyzed were irradiated with a proton beam of 2.5 MeV obtained from Universities 3 MeV Dynamitron accelerator. This is a variable energy high current accelerator. The proton beam was accelerated vertically downward and deflected through 90° in two stages by suitable bending magnets. The beam was then focused using a quadrupole pair of focusing magnets and directed onto a 5 micron thick aluminium foil, mounted 118 cm infront of the sample position, to diffuse the proton beam.

Figure 3.1 shows a schematic diagram of the experimental beam line employed. Two tantalum collimators A_1 and A_2 of diameter 2 mm and 4 mm respectively preceeding the scattering chamber served to define the diffused beam, selecting out the centre and most uniform portion. The beam area at the sample was determined by the collimator A_2, which could be changed to vary the beam area on the target.

After collimation, the resultant beam on the target was a spot of 0.255 cm^2 of approximately uniform intensity. The circular beam hits the target at 45° resulting in a beam spot of elliptical shape.

The collimators were sharply bevelled to minimize beam scattering and the proton current on the collimators was monitored continuously.

For thin targets the beam was collected in a Faraday cup which consisted of a cylindrical stainless steel tube, 40 cm long with a fixed aperture of 1.5 cm diameter at the open end to minimize electron loss. This was located about 15 cm from the target position and was sufficiently distant from the detector that the X-ray production in and around the cup were not detected. The tube was electrically insulated from its surround-
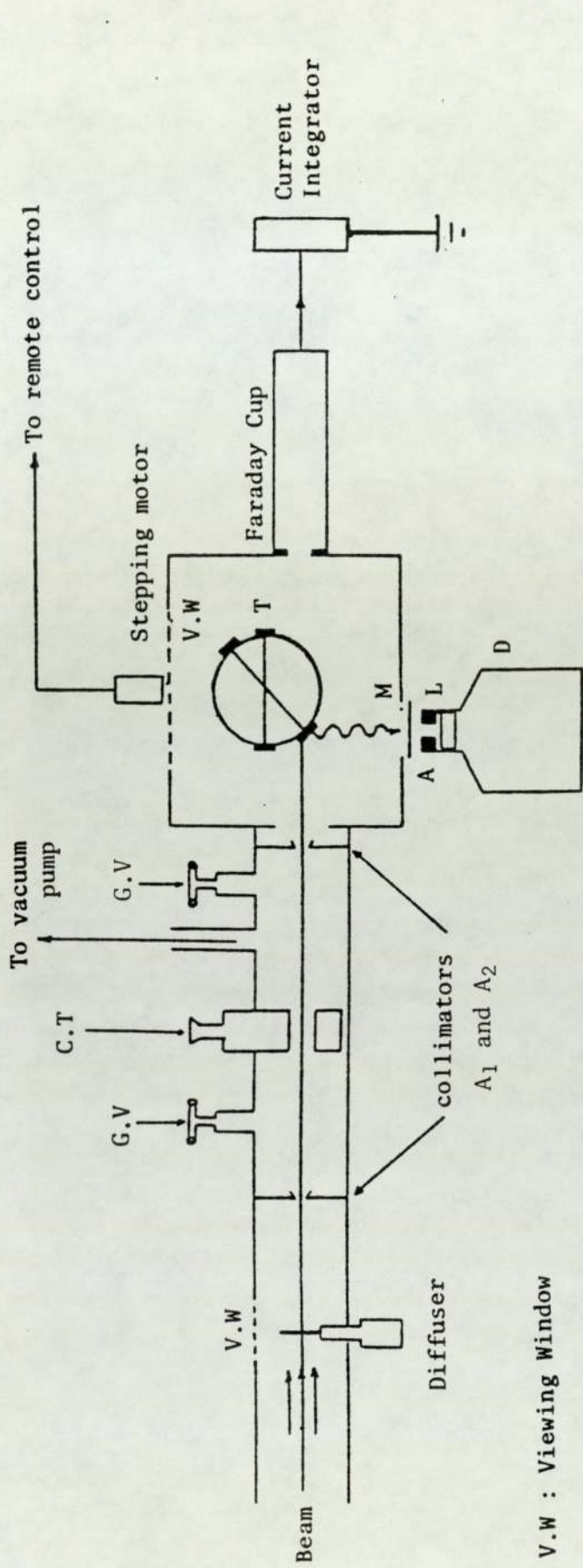
V.W : Viewing Window

G.V : Gate Valves

C.T : Cold Trap

T : Rotating Target

M : Melinex Window

A : X-ray Absorber

L : Lead Aperture

D : Si(Li) Detector

Figure 3.1   Schematic diagram of experimental set-up for PIXE analysis

ing. The number of protons incident on the sample was determined by in-
tegrating the charge collected in the Faraday cup, using a Kiethley elect-
rometer.

Initial results of the photon yield per proton obtained by analyzing
a single elemental foil at different times under identical experimental
conditions were not reproducible. Since the Kiethley electrometer is a
high impedance instrument, this was most likely due to leakage between
the Faraday cup and the chamber, coupled with secondary electron effects.
In order to eliminate these effects, the scattering chamber target assem-
bly and the Faraday cup were all electrically connnected and insulated
from the remainder of the apparatus. The whole assembly then acted as a
Faraday cup for charge integration. Following this, measurements of the
photon yield per proton were reproducible. The other advantages of this
arrangement was that thick target currents could also be monitored as well.

Vacuum System: The ion beam from the accelerator was transported in
vacuum to prevent energy loss and small angle scattering and the irradia-
tion also took place in vacuum. Stainless steel components were used for
the vacuum system with ion pumping to provide clean conditions.

The pressure throughout the beam tube and target chamber were usually
maintained near 10^{-5} torr or less. A clean system was maintained by means
of a cold trap located upstream of a vacuum gate valve. This was a hand
operated vacuum lock which isolated the scattering chamber from the acc-
elerator vacuum system.

The cold trap consisted of a cylindrical tube maintained at liquid
nitrogen temperature through which the beam passed. The cold trap reduced
condensation of hydrocarbons on the target and the vapour pressure to pro-
tect the accelerator vacuum. A second vacuum gate valve was positioned
behind the cold trap so that it could be isolated from the accelerator as
well as the target chamber.

The time required to replace the targets and to attain working vacuum was dependent on the targets analyzed. It could be as short as 15 minutes, but typically was about 30 minutes. Refilling the scattering chamber with inert gas instead of exposing it to atmosphere before opening the chamber is very useful to attain the vacuum in the shortest possible time.

3.2 BEAM DIFFUSER FOIL

In order to obtain reliable quantitative and reproducible information from samples smaller than the beam area and inhomogeneous samples larger than the beam area, it is essential to use an irradiating beam of uniform intensity distribution. Otherwise the target thickness and composition must be made uniform with an area larger than that of the beam. Since it is difficult to produce such targets from biological material and in particular from aqueous solution, it was necessary to make the beam uniform across the target area. Such beams are always useful in avoiding hot spots on the targets which could give rise to extra target damage.

A uniformly distributed beam can be achieved by passing the beam through a thin "diffuser foil". This diffuses the beam into an approximately Gaussian distribution about the axis of the incident beam. The parameters which have to be considered in the choice of the diffuser foil are the thickness, the atomic number of the foil material and the mounting position relative to the target. When a beam of charged particles passed through a foil, it will lose energy by collisions with electrons and nuclei of the target. This energy loss is accompanied by a spreading of the beam due to statistical fluctuations in the number of collisions.

In many cases of practical interest the distribution in energy loss is sufficiently close to a Gaussian that the spreading around the average value is completely characterized by the mean square fluctuations η^2 in

energy loss. η is known as the energy straggling.

In nuclear collision, because much larger masses are involved the collision does not usually make a significant contribution to the energy loss or degradation. However, a fraction of the incident beam will change direction slightly due to multiple collision or scattering. The angular distribution about the original beam direction is essentially Gaussian. The Gaussian assumption allows the angular straggling to be characterized by a width σ.

Hence, the ion beam in passing through a foil undergoes angular straggling as well as energy straggling.

The significant criteria for the selection of a diffuser foil are: energy loss and energy straggling and in addition, the angular straggling which determines the divergence of the beam and hence governs the loss of the beam current and the beam uniformity at the target.

The energy loss of the beam when it penetrates the foil can be corrected for, but the larger the energy loss the greater is the uncertainty in the beam energy due to straggling effect. The diffuser foil, therefore, has to be kept the thinnest possible. However, a compromise must always be made between the criteria and the stability and life time of the foil.

A theory which accounts for the dependence of the energy staggling on proton energy loss is given by Taschala (1968a, 1968b) when the foil thickness is less than half the proton range, the energy straggling can be calculated using a simple formula given by Bohr in 1915. The results are usually in good agreement with Taschala theory. Bearing in mind that in this formula the dependence of the straggling on proton energy is not considered, in addition, it holds only for a thin homogeneous material.

The state of the theories together with accurate experimental results have recently been reviewed by Besenbacher et al (1980). They have

defined Bohrs formula as very simple, high energy limit expression since it is independent of projectile velocity. The fact that we were only interested in rather low energy protons and low energy degeneration, justifies the use of Bohr's formula, where the FWHM of energy straggling Ω in (keV) is given as:

$$\Omega = 2 (Z_1 e^2) \sqrt{\pi n Z t} \qquad \text{(keV)} \qquad \ldots \ldots (3.1)$$

$$\eta = 2.355 \ \Omega$$

$$\eta = 935 \sqrt{\frac{Z(\rho t)}{A}} \qquad \text{(for protons)} \qquad \ldots \ldots (3.2)$$

where, η = FWHM of energy broadening (keV)

Z_1 = projectile atomic number

n = number of atoms per unit volume

t = the thickness of the diffuser foil

(ρt) = the mass thickness of the foil (g/cm^2)

A = atomic weight of diffuser material (g/mole)

The energy straggling was computed using this expression.

To achieve a uniformily distributed beam intensity a reasonable proton scattering has to be obtained in addition to a good collimation system. Therefore, before mounting a diffuser foil the multiple scattering angle must be calculated and the location of the foil relative to the target chosen. To keep the loss of beam current between the diffuser foil and the target moderate, the distance between the foil and the target should not be significantly large.

The multiple angular scattering has been treated in several papers. Spahn et al (1975) have measured the angular straggling of different projectiles including protons in solid targets of C, Al, Ni, Sb, Ag, Au in the projectile energy range (1 - 11) MeV. The straggling width was

- 34 -

studied as a function of foil thickness, projectile energy and atomic
number of the foil material. The agreement between theoretical and ex-
perimental values were not better than 25%.

Marion and Zimmerman (1967) have performed numerical calculations
and provide tabulations which can be used to estimate the distribution
function and the value of scattering angle for different charged parti-
cles.

The method for obtaining the scattering angle as determined by Marion
and Zimmerman (1967), Marion and Young (1968) based on Molier theory and
later simplified by Kivits (1980) to be used with non-relativistic proton
velocities was adopted in this work. This method permits the rapid eval-
uation of the angle at which the angular distribution has decreased to
1/e of its initial value in the forward direction, if a Gaussian angular
distribution is assumed. This is represented by:

$$\theta_{1/e} \;=\; X_c \; (0.869 + 0.34 \; b - 8.88 \times 10^{-3} \; b^2) \qquad \ldots\ldots \text{(3.3)}$$

where $\quad X_c \;=\; 0.0392 \; [Z(Z + 1) \; \frac{\rho t}{A \, E_i^2}] \qquad\qquad \ldots\ldots \text{(3.4)}$

$$b \;=\; \text{In} \; [Z^{1/3} \; (Z + 1) \; \frac{\rho t}{A \, E_i}] + 13.91 \qquad \ldots\ldots \text{(3.5)}$$

$\quad E_i \;=\;$ initial energy (MeV)

$\quad \rho t \;=\;$ foil thickness (g/cm^2)

$\theta_{1/e}$ is the half angle which defines a cone containing 69.5% of the
scattered protons, following the Gaussian distribution.

To justify the selection of a proper diffuser foil, we have investi-
gated the characteristics of some of the elements considered for this
diffusing foil.

For protons having an initial energy of 2.5 MeV, and an assumed

energy loss of 200 keV, the foil thickness, proton scattering and energy straggling were calculated. The formula from Zaidins (1974) was used to calculate the foil thickness in (mg/cm^2) and is given by:

$$(\rho t) = (E_i^{1.75} - E_f^{1.75}) \times \frac{4000}{7C} \qquad \ldots\ldots (3.6)$$

where
E_f = final proton energy (MeV)

C = a constant, depending on Z and given by the same author

These results with some physical characteristic of the foils are presented in Table 3.1, where it can be seen that the energy straggling increases with Z, increasing the uncertainty in the energy correction. The results of (ρt) are in agreement within 10% with the values given by Anderson and Zeigler (1977). The same energy degrading can be carried out with thicker foil of low Z elements, due to their lower density. This implies higher mechanical strength, while $\theta_{1/e}$ can still provide the required beam uniformity with a tolerable proportion of intensity lost. In addition, the foils of such small thicknesses are generally not light tight. It was therefore decided to make the diffuser foil from 5 μm thick aluminium, supplied pin hole free by Good Fellow Metal Ltd, Cambridge.

The calculated parameters using 5 μm aluminium with an incident proton energy of 2.5 MeV using equation (3.3) and (3.2) respectively are as follows:

$\theta_{1/e}$ = 0.020 radians, η = 24 keV and energy loss = 130 keV

The diffuser foil to target distance was chosen as 118 cm, thus the beam intensity at the target position had its 1/e value at radius of 2.4 cm (area of $2.4^2\pi$ = 18 cm^2). Hence, 69.5% of original beam intensity was contained in an area of 18 cm^2 at the target position. The collimated area of the beam on the target was 0.18 cm^2. Thus the solid angle

TABLE 3.1

CHARACTERISTICS OF DIFFERENT DIFFUSER FOILS

Element	Z	A g/mole	M.P C°	ρ g/cm³	C MeV$^{.75}$ · $\frac{cm^2}{g}$	ρt mg/cm²	t μm	η keV	$\theta_{1/e}$ rad
Al	13	26.98	560	2.7	184	2.09	7.75	29.70	0.027
Ni	28	58.71	1453	8.9	148	2.60	2.93	32.94	0.044
Ag	47	107.81	960	10.5	114	3.38	3.22	35.88	0.062
Au	79	196.97	1063	19.3	87	4.43	2.30	39.44	0.091

Note: Calculations for proton energy straggling and proton scattering in the foils are made, assuming an initial proton energy E_i of 2.50 MeV and a final energy E_f of 2.30 MeV

- 37 -

selected to subtend the area of the target was about 1.29×10^{-5} str. The above described scattering geometry is shown in Figure 3.2.

The beam intensity on the target was calculated, the non-uniformity of the beam at the centre to the edge of the beam cross-section was estimated to be only 1%. This represents the most uniform part of the Gaussian distribution.

The system was designed so that the diffuser foil could be withdrawn from the beam without disturbing the vacuum of the system. Mounting a glass window on the beam line in the position of the diffuser foil, made the viewing and checking the foil possible, while the foil was inside the beam tube. The foil was frequently examined for pin holes. The life-time of the foil were found to be relatively long (about 15-20 days of run) for beam currents on the foil typically 3.5 μA.

The diffuser foil is the least complicated arrangement for achieving a uniform beam but requires relatively high initial beam current to allow for intensity reduction. In addition, problems can arise due to heating damage and radiation damage. Over-heating the foil from the total proton energy dissipation can cause pin holes to develop. The target composition may change during irradiation due to radiation damage. Some atoms will inevitably be displaced by nuclear reaction, but more damage will result from ionization leading to breaking covalent bonds. However, the visual appearance of the foil did not indicate or reveal any serious change after irradiation and the slight damage to the filter was not uniform and the pin holes were in the centre which indicates that the melting of the fil-ter material took place due to formation of hot spots. Figure 3.3 shows a scanning electron micrograph of one of the foils used after it has been irradiated until pin holes had developed compared with one before irradi-ation.

However, while we have found   diffusing to be satisfactory the same results can be achieved with a more sophisticated method by sweeping
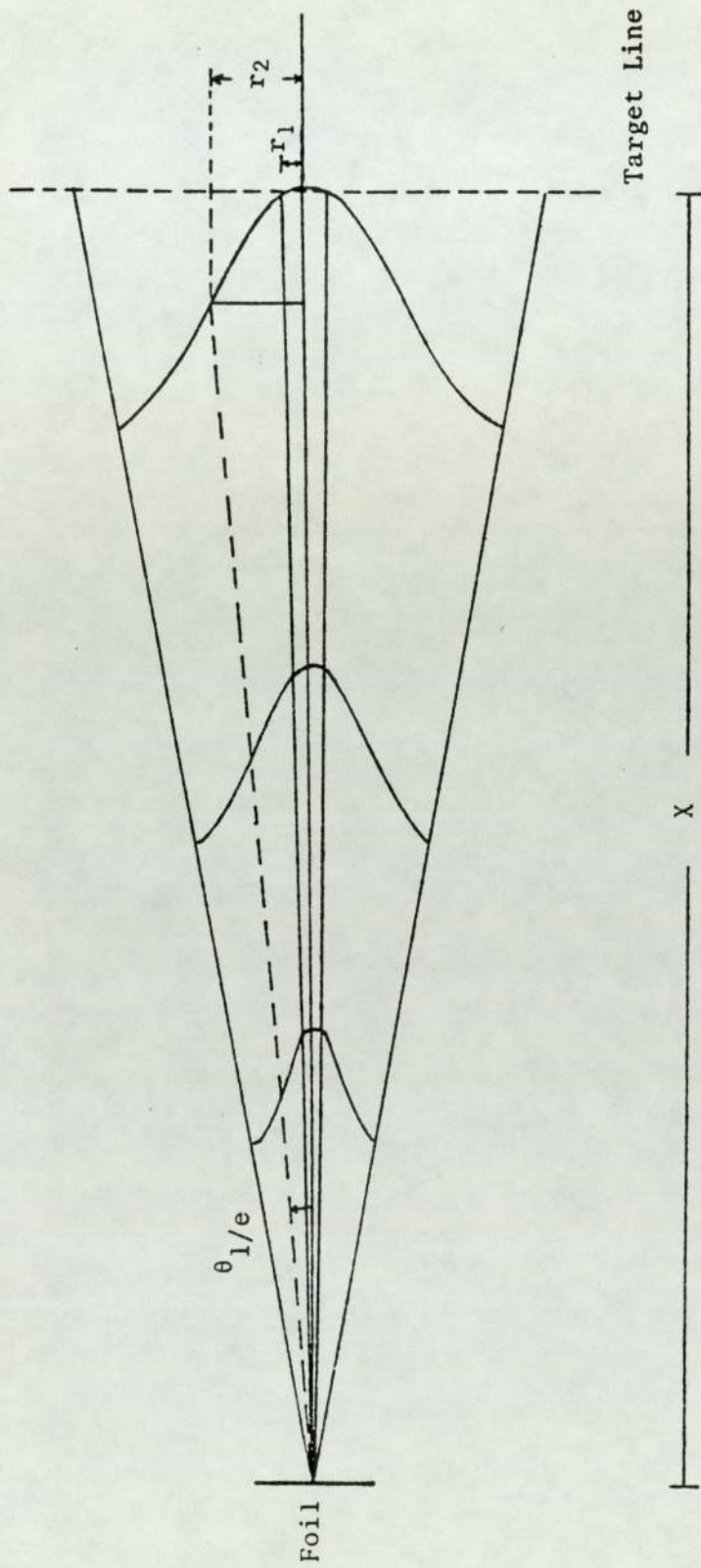
Figure 3.2   The scattering geometry of diffused protons

- 39 -

A

B

Figure 3.3   Scanning electron micrographs for
            A: Aluminum diffuser foil before irradiation (X10) and
            B: The same foil after irradiation with some developed pinholes
            (X10)

a well focused beam in the two perpendicular directions across the target face using electrostatic sweeping as employed by Johansson (1972), Cahill(1975) and Bearse(1974, 1977).

3.3   SAMPLE MOUNTING AND TARGET CHAMBER

The irradiation chamber positioned at the end of the accelerator beam line was a rectangular box constructed from 1 cm thick stainless steel plates. The chamber was fitted with a 50 μm Melinex window through which the Si(Li) detector collected X-rays from the target. A glass window of 1.25 cm thickness for target viewing was also incorporated. A front and back port were connected to the 10 cm diameter beam tube and a Faraday cup respectively. The chamber was electrically isolated from the beam tube by an insulation coupling.

The initial work commenced with a rotating target assembly with hinged mounting arms for eight targets. A rectangular target frame was held at the end of each arm. This target rotary system was suspended inside the evacuated chamber by a motor shaft which was rotated indirectly by a magnetic coupling. The hinged arms moved on a cam to bring each target sequentially to a position of 45° to the incident beam. A Faraday cup which consisted of an aluminium tube of 10 cm length and 1.5 cm diameter was located about 2 cm from the target.

The system performance was assessed by studying the reproducibility achieved when a set of semi-thick standard metal targets of Ti, V , Co, Ni, Cu, Zn, Nb and Zr were bombarded by 2.5 MeV protons. The X-ray yield obtained by irradiating these foils with proton beams under identical experimental conditions at different times were found to be unreproducible. This was considered to be due to (i) positional variation of the sample with respect to the beam and detector, (ii) incomplete charge collection by the Faraday cup.

To estimate the influence of the variation of the target - beam angle on the observed X-ray intensity, calculations were made on the X-ray yield as a function of the angular position of the targets. Changes in the horizontal and vertical position of the target affect the X-ray yield through the associated changes in target thickness seen by the beam.

Calculations have been made for the horizontal position θ, 38° to 52° and for the vertical position δ, - 5° to + 5°. Table 3.2 gives the variation of the number of X-rays detected (n) with θ, where n normalized to 1 at $\theta = 45°$, while Table 3.3 gives the variation of n with δ where n = 1 at $\delta = 0$.

The information provided in Tables 3.2 and 3.3 indicate that a variation of 1° in horizontal position gives rise to 2% variation in the X-ray yield per proton, while a 10° variation in the vertical position gives rise to a similar variation. A study of the rotary mechanism revealed that the torque of the indirect coupled motor was insufficient to fully overcome the friction associated with the motion of the targets on the cam . This resulted in a variation of horizontal position of ± 3°. In addition, variations in the vertical target position of ± 2° observed due to the friction in the hinges and the target clamping arrangements. More-over, the relatively small size of the Faraday cup and its close proxi-mity to the targets resulted in secondary electrons loss and incor-rect charge integration.

The situation was rectified by modifying both the movement mechanism of the rotating target assembly and the design of the Faraday cup.

In order to evaluate the precision and long term reproducibility of the PIXE analysis system a very simple design was adopted with a minimum of moving components. This consisted of an aluminium disc suspended from the chamber top plate by a shaft connected to its centre. Four target mounts were rigidly fixed at the outer edge of this disc into which the

TABLE 3.2

THE EFFECT OF HORIZONTAL MOVEMENT OF THE TARGET ON THE X-RAY YIELD

$\theta°$	38°	39°	40°	41°	42°	43°	44°	45°	46°	47°	48°	49°	50°	51°	52°
n	0.897	0.910	0.923	0.937	0.957	0.967	0.983	1	1.018	1.037	1.057	1.08	1.10	1.12	1.15

TABLE 3.3

THE EFFECT OF VERTICAL MOVEMENT OF THE TARGET ON THE X-RAY YIELD

δ	0	2	2	3	4	5	6	7	8	9	10
n	1	1.0001	1.0002	1.0011	1.0019	1.003	1.0044	1.006	1.0079	0.99	0.98

Note: The values are normalized to 1

at $\delta = 0$, and $\theta = 45$

target frames could drop into position. This ensured that the targets could be rotated repeatedly into four exactly reproducible positions. The target frame consisted of a (2 x 2.5) cm^2 and 0.1 cm thick piece of aluminium with 1.5 cm circular aperture. The target backings were held across the hole with the aid of a ring which was slightly smaller than the hole so that it could be pressed into it and clamp the backing.

The targets were positioned at 45° relative to the beam direction. For proper beam alignment, a laser beam was utilized to ensure that the small specimen deposit in the centre of the backing was covered by the beam. The laser beam was set up in the same direction as that of the proton beam and allowed to hit a metal foil placed in the sample holder. The specular reflection from the foil was observed at 90° to the beam direction on a mark on the wall $\sim$ 3.0 metres away from the chamber and in line with the axis joining the chamber and the detector.

For accurate positioning of the target, a rotary specimen manipulator, RD91 Minature Rotary Drive, was chosen to rotate the target assembly device. This was a direct method of rotating, employing bellows. The stop positioning was fully adjustable. The torque of the target assembly was found experimentally to be 60 gm.cm which was within the range of the rotary device torque. The chamber top plate was replaced by a new 1.25 cm thick stainless steel plate through which the rotary device was connected to the target holder. In order to make full use of the accelerator time, a remote change facility was designed. This involved the introduction of a stepping motor to operate the rotary drive and control the angular positioning of it, together with an associated remote control.

A high resolution stepping motor (FDTA/A51), Evershed Powertor, London) was installed on the top of the rotary manipulator. The movement of this stepping motor was operated by a remote control system which

was constructed from a Synchronous Digiplan Stepping motor drive (type 1016/1) which provided all of the required logic and power necessary to step the motor. This was interfaced with an incremental indexor (type 1041) to serve the dynamic performance of the stepping motor. The design of the last card was such that, it resulted in rotation of the motor shaft by $0.9°$. These cards were all mounted in an aluminium chassis in which the power supply was built and mounted, in addition to a small fan provided for heat dissipation. Proper connection from the driver card to the motor was made with shielded coaxial cables. The target position and the angle indicated on the rotary dial was observed with two T.V. cameras. Thus the targets were remotely interchanged and controlled from the computer room. This permitted fast and accurate repositioning of the targets.

A photograph of the general irradiation facility is given in Figure 3.4.

3.4 DATA AQUISITION AND ANALYSIS

The data aquisition electronics used in these experiments has been described in detail by R. Khan (1975) and O. Khan (1977) and only a brief description will be given here.

A schematic representation of the essential components of the data processing system is shown in Figure (3.5). X-rays produced by proton bombardment of the target were detected with a 30 mm^2 lithium drifted silicon Si(Li) detector. The targets were at an angle of 45° with respect to the detector. The X-rays leave the target chamber through a 50 micron Melinex window and pass through approximately 3 cm of air before entering the 12.5 micron beryllium window of the detector. Aluminium absorbers were usually placed between the two windows to reduce the intensity of low energy X-rays reaching the detector. Each X-ray entering

- 45 -

Figure 3.4   A photograph of the PIXE
              facility
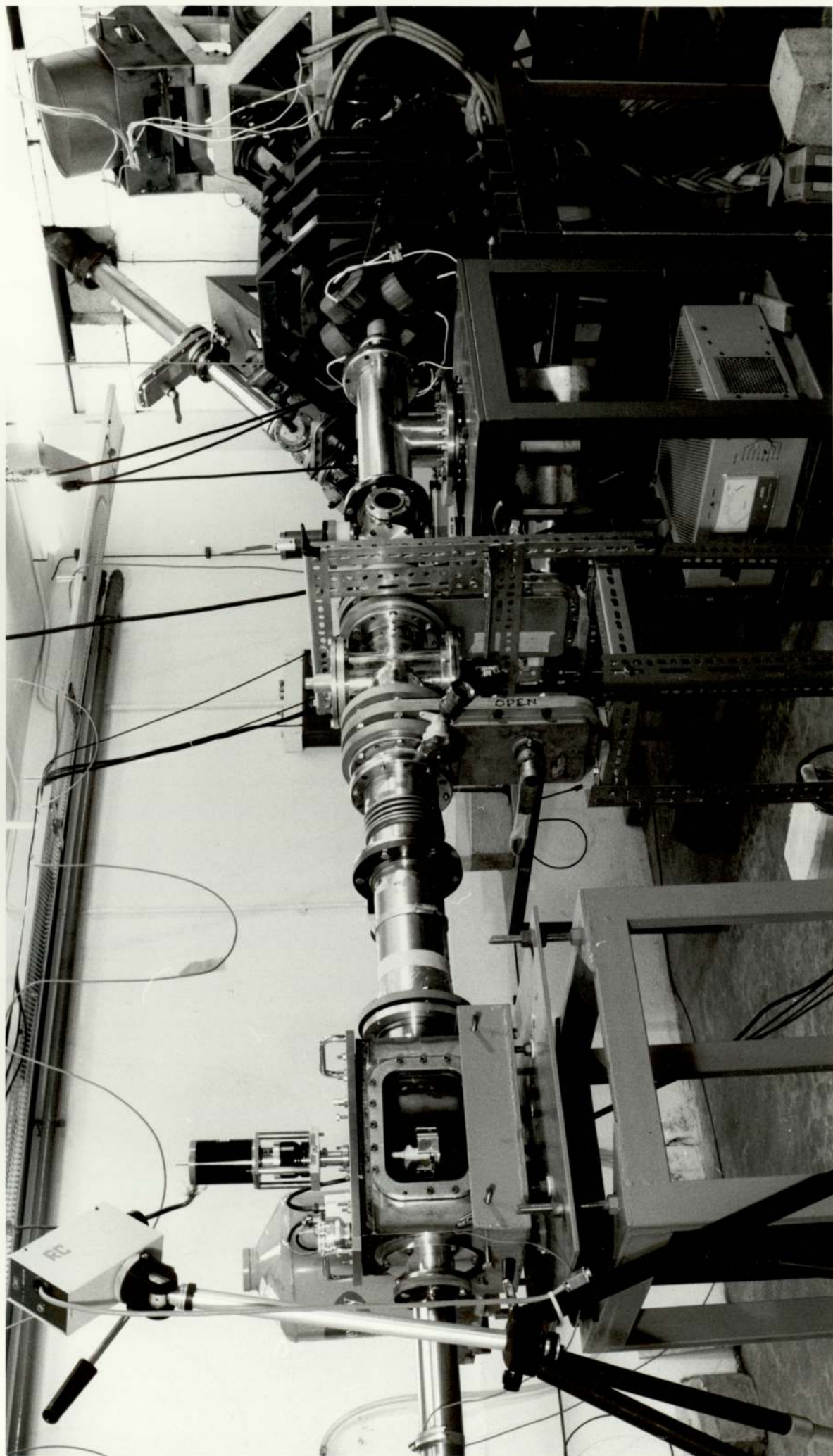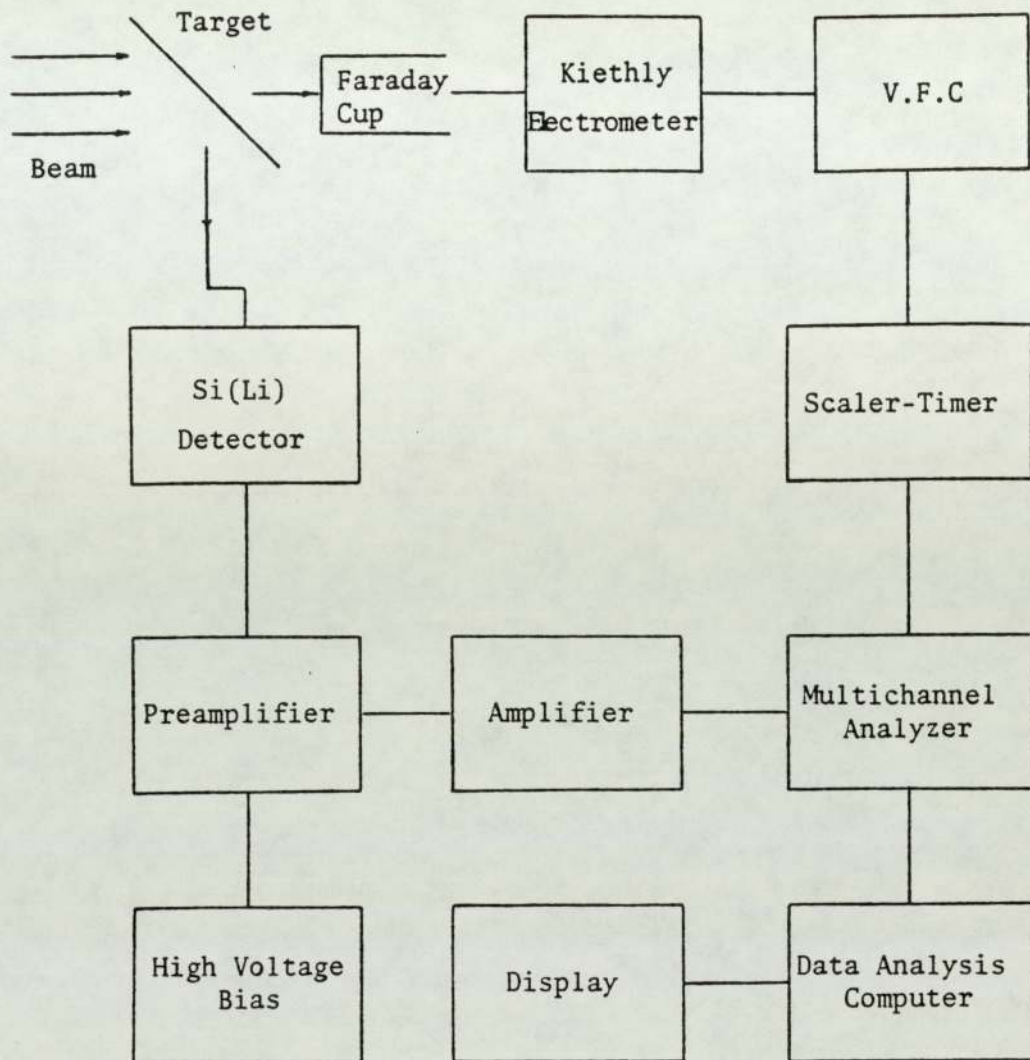
Figure 3.5   Electronic block diagram for X-ray detection and data processing

- 48 -

the Si(Li) detector gives rise to an electrical pulse which is proportional to the energy of the X-ray. These charge pulses were then collected by the applied potential of 1000 V. The preamplifier which is an integral part of the detector assembly, converts the charge pulse into a voltage signal using a cooled field effect transistor (FET), while keeping the proportionality between the energy deposited and the pulse height. To maintain the dc level, pulsed optical feedback was employed. The output of the preamplifier was coupled to a spectroscopy amplifier where the pulses were shaped and amplified before being allowed to proceed to multichannel pulse height analyzer, where the ADC sorted the input signals by pulse height into 2048 channels. This computer based data aquisition system was interfaced to Hewlett-Packard 2100 computer. A display unit working in conjunction with the ADC provided a visual display of the spectrum being accumulated. This helped greatly in whether to continue an experiment run by observing the intensity of a desired peak in the spectrum.

The overall system has an energy resolution of 160 eV at FWHM measured at 5.89 keV. The X-rays of the elements above atomic number, 13 (aluminium) can be detected.

For quantitative analysis, the proton charge accumulated on the sample had to be measured. As mentioned earlier the total current collected was fed into a current integrator which outputs a voltage pulse for the charge collected. These voltage signals were fed to a Voltage to Frequency Converter VFC, which produces a pulse chain of 10^5 Hz for 1 volt input. The output of VFC was again fed to a scaler through a decade deviding unit to make it suitable for counting. The scaler and divider were interfaced with an automatic stop device, to stop the collection of data once a present count on the scaler had been accumulated, which was directly proportional to proton charge. Thus the spectra were accumulated for a specific total charge since the beam intensity may vary with

- 49 -

time.

At the end of an analysis, the data was stored on a file manager (FMGR) which is a system for storing source information. The information on the FMGR can be stored on magnetic tape for analysis at a later time.

The on-line computer programme which controlled data acquisition provided the capability to analyze data from one of the spectra previously stored while the next X-ray spectrum was being accumulated.

3.4.1 X-ray Absorber Filters

A common experimental situation in the analysis of biological and environmental samples is that most of the low atomic number elements (e.g. S, Cl, K, Ca) are quite abundant. Combining this with the relatively large cross-section for both characteristic X-ray and bremsstrahlung production in the low energy X-ray region results in a high intense radiation into the detector. This intense flux deteriorates the detection efficiency for higher energetic X-rays due to its large count rate contribution. This reduces the system's sensitivity to the medium and high Z elements.

The count rate was decreased by the method of filtration utilizing either the use of single or multiple filters. The absorber was placed between the detector and the target.

The majority of thin samples such as hair and bovine liver were analyzed with a single filter of 7 μm aluminium. The effect of this absorber on a bovine liver sample is illustrated in Figure 3.6. This represented a compromise between optimized sensitivity for all the range of elements of interest and a moderate count rate of < 1000 counts per second (cps). Hence, a beam intensity of 100 nA/cm^2 could be used without any appreciable increase in the detector dead time.

For the thick bovine liver pellets a 10 μm aluminium filter was found to be most suitable.
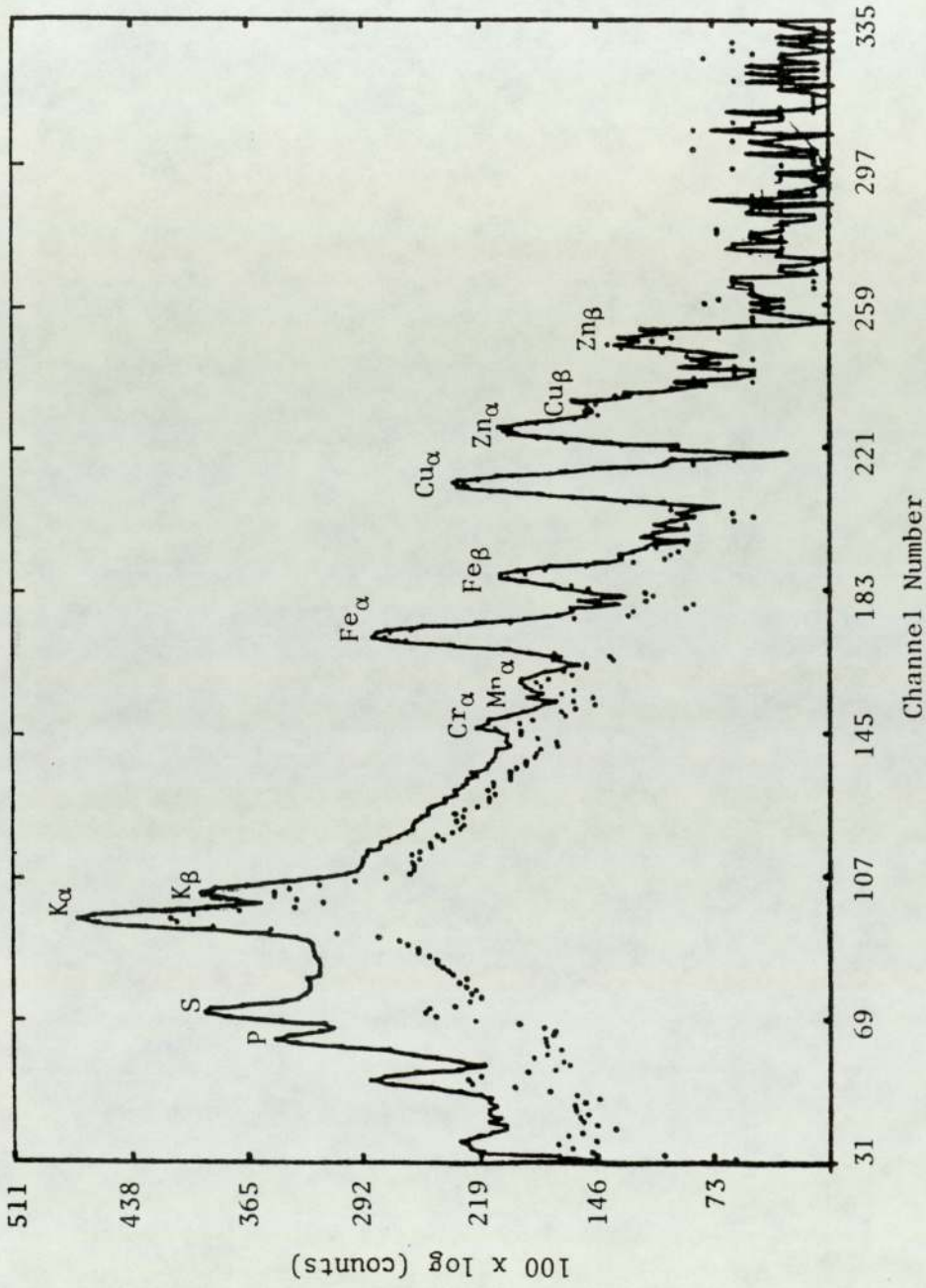
Figure 3.6   Comparison of PIXE spectra obtained from analysis of bovine liver target with and without 7 μm aluminium absorber

- 51 -

By employing filters of different thickness one can optimize the detection efficiency for a selected region of interest. This was the method followed when kidney and bladder stones were analyzed, which contained, for example, significant quantities of calcium. Therefore, to obtain optimal sensitivity over the range of elements of interest the samples were analyzed several times, each time using a different appropriate foil. The absorbers used were aluminium foils of thickness 5, 15, 30, 40, 50 μm. Typically, a short analysis for the low Z elements was performed using 5 or 15 μm aluminium filter, longer analysis was required with the thicker filters. When analysis was carried out for P, S and Cl, it was necessary to remove all the filters.

The advantage of using X-ray filters is demonstrated in Figure 3.7. The spectrum obtained without an additional absorber shows the poorest sensitivities for the high Z elements, while the spectrum accumulated using the absorber shows the best sensitivities for these elements. Figures 3.8, 3.9 and 3.10 show the effect of three different absorbers of 0, 10, 50 μm on a spectrum obtained from bladder stone. The effect of the thicker filter in low Z element is quite pronounced. However, the major benefit gained by X-ray filtration was reducing the count rate at low X-ray energies which allowed increasing the beam current and thus obtaining improved statics for heavier elements in shorter times.

3.4.2 Detection of X-rays

Basically, two types of X-ray detection are available: energy or wavelength dispersion. For PIXE work, energy dispersion detectors have proved to be very useful, mostly due to their ability to detect X-rays of many elements simultaneously. While wavelength dispersion techniques such as single crystal spectrometers detect only X-rays of a single wave-

Figure 3.7   PIXE spectra from analysis of a
              bladder stone with and without
              an absorber. The time required
              to accumulate the 10 μC charge
              for the sample with absorber
              was a fifth of the time required
              in the first case, due to higher
              permitted current used in the
              second case.
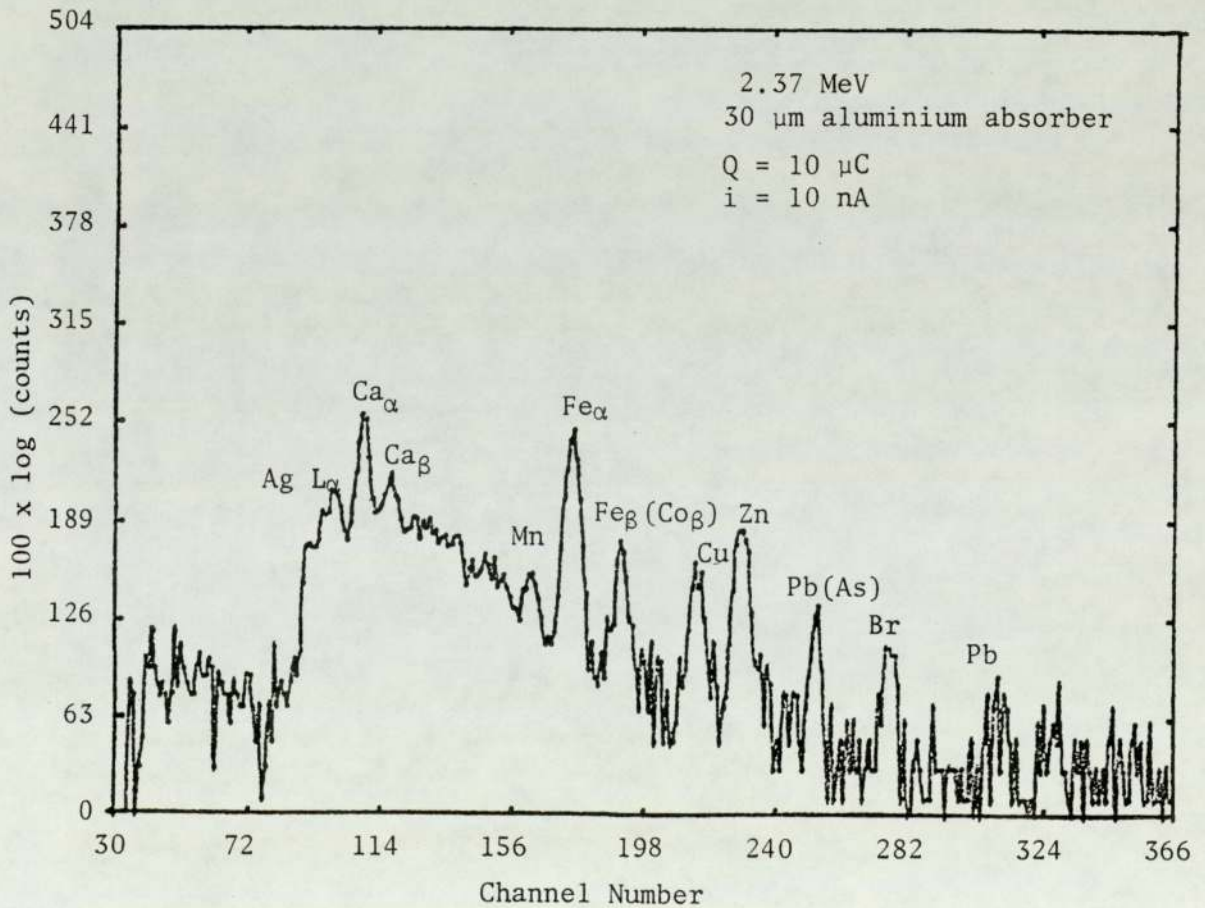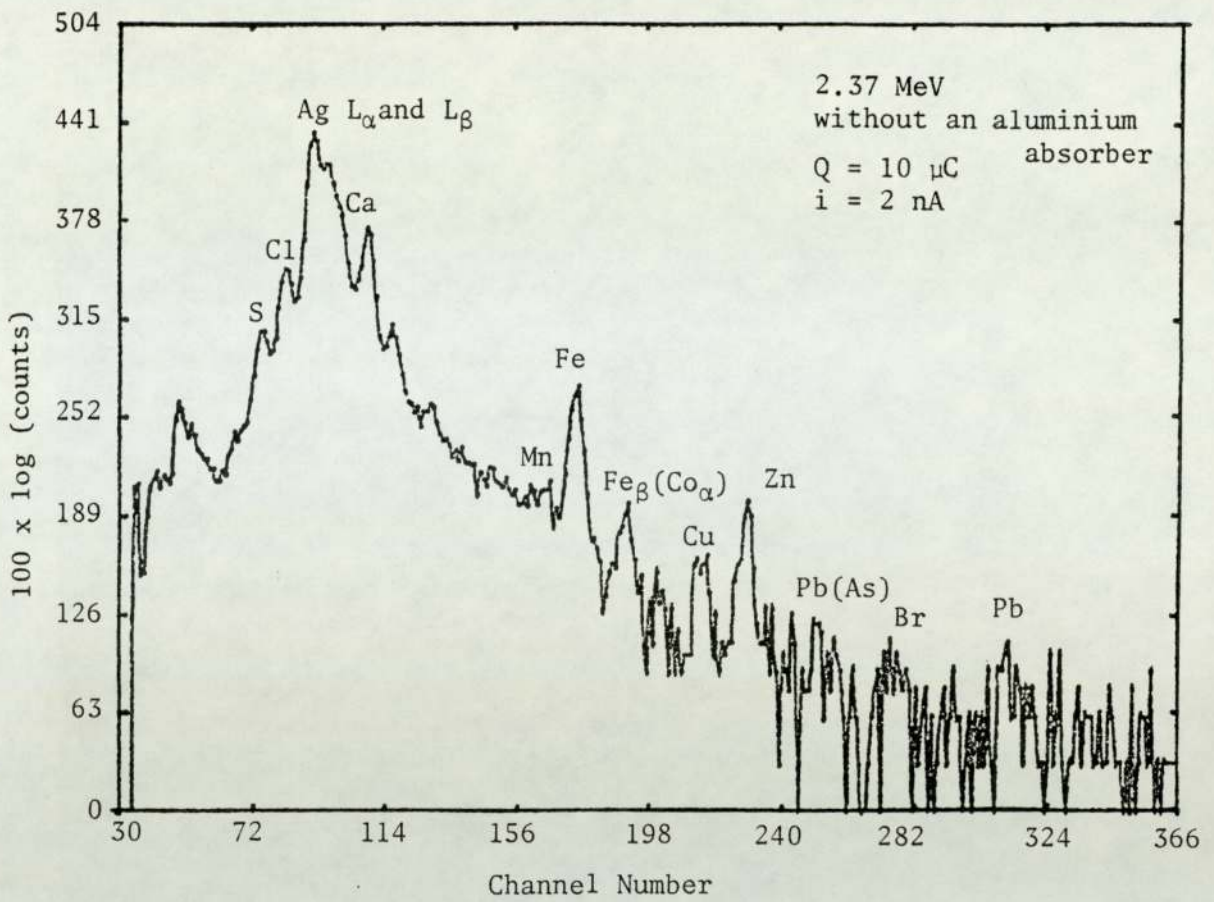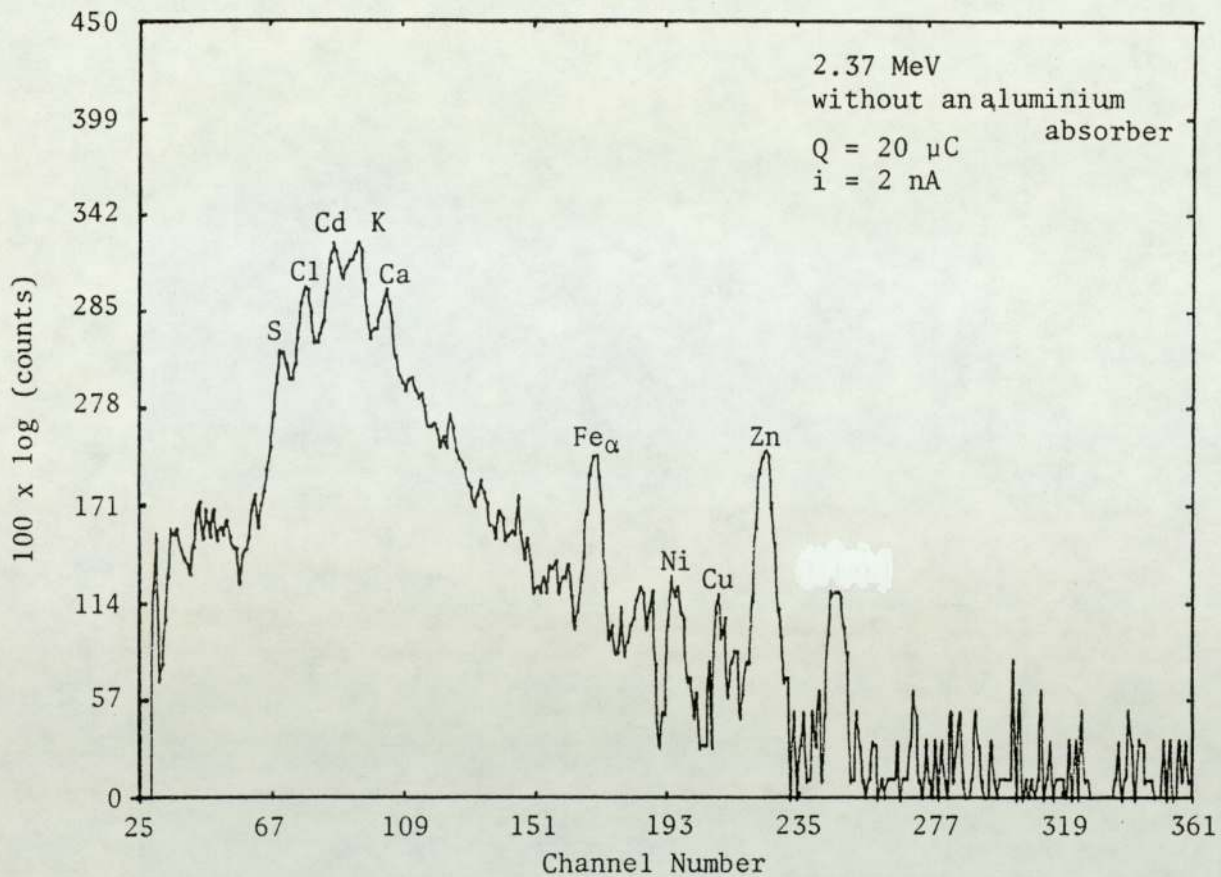
Figure 3.8
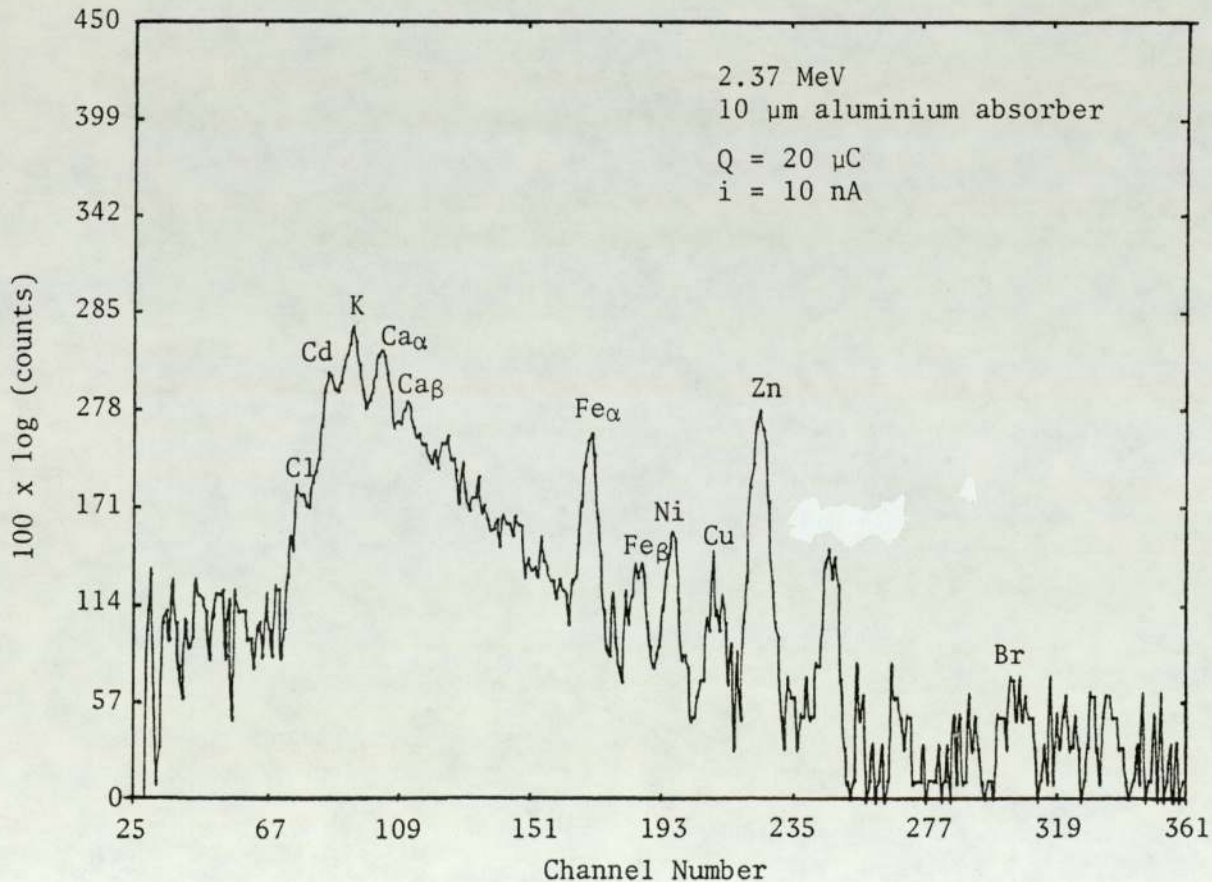
Figure 3.9
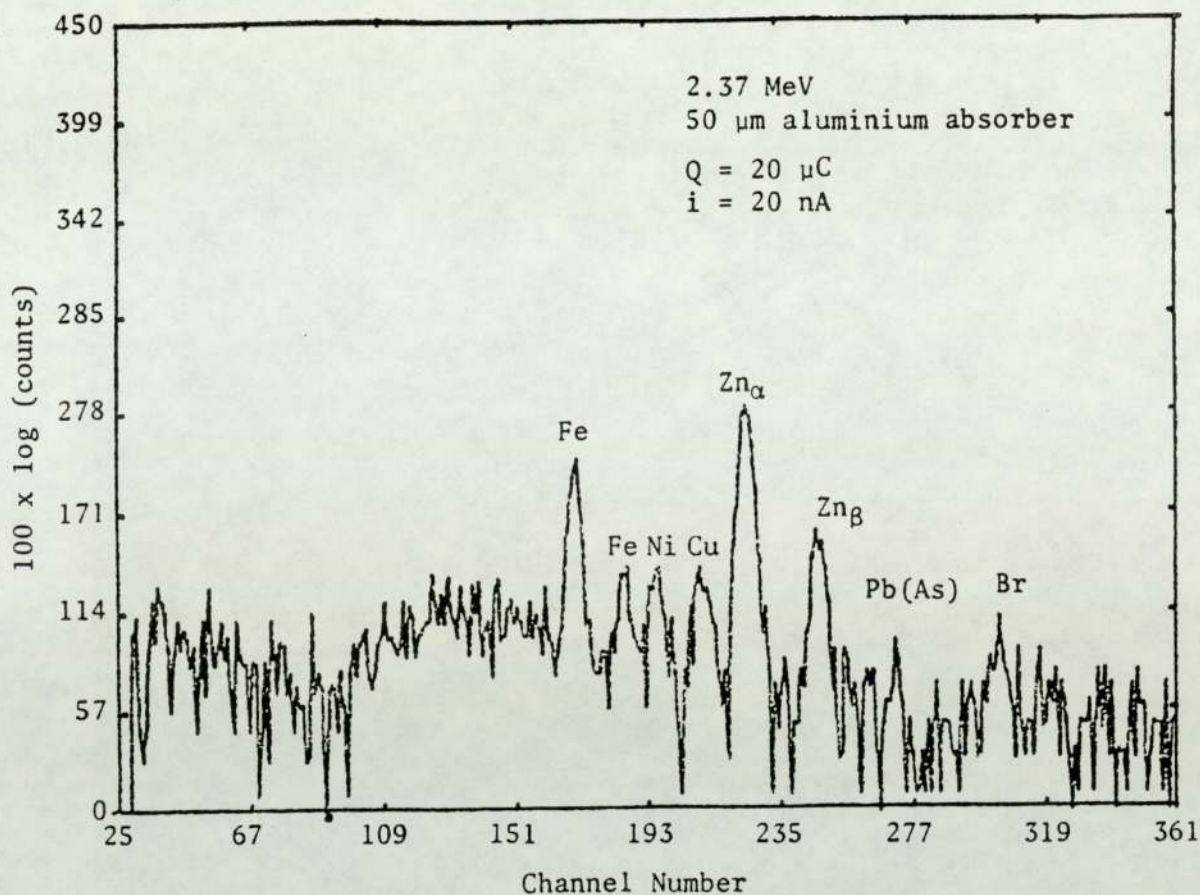
Figure 3.10

Figures 3.8, 3.9, 3.10

Pixe spectra of a kidney stone without an absorber
and with two different thicknesses of 10 and 50 μm
aluminium. Note the attenuation of low energy X-rays
in Figure 3.10 compared to spectrum in Figure 3.9 with
thinner absorber and the spectrum in Figure 3.8 without
any absorber.

length, (i.e. energy) and in addition have low efficiency.

The detector chosen for this system was an energy dispersive solid state Si(Li) detector, directly coupled to a pulsed optical charge sensitive preamplifier.

The Si(Li) detector (Kevex, 3201 cryogenic sub-system) comprised of a disc of 30 mm^2 area and 3 mm thick silicon crystal, drifted with lithium impurity atoms. This lithium creates an intrinsic region within the silicon which can then be regarded as a solid state ionization chamber. The detector and first stage of the preamplifier are cooled to liquid nitrogen temperature to minimize the electrical noise production by the thermally excited charge carrier in the crystal material and to prevent diffusion of the lithium through the crystal.

A high potential is applied between its parallel faces. The detector has a 12.5 μm beryllium window to protect the vacuum of the detection system and allows a reasonable efficiency for X-rays as low as 1 keV (sodium)

For accurate PIXE work, it was found that the reproducibility of the detector re-positioning was imperative. Therefore, the detector was kept rigidly in a fixed position at 90° with respect to the incident beam and subtended a solid angle of 0.014 steradian at the centre of the sample. The geometry was fixed by installing a perspex adapter, one end of it was attached to the chamber Melinex window mount and the other end was fitted to the detector. Two slots in the perspex allowed interposition of absorber filters. A fixed air gap of about 3 cm was maintained between the Melinex and beryllium windows.

When an X-ray enters this non-conducting material of the detector, silicon atoms are ionized via photoelectric and Compton scattering process. This results in the creation of an amount of "free charge" which is proportional to the amount of energy deposited in the detector by the X-ray.

This charge is swept out by the applied potential forming a charge pulse characteristic of the detected photon. The preamplifier effectively integrates this charge pulse and converts it to a voltage signal while preserving the proportionality between the intial energy deposit and the level of the output voltage signal.

The parameters which relate to the performance of Si(Li) detector and are basic requirement for a good detector are the detector efficiency, detector resolution and linear relationship for input and output signal. These parameters are discussed in the following sections.

6.4.2.1 <u>Detector Efficiency</u>: For any absolute quantitative analysis based on the calculation using X-ray production cross-section values, it is imperative that the detection efficiency is accurately known as a function of the photon energy.

The absolute detection efficiency of the detector crystal is given as:

$$\frac{\Delta\Omega}{4\pi} \ x \ \varepsilon$$

where, $\frac{\Delta\Omega}{4\pi}$ is the geometrical efficiency

and, ε is the intrinsic efficiency of the sensitive region in the crystal which is the probability that a photon entering the detector produces sufficient ionization that the output pulse fall within the corresponding full energy peak. This is usually expressed as:

$$\varepsilon = (1 - e^{-\mu_{si} X_{si}}) \qquad\qquad ..... (3.7)$$

where μ_{si}, X_{si} are the mass absorption coefficient and areal density of the sensitive region respectively.

Since the crystal is usually protected by a beryllium window, the

absorption of X-rays in this window must be accounted for. Apart from absorption in the Be window, there is appreciable absorption in the gold layer and dead layer of the silicon crystal, which is an inactive layer of silicon near the detector surface. Thus the effective efficiency is given by:

$$\eta = e^{-\sum_{i=1}^{3} \mu_i X_i} [1 - e^{-\mu_{si} X_{si}}] \qquad \dots \dots (3.8)$$

where μ_i and X_i are the mass absorption coefficient and areal density respectively for the layer i.

Figure 3.11 illustrates the theoretical detector efficiency for the detector as a function of energy upon using a 12.7 μm Be window and silicon diode of 3 mm thickness only. As it is seen the distinct feature of this curve is the fall in efficiency at high and low energies. Below 15 keV the crystal is expected to absorb all photons and be 100% efficient. However, as photons are attenuated by the Melinex window, air path and beryllium window before they reach the sensitive region, this causes a fall in the efficiency. At energies above 15 keV the drop in the detection efficiency is due to the increased transmission of the X-rays through the detector crystal. Thus the detection efficiency at higher energies is a function of the thickness of the crystal.

The efficiency curve for Si(Li) detector is usually provided by the supplier, in which it is accounted for absorption in Be window only. For accurate quantitative analysis the detector efficiency for the specified Si(Li) detector should be experimentally determined.

In the present quantitative analysis, the efficiency factor was not accounted for, since the use of the calibration factor F_{xz}, see section 4.2, eliminates the detection efficiency factor η.

Due to the significance of X-ray lines intensities to proceed the following experimental work, $\frac{K_\beta}{K_\alpha}$ ratios of thin standard targets, under

- 59 -
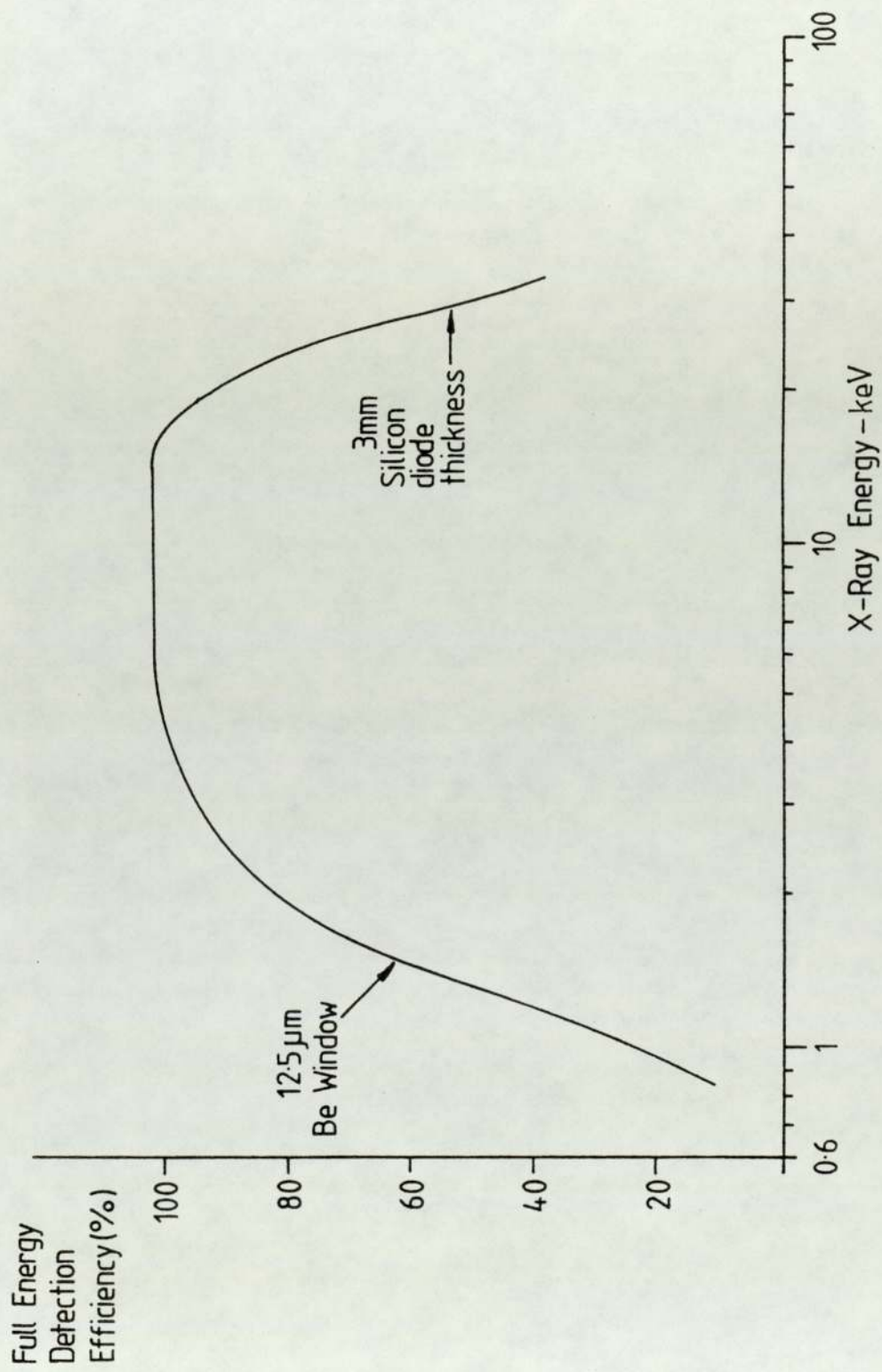
Figure 3.11   Detection efficiency of the Si(Li) detector with 12.5 µm Be
window and 3 mm silicon diode

- 60 -

proton irradiation were measured. Characteristics of these foils will be considered in detail later. These values were corrected for absorption in Be window, air path, Melinex window and compared to reported values in the literature as shown in Table 3.4. A good agreement with the values from review of Bambynek et al (1972) as well as those of the PIXE work of Barfoot (1980) is found for almost all elements, while the values given by Scofield show some disagreement with all the other values.

3.4.2.2 Detector Resolution: The energy resolution of the X-ray detector, is its ability to distinguish between K_α X-rays of adjacent element in the periodic table, is an essential parameter in the choice of an X-ray detector.

The resolution is conventionally defined as the full width of the energy peak at half maximum intensity (FWHM) measured in energy units.

In the present set-up, the detector resolution was measured to be 160 eV at 5.898 keV at 1000 cps, the K_α X-ray line of Mn from an Fe-55 source. This corresponds to 2.7% which is relatively a high resolution for Si(Li) detector.

The limit of resolution depends quite critically on the value of the Fano Factor (F) which is a measure of the ultimate theoretical statistical capability of ionization detector which includes the pair-creation statistics and inefficient charge collection.

However, the effective resolution of the X-ray detector is also limited by the noise and count rate capability of the associated electronics. This is considered random and independent. Therefore, the total resolution is the sum in quadrature of the intrinsic and electronics noise effect (Woldseth 1973).

$$ \text{FWHM} = [(2.35^2\, F\, \epsilon\, E) + (\text{FWHM})^2_{\text{noise}}]^{\frac{1}{2}} \qquad \ldots\ldots (3.9) $$

TABLE 3.4

COMPARISON OF MEASURED AND LITERATURE VALUES OF K_β/K_α RATIOS

Element	K_β/K_α ratio			
	PIXE present work	PIXE Barfoot 1980	Bambynek et al (1972)	Scofield (1974)
Ti	0.123 - 0.126	0.118 - 0.122	0.133	0.1355
Mn	0.127 - 0.137	-	-	0.1385
Co	0.126 - 0.133	0.131 - 0.135	0.134	-
Cu	0.133 - 0.135	0.135 - 0.143	0.135	0.1379
Ga	0.137 - 0.147	-	-	-
Ge	0.145 - 0.153	0.148 - 0.154	0.148	0.1504
Mo	0.193 - 0.197	-	0.193	0.1981

where ε is the average energy required to create an electron hole pair in silicon at liquid nitrogen temperature and equals 3.9 eV.

E is the photon energy.

The constant 2.35 relates one standard deviation of a Gaussian distribution σ to the FWHM.

It is shown in the above relation that the resolution varies with the the energy of detected photon. Thus it is more reliable to evaluate the resolution of the detection system for a range of different energies.

From equation 3.9 it is found that σ^2 is related to X-ray energy by:

$$\sigma^2 = (\varepsilon F) E + [\frac{(FWHM)_{noise}}{2.355}]^2 \qquad \ldots\ldots (3.10)$$

The resolution has been measured with the present system using 10 elemental standard foils. Figure 3.12 shows a plot of σ^2 vs Energy. The values corresponding to Cl and K are deviated from the straight line obtained. This appears to be due to slight under-estimation of the true FWHM since thses lines are composite and not properly resolved. From this plot F was calculated to be 0.117 ± 0.003, where the value of uncertainty was a consequence of the uncertainties in the FWHM. This range of (0.120 - 0.114) is in fair agreement with the recent experimental value for Si(Li) detectors Musket(1974), Jaklevic (1971) and Zulliger (1970).

The value of $(FWHM)_{noise}$ as supplied by manufacturers is 113 eV, while its value according to Figure 3.12 was found to be 119 eV. This small difference could be explained by the laboratory microphonic noise effect, Khan et al (1979).

Furthermore, to illustrate the resolution capability of the system over a large range of elements, energies of the characteristic K_α, K_β, L_α and L_β lines as a function of atomic number are illustrated in Figure 3.13. From this figure it can be noted that adjacent elements and K_α and K_β lines of high and intermediate elements can be separated by an energy
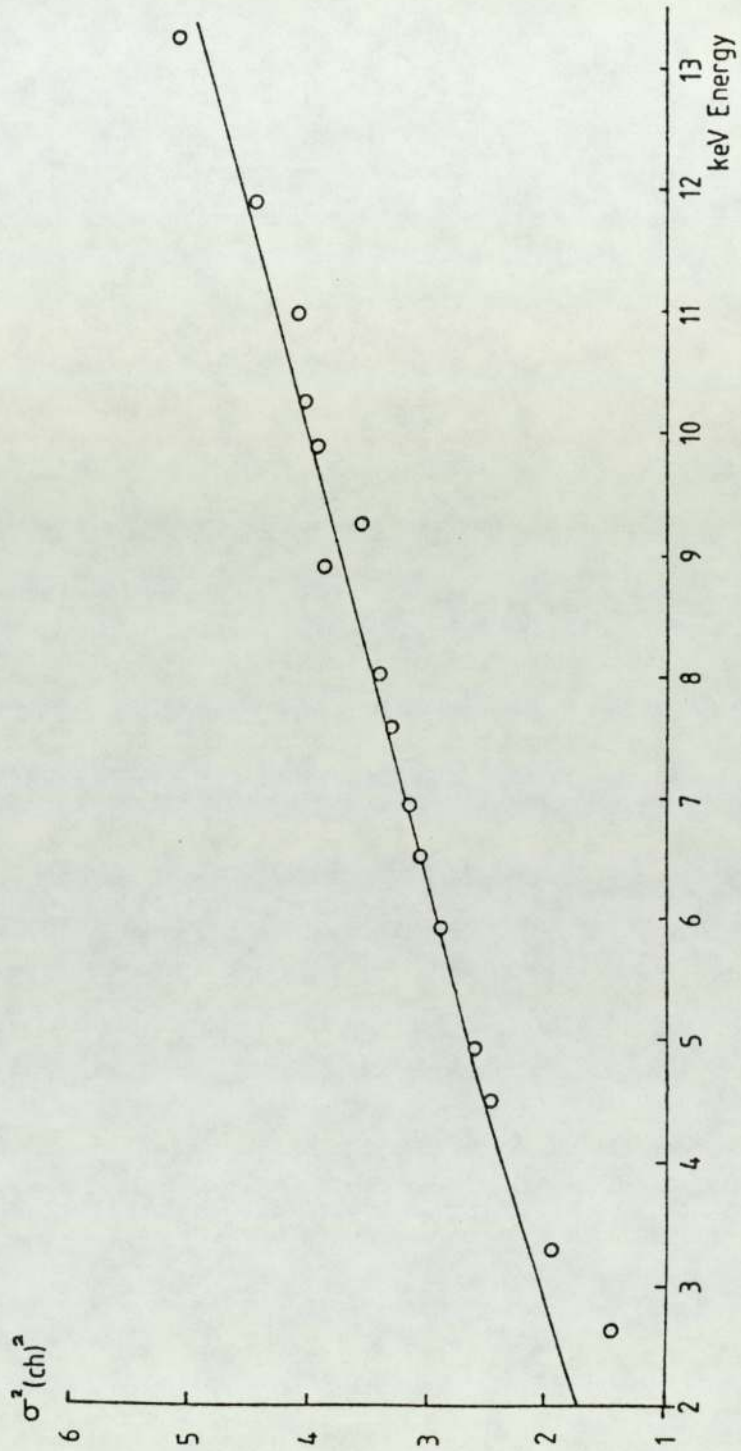
Figure 3.12   A plot of σ^2 versus X-ray energy presenting the measured FWHM resolution for the present system (where FWHM = 2.35σ)

Error bars were omitted since they were smaller than the symbol size

- 64 -
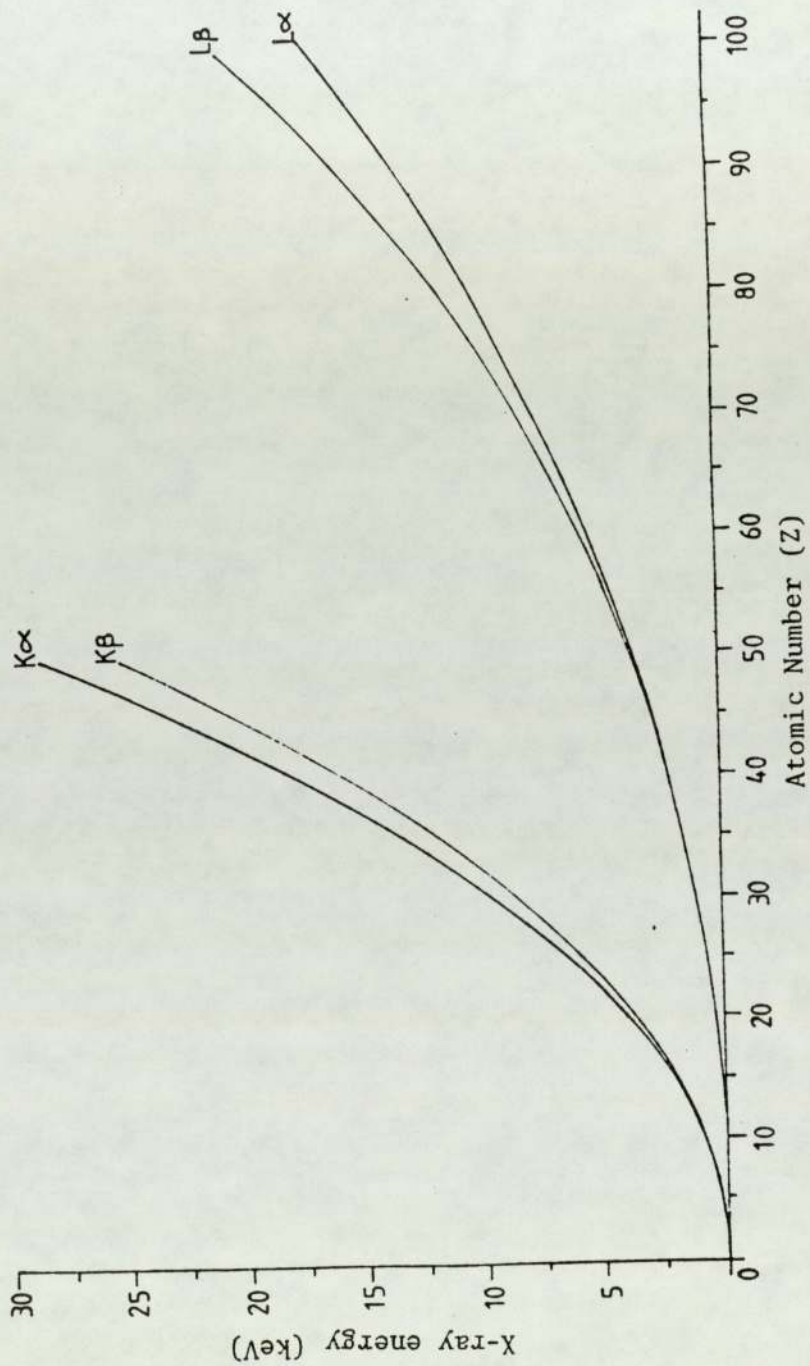
Figure 3.13   Weighted average energies of the characteristic K and L lines as
a function of atomic number

resolution of few hundred electron volts which is shown to be quite possible with our detection system. Interference nevertheless occurs because of overlapping K and L lines of widely different Z or overlapping K_α and K_β lines of neighbouring elements. Some of these interference could be handled and this will be treated fully later.

3.4.2.3 The Detector Linearity and Energy Calibration: The energy calibration of a detector system is an evaluation of the detector linearity. The calibration is based on the assumption that the mean energy required to create an electron-hole pair inside a detector has a constant value, indpendent of the photon energy. Thus, the measured output of the detector system should be linearly proportional to the incident radiation energy. Consequently, any deviation from a straight line established for measured output of known incident energy will be an estimate of the detection non-linearity. The non-linearities are ascribed to the inefficient charge collection by the detector and/or failure of a linear response of the electronics.

X-ray spectra from a variable X-ray source of 10 mc ^{241}Am ceramic sealed primary source of γ radiation of 60 keV energy with six different targets provided data for determination of relationship between detected pulse height (measured output) and X-ray energy, i.e. the energy calibration of the system.

At fixed count rate, a linear relation between the energies and their respective channel number (i.e. pulse height) was always observed.

During an experimental run the calibration linearity was usually checked, from the characteristic X-ray emitted by pure standard foils under proton irradiation.

The least square method was used to compute the slope and the intercept of the calibration line, then these data were stored in the

memory of the on-line computer. When peak areas were determined for a spectrum, the centroid of the peak was also calculated and the energy of the corresponding X-ray was given using these values. The dependence of the characteristic X-ray energy on atomic number Z was used to identify the specific elements in the analyzed sample.

3.4.2.4 The Limitation on X-ray Detection: The analysis of X-ray spectra utilizing solid state (Si(Li)) detectors is limited by a number of factors.

A.   Incomplete charge collection

B.   Counting rate

C.   Energy resolution

Each of these parameters will be considered briefly.

A.   Incomplete Charge Collection:

The processes in the detector, which result in a deposition of a fraction of X-ray's energy, give rise to some background in the X-ray spectra. This background includes   a tail to the characteristic X-ray peak extending to the lower energy and a silicon escape peak. Low energy tailing is caused primarily by incomplete charge collection in the edge region of the detector. This was eliminated in the present work, by highly collimating the X-rays to the central part of the sensitive active area of the crystal, by introducing a lead collimator of 0.4 cm diameter and 0.3 cm thickness infront of the beryllium window.

The other factor to be considered in peak identification is the possibility of silicon escape peaks. The energy transfer by a characteristic X-ray in the detector will create a silicon X-ray which in general will be absorbed by the detector. When such processes occur   near the surface, usually for low energy X-rays, a finite probability exists that a Si K_{α} X-ray (1.74)keV will escape from the detector leaving an energy deposit in the detector of energy (E - 1.74)keV. If the intensity of the X-ray

line of energy E is great enough, a noticeable peak will accumulate in the spectra at energy (E - 1.74). The (E - 1.74)keV peak from one element can lie very near to the characteristic X-ray peak of another element. Thus, it can lead to difficulties in identifying peaks and assigning peak areas.

In practice, however, the elemental concentration required to generate significant escape peaks rarely exist in biological samples. Silicon escape peaks were not observed in the spectra of bovine liver, hair, heart samples. Exceptionally, several bladder stone samples contained large Fe concentrations sufficient to produce a noticeable escape peak at energy (6.4 - 1.74 = 4.6 keV). This escape peak interfers with the Ti, K_α peak (4.51)keV, thus making quantitative analysis of Ti difficult. The expected ratio of the Si escape peak to the full energy peak for Fe K_α is 0.003 (Woldseth 1973), for more energetic X-rays this ratio is even lower. Thus silicon escape peaks were, usually, a negligible interference. Figure 3.14 from Woldseth shows the escape probability of Si K_α vs photon energy.

B.   Counting Rate

Another factor limiting the use of solid state detectors is their counting rate acceptance.

With a high count of X-rays in the detector, there is a probability that two or more X-ray signals will be detected simultaneously or within a short time interval. If two or more pulses arrive at the amplifier input within its shaping time constant, the time interval required by the amplifier to process a single pulse, this results in pulse pile up. For optimum energy resolution, the main amplifier is usually used with a long shaping time constant ($\sim$ 8 μs) which will enhance the pulse pile up phenomenon.

Pulse pile up increases the problems in analyzing a spectrum. One of its serious features is the pile up continuum which extends from just above the characteristic X-ray peaks to the pile up peaks which represent an energy equivalent to twice the original peak energy. This background continuum impairs the statistical precision and detection limit for elemental analysis in this energy region.

The pile up peaks can interfere with characteristic X-rays of the same energy and may be misinterpreted as peaks representing characteristic X-ray of an element not present in the sample. For example, the strong Ca K_α line (3.62 keV) in kidney stone sample produced a pile up peak at 7.38 (Figure 3.15) which may be misinterpreted as Ni K_α (7.48 keV), at the same time the X-ray lines of all other elements between Ca and Ni could not be identified and quantified satisfactorily.

Because this pile up loss dependence on the total counting rate is not linear, it is difficult to correct for (Woldseth 1973). Therefore, it is necessary to minimize the pile up. This could be accomplished either by decreasing the counting rate which increases the analysis time required to obtain the same statistical accuracy or by reducing the shaping time constant of the amplifier which is accompanied by a loss of resolution.

Introducing a commercial pile up rejector will reduce the pulse pile up phenomenon but not eliminate it, in addition, it contributes to overall uncertainty of the system due to the associated dead time correction.

The whole problem can be improved by the application of on-demand beam pulsing, Cahill (1975), whenever the detector responds to an X-ray, the proton beam is turned off until the system is ready to accept another pulse. Count rates up to 5000 can then be realised.

In the present work, a shaping time constant of 8 μs was employed and the count rates limited to less than 1000 cps.
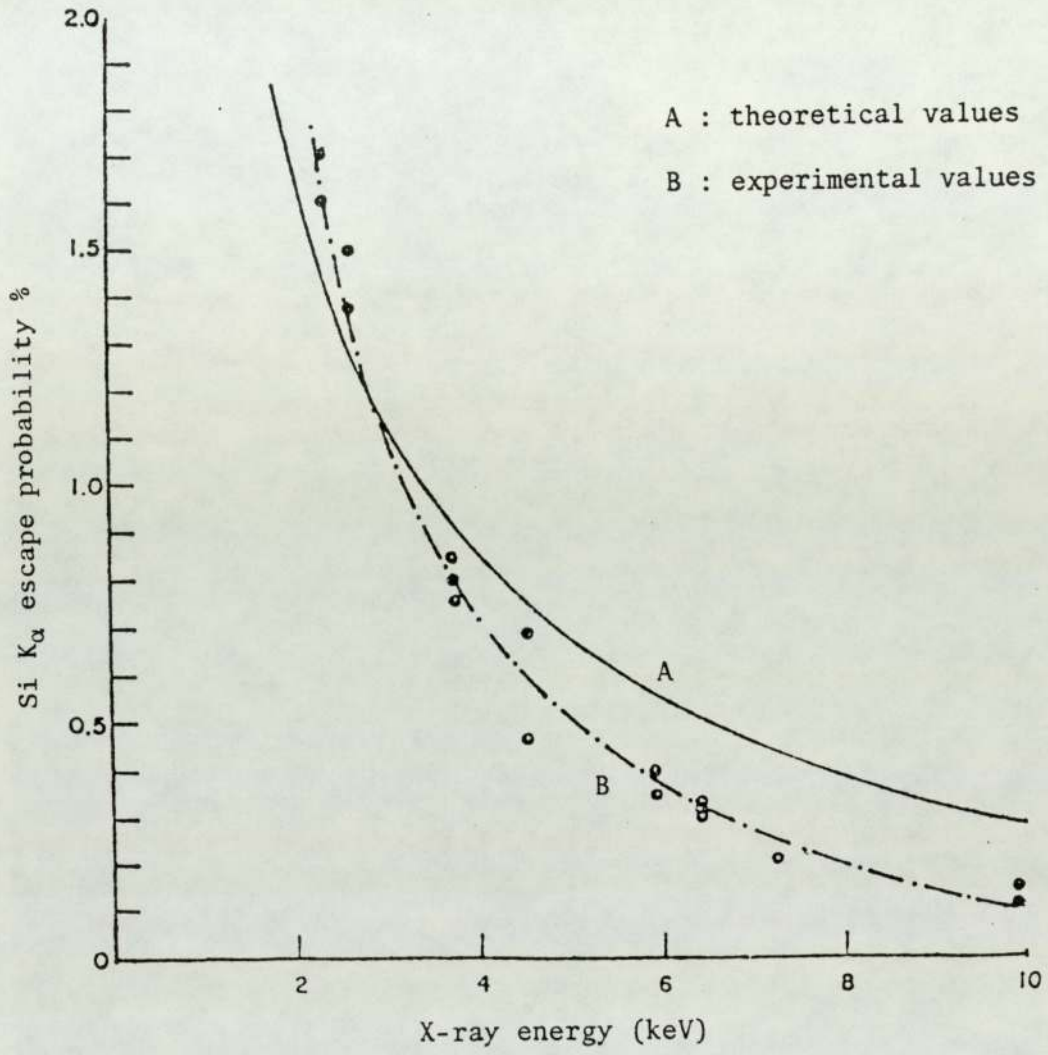
Figure 3.14   Percent escape probability of Si K_α as a function
of incident photon energy. Data from Woldseth (1973)
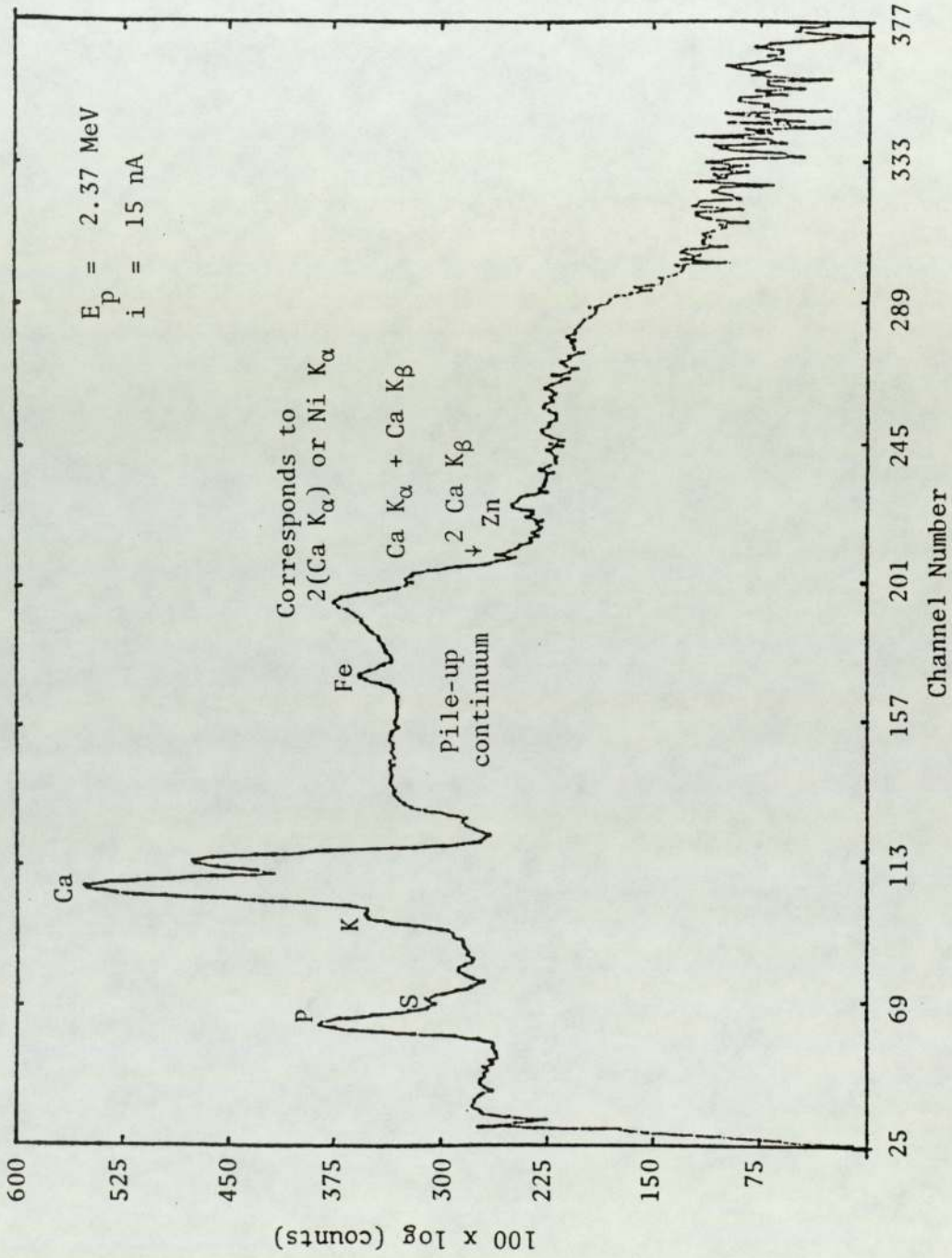
Figure 3.15   PIXE spectrum of bladder stone. Accumulated high count rate, the effect of pile up of Ca peak is shown, starting from Ca X-ray energy up to twice that energy

- 71 -

C. Resolving Power

The resolving power, i.e. element peak separation ability of the energy dispersive system is relatively limited.

By the fact that each element is characterized by more than one X-ray, the overlap between unresolved X-ray from interfering elements can often be distinguished. This problem will be treated more fully in chapter 7.

CHAPTER FOUR

REPRODUCIBILITY STUDIES AND SYSTEM CALIBRATION

4.1 REPRODUCIBILITY STUDIES

To test the applicability of the technique as an analytical tool,
the precision of the analysis has first to be assessed. This is to est-
ablish that the system gives reproducible results for many replicate
targets from the same specimen under identical experimental conditions,
over a long period of time. The precision attained by different workers
following such procedure is generally worse than that expected from stat-
istical uncertainty alone. Bearse et al (1974) have investigated the
attainable precision by analysing human whole blood. The elements Fe,
Cu, Zn, Se and Rb were detected with a precision of 7, 18, 7, 50 and 19%
respectively. Valkovic et al (1974) reported a 5-10% precision for Fe,
Cu and Zn analysing 150 blood serum samples. Similar findings have been
reported by other authors, Kubo (1974), Lear (1976). This is thought to
be due to target preparation techniques which produce non-uniform tar-
gets combined with imperfect homogeneity of the beam. In addition, sam-
ple deterioration during bombardment is another contribution on this.
The determination of precision provides a check on both the target pre-
paration procedure and the measuring system.

It is obvious that overall precision of both the system and prepara-
tion must be ascertained in order to provide reproducible results. The
reproducibility was therefore investigated in two different ways: first,
to check the consistency of the system developed in this research, diff-
erent thin metal foils were analyzed, thin enough that the proton energy
loss traversing these samples and X-ray self absorption could be ignored.
Second, both thick and thin samples prepared from NBS bovine liver were
analyzed to evaluate the sample preparation procedure and to establish
the accuracy of the analytical technique for biological samples. NBS

bovine liver is a standard biological material which is a secondary standard of specified composition.

4.1.1 THIN FILM PREPARATION

To assess the reproducibility and simultaneously calibrate the system as detailed in section 4.2, thin standard targets with an accurately known areal density are required. Pure metals needed for preparing these films are not easily attainable. Furthermore, the evaporation temperature of most of these pure metals is either higher than or close to the melting point of normal vacuum evaporation boats. Therefore, undesirable contamination will follow from employing these boats.

Evaporation with a steady vacuum beam is difficult without the availability of a sophisticated shuttering device over the evaporation source. In addition, errors due to irregularities and fluctuation in the vapour beam are possible which can result in non-uniform evaporated layers. Geometrical variations of vapour density can hardly be avoided and may also cause significant uncertainties.

An alternative method is sputtering, in which a bulk of material has to be used and is therefore economically disadvantageous.

However, the mass of the produced layer, which was intended to be about 40 $\mu g/cm^2$, may change under atmospheric conditions. The mass change due to sorption and handling the substrate, besides oxidation and other reaction of film, prevent the application of weighing under atmospheric conditions. Therefore, for high accuracy, a vacuum micro-balance weighing procedure is imperative to determine the thickness of vacuum evaporated layers. The detail of which is discussed by Moret et al (1966). Since this facility is not generally available and determining the film mass thickness with one of the other available techniques produces results of more questionable accuracy, commercially available films were

employed.

4.1.2 Characteristic of Commercially Available Thin Standards

These readily available standards can be made from almost any mat-
erial, in the form of a single element or stable compound of known areal
density ranging from 10-100 $\mu g/cm^2$ (Micromatter Co.). They are spectro-
scopically pure vacuum evaporated on Mylar, carbon or polycarbonate sub-
strates. One desirable feature of these films is the ability to with-
stand the proton beam heating. It was found in the present work that
beam current densities between 15 and 60 nA/cm^2 at 2.5 MeV could be safe-
ly used with all the range of elements analysed without any noticeable
damage. Consistent with this finding Stiles et al (1976) reported that
protons currents between 30 and 70 nA/cm^2 at 3 MeV were safe for all
their 12 investigated deposits for periods of several minutes. Some low
melting point materials such as $Rb(No_3)$ were among the analysed elements.
There is a significant lack of agreement between these findings and that
obtained by Kivits (1980) in analyzing different inorganic chlorides and
bromides of 7.5 $\mu g/cm^2$ areal density. The percentage loss of Cl and Br
in these samples ranged between (5-20) and (6-20) respectively. The
author reported that the losses occurred in the first 8 minutes of bom-
bardment with 3.05 MeV protons of 50 nA/cm^2 current density. These
parameters depend on the composition of the target and the mass of the
material irradiated. The targets bombarded in these two contrary cases
were different since the thicknesses of target deposits were diffi-
cult in addition to different backing materials. The backing substrate
used by Kivitz was selectron $(C_{32} H_{44} O_{23})$ of 5 mg/cm^2 thickness while
the backing used by the other workers were Nuclepore polycarbonate of
1 mg/cm^2 so the disagreement may well be ascribed to this.

Radiation damage and heat damage may lead to loss of elements

analyzed as reported by various authors such as Valkovic (1974), Ishii (1975), Johansson (1976), Whitton et al (1978), Mitchell et al (1979), Legge (1980). The observed phenomena of radiation damage in the present work is illustrated from the comparison of scanning electron micrographs of three of the standard foils Ge, Ti and Cu before and after irradiation in Figures 4.1a, 4.1b and 4.1c respectively.

Since inhomogeneous standards can introduce uncertainties in the system calibration, section 4.2, the homogeneity of the foils employed in the present work was determined. The standard foils were cut into four different pieces and irradiated. The agreement between the measured X-ray yield from the separate pieces of the same standard within statistical uncertainty of 1-4% shows the good uniformity of the film thickness. Stile et al (1976) measured the uniformity of three similar sets of these vacuum deposits, each set containing 11 different single deposits by scanning a 6 mm diameter proton beam at 6 to 8 positions along the deposit diameter. They estimated the non-uniformity to be less than ± 2%. Baum et al (1977) determined the uniformity of these foils, by scanning three replicates from each of five investigated elements. They reported that these were quite uniform. Johansson et al (1981) reported that non-uniformity to be typically ± 3% although some standards showed larger deviations confirming the need to make an experimental check on each standard.

The other attraction of these standards as calibrators is the accurately known weight of the deposit within the manufacturers quoted accuracy of ± 5%. Dzubay et al (1978) believe that the 1σ accuracy is about 8%, although it is not reported how this uncertainty was estimated. The mass stability is fairly satisfactory since no change was observed in the measured X-ray yield from the same target during irradiation for relatively long periods of time. This is inconsistent with the finding of Stile et al (1976) who claimed that some attention had to be paid to

A
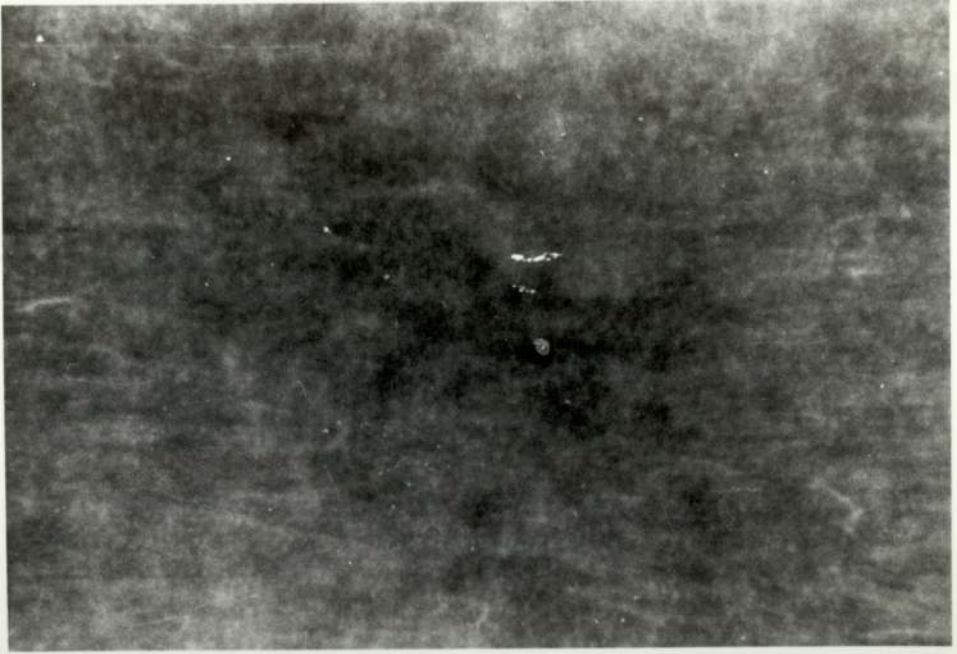
B
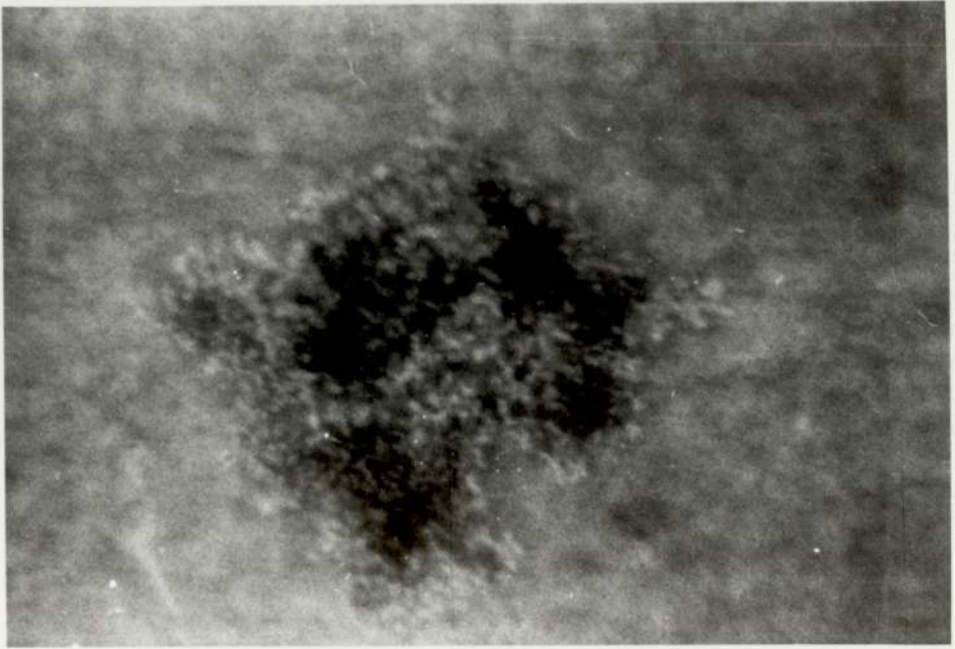
Figure 4.1a   Scanning electron microscopy micrographs of Germanium foil
               A: before it has been irradiated (X500)
               B: after irradiation (X500)

A
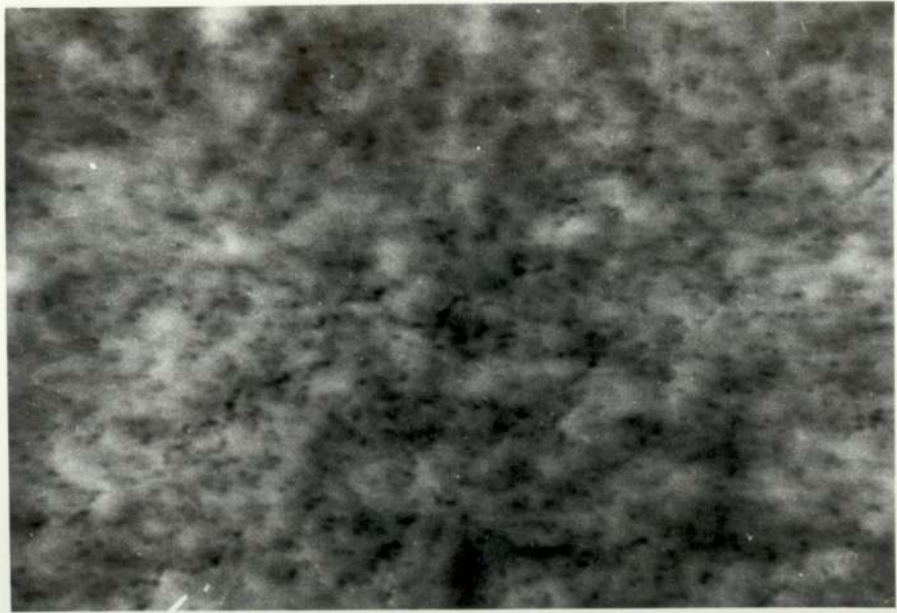
B

Figure 4.1b   Scanning electron microscopy micrographs of Titanium foil
                A: before irradiation (X1000)
                B: after irradiation (X1000)

A
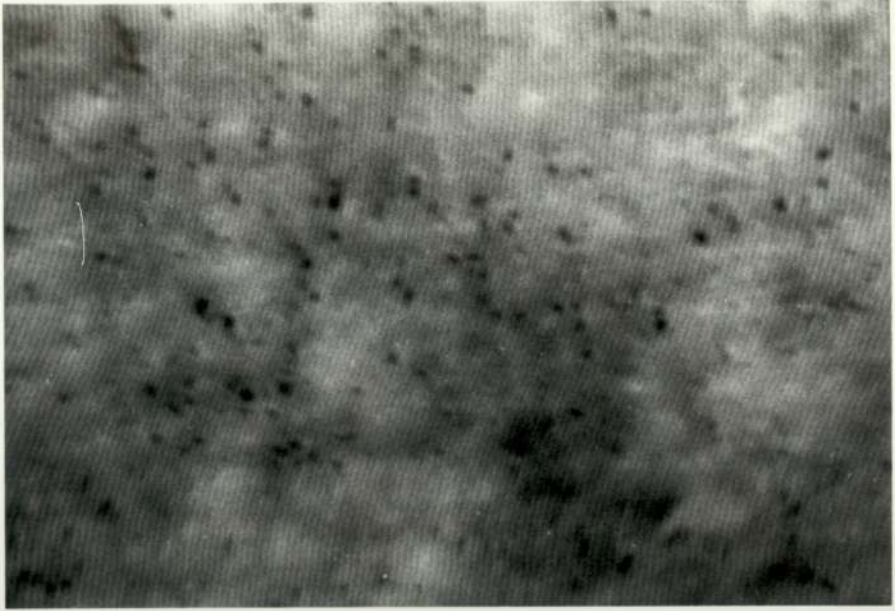
B
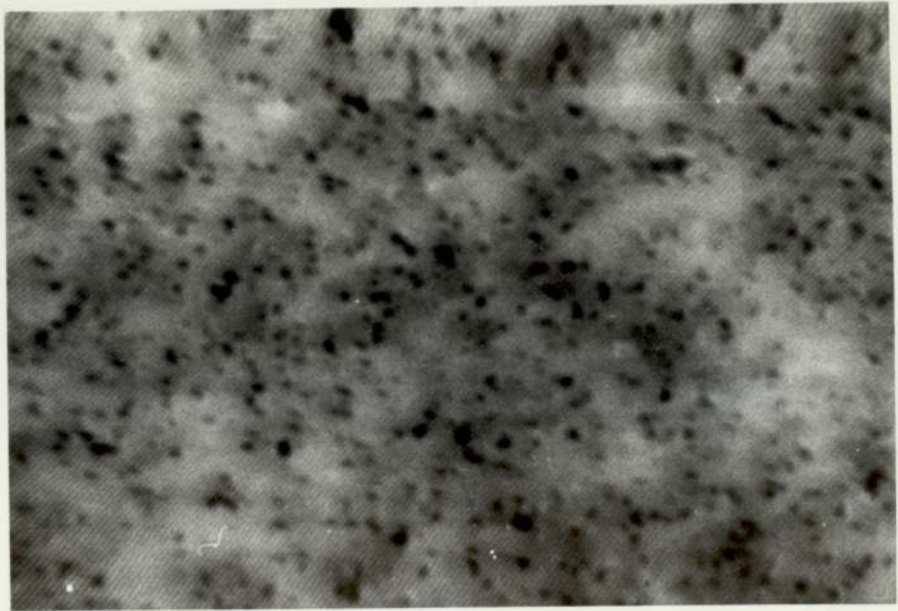
Figure 4.1c   Scanning electron microscopy micrographs of Copper foil
A: before irradiation (X500)
B: after it has been irradiated (X500)

the possibility of degradation in the standards as losses can occur with frequent use and handling. Nevertheless, flake-off material was observed in scanning electron micrographs of some foils used in the present work, Figure 4.2. However, this flake-off only occurred at the edge of the target frame holder and was due to the method of clamping.

A yield increase of 5% due to shrinkage (thickening) within the irradiated area has been reported by Mitchell(1980) since the uncertainty quoted in the current work is higher than this figure, this consequent phenomenon of radiation damage was not observed. On the other hand, it could be argued that the method of mounting the targets could affect the phenomenon's appearance. Perhaps the tension used in clamping the targets in this work would prevent the shrinkage.

TABLE 4.1

CHARACTERISTICS OF THE FOIL CALIBRATORS EMPLOYED

Element	Mass/Unit area $\mu g.cm^{-2}$	Form
Chlorine Potassium	35	KCl
Titanium	41	Element
Manganese	71	Element
Cobalt	25	Element
Copper	40	Element
Gallium	21	GaP
Germanium	54	Element
Rubidium	29	$Rb(NO_3)$
Yttrium	44	Element
Molybdenum	56	MoO_3

A
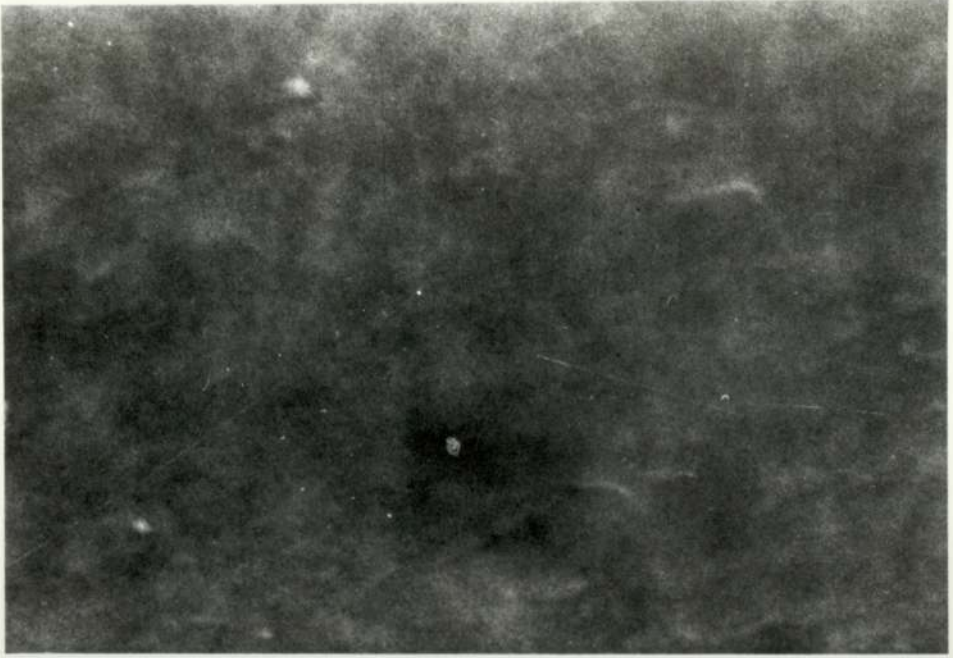
B
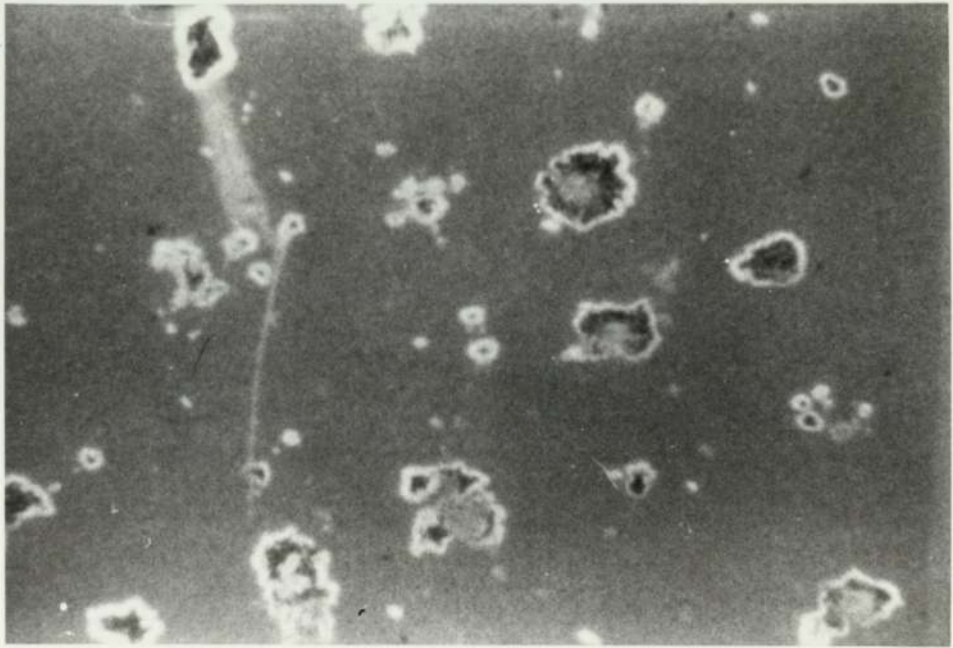
Figure 4.2   Scanning electron microscopy micrographs showing
A: a typical homogeneous surface of a foil (Ge) before it was
used, and
B: the flaking off phenomena at the edges of the same foil, after it
was used, as a consequence of the tension experienced from the
holding ring.

4.1.3 Consistency Check and One Way Analysis of Variance

A frequent check on the stability and consistency of the analysis is imperative to assess the analytical reliability. Experiments were carried out periodically on standard foils and afforded a good test of the system consistency. No external uncertainties are introduced from target formation or caused by problems of uniformity and stability of these targets. The foils listed in Table 4.1 were analyzed frequently in order to test the consistency and reproducibility of results.

A set of four metal foils were mounted and analyzed preceeding each biological sample analysis. Typically 8-20 sets of X-ray yield data were obtained from each foil and compared with similar previous results. This was followed with further checks by mounting one different foil with each set of biological samples to enable standard data collection for comparison with previously stored standard data.

A summary of the results from some of the elements investigated is shown in Table 4.2. It should be emphasised that the six sets of data presented in this table is a typical representative of the large number of data sets obtained from repeated measurements on standard foils over the whole period of the work. For most of the standards more than one target was used. The proton current used was normally in the range of 1-10 nA and a beam area of 0.25 cm^2. The maximum value of the current selected depends on the ability to dissipate the heat and melting point of the sample irradiated. The count rates were below 1000 c/s to reduce pile-up peaks in the spectra. The time of analysis was chosen to give a statistical uncertainty below 4%. The foils were analyzed for their K-lines. The uncertainty of the measurements for a given foil represented by the standard deviation of the mean of 8-16 measurements is typically 2-5%.

The statistical uncertainty associated with an individual measure-

TABLE 4.2

TYPICAL REPRODUCIBILITY MEASUREMENTS OBTAINED WITH THE CALIBRATOR FOILS OVER A PERIOD OF THE WORK

Chlorine n = 10 - 12		Potassium n = 10 - 12		Titanium n = 10 - 20		Manganese n = 8 - 10		Cobalt n = 8 - 15		Copper n = 10 - 15		Gallium n = 8 - 10		Germanium n = 8 - 10	
$\bar{x}$	c.v	$\bar{x}$	c.v	$\bar{x}$	c.v	$\bar{x}$	c.v	$\bar{x}$	c.v	$\bar{x}$	c.v	$\bar{x}$	c.v	$\bar{x}$	c.v
1402	5%	3130	3%	2911	2%	3728	3%	1737	3%	2001	3%	1338	2%	1639	4%
1380	2%	3173	2%	2891	3%	3750	3%	1701	2%	2016	2%	1387	3%	1646	2%
1393	5%	3204	1%	2863	4%	3665	2%	1717	4%	2036	2%	1361	2%	1776	3%
1383	5%	3184	2%	2881	2%	3645	2%	1645	2%	20158	3%	1294	3%	1759	2%
1352	5%	3202	2%	2883	3%	3620	4%	1719	2%	1973	2%	1311	3%	1640	2%
1387	4%	3260	2%	2922	2%	3601	2%	1638	4%	1976	1%	1280	3%	1667	3%

n = number of measurements in each set

c.v = Coefficient of Variation

$= \dfrac{SD}{\bar{x}} \times 100$

ment, which is comparable with this, shows that the statistical uncert-
ainty is the major contributor to the overall precision of the measure-
ment at this level of precision. The long term stability of the analyti-
cal system was estimated, through determining the reproducibility of the
groups of data over the experimental period. This assessment of reprod-
ucibility was accomplished using one way analysis of variance. This
approach involves the comparison of two variance estimated through the F test,
where F is the ratio between the two variances. The first variance is
based on the variation between the means of the groups and the second is
based on the variation within all the data. This is to determine whether
the difference is large enough to be significant, and hence the groups
are not from the same population or whether the difference can be ascrib-
ed to sampling fluctuation. In this latter case the null hypothesis is
true, i.e. that the samples are randomly drawn from the same normally
distributed population.

A summary of typical calculation is shown in Table 4.3 where the sum
of squares within the groups was computed, which is a measure of experi-
mental error. Then the sum of squares between groups was computed which
is a measure of the dispersion of group means about the combined mean and
combines the experimental error with any other variation.

From the obtained F value it can be seen that no evidence exists at
the 5% level of significance to reject the null hypothesis for these ele-
ments. Thus the null hypothesis is true and the groups all represent
random samples from the same population, and the observed difference
among the means of the samples may be ascribed to sampling fluctuation.

It was observed that if the precision of the individual measurements
is improved beyond the 3 to 4% level, data taken with a significant time
separation occasionally result in a rejection of the null hypothesis. In
these cases it may be that the groups do not come from the same distribu-

tion. This is brought about by the contribution of other artifacts, such as current leakage, sample positioning, which come into play over a long period of time. For biological samples one is seldom interested in a precision better than 5% level so that the system as evaluated is more than adequate for this purpose.

TABLE 4.3

ONE WAY ANALYSIS OF VARIANCE, TABLE FOR

CHLORINE AND TITANIUM MEASUREMENTS

Chlorine measurements, 10 groups			
Source of Variance	Sum of Squares	Degree of Freedom	Mean Square
Between Groups	47251	9	5250
Within Groups	302343	91	3322
Total	349594	100	

$$F = \frac{5250}{3322} = 1.58 \qquad F(0.05, 9, 100) = 1.97$$

Titanium measurements, 5 groups			
Between Groups	24917	4	6229
Within Groups	130007	43	3023
Total	154924	47	

$$F = \frac{6229}{3023} = 2.06 \qquad F(0.05, 4, 43) = 2.58$$

4.1.4 Evaluation of the Sample Preparation Technique

Evaluation of the sample preparation procedure by ascertaining the accuracy is essential to estimate the potential of a system for trace

element studies. However, not all accurate results are precise and the precision of PIXE data as opposed to their accuracy is also related to specimen preparation. Therefore, to evaluate any preparation procedure it is necessary to estimate its precision as well as its accuracy. The procedure adopted in this work is to employ NBS standard reference materials to investigate the precision and accuracy of the system for biomedical samples.

4.1.4.1 Precision and Reproducibility of Biological Samples

a) Thin Targets: Four digestion solutions A, B, C, D from 1577 NBS bovine liver were prepared following the same preparation procedure discussed in detail in Chapter 6. From solutions A, B and C, 15 replicate thin samples were prepared by micropippeting 3 µl aliquots onto Nuclepore substrates of 1 mg/cm^2 areal density. After evaporation of the solvent, the samples were ready for irradiation. Extreme caution was exercised to prevent contamination resulting from the sample manipulation and drying process. The target frames were washed ultrasonically using a 150 - PROPYLE ALCOHOL $[(CH_3)_2 CH OH]$ bath. The backings were mounted prior to sampling in a glove box. The targets made were kept and transferred in a desiccator.

Initial analysis with a focused beam indicated that samples made from these very clear solutions were not uniform in their trace element distribution. Therefore the beam was diffused and made larger than the target area.

The samples were then analyzed under the diffused proton beam, seperated by several weeks during which time the accelerator was running on other beam lines. This afforded a much more rigorous test of reproducibility than simply running duplicates one after the other.

Beam currents of 60 nA/cm^2 at 2.5 MeV were employed and a 7 µm

aluminium absorber was located infront of the detector to reduce the
intense low energy portion of the X-ray spectrum incident on the detector.

A comparison between different targets from the same solution was
made in terms of the ratio between different elements. The significance
of this ratio technique is that it does not require accuracy in the sam-
ple thickness, size and weight. In addition, systematic errors are eli-
minated.

The typical mass ratios, Fe-Cu, Fe-Zn and Cu-Zn represented by their
X-ray peaks were determined. These sets of data, shown in Table 4.4,
include the mean ratios and their relative standard deviations. It
should be noted that there is no significant difference between the means.

From solution D 20 replicate targets were prepared from 9 μl deposit
and analyzed under identical experimental conditions. Larger amounts of
digested material were used to check the effect of X-ray attenuation and
proton energy loss in larger samples on reproducibility achieved. Simi-
lar results to those of A, B and C solutions were obtained. Thus assur-
ed that 9 μl deposit, also gave thin targets, since no evidence could
be found for any X-ray absorption or proton energy loss. The mass ratios
Fe-Cu, Fe-Zn and Cu-Zn determined similarly to those of previous sets
are shown in Table 4.4a. A typical PIXE spectrum from analysis of a tar-
get made from this solution is shown in Figure 4.3.

In addition a comparison of the average elemental ratios obtained
from these different digestion solutions with those obtained from the ab-
solute mass concentrations reported by other authors and those of NBS is
made in Table 4.5. The agreement is seen between the different results.

Consequently, we may conclude that the reproducibility of both the
system and sample preparation is reliable. The precision represented
by the standard deviation of each set was found to be less than that
obtained with the standard foils. This is due in part to contribution

TABLE 4.4

INTENSITY RATIOS OBTAINED FOR THIN TARGETS OF NBS BOVINE LIVER

FROM THREE DIFFERENT DIGESTION SOLUTION, A, B AND C

	(Fe/Cu)			(Cu/Zn)			(Fe/Zn)		
	Group A	Group B	Group C	A	B	C	A	B	C
	2.268	2.62	2.28	2.027	1.67	1.80	4.58	4.37	4.06
	2.52	2.37	2.23	1.63	1.63	1.82	4.64	3.86	4.12
	2.10	2.31	2.43	1.90	1.67	1.68	4.02	3.80	4.02
	2.35	2.34	2.33	1.64	1.55	1.63	3.97	3.60	3.80
	2.24	2.31	2.29	1.80	1.84	1.80	4.03	4.18	4.20
	2.50	2.31	2.24	1.71	1.77	1.50	4.27	4.00	3.70
	2.69	2.52	2.36	1.57	1.73	1.99	4.32	4.37	4.70
	2.74	2.29	2.61	1.68	1.68	1.78	4.61	3.80	4.33
	2.32	2.26	2.41	1.75	1.92	1.48	4.03	4.32	3.60
	2.22	2.38	2.34	1.69	1.60	1.68	3.75	3.66	3.90
	2.35	2.43	2.38	1.77	1.46	1.64	4.18	3.56	3.90
	2.33	2.49	2.50	1.79	1.85	1.64	4.41	4.60	4.09
	2.27	2.38	2.37	1.67	1.70	1.60	3.80	4.07	3.79
	2.35	2.38	2.49	1.56	1.88	1.72	3.75	4.45	4.37
	2.36	2.23	2.49	1.63	1.71	1.61	3.84	3.94	4.08
M	2.37	2.37	2.38	1.72	1.71	1.70	4.14	4.039	4.044
SD	0.17	0.11	0.11	0.125	0.127	0.13	0.31	0.33	0.285
c.v	7%	5%	4%	7%	7%	8%	7.5%	8%	7%

TABLE 4.4a

INTENSITY RATIO OBTAINED FOR TARGETS OF NBS BOVINE LIVER

WITH SAMPLE SIZE LARGER THAN ASSUMED THIN TARGETS

	Fe/Cu n = 20	Cu/Zn n = 20	Fe/Zn n = 20
	2.33	1.66	3.85
	2.58	1.79	4.61
	2.51	1.65	4.11
	2.40	1.62	3.75
	2.40	1.75	4.20
	2.42	1.73	4.18
	2.72	1.72	4.68
	2.28	1.73	3.93
	2.62	1.84	4.79
	2.52	1.65	4.17
	2.50	1.68	4.19
	2.57	1.65	4.24
	2.43	1.80	4.40
	2.59	1.65	4.30
	2.65	1.67	4.42
	2.48	1.72	4.26
	2.59	1.70	4.42
	2.53	1.63	4.13
	2.53	1.84	4.65
	2.50	1.90	4.70
Mean	2.5	1.72	4.29
SD	0.108	0.079	0.28
c.v	4%	5%	7%
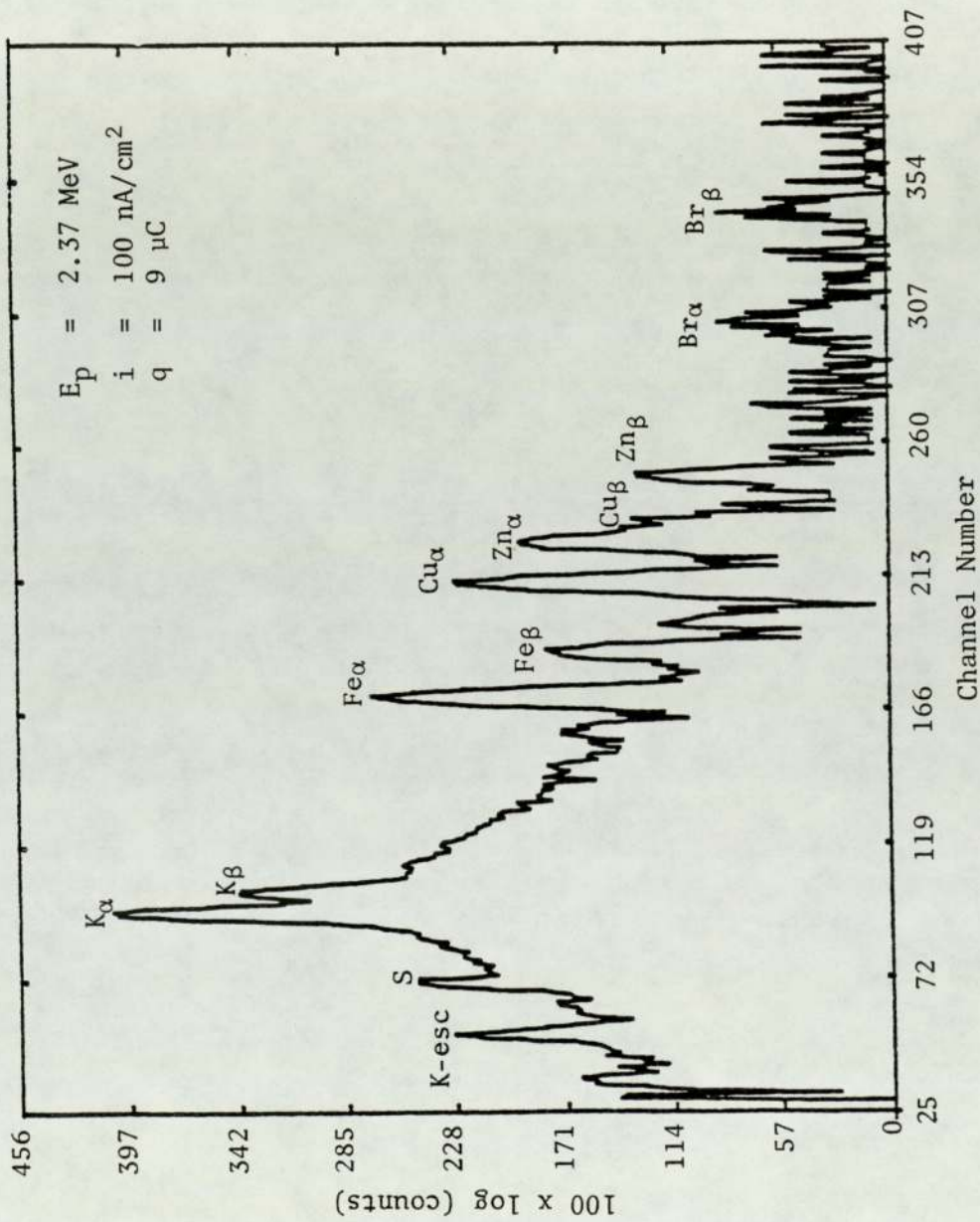
Figure 4.3   A PIXE spectrum of NBS bovine liver sample

- 90 -

TABLE 4.5

A COMPARISON OF THE ELEMENTAL RATIOS OBTAINED IN THE PRESENT STUDY FOR THIN

TARGETS WITH THOSE OBTAINED FROM THE ABSOLUTE MASS CONCENTRATION REPORTED

BY OTHER AUTHORS AND THOSE OF NBS

Ratio	Present Work		NBS Values		Willis (1977)		Jolly (1978)		Maenhaut (1980)		Navarrete (1978)	
	X	c.v %	X	c.v %	X	c.v %	X	c.v %	X	c.v %	X	c.v %
Fe/Cu	1.44	8	1.4	9	1.51	10	1.56	9	1.26	10	1.42	8
Cu/Zn	1.38	8	1.48	9	1.35	11	1.38	12	1.7	17	1.47	11
Fe/Zn	1.99	8	2.08	11	2.03	11	2.16	9	2.14	17	2.08	12

from slight inhomogeneity of the beam and the non-uniformity of sample, in addition to variable amounts of noticable impurity in the backing material. Comparison of the three spectra, Fig. 4.4, in which each spectrum represents a different target from one of the digestion solutions, shows agreement between the intensities of the other elements such as P, K, ... etc.

b) <u>Thick Targets</u>: Thick pellets were prepared from 200 mg quantities of NBS bovine liver powder as described in section 6.4.2.1.

The amount of material which is recommended by NBS to ensure a representative sample is > 250 mg. The irradiated area, however, was only 0.25 cm^2 and combined with the limited range of the proton penetration resulted in an irradiated mass < 250 mg. Thus the analysis does not sample the entire 250 mg as it is recommended. This suggests that representative test must be performed to evaluate the preparation procedure. This could be performed either by checking the accuracy or assessing the reproducibility over a large number of replicate targets. The estimated reproducibility also determines the reliability of the analytical system.

Observations were made on two replicate sets of pellet samples each containing 10 samples. Each set was made from different purchases of NBS powder. These samples were irradiated under similar experimental conditions to that of the thin targets, except that the pellets were each exposed to 10 μc of protons. The irradiations were performed at different times over a period of several months. Fe/Cu, Cu/Zn and Fe/Zn intensity ratios of these three sets are listed in Table 4.6. Comparison of the mean values as well as the relative standard deviation of each ratio of different sets show the reasonable reproducibility achieved.

A

B
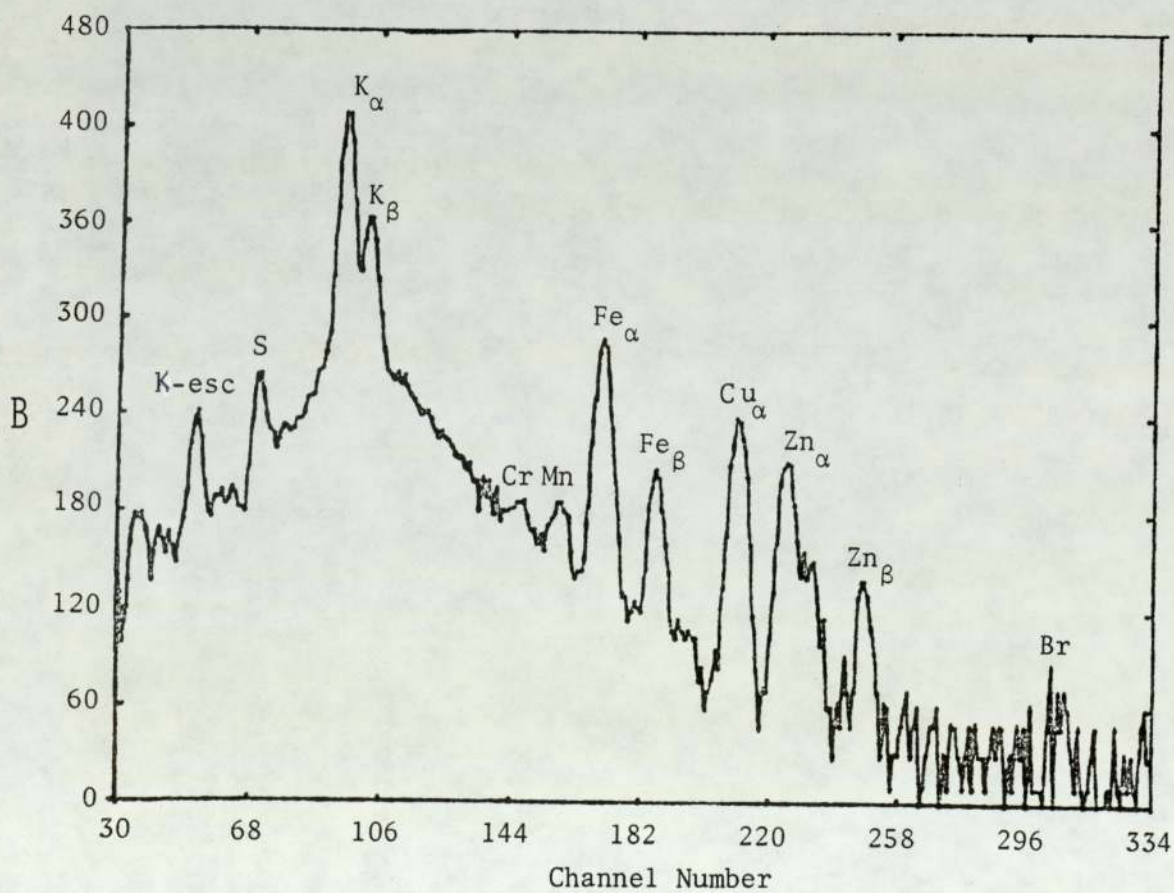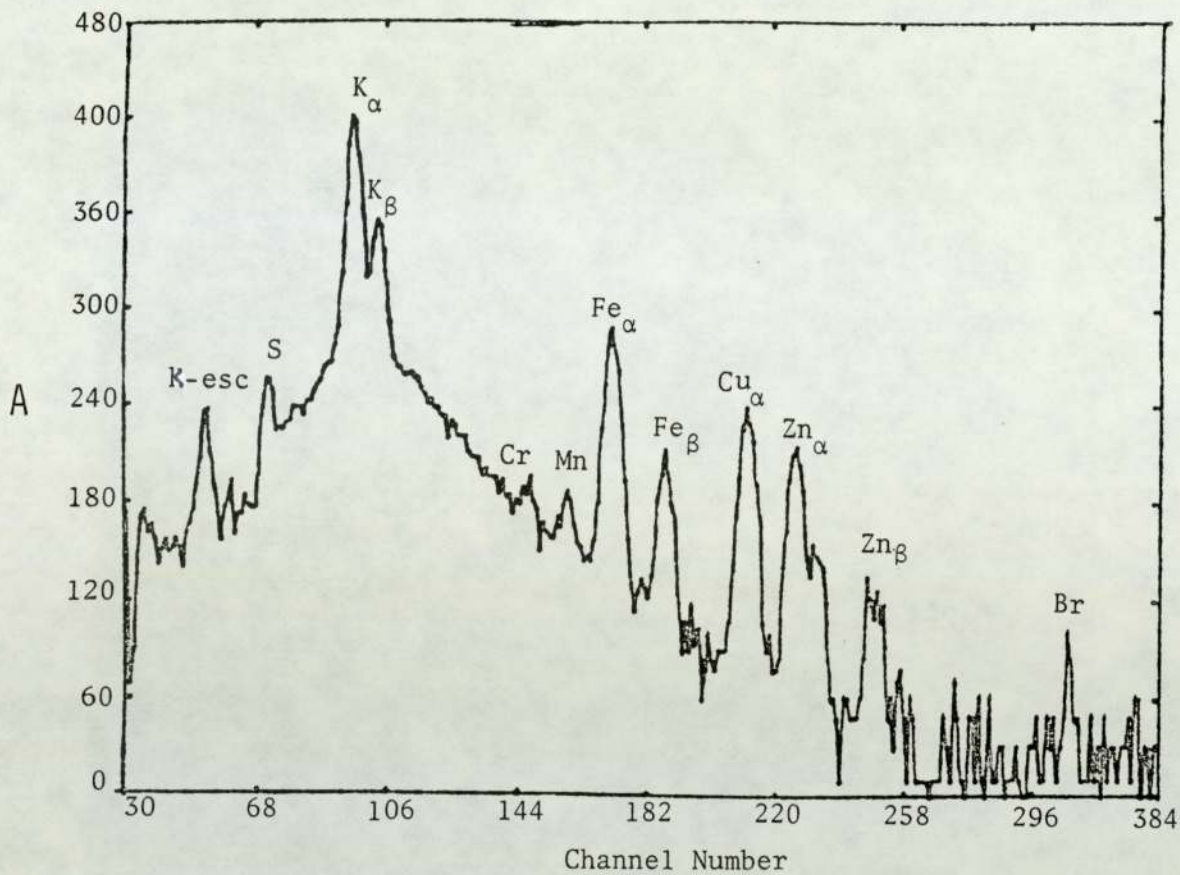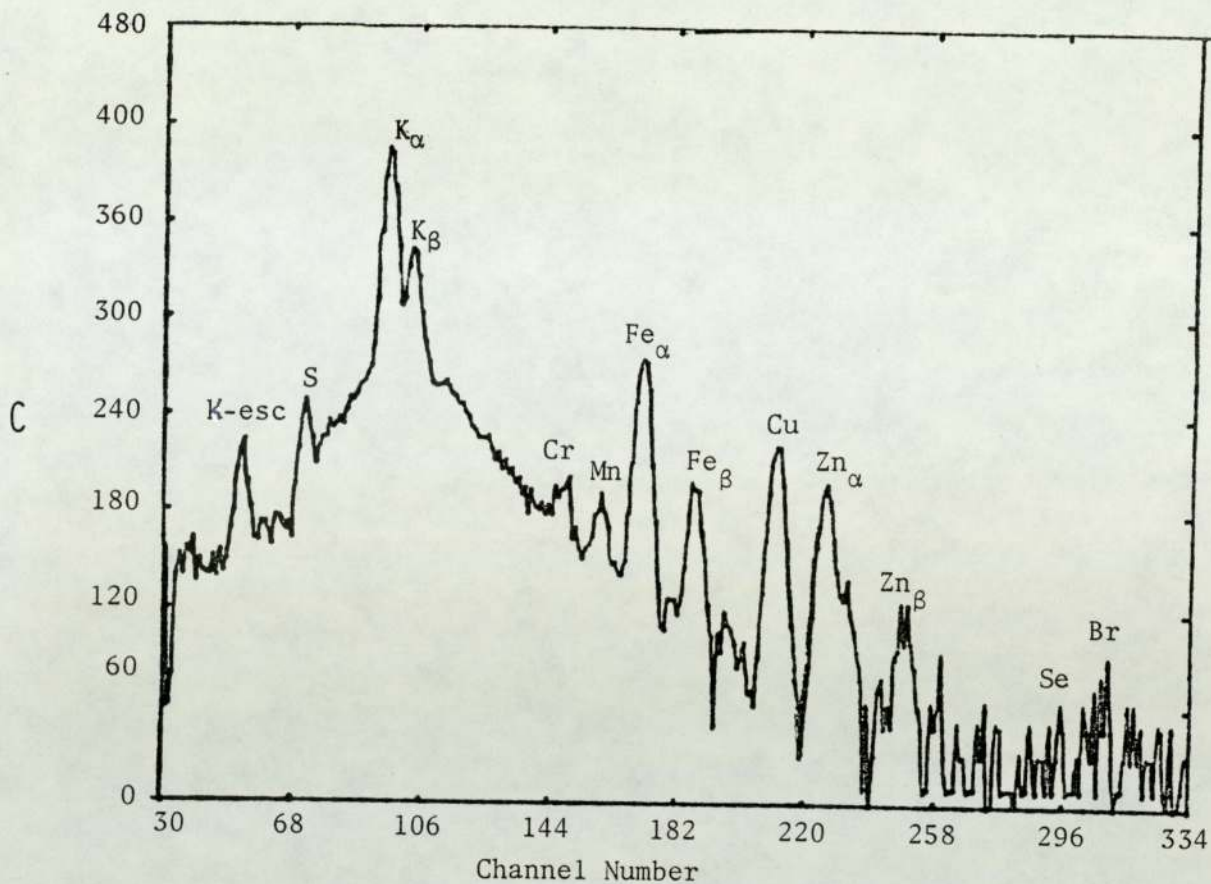
Figure 4.4   Comparison of three PIXE spectra of thin samples
               fabricated from three different NBS bovine liver
               digestion solution A, B and C, illustrating the
               reproducibility achieved.

               Note: a) y-axis represents 100 x log(counts)
                      b) The amount of Br and Cr detected are
                          ascribed to the impurity present in
                          the backing material

- 94 -

TABLE 4.6

INTENSITY RATIOS OBTAINED FOR THICK SAMPLES OF

NBS BOVINE LIVER FROM TWO DIFFERENT SETS

	Set 1			Set 2		
	Fe/Cu	Cu/Zn	Fe/Zn	Fe/Cu	Cu/Zn	Fe/Zn
	2.46	1.42	3.50	2.50	1.34	3.40
	2.41	1.40	3.48	2.44	1.41	3.43
	2.42	1.36	3.31	2.40	1.40	3.30
	2.48	1.33	3.32	2.44	1.46	3.58
	2.56	1.39	3.57	2.63	1.35	3.55
	2.56	1.35	3.46	2.46	1.39	3.42
	2.53	1.36	3.44	2.50	1.50	3.42
	2.63	1.29	3.39	2.85	1.36	3.86
	2.53	1.34	3.44	2.50	1.39	3.48
	2.51	1.45	3.59	2.47	1.41	3.53
M	2.51	1.37	3.45	2.52	1.40	3.50
SD	0.068	0.047	0.093	0.13	0.049	0.15
c.v	2.7%	3.4%	2.7%	5.2%	3.5%	4.3%

4.1.4.2 Accuracy

Obviously, no evaluation of the sample preparation technique is
complete without assessing the accuracy.

The procedure, which has been increasingly employed by different
workers to assess the ability to perform quantitative analysis is to
analyze a standard reference material provided by NBS and then compare
the results obtained with the NBS recommended values. These values are

obtained from determinations with six different analytical techniques. This was the procedure adopted in the quantitative analysis in the present study.

The quantitative results obtained for Fe, Cu and Zn in analyzing thin samples made from 1577 bovine liver were compared to the certified values provided. These results together with those achieved by other laboratories are summarized in Table 4.7. The results obtained in this work represent mean values of 3 sets of samples each consists of 15 targets. The good overall agreement obtained gives confidence that for elements considered preferential loss or absorption of these elements does not take place during the sample preparation procedure. It is worth noting that the authors mentioned in Table 4.7 report measurements made relative to an internal standard, whereas in the present work no internal standards were employed.

Moreover, to check the accuracy of the preparation technique only and to avoid uncertainties, which would be introduced by the PIXE system, the prepared NBS digestion solutions were analyzed by Atomic Absorption Spectroscopy (AAS). Table 4.8 compares the results obtained by these two methods. With the expected systematic error, the agreement is reasonable.

However, the absolute accuracy for the biological samples was obtained by comparing the mass concentrations obtained, shown in Table 4.8, with the certified values of NBS and AAS. The agreement is about 6% or better for almost all intermediate elements, which is again very satisfactory. A number of workers have also followed the same approach comparing their results with that of AAS, to test their accuracy.

Bearse et al (1974) arrived at 10% accuracy when analyzed Zn in whole blood with both of these methods. For the analysis of Fe, Cu, Zn and Pb in animal liver, Campbell (1974) obtained good agreement of the

order of 15% on the other hand he found a very bad agreement between the
PIXE and AAS when analyzing Pb in non-uniform samples of kidney medulla
tissue. This is an example which indicates the importance of represent-
ative sampling.

<div align="center">TABLE 4.7</div>

A COMPARISON OF THE MASS CONCENTRATIONS OBTAINED IN THE PRESENT WORK

WITH THE CERTIFIED VALUES OF NBS AND THOSE OF OTHER

WORKERS CONCENTRATIONS ARE IN µg/g

Element	NBS	Present Work	Jolly (1978)	Willis (1977)	Maenhaut (1980)
Fe	270 ± 20	262 ± 18	271.5 ± 11.5	293 ± 21	248 ± 16
Cu	193 ± 10	182 ± 13	173.5 ± 13.9	194 ± 13	197 ± 16
Zn	130 ± 10	132 ± 10	125.7 ± 10.6	144 ± 12	116 ± 18

4.2 SYSTEM CALIBRATION

An essential feature of the PIXE technique is that it is quantita-
tive. In addition qualitative information and the relative quantities
of elements present in thin samples may be determined on line during the
collection of data. In order to determine for a particular element,
either the absolute mass presented in the irradiated area or the mass
concentration of that element in a given sample a calibration for the
system is required. The detected X-ray intensities can then be precise-
ly related to the physical quantities of all elements of interest. Hence
analysis of the intensity of each X-ray peak can provide a value for the
element abundance. The number of X-rays generated n_x due to an element

TABLE 4.8

MASS CONCENTRATIONS OBTAINED IN THE PRESENT WORK FROM ANALYZING

THREE DIFFERENT DIGESTION SOLUTIONS A, B AND C; A

COMPARISON OF THEIR AVERAGE VALUES WITH THE

CERTIFIED VALUES OF NBS AND THOSE OF AAS

Content (μg/g) - Dry Weight

Element	A n = 15	B n = 15	C n = 15	Average V	NBS Value	AAS Analysis
K	0.76%	0.75%	0.79%	0.77 ± 0.14%	0.97 ± 0.06%	-
Mn	8.75	10.2	9.94	9.63 ± 0.83	10.3 ± 1.0	13.6
Fe	262	260	264	262 ± 18	270 ± 20	201.7
Cu	182	181	183	182 ± 13	193 ± 10	170
Zn	129	132	135	132 ± 10	130 ± 10	99.7
Rb	19.60	17.5	17.8	18.3 ± 2	18.3 ± 1	-
Se	-	3.15	-	1.05 ± 0.16	1.1 ± 0.1	-
Pb	1.85	1.87	1.55	1.75 ± 0.26	0.34 ± 0.08	< 0.45

Z present in a thin target (thickness t) is related to the number of protons n_p incident onto the target by:

$$n_x = n_p \, n_z \, \sigma_{xe} \, t \qquad \qquad \ldots\ldots (4.1)$$

where σ_{xe} = x-ray production cross-section for a fixed proton energy E

n_z = the number of atoms of the element Z per unit volume

t = target thickness

$$\text{since} \quad n_z = \frac{N_A}{A} \rho$$

where N_A = Avogadro's number

A = Atomic weight of element Z

ρ = density of element Z in the sample

$$n_x = n_p \frac{N_A}{A} \rho t \, \sigma_{xe} \qquad \qquad \ldots\ldots (4.2)$$

If the X-rays are detected in a solid angle $d\Omega$ steradian by a detector of efficiency ε including absorption losses in chamber exit window, air passage, detector front window, we have the yield N_x given by:

$$N_x = n_p \frac{N_A}{A} (\rho t)_z \frac{d\Omega}{4\pi} \varepsilon \, \sigma_{xe}$$

$$(\rho t)_z = \frac{N_x}{n_p} \left[\frac{A}{N_A \, \sigma_{xe} \frac{d\Omega}{4\pi} \varepsilon} \right] \qquad \qquad \ldots\ldots (4.3)$$

$$(\rho t)_z = \frac{N_x}{n_p} \left[\frac{1}{F_{xz}} \right] \qquad \qquad \ldots\ldots (4.4)$$

where F_{xz} is the "Calibration Factor" which is constant for a given element Z, X-ray transition, fixed proton energy and geometry. It is obvious from equation (4.4) that inserting the appropriate value of F_{xz} will lead to an absolute quantitative analysis of thin targets. Therefore

- 99 -

the task of calibrating involves the accurate determination of the F_{xz} values. There are a number of possible approaches to obtain this absolute calibration

1. Theoretical evaluation of F_{xz} values

2. Experimental evaluation of F_{xz} values through:

   a) using standard reference materials

   b) using elemental thin film standards

The alternative method to this absolute calibration is to calibrate the system on a relative basis, that is:

Relative calibration through internal standards

In the following, the different methods of calibration are studied:

4.2.1 Absolute Calibration

The procedure adopted to calibrate the system in the present work is absolute calibration which was performed as described in the following sections:

4.2.1.1 Theoretical Evaluation of F_{xz} Values

This method is a semi-empirical approach since it relies upon published values for most of the parameters in the F_{xz} expression:

$$\left(\frac{N_A}{4\pi}\frac{d\Omega}{A}\,\varepsilon\,\sigma_{xe}\right)$$

The solid angle $d\Omega$ subtended by the detector was determined by the geometry of the experimental set up which was fixed through the experiment period. Since the size of the detector is not accurately defined due to the presence of an annular dead-layer, a lead collimator of 0.3 ± 0.05 cm thickness was introduced with a precise aperture of diameter

0.4 ± 0.05 cm. The target aperture distance was fixed and carefully measured to be (9.4 ± 0.2) cm.

A proportion of the X-rays emitted from the target are absorbed by the chamber Melinex window, air path and the detector combination of the beryllium vacuum window, the gold-layer electrical contact on the front surface of the crystal and a silicon "dead layer".

The gold and silicon dead layer thicknesses are not usually given by the manufacturer, but they are comparatively thin; Goulding (1977) determines that the dead-layer should be about 0.3 μm thick.

For the elements of interest in the present study the X-ray absorbion in such thickness is negligible.

The fraction of X-rays transmitted through the absorbers may be expressed as:

$$e^{-\Sigma \mu_i (\rho t)_i} = e^{-[\mu_{air}(\rho t)_{air} + \mu_{mx}(\rho t)_{mx} + \mu_{be}(\rho t)_{be}]} \quad \ldots \ldots \text{ (4.5)}$$

where (ρt)'s are the mass thicknesses that X-rays must transverse, μ_{air}, μ_{mx} and μ_{be} are the mass absorption coefficient of air, Melinex and beryllium respectively. The absorption coefficient for Melinex was calculated by assuming:

$$\mu_{mx} = \Sigma P_i \mu_i \quad \text{(Bragg Additivity Rule)}$$

where P_i is weight fraction of element i in the compound and μ_i is the absorption coefficient for the X-ray of interest by the element i. The mass absorption coefficient of air is given by:

$$\mu_{air} = \Sigma c_i \mu_i$$

where c_i is the concentration of element i.

The absorption of X-rays by the combination was calculated using the appropriate absorption coefficient taken from the compilation of

Storm and Israel (1970)

The efficiency of the detection ε is given by:

$$\varepsilon = e^{-\Sigma \mu_i (\rho t)_i} \times \eta \qquad \qquad \ldots\ldots (4.6)$$

where η is the detector efficiency obtained from data provided by manu-facturer.

The ionization cross-sections employed were computed from the poly-nomial of Khan et al (1975), which is based on thick target measurements of K X-ray ionization cross-sections of several elements between Z = 20 and Z = 50, and is given by:

$$
\begin{aligned}
\ln \sigma_i = {} & (41.46 - 37.32\, E + 8.448\, E^2) \\
& - (12.212 - 21.242\, E + 4.864\, E^2)\ \ln Z \\
& - (0.0107 + 2.737\, E - 0.655\, E^2)(\ln Z)^2 \qquad \ldots\ldots (4.7)
\end{aligned}
$$

where Z = atomic number of element of interest

E = proton energy in MeV

This formula is valid within the range $\quad 1.3 < E < 3$ MeV

$$20 < Z < 50$$

For use in trace analysis the production cross-section is of interest rather than the ionization cross-section. These are related to each other through the fluorescence yield, values of which were taken from Bambynek et al (1972). The values published more recently by Krause (1979) are not significantly different than that of Bambynek. For example, there is no difference for Ca, for Cu the difference is 1%, while for Mo it is 0.1%.

The F_{xz} values computed as described above are tabulated in Table 4.9. The experimental accuracy in F_{xz} values quoted from comparison with calculated values is between (2.4 - 10)% which is acceptable considering the uncertainties quoted. That is except for Ti and Mo, where the uncertainty is of the order of 20%. The disagreement is ascribed to

uncertainties in the data used in F_{xz} calculations including production cross-sections.

4.2.1.2 Experimental Evaluation of F_{xz} Value

4.2.1.2.1 Using Elemental Thin Standards: In addition to the theoretical evaluation of F_{xz}, an experimental determination was made. Ten thin elemental standard foils of low X-ray self absorption were chosen to span the elemental range of interest. They were in the form of single elements or stable compounds the characteristics of which were discussed in section 4.1.2. These standards of known areal density were exposed to the proton beam and the number of K_α X-rays per proton $(y_x = \frac{N_x}{n_p})$ were measured as a weighted average of (8 - 20) sets of data, each set comprises of (8 - 16) measurements. F_{xz} values were then directly determined from:

$$[(\rho t)_z = \frac{N_x}{n_p F_{xz}} \quad \ldots \ldots \text{ eq.(4.4)}]$$

since all parameters in F_{xz} are either constant or vary smoothly with both X-ray energy and atomic number, the X-ray yield per proton per $(g.cm^{-2})$, i.e. F_{xz}, of several analyzed standards as a function of atomic number resulted in a smooth calibrating curve as shown in Figure 4.5.

Intermediate elements also could be quantitatively obtained through this calibration curve.

The calibration curve is seen to peak in the region of $19 < Z < 22$ and drops on both the low energy and high energy X-ray (low and high Z) sides. At low energy the drop is due to X-ray attenuation in passing from target to detector crystal as well as falling detector efficiency in that region, in addition to the decreasing fluorescence yield value. At high Z the X-ray production cross-section drops off rapidly resulting
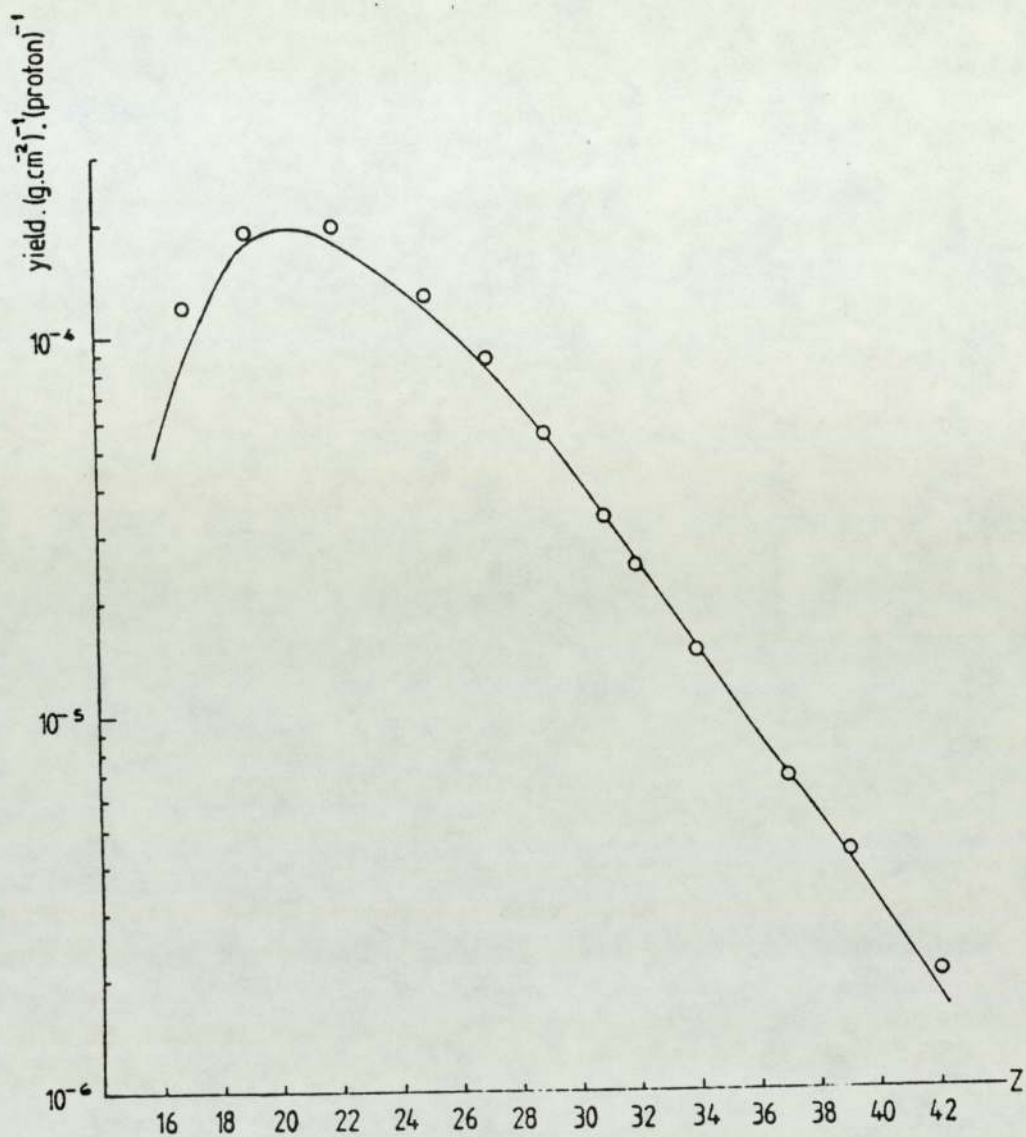
Figure 4.5   Calibration curve for PIXE analysis system

The curve represents experimental values and the symbols are calculated values

Error bars were omitted since they were smaller than the symbol size

TABLE 4.9

A COMPARISON OF COMPUTED CALIBRATION FACTORS $(F_{xz})^a$ OF THE

PRESENT SYSTEM COMPARED WITH EXPERIMENTAL VALUES

Element	F_{xz} (theo.)	F_{xz} (exp.)
Cl	-	$8.9 \times 10^{-4} \pm 0.44 \times 10^{-4}$
K	-	$1.83 \times 10^{-5} \pm 0.9 \times 10^{-6}$
Ti	$2.015 \times 10^{-4} \pm 2.3 \times 10^{-5}$	$1.6 \times 10^{-4} \pm 0.8 \times 10^{-5}$
Mn	$1.27 \times 10^{-4} \pm 1 \times 10^{-5}$	$1.15 \times 10^{-4} \pm 0.6 \times 10^{-5}$
Co	$8.42 \times 10^{-5} \pm 6.3 \times 10^{-6}$	$8.01 \times 10^{-5} \pm 4 \times 10^{-6}$
Cu	$5.31 \times 10^{-5} \pm 4 \times 10^{-6}$	$5.44 \times 10^{-5} \pm 3 \times 10^{-6}$
Ga	$3.2 \times 10^{-5} \pm 2.4 \times 10^{-6}$	$3.3 \times 10^{-5} \pm 2 \times 10^{-6}$
Ge	$2.47 \times 10^{-5} \pm 1.9 \times 10^{-6}$	$2.4 \times 10^{-5} \pm 2 \times 10^{-6}$
Rb	$7.04 \times 10^{-6} \pm 5.2 \times 10^{-7}$	$7.9 \times 10^{-6} \pm 4 \times 10^{-7}$
y	$4.35 \times 10^{-6} \pm 3.2 \times 10^{-7}$	$4.2 \times 10^{-6} \pm 2 \times 10^{-7}$
Mo	$2.08 \times 10^{-6} \pm 1.56 \times 10^{-7}$	$1.57 \times 10^{-6} \pm 0.8 \times 10^{-7}$

F_{xz} (Calibration Factor) = Counts. $(\text{proton})^{-1}.(\text{g}.\text{cm}^2)^{-1}$

a: K_α X-ray energies of Cl and K are not within the

limits imposed by Khan's polynomial employed to calculate

K shell production cross-sections. In order to maintain

the consistancy of the present data, it was preferred to

omit the F_{xz} (theo.) values to these elements rather than

to use the cross-sections of other workers

- 105 -

in the fall in yield. The decrease in the detector efficiency for Z > 32 is another contributing factor to this. The calibration curve was obtained from a uniformly distributed proton beam bombarding a standard target of area larger than the area of the beam. The calibration was valid for targets either the same size as or smaller than the beam spot regardless of the target homogeneity or larger than the beam area where the target has to be uniformly distributed. In this case the areal density of unknown sample $(\rho t)_{sm}$ could easily be determined through evaluation of X-ray per proton then comparison of this with the appropriate F_{xz} as found in the calibration curve, utilizing the following equation:

$$(\rho t)_{sm} = (\frac{N_x}{n_p})_{sm} \times \frac{1}{(F_{xz})_{st}} \qquad \ldots . . (4.4)$$

In the current PIXE work samples smaller than the area of the beam were employed. The value of n_p used to derive F_{xz} in equation (4.2) represents the number of protons that are incident on the sample during the measurement. Accordingly for samples smaller than the beam, n_p was determined from the ratio of specimen and beam area and from the total integrated change on a Faraday cup, i.e.

$$n_p = N_p \times \frac{d S_{sm}}{d S_b}$$

where N_p = total number of integrated proton

$d S_{sm}$ = area of the sample

$d S_b$ = area of the beam

Then equation 4.4 may be written as:

$$(\rho t)_{sm} = \frac{N_x}{N_p} \times \frac{d S_b}{d S_{sm}} \times (\frac{1}{F_{xz}})_{st} \qquad \ldots . . (4.8)$$

Since the absolute mass of a sample $M_{sm} = (\rho t)_{sm} \times d S_{sm}$, then:

$$M_{sm} = \frac{N_x}{N_p} \times (\frac{1}{F_{xz}})_{st} \times dS_b \qquad \qquad \dots \dots (4.9)$$

Since the total specimen mass was measured prior to placing onto the backing the concentration was obtained from the ratio of M_{sm} to this measured mass.

Considering now the accuracy of this method, from equation 4.8 we see that the accuracy of the absolute mass (M_{sm}) of the sample is determined mainly by the accuracy of $(N_x)_{sm}$, N_p, dS_b and $(F_{xz})_{st}$. The accuracy of $(N_x)_{sm}$ and $(N_x)_{st}$ was obtained from counting statistics and systematic errors due to peak programme discussed in section 4.3, which was estimated to be (2-10)% for large and intermediate peaks. The accuracy of N_p depends on the Keithley current integrator, which is typically not more than a few percent. The accuracy of $(\rho t)_{st}$ is also about 5%. Clearly, all uncertainties from Ω, w, σ are not involved through employing this approach which is advantageous for assuring high accuracy.

To check the accuracy obtained relative to the semi-empirical approach where F_{xz} values were calculated (section 4.2.1.1), a comparison was made between the values obtained from these two methods. The summary of this is shown in Table 4.9, which shows the reliability of the data obtained. Moreover, Figure 4.5 shows the plotted experimental calibration curves and theoretical F_{xz} values.

The further advantage of this method is that it requires a very simple observation to check the stability of the system calibration. One or two standard targets are needed for such a check and only short time is required to perform the measurements, depending on the atomic number of the standard used. For some standards such as Ti or Mn, 5 minutes are adequate to obtain the sample and obtain ten readings in which the counting statistics are better than 5% on each reading. Usually, such standards were analyzed; three to four different times each run day, providing a continuous check on the system.

An alternative approach to the above is to prepare thin standards in the laboratory in a liquid deposit form, which are analogous to commercial standard metals, in that they are thin enough to ignore X-ray self absorption and X-ray production variation. Many authors have reported such an approach, Walter et al (1974), Kubo (1974), Deconnink (1977) made standard films by depositing known volumes of solution onto suitable substrates and evaporated to dryness; the solutions contained a known quantity of the standard element. Mostly, atomic absorption liquid standards are used. Simms et al (1978) employed the two methods and compared calibration curves obtained from commercial standards with that obtained from liquid deposit standard, in which they obtained reproducible results.

4.2.1.2.2 Using Standard Reference Materials: A number of Standard Reference Materials (SRMs) have been developed and produced by the National Bureau of Standards (NBS) as a result of the necessity to establish criteria for evaluating and confirming the reliability of the data obtained from analytical techniques. These standards include finely powdered, homogeneous biological Standard Reference Materials, which are certified for their trace element content on the basis of determinations made using a variety of independent techniques. The evaluation and preparation procedure of the two common biological standards, SRM - 1571 orchard leaves and SRM - 1577 bovine liver have been discussed by LaFleur (1974). They are secondary standards of initially impure mixture of largely unknown compositions therefore they differ from the primary standards of pure chemicals of defined composition. As the impurity is homogeneously distributed within the sample, they are particularly suitable for calibrating analytical techniques.

Since these reference materials are in the form of a homogeneous

powder, several preparation methods are available. They are easily made into fairly rugged, thick pellets. In addition, thin targets can be prepared by carrying through a wet digestion procedure and depositing the solution onto a suitable backing. The X-ray yield from each element, which is present in a known amount, can be determined. F_{xz} values for each element could then be evaluated from equation 4.4 and interpolated for other elements, hence providing a calibration of the system.

In the present work it was found more useful to employ SRM's to obtain information on the target preparation techniques employed and also to assess the overall accuracy.

4.2.2 Relative Calibration Through Internal Standard

It is advantageous to add internal standards to thin targets when the beam area is smaller than the specimen, and to thick inhomogeneous samples where applying the various corrections required are difficult. Adding internal standards is possible if the sample preparation procedures lend themselves to this process. Obviously, samples in solution form are most suitable for internal standardization. A known volume of standard solution, which does not exist in the sample, is added to the sample to be analyzed. The unknown concentration of an element of interest Z in thin samples is determined simply. From equation (4.8) areal density of the element of interest may be expressed as:

$$(\rho t)_z = (\rho t)_{st} \frac{(N_x)_z}{(N_x)_{st}} \times \frac{(F_{xz})_{st}}{(F_{xz})_z} \qquad \ldots\ldots (4.10)$$

Since both the standard and the unknown element occupy the same area then:

$$M_z = M_{st} \frac{(N_x)_z}{(N_x)_{st}} \times \frac{(F_{xz})_{st}}{(F_{xz})_z} \qquad \ldots\ldots (4.11)$$

or $\quad M_z = M_{st} \dfrac{(N_x)_z}{(N_x)st} \times \dfrac{A_z}{A_{st}} \times \dfrac{(\sigma xe)_{st}}{(\sigma xe)_z} \times \dfrac{\varepsilon_{st}}{\varepsilon_z}$ $\quad$ ..... (4.12)

where the symbols and the subscripts are defined previously.

It is noticable that uncertainty in the unknown sample mass (M_z) is much lower due to replacement of the absolute values by their ratios. This is because the uncertainty in the absolute value is higher than that of the ratios. In addition to this, is the equal effect of the systematic errors on both standard and the unknown (e.g. improper integration of the beam current) which does not appear in equations 4.10, 4.11 and 4.12.

The conditions to be observed in selecting these standards which affect the calibration are: they should not volatilize during proton irradiation; the compound used must not cause precipitation of any element in the sample and finally it must distribute uniformly throughout the sample. In addition, the cross-section needs to be known.

4.3 SOURCES OF EXPERIMENTAL UNCERTAINTIES

The uncertainties which contribute to the final uncertainty in the absolute mass of an unknown element determined by PIXE analysis, can be summarized with reference to equation 4.8;

$$M_{sm} = \dfrac{N_x}{N_p} \times (\dfrac{1}{F_{xz}})_{st} \times d \; S_b$$

These uncertainties are as follows:

1. Uncertainties in N_x which are due to:

   a) Counting statistics

   b) Peak fitting

      1 - Background determination

      2 - Inter-element interference correction

- 110 -

c) Sampling error

    1 - Volume error

    2 - Positioning

    3 - Flake off probability

    4 - Non-uniformity

    5 - X-ray absorber

d) Beam energy

2. Uncertainties in beam integration n_p

a) Instrumental

b) Leakage

3. Measurement error in d S_b

4. System calibration factor F_{xz} uncertainties

a) Uncertainties in N_x which are due to

    1 - Counting statistics

    2 - Peak fitting

    3 - Areal density

    4 - Beam energy

b) Uncertainties in beam integration

1. Uncertainties in N_x

a) Counting Statistics

The statistical uncertainty associated with the number of counts, N_p in a well defined peak in a recorded X-ray spectrum is given by:

$$\sigma_p = \sqrt{N_t + N_b} \qquad \ldots\ldots (4.13)$$

where N_t is the total number of counts in the peak region and N_b is the summation of the background counts in the same region.

Thus the smallest peak area gives the largest fractional counting error. In the present experiments, this error varied from 1% for the

- 111 -

largest peak to 15% for the smallest peak.

b)   Peak Fitting

The PEAK integrating programme used for analysis of PIXE spectra, outputs the area of the peak representing the intensity of a character- istic X-ray together with its standard deviation and location of its centroid. The procedure used to find the peak area is as follows. Two background regions, one region on the high energy and one on the low energy side of the peak are selected from a visual inspection of the spectrum. The programme computes the average of the background per channel from the total background in the 2B channels of the background region and then draws a straight line between these averaged values. The area function computes the number of counts in the peak that are above a background level.

This is computed as follows:

$$\text{sum} = \sum_a^b (C_i - Y_i) \qquad \qquad \dots\dots (4.14)$$

$$\text{Mu} = \frac{\sum_a^b X_i (C_i - Y_i)}{\text{sum}} \qquad \qquad \dots\dots (4.15)$$

$$\text{sigma} = \left[\frac{\sum_a^b X_i^2 (C_i - Y_i)}{\text{sum}} - (\text{Mu})^2 \right]^{\frac{1}{2}} \qquad \dots\dots (4.16)$$

where sum = the sum of the counts under the peak with background

        subtraction starting at a and ending at b.

    C_i = the total counts at the ith channel

    Y_i = the background counts at the ith channel

    X_i = the ith channel

    Mu = the centroid or the mean

  sigma = the standard deviation

    This is shown graphically in Figure 4.6.

- 112 -
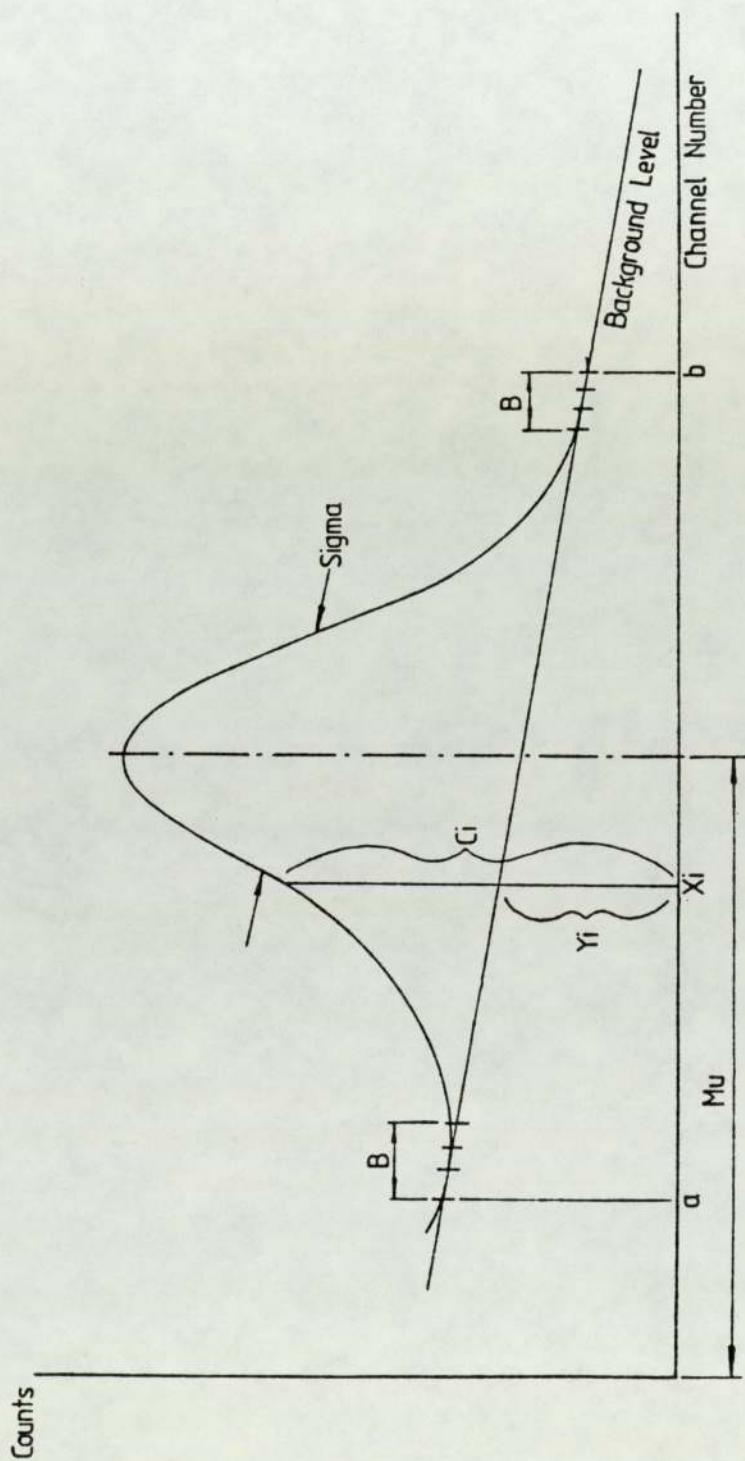
Figure 4.6   A diagram to illustrate the integration of peak area

- 113 -

It was found in the present study that an error up to 20% in the peak area could result if care was not exercised in choosing appropriate channels for the background estimation for the analyzed peak. A plot of standard deviation vs atomic number, Figure 3.12, provides the accurate standard deviation expected for each elemental peak of interest analyzed by the present system. These values were extracted from the analysis of standard foils and employed in addition to the PEAK routine to define the peak width accurately, thus resulting in reliable peak area estimations.

In certain circumstances adjacent peaks are very close together and there is little room for manipulation for selecting the background channels on either one or both sides of the peak. It is then difficult to obtain the expected standard deviation, resulting in some uncertainty in the final peak area.

Occasionally, a peak of interest is not fully resolved from an interfering peak and the above procedure cannot be employed.

In order to separate these overlapping X-ray lines, line intensity ratios are required. The common overlap is that of K_β line on an element with the K_α line of the next higher Z element. The experimental $\frac{K_\beta}{K_\alpha}$ ratios, section 3.4.2, were used to separate out K_α intensities. This correction adds further uncertainty to the peak of interest.

c)   Sampling Error

One important source of uncertainty in the target fabrication from deposited solution is the uncertainty in the sample size. Errors in the measurement of the sample using pipetting procedures are considerable, particularly when small volumes are involved. At the level of 3 µl and 5 µl sample size the manufacturers are unwilling to quote an error figure, but suggest it would be 3 - 5%.

In order to maximize the detector solid angle the detector was

positioned as close as possible to the target. Consequently, any small variation in the sample position relative to the detector affects the total number of X-rays reaching the detector due to changes in the solid angle. The target detector geometry, however, was rigidly fixed to minimize this error. The only other anticipated uncertainty is due to target rotation, which was reproducible to better than ± 1% resulting in an uncertainty of the order of 2% in the detected X-ray yield.

The effect of different possible X-ray paths through the air-Melinex-beryllium combination due to positional variation will alter the X-ray attenuation only marginally.

For moderate currents of about 100 nA/cm^2 used in these experiments, no significant effect of heating or loss of volatile element from biological material was observed. Further study on this effect is presented in section 7. However, with the crystallization phenomena of solution deposited samples, there is some possibility of small loss of crystallized material through flaking off from the specimen. In addition X-ray absorption in the crystal has to be considered.

Targets that are crystallized and non-uniformly distributed coupled with any slight imperfection in the homogeneity of the beam will affect both the accuracy and precision of the results.

In order to prevent the intense low bremsstrahlung associated with biological samples from being detected and causing large dead time problems, 7 μm aluminium absorber was usually positioned infront of the detector. The determined X-ray count, N_x was corrected for attenuation effect of the absorber. The absorption coefficient was taken from Storm and Israel (1970) and is quoted as 10% for X-rays in the energy range of 1 keV to 6 keV and 3% for X-rays above 6 keV. The total uncertainty in this correction factor which includes the uncertainties in absorber thickness was < 7% except for the detected low Z elements. For the ele-

ments Ca, K, Cl, S and P the uncertainties were significant and ranged from 10 - 50% respectively.

d) Beam Energy

Any uncertainty in the proton beam energy contributes to the uncertainty in elemental abundance. Energy calibration tests made indicate that the uncertainty in the beam energy is usually less than 10 keV at 2.5 MeV, which is only 0.4% of the beam energy. Since the cross-section depends on E_p^4, this uncertainty will produce 1.6% error in the cross-section and hence the same uncertainty introduced to thin target X-ray yields (due to direct proportionality which relates cross-section to X-ray yield).

2. Uncertainty in the Beam Integration

Uncertainty in the total accumulated charge can arise from instrumental error and leakage current problems. The uncertainty in the Kiethley electrometer measurement introduced an error of 1% at full scale deflection and was checked periodically against a calibrated ORTEC current digitizer.

3. Measurement Error in dS_b

The beam area dS_b was measured using a shadowgraph with a magnification of x 50. The uncertainty in dS_b due to the measured r_b was estimated to be of the order of ± 4%.

4. System Calibration Factor F_{xz} Uncertainties

Obviously, the system calibration factor determines to a large extent, the accuracy of the system. Most of the errors introduced in

evaluating this factor by the uncertainty in the physical parameters involved have been discussed. The uncertainty for the areal density of the standard foil calibrators is quoted by the manufacturers to be ± 5%.

The system calibration was compared with the computed F_{xz} values, section 4.2.1.1, and is shown graphically in Figure 4.5. The difference between the two F_{xz} values for one element in expressed as:

$$\Delta = \frac{R_1 - R_2}{(R_1 + R_2)/2} \times 100 \qquad \ldots\ldots (4.17)$$

These results are summarized in Table 4.8. The difference varies from 2.4% to 10%. The calibration uncertainty in the calculated F_{xz} values were taken from the parameters involved. These parameters could be found from:

$$F_{xz} = \frac{N_A}{A} \sigma_{xe} e^{-\varepsilon} \mu_i x_i \frac{d\Omega}{4\pi} \varepsilon$$

in which the uncertainties were assessed as follows. The error in the Avogadro's number and atomic weight are negligible. The uncertainty in the production cross-section were estimated to be 10% for X-ray energies below 5 keV and 6% for energies above 5 keV, Khan et al (1975). The total uncertainties in the absorption corrections due to all absorbers varied from about 2% at 5 keV rising to 8% at 3 keV. At energies higher than 5 keV uncertainties are less than 1% which is negligible. The errors due to uncertainty in ε are zero for all X-rays between 5 keV and 15 keV and above this increases to 1.6% for 40 keV X-rays. The error in the measured solid angle $d\Omega$ was estimated to be 1.5%. All these sources of uncertainty can be assumed to be independent, therefore the total uncertainty can be obtained from adding these in quadrature.

$$E_T = \sqrt{\sum_i^N E_i^2} \qquad \ldots\ldots (4.18)$$

where E_i's are the individual independent sources of uncertainty and E_T is the total uncertainty . The overall uncertainty in the calculated F_{xz} values was estimated to be 6% at 40 keV rising to 12% at about 3 keV energy.

The uncertainties quoted in this work were obtained following the above procedure.

CHAPTER FIVE

THE SENSITIVITY

5.1 SENSITIVITY VERSUS TARGET BACKING THICKNESS

Sensitivity is defined as the minimum amount of an element present in a sample that can be detected. In order to detect this quantity it is necessary to generate a number of characteristic X-rays, N_x, which is in a statistically significant way greater than the uncertainty in the corresponding background. From this definition it is evident that the major factors limiting the analysis of a sample being bombarded for a fixed excitation condition are the X-ray production cross-section of the element of interest in the sample and the shape and intensity of the generated background.

The lower the background intensity the higher the sensitivity achievable.

For the case when a thin sample is deposited from liquid form with negligible matrix onto a supporting substrate the main cause of background is the bremsstrahlung radiation resulting from the slowing down of the secondary electrons produced in the backing by the incident proton beam. This bremsstrahlung X-ray spectrum is a broad continuum of maximum intensity at low energy, falling steeply with its maximum energy at:

$$E_x = \frac{4m\ M}{(m + M)^2}\ E_p$$

where E_x is the maximum energy transfer from a projectile of mass M and energy E_p to a free electron of mass m. It is clear that for a pure backing, free from elemental impurity, the background does not interfere with the X-rays of elements that have characteristic X-ray energies above E_x. Therefore, it is useful in terms of minimizing the electron bremsstrahlung to make E_x as small as practically possible. It is seen from

the above relation that this can be accomplished by reducing the pro-
jectile energy E_p. This will cause, however, a corresponding decrease
in the characteristic X-ray yield due to lowering the production cross-
section. It has been shown by several workers that the optimum choice
of E_p for protons, in analyzing biological and environmental samples, is
between 2.0 - 4.0 MeV depending upon the elemental region of interest,
present work, Willis (1977), Folkmann (1974) and Johansson et al (1976).

Since the background contribution from bremsstrahlung is larger for
thicker backings the highest sensitivity is obtained by using the thinest
possible backing.

Experiments performed by Johansson et al (1976) demonstrated how
the background intensity sets the limit of sensitivity. Their comparison
of thin backings such as polystyrene and thick foils indicate that an in-
creased bremsstrahlung by a factor 15 in the region of interest will
cause the lower limit of detection to increase by a factor 4.

The authors, Johansson (1970), Watson (1971), Gilfrich (1973),
Umbargar (1973) are among those who have demonstrated the merits of using
thin backings and achieved sensitivities in the sub-nanogram region for
small quantities of material mounted on thin backings. A study of sen-
sitivities as a function of backing thickness in the region of 700 -
8000 $\mu g/cm^2$ has been published by Flochini et al (1972); this study show-
ed the effect of the physical nature as well as thickness of these targets.
Equal thickness of Mylar $(C_{10} H_8 O_4)_n$ and Kapton $(C_{22} H_{10} N_2 O_4)_n$ gave
similar background rates, but Teflon $(CF_2)_n$ generated significantly high-
er background for the same thickness. The background arose from brems-
strahlung rather than impurity X-rays, and is due to the effective atomic
number of the backings.

Watson et al (1971) recorded the background for thin backings of
carbon, aluminium, Mylar and 4.3 mg/cm^2 Millipore filters. They found

that the shapes of all the background spectra were identical and that the intensity varied linearly with the number of atoms per cm^2 indicating that the cross-section for the production of background events was essentially the same for the four analyzed backings. Johansson et al (1972) found the background from 270 µg/cm^2 aluminium foil was four times the background from carbon foil of 20 µg/cm^2 which is not quite a linear variation with number of atoms per cm^2 as is claimed by the previous authors.

Shown in Figure 5.1 are the background spectra obtained from experiments performed in this study of a polycarbonate substrate of 10 µm thickness Nuclepore and Kimfol of 5 µm thickness. The measurements were made under the same experimental conditions with the presence of 7 µm aluminium absorber infront of the detector. The average integrated background in the region of 1.8 keV - 5.4 keV was determined from ten analyzed backings, each exposed to 25 µC, and found to be 279 and 143 counts per keV per µC for Nuclepore and Kimfol respectively. The end point energy of the bremsstrahlung produced in the current work employing 2.5 MeV protons was 5.4 keV.

These results suggest that for thin targets considered the bremsstrahlung is proportional to the thickness.

It is clear that both the composition and thickness of the backing material critically affects the bremsstrahlung background and hence the ultimate sensitivity. It should be noted, however, that other factors relating to the backing material also affect the sensitivity. For example, severe limitations can arise due to impurities in the backing material. In addition, several other considerations may control the selection of the backing material, as follows:
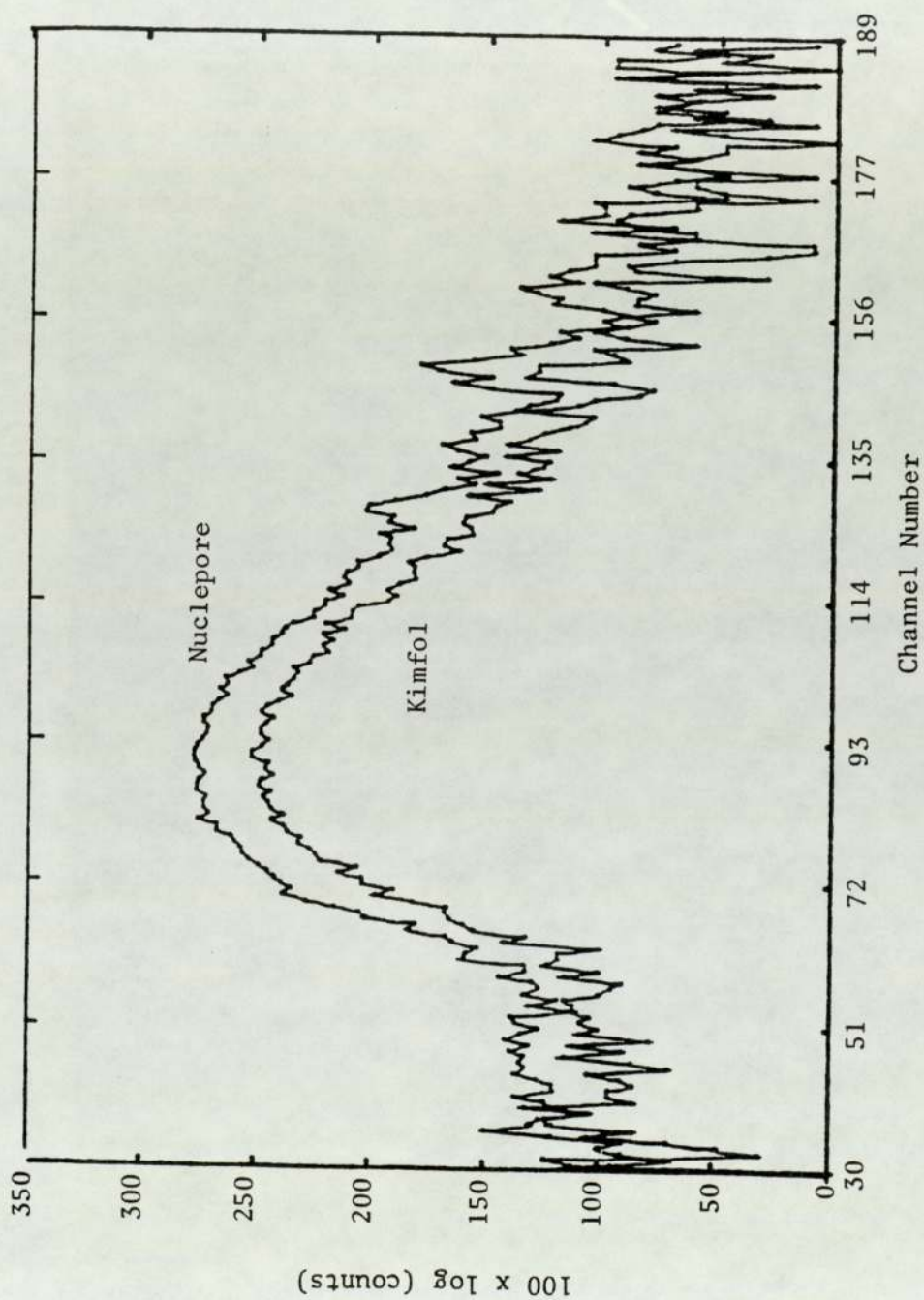
Figure 5.1   PIXE spectra from the analysis of Nuclepore and Kimfol backing illustrating the difference in the background level produced in these backings

5.2 TARGET BACKINGS

5.2.1 The Criteria for Selection of Target Backing

The criteria for the selection of target backing material could be summarized as follows:

1) Low areal density

2) Freedom from metallic impurity

3) Good mechanical strength

4) Ability to withstand the required beam intensity

5) Chemical resistant

Below each of these factors is discussed.

Ideally, a target support should be composed of low Z material with a minimum areal density. The low Z composition ensures that X-rays emitted from the backing do not interfere with the characteristic X-rays of the elements of interest. The low areal density ensures a low intensity bremsstrahlung background so that optimum sensitivity can be achieved.

When the lowest background has been achieved, the main criterion is the trace elements content. Ideally, the backing should be entirely free from high Z elements which produce unwanted characteristic X-rays and complicate the analytical procedure and introduce a great deal of uncertainty into the results.

The backing material should give sufficient mechanical strength to withstand handling and target preparation procedures.

To prevent deformation of the backing material and evaporation of the sample due to heating, the energy loss of the protons in the backing should be small.

The ability to resist acids is essential for specimens prepared by digestion in concentrated acid.

Rarely are all these requirements fulfilled simultaneously. So the optimum choice depends on the specific analytical problem. However, one of the aspects in which the experimenters in PIXE analysis have not yet reached agreement and have very different approaches and preferences is the target support backings. Because of this, it is thought that perhaps an investigation of the common available backing is useful, to study carefully all the relevant characteristic of these materials.

5.2.2 Brief Studies on Different Available Backings

The properties of the backings most commonly used are summarized in the review by Johansson (1976). Essentially, the choice is between thin foils and semi-thick materials, the characteristics of which are discussed below:

5.2.2.1 Thin Foil Backings: These are mainly carbon foils or plastic films.

Carbon foils: Thin carbon foil of 40 $\mu g/cm^2$ was employed as the backing material by Johansson (1970) when he introduced the PIXE analysis technique. Carbon has low associated bremsstrahlung background and the ability to withstand a high beam intensity. A 2.5 μA, 1.5 MeV well collimated proton beam was used to irradiate the carbon foil for one hour without any adverse effect. Herman et al (1973a, 1973b) also advocated carbon foils and compared them with several plastic foils which possess lower beam tolerance. They found that carbon foils have more ability to withstand the destructive effect of the charged particle beam. Moreover, carbon foils are not attacked by acids. The main objection to carbon is the presence of different impurities of a significant level such as Cl, Ca, Cr, Fe, Ni, Cu and Zn in an unreproducible manner. After fabricating carbon foils Kaji et al (1977) suggested that they were unsuitable as

backing on the basis of their impurity. Moreover, apart from the frag-
ility, making specimen of small area deposit from liquids onto these
foils is rather difficult, since the liquids spread very readily across
the backing.

Umbarger et al (1973) investigated different backings and from the
standpoint of rigidity they preferred Mylar and Kapton to carbon and
further they obtained similar detectability curves for carbon, Mylar and
Kapton of similar thicknesses.

Plastic Films: These are more widely used than carbon foils. They
are cheaper and more easily made. In addition, the advantages of low
bremsstrahlung can be kept by using these foils. The most commonly used
foils are Formvar $(C_{15} H_7 O_2)_n$, Polystyrene $(CH_2)_n$ and Collodion $(C_{12} H_{11}$
$O_{22} N_2)_n$.

Formvar shares with carbon the disadvantage of fragility but poly-
styrene and Collodion are mechanically stronger. The most important
difference between these organic films and carbon foil is their lack of
electrical and thermal conductivity. Hence, films are unable to with-
stand high beam intensities leading to longer analysis times. Herman et
al (1973a) found that polystyrene withstood 100 nA of 2 MeV protons,
spread over an area of about 0.18 cm^2 for only a few minutes.

Formvar has been frequently used by various workers, Bearse et al
(1974) described the preparation of foils of 10 $\mu g/cm^2$ mass thickness
and used them satisfactorily. They have reported that, "they were tough
enough to endure the abuse of target preparation and subsequent handling".
On the contrary, Walter et al (1977) after investigating these films
found that they are fragile and not practical unless maximum sensitivity
is required, since they produce the least bremsstrahlung due to their
small mass thickness and low Z composition.

Alexander et al (1974), Valkovic et al (1974), Kaji et al (1977)

circumvented the problem of non-conductivity of these foils by evaporating a layer of aluminium on the foil. But they found that the fragility of the foils was not improved by this process.

Kubo (1976), Lear (1977), Guffey (1978) have satisfactorily used Formvar to encapsulate their targets to prevent possible loss of volatile elements from the targets.

Traces of iron and bromine have been observed by Barrette et al (1976) in Formvar (> 15 $\mu g/cm^2$), while Walter et al observed Mn, Fe, Cu and Zn. However, Valkovic et al (1974) did not observe any characteristic X-rays. Sharon (1977), Zambola (1978) and other mentioned authors make no mention of impurity. This relative freedom from metallic impurity makes it a popular choice for PIXE technique, but unfortunately, the advantages are limited due to its inability to support acid specimens, which are very common specimen type. In addition, large area targets result when preparing samples from liquids as is the case with carbon.

Johansson et al (1975) discussed the preparation of backing of 40 $\mu g/cm^2$ Polyethylene; 100 nA beam current of 3.7 MeV energy was used to irradiate these films where the beam area was about 0.28 cm^2, without any evidence of deformation. The acid resistance feature makes them more useful but several impurities such as Ca, S, Mn, Fe and Zn were observed. Kemp et al (1975) have used Polyethylene as a backing for their microtome sliced tissue.

Collodion foil of 0.25 μm has been used by Kubo (1974), who employed two layers of Collodion to encapsulate his targets which withstood 30 nA/ cm^2 of current with an energy of 2.5 MeV. The low beam tolerance was improved by evaporating carbon or aluminium onto the film. No mention was made of the trace element content.

5.2.2.2 Semi-Thick Material Backing: Mylar $(C_{10} H_8 O_4)_n$, 400 - 2300 µg/cm^2; Kapton $(C_{22} H_{10} N_2 O_4)_n$ Millipore and Nuclepore filters 1000 - 6000 µg/cm^2 are considered as semi-thick backing since they are usually used as a support for thin targets (1000 µg/cm^2). These have the advantages of commercial availability, physical strength, a fair thermal conductivity which enables them to withstand beam intensities and they are resistant to acid attack. The bremsstrahlung produced however is much more intense than that emitted from thin foils. Walter et al (1977) found that the bremsstrahlung induced by 3.0 MeV protons at the Fe K_α region in 0.6 mg/cm^2 Mylar spectrum is 20 times greater than that from thin layer of Formvar.

Among the different workers who studied Mylar and adapted it as a support for their specimens because of low impurity concentration and the relatively low continuum background are Mangelson et al (1977) and Kaji (1977) while Sharon (1977) claims that Mylar (2300 µg/cm^2) and Kapton (860 µg/cm^2) produced the highest background compared to that produced by Millipore membrane (6000 µg/cm^2) and Nuclepore membrane (1400 µg/cm^2).

Kaji et al (1977) have observed small amounts of Cu, Fe and Zn in analyzing 10 µm Mylar foil, while Barrette et al (1976) have reported only the presence of Zn. Other authors Umbarger (1973), Baeri (1978) and Navarette (1978) have employed Mylar as backing but have not reported on the impurities of their foil. It should be noted that the majority of workers have used a wetting agent with Mylar to give acceptable wetting properties. This requires extra time and effort, and could introduce impurities.

Kapton foil is more heat resistant than the plastic foils noted above. Gorden et al (1972), Flochini et al (1972), Umbarger et al (1973) have investigated the use of Kapton as a backing material. Barrette et al (1976) have selected Kapton as backing for their targets as a result of

the study made by Gordon et al. Kapton can take up to 1 μA beam of 2 MeV protons; this was a finding by Umbarger et al but no mention was made to the beam area. Gordon et al pointed out that 0.3 mm Kapton could withstand a 30 minutes irradiation by 200 μA protons at 3.5 MeV, but burned away after a few minutes of irradiation with 350 μA. However, Sharon considers Kapton an undesirable backing for trace analysis due to its high bremsstrahlung compared to the other plastic foils.

Nuclepore and Millipore filters are now increasingly used as a backing in different laboratories. Liquid samples as well as tissue slices adhere very well to these filters due to their porous feature. The wetting properties of these two filters are however different.

Small porous size Nuclepore (0.2 - 0.6) μm produce an uncontrolled large spot from a drop of deposit on the surface while the deposit is in a small defined area on the larger porous size (8 μm) diameter porous (present work). Millipore acts similar to small porous size, although Nuclepore is preferable because it is thinner and withstands more beam. Millipore suffer usually either from beam heating or from radiation damage to the long chain molecules.

However, Gilfrich et al (1973) claims that Nuclepore and Millipore showed acceptable low impurity and mass thickness which makes them desirable backing. Bearse et al (1974), Nielson et al (1976), Walter et al (1977) and Mangelson et al (1977) are among the authors employing Nuclepore satisfactorily as a target backing.

The conclusion emerging from this study is that the issue of thin foils versus thick material cannot be settled easily. For example, thin foils low bremsstrahlung is set against the availability and ease of handling of thick backing, and each one of these possesses advantages for a specific situation and deficiency for the others. Therefore, the condition of the analytical situation will have to determine the appropriate backing

to be used. It is obvious that it is less convenient to mount tissue samples on thin carbon film than to mount them on Nuclepore filters which have excellent strength and adhesion property. Serious flaking occurs for crystalline materials such as the deposits from ashing unless membrane filters are used as backings. However, this problem can be circumvented either by using glue which increases the bremsstrahlung and perhaps introduces more impurity or by sandwiching the specimen with another layer of backing which will cause an increase of bremsstrahlung by a factor of 2 and also requires extra manipulation.

So unless optimum sensitivity is required, the sensitivity loss has to be balanced against the good properties of thick backings. Therefore semi-thick foils are preferably accepted. According to some of the points discussed and the experience gained by the other workers, it was thought that membrane filter is the backing of choice to start with in the present research.

An Investigation on Nuclepore as Backing

To select an appropriate filter meeting the requirement of the present experiment, consideration was given to the investigations of other workers, such as Walter et al (1977) who evaluated backing materials including Formvar, Polystyrene, Mylar, Millipore and Nuclepore filters. They found 8-micron Nuclepore material to be most suitable because it had the lowest contamination level of any of the materials tested. Sharon (1977) considers Nuclepore membrane as the preferred alternative to their thin backings. In addition, Bearse et al investigated several possible materials and found 8-micron porosity Nuclepore the most suitable.

Consequently, Nuclepore filters were chosen as the initial backings for the targets in the present work.

5.2.3 Nuclepore Filters

These filters are standard polycarbonate membranes. Being strong
of tensile strength = 30,000 psi (manufacturers) handling and mounting is
easy. They are flexible, will not crack and are not easily split. They
are available in different pore sizes ranging from 0.2 µm diameter to
10 µm diameter.

Three different porous sizes 0.2, 0.4, 0.6 µm diameter of areal den-
sity typically 1 mg/cm^2 were studied. No difference was observed in
their physical strength or in their bremsstrahlung and characteristic X-
ray spectra from these foils. They withstood beam intensities which
produced a count rate of 1000 count/sec which was the maximum count rate
limit of our electronics. However, higher current, corresponding to 100
nA/cm^2 beam intensity was used, since 7 µm aluminium absorber was placed
infront of the detector, in order to prevent the intense low energy
bremsstrahlung from being detected and causing long dead time problem.
Tissue slides as well as residue from fluids were found to adhere very
well to these backings. Sample solutions generally penetrated Nuclepore
filter matrix and were distributed through it, Nielson (1976), Campbell
(1977), Mangelson (1977), this work. Some of the workers claimed that
a small well defined area deposit forms on the Nuclepore surface without
any mention of the porous size effect. However, from the experience
gained from the present work it was found that for the same sample size
the spatial distribution through the matrix material of the filter de-
pends on the porous size, the smaller the size the larger is the wetted
area. With the three filters used it was found that unless a very small
size of about 2-3 µl was deposited, the drop spread out to form uncontrol-
lable large spot. This is unsuitable for proton irradiation since usu-
ally the sample sizes are not that small (3 - 5) µl and the target has
to be covered by the beam area, which was usually smaller than 0.3 cm^2.

To overcome this problem, larger porous size 8 µm were successfully tried. The deposit from wet ashed solution resulted in a small well defined area. However, skill is required to manipulate the deposition.

The detail of pore construction and distribution is shown in scanning electron microscopy micrograph of this foil in Figure 5.2.

In order to assess the impurity level in the Nuclepore filters forty-two filters were analyzed and the trace elemental concentration was determined.

The areal density of the detected elements was calculated using the following equation:

$$[(\rho t)_z \;=\; \frac{(N_x)_z}{n_p} \; x \; \frac{1}{(F_{xz})_{st}}]$$

The elements observed and their measured areal densities are given in Table 5.1 and 5.2.

In Table 5.3 the results are compared with those certified by the manufacturers.

The impurity trace elements detected represent more or less the elements of interest in biological samples.

In the case of the (0.2, 0.4, 0.6 µm) diameter foils, group 1, Table 5.1, the average weight of the trace elements detected (represented by mass thickness) was comparable in some instances to the maximum weight certified by the suppliers. However, a considerable variation in the trace element content was observed from one foil to another. For example, Fe varied from zero to 181 ng/cm², Cr from zero to 39 ng/cm²; any correction to be made on this account would introduce unacceptable uncertainty to the data to be analyzed.

On this basis any result obtained from samples deposited on these foils were not taken into account.

Investigating Table 5.2 which represents trace analysis of the
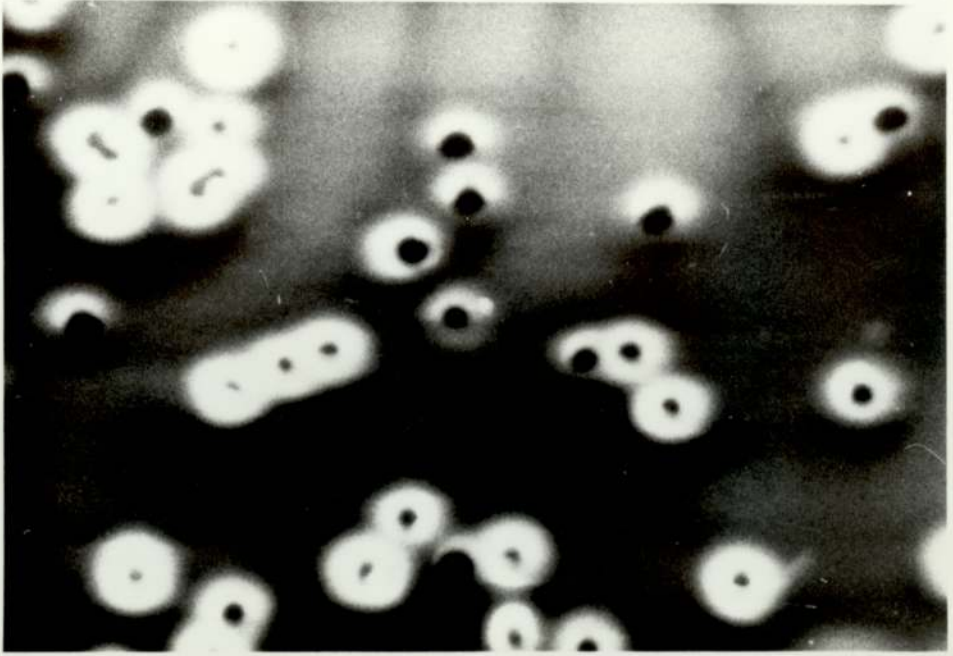
Figure 5.2   Scanning electron microscopy micrograph of 8μm pore size Nuclepore, illustrating the construction and distribution of the pores. (X500)

TABLE 5.1

ELEMENTAL IMPURITY ABUNDANCE IN NUCLEPORE FILTER

THE DATA ARE TAKEN FROM ANALYSIS OF 24 SAMPLES OF THE FIRST

GROUP (0.2, 0.4 AND 0.6 μm PORE SIZES) FOR 25 μC CHARGE[a]

Cr (ng/cm^2)	Mn (ng/cm^2)	Fe (ng/cm^2)
26.6	-	92.2
26.0	-	72.0
30.0	-	46.4
38.7	-	26.0
-	-	-
-	-	37.0
-	-	181.0
12.8	-	-
22.0	-	25.0
11.0	4.0	49.0
9.3	3.4	33.8
-	5.8	
18.7	6.0	106.0
10.5	-	21.8
30.0	-	-
-	-	72.7
-	4.5	25.6
-	9.5	26.7
-	9.6	42.0
7.6	10.3	34.0
27.2	8.9	41.0
21.6	10.3	38.0
28.7	29.0	37.0
17.7	2.8	35.0
Mean = 13.5	Mean = 4.3	Mean = 43.5

a: - sign indicates that the element in the analyzed filter was not detected

TABLE 5.2

ELEMENTAL IMPURITY ABUNDANCE IN THE SECOND GROUP

OF 8 μm PORES NUCLEPORE, THE DATA ARE TAKEN FROM

ANALYSIS OF 15 SAMPLES FOR 25 μC CHARGE

Cr (ng/cm^2)	Mn (ng/cm^2)	Fe (ng/cm^2)	Br (ng/cm^2)
15.7	-	29.6	45.6
-	6.5	27.2	57.0
11.5	-	12.5	-
15.1	-	26.3	42.3
14.2	-	18.5	50.6
12.5	-	22.6	45.6
15.1	8.2	28.4	30.3
13.2	5.0	30.0	41.7
13.8	-	21.3	24.5
13.8	-	13.4	43.8
15.1	5.67	35.6	46.7
20.0	4.3	20.4	33.9
21.0	4.9	28.0	36.0
19.0	6.1	11.8	x
18.8	5.9	20.1	x
Mean = 14.5	Mean = 3.06	Mean = 22.4	Mean = 38.7

x   indicates a relatively high amount of Bromine.

This is most likely due to contamination

rather than a proper impurity

- 134 -

TABLE 5.3

COMPARISON OF MAXIMUM AND MINIMUM VALUES OF THE DETECTED

ELEMENT IN ANALYZED NUCLEPORE (TABLES 5.1 AND 5.2) WITH

THAT PROVIDED BY MANUFACTURERS

Element		First group			Second group			expected
		Mav	Mmin	Mmax	Mav	Mmin	Mmax	Mmax
1.	Cr	13.5	0	39	14.5	0	21	12
2.	Mn	4.3	0	29	3.1	0	6.5	3
3.	Fe	43.5	0	181	22.4	11.8	35	90
4.	Cu	0.15	0	3.6	0	0	0	3
5.	Ni	0	0	0.8	0	0	0	7
6.	Br	0	0	0	38.7	0	57	0
7.	Zn	0.13	0	3.2	0	0	0	6

second group - 8 μm porous Nuclepore - denote that the mean values obtained for trace element content were comparable to the maximum given value. The variation between these results was significantly less than with group 1 and the maximum values detected were within the limit of the values quoted. That is, with an exception of bromine which was present in a large amount and with a typical large variation of zero to 2821 ng/cm^2. Hence, on analyzing the deposited samples on these filters no reliable estimation for bromine could be reported.

To ensure that the X-rays detected came from the Nuclepore filters a careful check of the proton beam and sample alignment was made. The background spectrum from the chamber was regularly monitored following the beam and detector collimator alignment. In addition, X-ray spectra from Nuclepore filters were recorded under fixed sample-detector geometry with both a 1 mm diameter focused beam and 0.25 cm^2 area diffused beam. No significant difference was observed in the spectra indicating that proton scattering at the sample did not contribute to the detected X-ray spectrum.

It is clear from the above study that Nuclepore backing are only satisfactory if free from contaminations.

5.2.4 Kimfol Filters

At the 2nd International PIXE Conference - Lund, Sweden, June 1980, Campbell et al (1981) reported the use of Kimfol filters for mounting samples. They found that they were more suitable than the commercial foils Kapton, Mylar and carbon because of their low elemental and bremsstrahlung background.

Kimfol polycarbonate (Kimberly-Clark Corp. Mass U.S.A.) is manufactured from a high molecular weight polycarbonate polymer, having basic repeating unit of
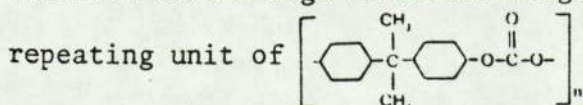
They are made in a wide range of thicknesses commencing at 2 micron thickness. They have a very good mechanical strength; tensile strength 11,000 psi (manufacturers). They are resistant to the action of many chemicals including nitric and sulphuric acid. They are available either as a basic film or metallized with aluminium. Due to their small thickness no charge accumulation or heating effect is expected. However, using metallized foils is always advantageous provided that trace element content is small.

In the present work a group of 10 samples from plain Kimfol were analyzed to investigate the elemental impurity. Each foil was exposed to a charge of 25 μC. It was found that the amount of impurities detected were slightly more than what was expected. This was thought to be due to scattered protons which might have been caused by slight imperfect alignment. To eliminate the elemental background induced by scattered protons the detector was collimated to view the target only. This was achieved by an aperture made of a large piece of 2 mm thick aluminium with a hole of 2 cm diameter, positioned 3.5 cm from the target. Any induced X-ray not from the target was absorbed by this aluminium aperture.

To check the effectiveness of this aperture another set of 10 targets were analyzed, some difference in the trace levels was observed. The only elements detected were 12 ng/cm^2 Fe, 0.3 ng/cm^2 Cu, 1 ng/cm^2 Zn.

These numbers represent the average of the 10 backings investigated, in each case the exposure used was 25 μC at 2.37 MeV.

A set of four targets, made from aluminized foils, was investigated, several elements such as Fe, Cu, Zn were observed in large quantities. Consequently, plain foils only were employed as backing in the present work.

The only drawback of these foils is the problem with the flaking of sample deposits. It was observed that there was a possibility of loss of mass due to the sample flaking off the foil immediately upon irradiation

- 137 -

with the proton beam.

To overcome this problem a procedure was adopted for gluing the sample to Kimfol, based on the technique used by Russell et al (1981) who covered their samples with a thin layer of polystyrene. From the view point of health protection, it is preferable to avoid using benzene, which is commonly used by others. However, Kimfol is attacked by both chloroform and toluene, and hence it was necessary to employ benzene. We dissolved 0.25 g of polystyrene (Aldrich Chemical Co., Gillingham, England) in 6.7 g of benzene (certified Analar, BDH Chemical Ltd., England) giving a 3.5% solution by weight. The "glue" was stored in a clean Pyrex glass bottle and thoroughly mixed.

After the solution had settled, a 2 µl drop was deposited onto the specimen using a micropipette. The drop quickly spread into a circle covering the entire specimen. The samples then required further drying for about one hour before they were ready to be analyzed.

To check for possible trace metal contamination from this glue, four samples were prepared from 2 µl drop of Polystyrene solution, placed onto clean Kimfol backing and bombarded under the same experimental conditions as the blank Kimfols. No additional characteristic peaks were introduced to the Kimfol spectrum by the addition of polystyrene, only the continuum background increased due to the additional mass of polystyrene and benzene residue. The background in the region between 1.8 keV - 5.4 keV increased from 143 counts per keV per µC to 206 counts per keV per µC, which is nearly equivalent to 2 µm thick Kimfol for producing bremsstrahlung background. The results are illustrated in Figure 5.3 which compares the two spectra.

However, the increased bremsstrahlung could be halved by using 1 µl glue instead of 2 µl which would be quite adequate to adhere the sample.
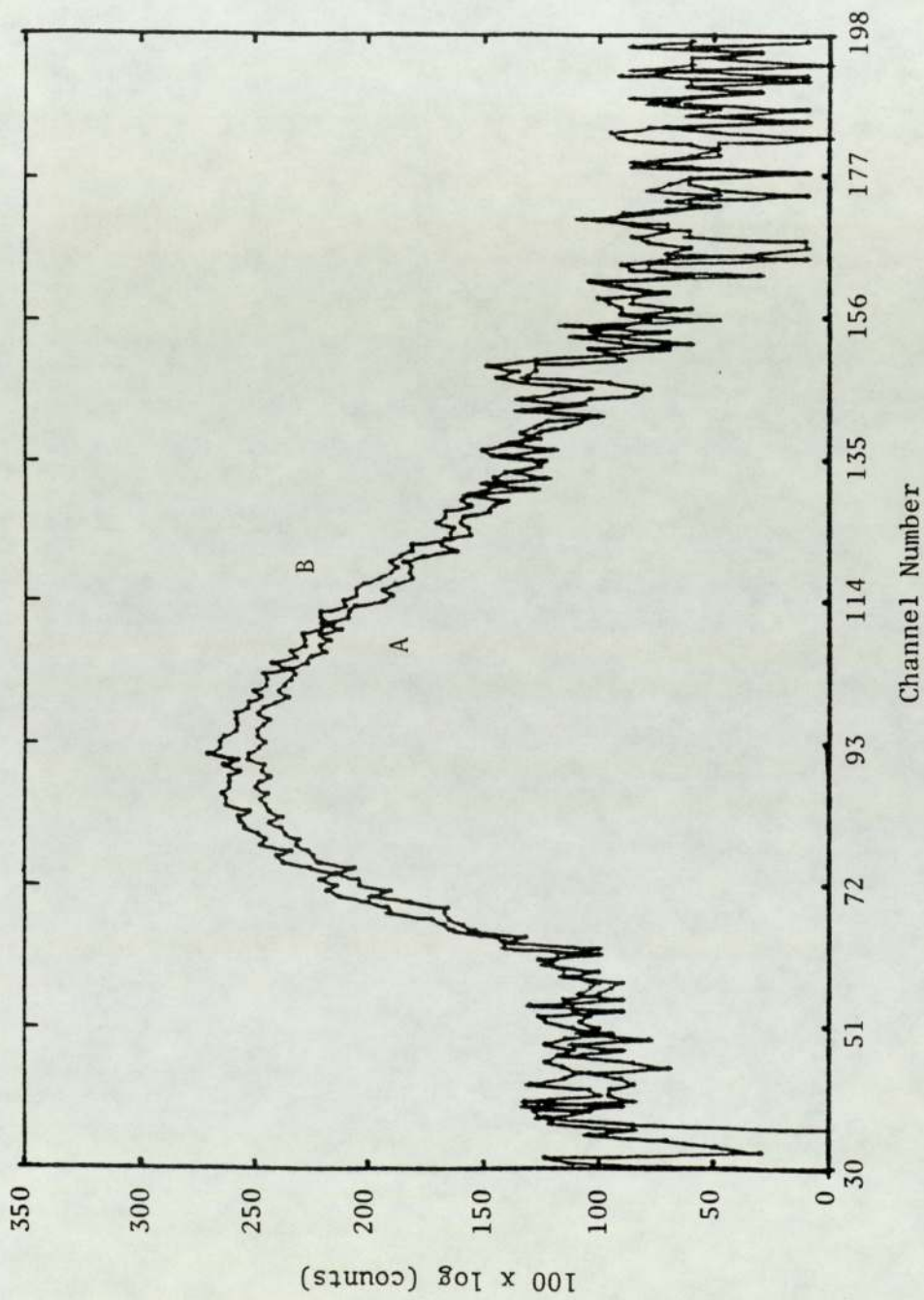
Figure 5.3   Comparison spectra obtained from:

A: Blank Kimfol substrate, and
B: The same substrate onto which 2 μl glue have been deposited

The increased level of bremsstrahlung due to the mass of the deposit is illustrated

- 139 -

5.3 SYSTEM SENSITIVITY AND MDL

In dealing with charged particle induced X-ray analysis it is nec-
essary to evaluate the sensitivity as a function of Z for different pro-
jectiles at various energies. The detection limit is widely used as a
criterion to evaluate and compare the capability of different analytical
techniques. The optimization of the present system with respect to ex-
perimental parameters was performed on the basis of MDL. The optimiza-
tion of the bombarding particle and its energy is discussed earlier in
chapter 2.

Currie (1968) of the National Bureau of Standards (NBS) critically
reviewed the methods available for calculating the Minimum Detection
Limit (MDL) for analysis experiments in which the signal follows Poisson
statistics.

The MDL of a measuring system is determined by statistical uncer-
tainty in the background in the region of the signal from the element of
interest.

However, the sensitivity of an analytical method is best expressed
using the following two concepts:

i)   the quantitation limit C_Q defined recently by Currie (1978) as "the
concentration for which the relative standard deviation of the measured
concentration is 10%", and,

ii)   the detection limit C_D defined as "the smallest concentration that
a particular process can reliably detect".

According to the same author, detection is considered "reliable"
when the probability for detection concentration C_D is 95%.

The critera employed to meet these conditions are:

$$L_D \;=\; 2.71 \;+\; 3.29 \;\sqrt{N_B} \qquad\qquad \ldots\ldots \text{(5.1)}$$

- 140 -

$$L_Q = 50[1 + \sqrt{1 + \frac{N_B}{25}}] \qquad \dots \dots (5.2)$$

where N_B is the number of background counts under the peak in an inter-
val having a width equal to the FWHM of the peak. C_D and C_Q correspond-
ing to L_D and L_Q counts respectively.

As it is stated a number of definitions of MDL are still in use.
In order to stress the importance of choosing a statistically meaningful
definition, three common criteria of statistical detectability are con-
sidered.

1) The integrated number of peak counts has to be larger than a
certain value, which is needed to give a well defined peak with a good
statistical uncertainty, e.g. 100 counts for 10% statistics. This will
enable calculation of MDL for any specific element observed, directly
from the detection efficiency of the system employed. This criterion
has been used by Johansson et al (1970, 1972) Gordon et al (1972) and is
inherent in the compilation of detection efficiencies by Gilfrich et al
(1973). Katson (1978) used 1000 counts to specify the peaks in his
spectra. The criterion is satisfactory for studying elements present in
high concentration in the matrix, leading to large X-ray signals compared
with the background.

2) The peak-to-background ratio must exceed a certain value. This
criterion emphasizes the significance of the background radiation at the
position of the peak. Several authors have employed a peak-to-background
ratio of 1 including Folkmann et al (1974), Raith et al (1977), Moriya
et al (1978). H e r e   the number of counts in the X-ray peak is equal
to the number of background counts within an interval equal to the width
of the peak. This criterion does not depend on the experimental para-
meters such as geometry or beam current, since peak and background have
the same dependence on these factors. Furthermore, peak and background
are in the same energy region, so attenuation of the X-ray and the energy

dependent detector efficiency are cancelled. The drawback of this criterion is that peaks with many or relatively few counts may give the same ratio, although the intense peak has a better precision and is easier to distinguish from the background. The deficient point of this criterion is that it is used without any apparent theoretical justification and the MDL never improves with increased beam current, which is clearly contrary to experience.

3) The peak counts must be greater than the statistical uncertainty of the associated background in a statistically significant way, i.e.

$$N_X = K \sqrt{N_B} \qquad \dots \dots (5.3)$$

where the coefficient K varies for 1 to 10 depending on the particular definition of reliable data, Currie (1968) and Strashinskii (1975). Both the International Union of Pure and Applied Chemistry (IUPAC) and International Union of Pure and Applied Physics (IUPAP) recommend a value of 3 for K.

However, the (IUPAC) takes N_B as the number of background counts present within an interval equal to the full width half maximum of the peak, while (IUPAP) defines N_B as the background taken over the same interval as the peak. Cahill (1975) has discussed the latter definition and decided that, according to student t-test the correct definition is given by:

$$N_p = 2 + 2 \sqrt{2N_B + 1} \qquad \dots \dots (5.4)$$

The most popular criterion is to use equation (5.3) with K = 3, but different workers employ different intervals for the integration of N_B. The authors Perry (1973), Goulding (1973, 1977), Cooper (1973), Sharon (1977) and Khaliquzzaman (1981) considered the peak reliable if N_p exceeds three

- 142 -

times the square root of the background N_B associated with the FWHM of
the peak, While Strashinkii (1975), Johansson (1975), Ahlberg (1976)
and Mommsen (1978) take N_B with 2 FWHM of the peak. Other authors have
not published the selected interval to integrate the background over.
Flocchini et al (1972), Strashinkii (1975) and Khan (1976) suggest a
valuable supplement to this criterion which is $N_X > 10$. This is useful
where the background is very small.

This criterion is dependent on external parameters; for example, it
is seen that the MDL will improve with increased beam fluence. This
criterion has been chosen to evaluate the capability of the present sys-
tem.

5.3.1 The Factors Affecting the MDL

To assess how various experimental parameters affect the minimum
detection limit it is convenient to employ the three sigma criterion
which has been used to evaluate the sensitivity of the present system,
i.e.

$$N_X = 3 \sqrt{N_B}$$

Here, N_B is the number of background counts taken within an interval of
2 FWHM of the X-ray signal of interest.

The minimum detectable limit, measured as X-ray counts, is related
to the physical quantities of interest, namely the areal density (ρt) and
the absolute mass (M), through the following equations:

$$(\rho t)_{MDL} = \frac{3\sqrt{N_B}}{F_{xz} \; n_p} \qquad (5.5) \; \ldots \ldots \text{ derived from } (4.4)$$

$$(M)_{MDL} = \frac{3\sqrt{N_B}}{F_{xz} \; N_p} \; dS_b \quad (5.6) \; \ldots \ldots \text{ derived from } (4.8)$$

- 143 -

where F_{xz} is thin target calibration factor for the element of interest [counts.proton^{-1}. (g.cm^2)$^{-1}$] and corresponds to the theoretical value of

$$\left(\frac{N_A \, \sigma_{xe} \, \frac{d\Omega}{4\pi} \, \varepsilon}{A} \right) \quad \text{and}$$

$$N_B = (\rho t)_B \, N_p \, x \, (F_{xz})_B$$

Hence,

$$(M)_{MDL} \propto \sqrt{(\rho t)_B} \sqrt{\frac{\sigma_B}{\sigma_{xe}^2}} \; x \; \frac{1}{\sqrt{N_p \, \varepsilon \, d\Omega}}$$

and since,

$$N_B \propto \Delta E, \text{ MDL is also proportional to } \sqrt{\Delta E}.$$

Thus MDL scales as follows:

$$MDL \propto \sqrt{(\rho t)_B} \sqrt{\frac{\sigma_B}{\sigma_{xe}^2}} \; x \; \sqrt{\frac{\Delta E}{N_p \, \varepsilon \, de}}$$

where:

$(\rho t)_B$ = areal density of both the backing material and the matrix material.

σ_B, σ_{xe} = are background and characteristic X-ray production cross-section respectively.

ΔE = FWHM resolution of X-ray detector

ε = detector efficiency for the element of interest.

This expression represents the response of the detection limit to change in the various parameters as follows:

$(\rho t)_B$: The amount of background radiation produced is proportional to

this, therefore any increase in this parameter leads to higher
MDL. Thus, sensitivity is improved by reducing the matrix and
backing material mass thicknesses.

$\dfrac{\sigma_B}{\sigma_{xe}^2}$ Both of these cross-sections are a function of proton energy,
optimization of the energy can be achieved for a given sample
analysis as discussed previously.

ΔE: The integrated background is proportional to this, and the
FWHM for a given X-ray energy is constant for a given detector.

$d\Omega$: The solid angle should be as large as possible. This can be
achieved by decreasing the detector-target distance and/or
increasing the area of the detector, providing the counting
rate limitation is not exceeded.

ε: Manipulation of the counting rate can result in some gain in
sensitivity. Often, for biological samples, the majority of
X-rays entering the detector are bremsstrahlung background,
which may cause excessive counting rates. This can be reduced
by using specific absorbers, thus effectively improving the
sensitivity for the more energetic X-rays.

N_p: This could be increased by accumulating more charge on the sam-
ple either by using a higher current, which may cause target
damage due to excessive beam heating and also higher count rates;
or by increasing the analysis time.

(ρt): When the MDL is expressed as concentration of the element of
interest it scales with $(\rho t)^{-\frac{1}{2}}$. Hence the preconcentration of
certain samples leads to a substantial improvement in sensitiv-
ity. This is typically performed by ashing or condensing the
sample material.

Sensitivity for thin targets is improved by increasing target
thickness within the limitation of "thin target criterion" so

that the slowing down of the proton and the absorption of the X-ray, can be neglected. Accordingly, the target thickness is not regarded as free parameter in the optimization of the sensitivity.

It is clear that the scaling law is only valid if there is no limitation to the counting rate of the detector.

5.3.2 The Selected Criteria to Determine the MDL

Although it was decided to use the "$3\sqrt{N_B}$" criterion for the analysis in the present work, the two other criteria, i.e. $N_X = N_B$ and $N_X = 100$ discussed previously, were determined to test the dependences of the MDL on the specific criterion definition.

In order to determine a MDL using the criteria:

(i)   "The minimum peak area is three times the square root of the background counts taken within 2 FWHM"

(ii) "The peak to background ratio is 1"

the following procedures were adopted:

Background spectra from blanks of 10 µm Nuclepore and 5 µm Kimfol which were used as target backings were taken. Each blank was taken as an average from a group of 10 backings. Obtaining the background count level from these spectra, the limit of minimum detectability calculation are based on the following conditions:

(a) standard running conditions: implies the system set up as for normal analytical work with the presence of 7 µm aluminium absorber infront of the detector.

(b) Each target is exposed to 25 µC of protons, the average of 80 nA/cm^2 for the beam intensity and about 20 minutes analyzing time.

(c) The targets are thin enough that the sensitivity is determined

by the bremsstrahlung from the target backings only, therefore it represents the lowest detection limit which can be achieved.

(d)   No interference exists between characteristic X-rays from different elements.

(e)   Ideal backing materials are used which possess no elements whose characteristic radiation is seen by the detector. This was accomplished by stripping off the characteristic X-ray peaks from the original spectra of the backings.

(f)   The quantitative estimate is carried out by using the experimental F_{xz} values.

The criteria adopted for the determination of the (MDL) are:

(1)   The MDL obtained using the criteria (i), MDL $= 3\sqrt{N_B}$ is shown in Figures 5.4 and 5.5 as function of atomic number for Nuclepore and Kimfol respectively.

The comparison between the MDL obtained using this criteria with both of the backings is made in Figure 5.6. The effect of using thinner backing (Kimfol) for achieving lower detection limit is obvious in this Figure. The experimental minimum detection limits for a range of elements Cl through Rb using the data from both Nuclepore and Kimfol backing are summarized in Table 5.4. Two different amounts of exposed charges are used to show the positive effect of larger exposure. The (MDL)'s are expressed as absolute mass and areal density.

In addition the MDL is expressed as concentration in ppm ($\mu g/g$) of dry weight of bovine liver. In doing this it is assumed that the bovine liver deposit on the backing material does not add significantly to the background. This assumption is clearly valid as can be seen in Figure 5.7, which compares the background with and without the sample. It should be borne in mind that the MDL quoted in this manner depends on
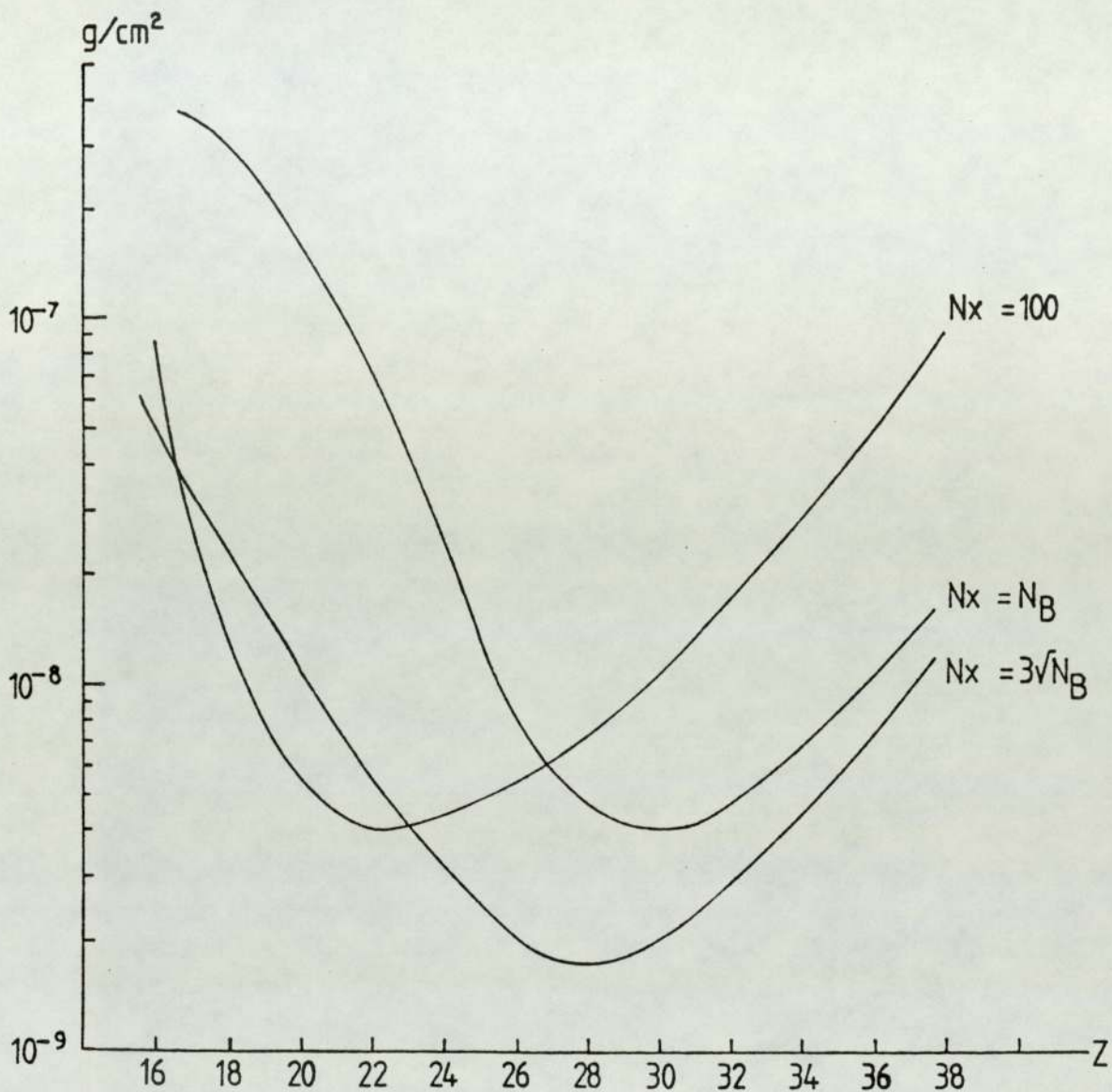
Figure 5.4   Calculated minimum detection limit MDL, using
              experimental calibration factor F_{xz} values, for
              Nuclepore backing, versus atomic number (sensitivity
              curves), utilizing the three criteria $N_X = 3\sqrt{N_B}$,
              $N_X = N_B$ and $N_X = 100$ for 25 μC of charge
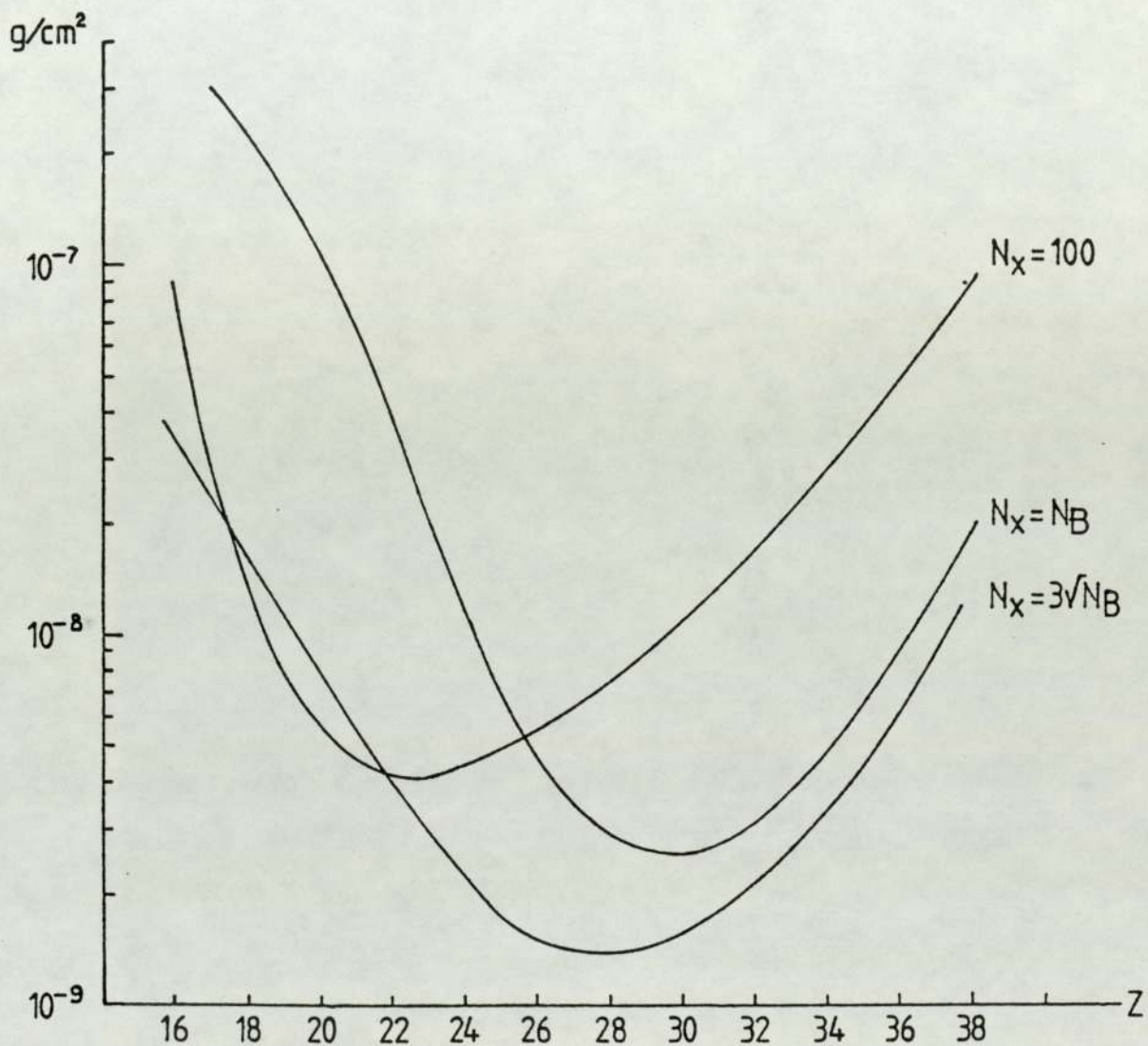
Figure 5.5   Sensitivity curves for Kimfol backing using experimental
F_{xz} values and utilizing the three normal criteria for
25 μC of charge
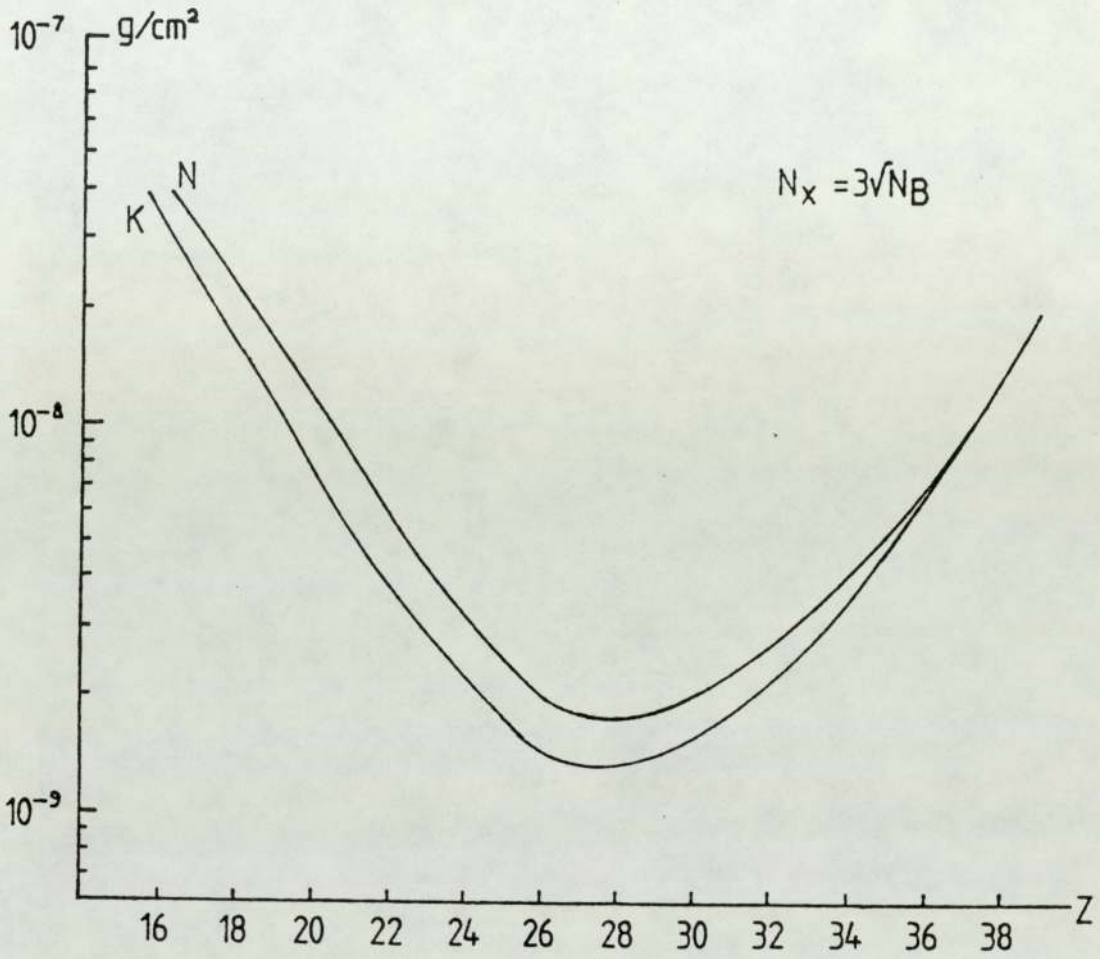
Figure 5.6   Comparison of MDL curves produced for each of Nuclepore and Kimfol backing employing the 3σ criterion illustrating the improved detection limit for thinner target

TABLE 5.4

PIXE MINIMUM DETECTION LIMITS FOR ELEMENTS IN A THIN TARGET DEPOSIT ONTO NUCLEPORE AND KIMFOL, FOR 25 AND 15 μC

CHARGE OF 2.37 MeV PROTON WITH THE PRESENCE OF 7 μm Al ABSORBER INFRONT OF THE DETECTOR[a].

Element	10 μm Nuclepore						5 μm Kimfol					
	q = 25 μC			q = 15 μC			q = 25 μC			q = 15 μC		
	ρt	abs. m	conc.	ρt	abs. m	conc.	ρt	abs. m	conc.	ρt	abs. m	conc.
Cl	3.20×10^{-8}	8.0×10^{-9}	21.30	4.13×10^{-8}	1.03×10^{-8}	27.50	2.30×10^{-8}	5.80×10^{-9}	15.40	2.97×10^{-8}	7.48×10^{-9}	19.90
K	1.60×10^{-8}	4.0×10^{-9}	10.60	2.06×10^{-8}	5.16×10^{-9}	13.70	1.10×10^{-8}	2.80×10^{-9}	7.40	1.42×10^{-8}	3.60×10^{-9}	9.55
Ca	1.10×10^{-8}	2.8×10^{-9}	7.40	1.42×10^{-8}	3.60×10^{-9}	9.55	7.80×10^{-9}	2.00×10^{-9}	5.30	1.00×10^{-8}	2.58×10^{-9}	6.84
Ti	5.20×10^{-9}	1.3×10^{-9}	3.50	6.70×10^{-9}	1.67×10^{-9}	4.51	3.80×10^{-9}	9.60×10^{-10}	2.56	4.90×10^{-9}	1.24×10^{-9}	3.30
Cr	3.10×10^{-9}	7.9×10^{-10}	2.10	4.00×10^{-9}	10.20×10^{-10}	2.70	2.10×10^{-9}	5.30×10^{-10}	1.40	2.70×10^{-9}	6.80×10^{-10}	1.80
Mn	2.50×10^{-9}	6.3×10^{-10}	1.68	3.23×10^{-9}	8.13×10^{-10}	2.17	1.80×10^{-9}	4.50×10^{-10}	1.20	2.32×10^{-9}	5.80×10^{-10}	1.55
Co	1.70×10^{-9}	4.3×10^{-10}	1.14	2.19×10^{-9}	5.55×10^{-10}	1.47	1.38×10^{-9}	3.50×10^{-10}	0.93	1.78×10^{-9}	4.50×10^{-10}	1.20
Ni	1.80×10^{-9}	4.6×10^{-10}	1.20	2.32×10^{-9}	5.94×10^{-10}	1.55	1.40×10^{-9}	3.56×10^{-10}	0.95	1.80×10^{-9}	4.60×10^{-10}	1.23
Cu	1.90×10^{-9}	4.8×10^{-10}	1.28	2.45×10^{-9}	6.20×10^{-10}	1.65	1.60×10^{-9}	4.00×10^{-10}	1.06	2.06×10^{-9}	5.16×10^{-10}	1.37
Zn	2.00×10^{-9}	5.1×10^{-10}	1.36	2.58×10^{-9}	6.58×10^{-10}	1.75	1.67×10^{-9}	4.30×10^{-10}	1.14	2.15×10^{-9}	5.55×10^{-10}	1.47
Ga	2.40×10^{-9}	6.1×10^{-10}	1.60	3.10×10^{-9}	7.80×10^{-10}	2.06	1.86×10^{-9}	4.70×10^{-10}	1.25	2.40×10^{-9}	6.06×10^{-10}	1.60
Ge	2.60×10^{-9}	6.6×10^{-10}	1.76	3.35×10^{-9}	8.52×10^{-10}	2.27	2.16×10^{-9}	5.50×10^{-10}	1.46	2.78×10^{-9}	7.10×10^{-10}	1.88
Br	5.65×10^{-9}	1.4×10^{-9}	3.73	7.29×10^{-9}	1.80×10^{-9}	4.80	5.20×10^{-9}	1.30×10^{-9}	2.60	6.70×10^{-9}	1.68×10^{-9}	3.35
Rb	9.20×10^{-9}	2.3×10^{-9}	6.13	1.19×10^{-9}	2.97×10^{-9}	7.90	9.20×10^{-9}	2.30×10^{-9}	6.13	1.19×10^{-9}	2.97×10^{-9}	7.90

a: 1. To express the MDL as a concentration (μg/g) a typical thin target
   deposit of 0.375 mg dry weight bovine liver powder is assumed.

2. abs. m corresponds to absolute mass in grams.
   ρt is areal density in g/cm² and conc. is concentration in μg/g
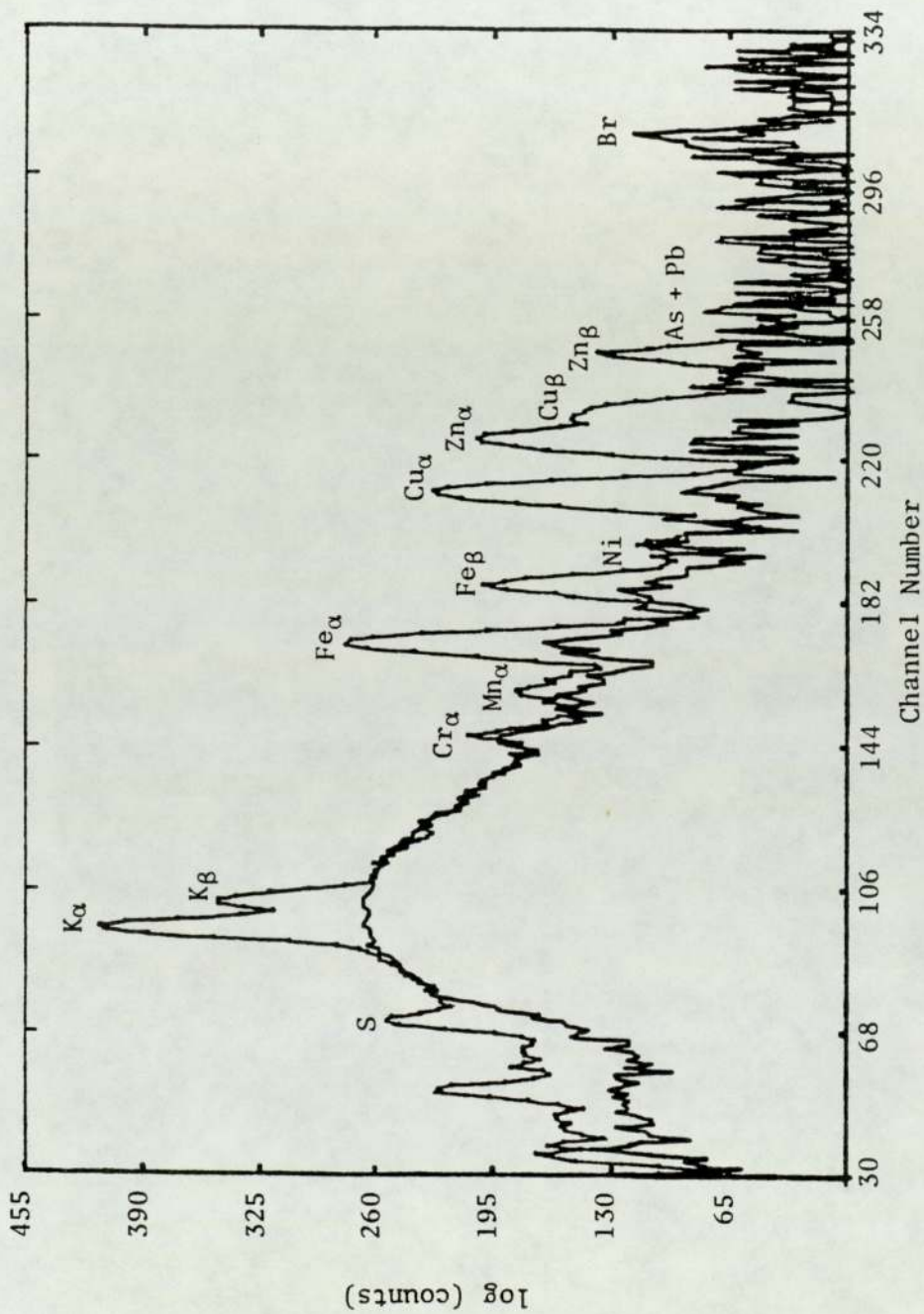
Figure 5.7   Comparison of background level produced from blank Nuclepore and a Nuclepore with 3 μl digestion bovine liver to show the low level of continuous background produced by the deposit

the level of preconcentration of the initial sample and could, therefore, under appropriate conditions, be less than that quoted in Table 5.4.

Therefore, the sensitivities reported here are not the ultimate that can be achieved, but are those that can be readily obtained for routine work. However, better sensitivity can be achieved when required employing the same system, either through mounting samples on extremely thin backings and/or exposing the samples to a greater number of protons.

The obvious feature in all sensitivity curves is that they are a smoothly varying function of atomic number Z, having a minimum (corresponding to maximum sensitivity) for Z between 20 - 30. For low and high Z elements, the sensitivity curve increases to a maximum value (poorest sensitivity). For low Z elements, this is due to the relatively large background intensity which reaches a maximum value in this region, the fall off in the fluorescence yield, the attenuation of low energy X-ray between the target and the detector and finally due to the decreasing detector efficiency. The decreasing sensitivity for heavier elements is mainly due to the decreasing X-ray cross-section, while the background is relatively constant, and to the fall in detector efficiency.

The plot of MDL against Z in Figures 5.4 and 5.5 indicates the other feature of these sensitivity curves which is the strong dependence of the MDL on the definition of that limit.

(2) "The Peak to Background Ratio is 1"

This criterion was applied to show the dependence of (MDL) on the definition of this limit. Figures 5.4 and 5.5 show the evaluated minimum areal density using the above criterion using both backings. The minimum detectable areal densities from these backings are summarized in Table 5.5. It can be seen that the (MDL) is lower for Kimfol than for Nuclepore due to the difference in thickness as described in section 5.1.

(3) The theoretical lower limit of detection was evaluated by assuming that the number of counts N_X in the peak is 100

TABLE 5.5

(MDL)s CALCULATED USING CRITERIA $N_X = N_B$; DATA ARE
FROM NUCLEPORE AND KIMFOL BACKING FOR 25 μC CHARGE
OF 2.37 MeV PROTONS AND 7 μm ALUMINIUM ABSORBER
INFRONT OF THE DETECTOR

Element	Nuclepore (ρt) g/cm^2	Kimfol (ρt) g/cm^2
Cl	4.06×10^{-7}	2.00×10^{-7}
K	3.45×10^{-7}	1.70×10^{-7}
Ca	2.35×10^{-7}	1.80×10^{-7}
Ti	7.40×10^{-8}	4.00×10^{-8}
Cr	2.50×10^{-8}	1.00×10^{-8}
Mn	1.40×10^{-8}	7.10×10^{-9}
Co	5.86×10^{-9}	3.48×10^{-9}
Ni	4.70×10^{-9}	2.98×10^{-9}
Cu	4.52×10^{-9}	3.26×10^{-9}
Zn	4.00×10^{-9}	2.78×10^{-9}
Ga	4.40×10^{-9}	2.78×10^{-9}
Ge	4.20×10^{-9}	2.97×10^{-9}
Br	8.43×10^{-9}	7.16×10^{-9}
Rb	1.38×10^{-9}	1.38×10^{-9}

The calculations were made for K_α peak for most of the elements of interest, using experimental $F_{(x,z)}$ values assuming the existance of 7 μm aluminium absorber infront of the detector, i.e.

$$100 = (\rho t)\ n_p\ F_{xz}$$

The value of "n_p", the number of protons striking the target, corresponds to the collected charge of 25 μC which is the total accumulated charge on the analyzed real targets in this research. The sensitivity curve obtained from this calculation is also shown in Figures 5.4 and 5.5 for comparison.

The typical values obtained for lower limits are 9.5 ng K, 1.04 ng Ti, 1.59 ng Co, 2.8 ng Zn, 8.2 ng Se and 16.8 ng Rb.

This criteria is not satisfactory for high Z elements which are present in very small amounts even when the background intensities in the corresponding region are very small.

CHAPTER SIX

TARGET PREPARATIONS

6.1 TARGET PREPARATION FOR PIXE

In any trace elemental analysis of biological material the process
of target preparation is still the major difficulty, partly due to the
low concentration of elements and the nature of the samples. In addition
in the case of organs, only a small portion is used to perform trace ele-
ment analysis which means that the results may not be representative of
the complete organ. Furthermore, the necessary drying of the sample in
some cases is very critical and will affect the results drastically, due
to evaporation of the volatile compounds. Finally, in the case of thick
samples the problem of X-ray attenuation and energy loss of the proton
beam in traversing the sample needs to be considered.

An ideal target for PIXE analysis would have the following charact-
eristics:

(1) Sufficient concentration so that the element of interest could
be detected.

(2) Homogeneity

(3) Prepared in such a way so as to be representative of the bulk
material and at the same time minimal sample preparation to avoid con-
tamination.

(4) Thin enough to overcome proton beam energy loss and X-ray self-
absorption or self-fluorescence effect.

(5) Stability to proton beam bombarding and resistant enough to be
placed in vacuum.

(6) High electrical and thermal conductivity.

A sample can be prepared either as a thick target or as a thin tar-
get. The properties and relative merits of thin and thick targets are

discussed in the following section.

6.2 THICK TARGET VERSUS THIN TARGET ANALYSIS

The term thin and thick target have to be defined with respect to the typical bombarding energy and target material. Thin targets have to be sufficiently thin such that the energy loss of the proton beam traversing it is negligible, consequently the ionization cross-section can be taken as that at the incident energy E_O of the proton beam. Campbell (1977) has adopted a definition of a thin specimen as one when the effective cross-section σ_E is 5% less than σ_{E_O}. In addition, the X-ray attenuation must be negligible.

A thick target is defined as being thick enough to completely stop the proton beam. Hence, account has to be taken of energy loss of the proton beam in the sample and the attenuation of the emitted X-ray in passing through it. Campbell in his criterion has considered that several $(2 - 4)$ mg/cm^2 of biological material constitutes a thick target, for $2 - 4$ MeV protons, while Willis et al (1977), has found that for proton energy of 3 MeV the dividing line between thin and thick targets of biological material is about 1 mg/cm^2.

Many samples occur naturally in liquid form or can be reduced to a solution by suitable techniques.

Thin samples are most commonly prepared from liquid samples by depositing a drop of solution onto a clean backing substrate such as Nuclepore, Formvar or Mylar filter.

From the standpoint of quantitative measurement it is generally preferable to use targets which require no correction for X-ray absorption or proton energy loss due to matrix effects.

Samples in solution form can be calibrated easily by doping with a known amount of standard material. This doping method has the advantage

that any systematic error affects both standard and sample in the same way and removes the necessity of determining the beam current accurately. In addition, one may make use only of cross-section ratios instead of absolute cross-sections. Thin specimen results may also be compared with those from separate external standards of negligible thickness made from a suitable matrix material.

Finally, thin specimens are generally not subject to the problems of charge accumulation and beam heating.

The major difficulty with thin targets is in their preparation. In addition, the background interference from impurities in the backing material can often cause problems.

Thick targets are usually easier and faster to prepare since the actual thickness is not important and the preparation procedures involve less risk of contamination. A variety of samples have been irradiated by different workers with no preparation other than mounting them on a target support. Additional advantages are high counting rate and no background contribution from the backing material.

In order to make the results quantitative, the specimens of finite thickness have to be compared with separate standards which have the same matrix as the target. The amount of material irradiated is very small. Hence, thick samples have to be sufficiently uniform such that the effective irradiation mass be representative of the bulk sample.

When the proton beam irradiates the target material, the proton loses its energy as it slows down in the material. Since the ionization cross-section has to be calculated by integrating this cross-section over energy losses, the effective cross-section is then given by:

$$(\sigma)_{eff} = \int_{E_o}^{0} \frac{\sigma_{E_o}}{(\frac{dE}{dX})} \, dE \qquad \ldots \ldots (6.1)$$

- 158 -

Accordingly, a degree of uncertainty will be introduced into the analysis. In addition, further corrections will be introduced due to corrections for X-ray attenuation and enhancement effects due to the matrix material. Another problem caused by this energy loss in the sample is the heating of the sample leading to possible loss of volatile elements.

The other form of targets which are not as common as the other two mentioned, are those which are semi-thick. These targets are not thick enough to stop the proton beam, nevertheless, the amount of proton energy loss is not negligible. Consequently, matrix corrections have to be applied when a quantitative analysis is required. Kivits (1980) considers that semi-thick targets have a mass thickness of between 1 and 10 mg/cm^2. They prepared solution deposit targets of 5 mg/cm^2 and claimed that their samples were more representative for target composition than the other two forms of targets. Another advantage of these targets compared to thick targets is that the intensity of the proton beam incident on the target can easily be measured. Also, the effect of charge build up may be reduced.

However, these targets should meet the requirement of uniformity because a constant areal density over the target area has to be analyzed. For thin targets, uniformity is not a strict requirement because variation in thickness has only a minor effect.

Due to the manipulation and preparation technique, the preparation of targets for PIXE analysis from the biological material can be summarized as follows:

(1) Direct preparation

    A - solution deposit technique

    B - sectioning with a microtome

    C - direct irradiation without preparation

(2) Enrichment methods

   A - freeze drying or lyophilization

   B - ashing methods

      (i) dry ashing

      (ii) wet ashing

Each of the above mentioned methods is discussed in the following section.

6.3 DIFFERENT PREPARATION METHODS

6.3.1 Direct Preparation

This is the direct analysis of biological material with a minimum of physical manipulation and can be divided into three sections.

6.3.1.1 Solution Deposit Technique: This involves spotting a small quantity of liquid material which is naturally in liquid form onto a thin backing with a hypodermic syringe or micropipette and subsequent air dry- ing. Examples of specimens studied by different workers include water, milk, urine, beer, synovial fluid [Walter et al (1974, 1977), Campbell (1977), Wheeler (1974)]. Chipperfield et al (1977) have used this pro- cess with blood serum and reported that the following elements could be detected, Na, Mg, S, P, Cl, K, Ca, Fe, Cu, Zn, Se and Br, they found the whole blood cannot be applied in a reproducible manner, since the filter covered with whole blood exhibits a very wrinkled surface and this leads to relatively large errors in analysis. However, in other cases, pro- blems arise because of flaking or when the backing is torn by the deposit. Walter et al (1974) found that with the more crystalline substances like whole blood, serious flaking occurs. They reported that the only rea- sonable method for solving the problem for various fluid samples might be

to cover the sample with a thin plastic foil.

One of the more serious drawbacks of the solution deposit technique is that a uniform distribution of trace elements in the resulting spot cannot be expected, since the trace elements are deposited differently along the radii. In addition, a careful measurement must be made for the elemental abundance in the target supporting material.

6.3.1.2 Sectioning with a Microtome: Sections of tissue can be cut from either frozen primary material or tissue embedded in a hardening agent to enable slicing with a cryostat microtome. These sections can be analyzed as a self-supporting target or can be supported with a thin backing material.

Kemp et al (1975) have studied self-supporting sections of liver, Walter et al (1974) have analyzed thick sections such as muscle tissue. Campbell (1975, 1977) reported the use of a freezing microtome to prepare slices of organic material of about 10 μm in thickness. Hasselman et al (1977) have analyzed frozen sections of liver and spleen of about 10 μm thickness. Jundt et al (1974) also used thin frozen sections and formalin-fixed, paraffin embedded sections of various tissues.

It has been observed that the small specimens obtained by microtome slicing may be quite unrepresentative of the bulk material in certain tissues. In the study of liver and kidney cortex and medulla by Campbell (1977), the reproducibility varied from fair to poor. These results are expected since liver is rather uniform in trace metal distribution while others are not.

6.3.1.3 Direct Irradiation without Preparation: Certain samples are suited to direct irradiation without any manipulation, these include hair and teeth. Air particulate deposits as obtained from air sampling

systems are ideally suited to direct analysis.

Mangelson et al (1977), Jolly et al (1974) and Valkovic et al (1973) have irradiated hair directly to study the relative concentration of elements as a function of distance along hair. Human teeth were analyzed directly by Ahlberg (1976) who examined the trace element concentration as a function of tooth structure. Thick samples of leaves have been analyzed directly by Walter (1974).

6.3.2 Enrichment Methods

These are the methods which are used in order to improve sensitivity and to determine elements which are present in low concentration of less than 0.1 - 0.2 ppm. In addition, more meaningful results can be obtained in this manner by producing more homogeneous samples, since the irradiation of the very limited area of the tissue gives rise to concern about representative samples of the whole material.

6.3.2.1 Freeze Drying or Lyophilization: In this process, the tissue is reduced by a physical method, the tissue or any organic substance is pre-frozen and then pumped for a relatively long time to sublimize the ice to leave a porous, friable solid residue which should be thoroughly powdered to ensure uniformity of elements throughout the target. Campbell et al (1977) have found that freeze drying technique is a standard method for concentrating the mass by a factor of 5. Walter et al (1977) have described the lyophilization of certain sample types, e.g. liver, whole blood, placenta and suggest that lyophilization material is often suitable for easily making pellet samples. However, Campbell et al criticized this method on the grounds that the powder produced by the lyophilization is not sufficiently homogenous. For example, a sample of 1 mg/cm^2 cannot be representative of the bulk material.

6.3.2.2 Ashing Method: Ashing is the process of increasing the concentration of intermediate atomic number elements by removal of the low atomic number elements such as H, C, N and O. These elements comprise most of the matrix which is the major constituent of biological samples. This can be achieved by destruction of the biological material by oxidation. There are two main techniques or a combination of them for this purpose, i.e.

(1) Dry ashing, which includes:

  a) low temperature

  b) high temperature

(2) Wet ashing

(1) Dry ashing: In dry ashing either the sample is raised to a high temperature where the organic matter is oxidized by air or the sample is subjected at low temperature to the oxidizing action of excited oxygen. In both situations, the organic material is oxidized by reaction with gaseous oxygen. This means that further concentration may be achieved, thus a lower detection limit is obtained. Dry ashed samples have been used by different workers such as Rudolph (1972), Nielson (1976), Bearse (1974, 1977) and Pallon (1981). Gorsuch (1970) suggested in his monograph (Destruction of organic matter) that dry ashing at high temperature should be avoided unless it is absolutely necessary as volatile elements are lost in this process. It is obvious that the loss of volatile material with high temperature is much more than with low temperature ashing. Pallon et al (1981) reported that low temperature ashing yields a good elemental recovery and mass reduction factor of 7. Mangelsson's low temperature ashing of tissue removes 95% of the organic mass (1981).

(2) Wet ashing: This is a well established technique, in which the

sample is exposed either at low or elevated temperature to the oxidising of the liquid reagent. As a result of these reactions, the biological material reduces to a homogenous solution of oxidized material providing a complete representative sampling.

Various methods have been reported for wet ashing. A good review of many methods is given by Gorsuch (1970), which covers the details of this process in all aspects. Concerning the volatilization he reported that the recovery rate of trace metals when organic materials are destroyed by acid digestion is generally greater than 95%.

This procedure has been used successfully by numerous workers. However, Nielson et al (1976) have claimed that wet ashing may not reduce the matrix material as much as dry ashing because the material is not oxidized completely, thus leaving some of the matrix as a residue. The method is however very rapid and effective provided all possible sources of error are avoided. For example, the problem of contamination due to the chemical agents employed is negligible with acids of ultra high purity. In addition the use of sealed digestion vessels is more rapid than the conventional acid digestion method, and prevents loss of volatile material. The non-combustive high pressure method has been successfully used for different biological materials. Pioneer of this method was Bernas (1968).

The uniformity of the deposit from a digestion solution depends on the uniformity and size of the particles in the solution. This depends to some extent on the chemical reagent used. Mangelson et al (1977) suggested that nitric acid, nitric acid with hydrogen peroxide or nitric acid with a small amount of sulphuric acid gives satisfactory results. Walter et al (1977) have found that a mixture of concentrated nitric acid and sulphuric acid (2:1) is necessary to yield a clear solution. Nielson (1975) has used Tetra methylammonium hydroxide (TMAM) as a basic agent for wet ashing. Some of the workers combine the method of wet digestion

with lyophilization. Consequently, greater sensitivity is expected, however, Campbell et al (1975) criticized this on the grounds that the increased trace element concentration achieved is negated by proportionally greater volume of acid required to dissolve the lyophilized tissue.

6.4   THE SELECTED PREPARATION METHODS

The process of sample preparation must receive more attention in case of biological samples, since these samples are generally characterized by containing very small amounts of element in the presence of large amounts of water and organic matter. The biological material, whether in the form of tissue or liquid, has to be sampled and converted into a form suitable for PIXE irradiation without any significant loss or addition of the trace elements by the preparation technique.

In principle, the best case is when the sample is already in a suitable form for analysis. But the existence of a wide range of sample types and states indicates the need for a correspondingly wide range of target preparation methods. The choice of a particular technique is governed by the original sample state and consideration of the required accuracy and precision.

The methods adopted in the present work for preparing thin and thick targets are discussed below.

6.4.1   Thin Target Preparation

A variety of techniques have been employed for preparation of thin targets in the present work. Samples were deposited onto a thin supporting substrate either in a solution form or as a solid microtomed tissue slice.

6.4.1.1 Wet Digestion: As previously stated, wet digestion is the

oxidation of organic material. This results in volatilization of the majority of the organic material by the oxidizing action of the chemical reagents. Most of these reactions involved in ashing of organic matter are obscure. They are varied not only according to the reagent and material used but with the nature of substances concerned. For example, a sample consisting largely of carbohydrate offers no problem with ashing, since carbohydrate gives on heating a residue of carbon that burns away easily at a fairly low temperature. On the other hand, animal tissue which consists mostly of protein and fat, often gives trouble. That is because proteins are among the most difficult substances to decompose by wet ashing. It is necessary to use a considerably higher temperature before the decomposition is complete. Fats are also difficult to destroy by wet ashing partly because they sublime on the upper part of the vessel (Middleton, 1953, 1954).

However, there is no single procedure for wet ashing which will effectively digest a variety of biological samples. The common procedure for wet oxidation involves the use of nitric or sulphuric acid or a combination of them. The use of oxidizing agents which are not acids is restricted to specialized application (Gorsuch, 1959).

The interaction of sulphuric acid with organic compounds is very complex. The most important reactions from the view point of wet digestion are oxidation and dehydration. The oxidation action of sulphuric acid is ascribed to the simplified reaction:

$$H_2 SO_4 \rightarrow H_2 O + SO_2 + O$$
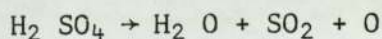
It should be borne in mind that the function of sulphuric acid is more to facilitate the action of the other oxidizing agents than to serve as a primary oxidant itself. Generally, the charred residue produced by sulphuric acid treatment is further treated with another oxi-

dant, such as nitric acid.

The primary oxidant nitric acid is the most widely used for destructing organic matter. The nitrating power of nitric acid can sometimes be troublesome, therefore it may be useful either to start the oxidation with dilute nitric acid or degrade the material with sulphuric acid before adding the nitric acid.

The methods and reagents used to perform the digestion are discussed.

6.4.1.1.1 Using 0.1 N Butyl-n-Amonium Hydroxide: The initial work involved the digestion of one of the most intractable materials, lyophilized bovine liver - NBS. A satisfactory method to achieve complete digestion of this, would ensure the successful digestion of other less intractable tissues.

In attempting to obtain an ashed solution 0.1 N Butyl-n-Amonium hydroxide was used as the solvent following the procedure described below.

300 mg of the sample were weighed out and homogenated with 3 ml of deionized water using a mortar and pestel or in a rotary tissue homogenizer. Complete homogenation was rarely achieved, as this required a relatively long time. The homogenated mixture was put in sample vials and 3 ml of the solvent agent was added then mixed and agitated vigorously to dissolve the material. The resulting solution was a suspension more than a clear solution. 10 µl was measured out and deposited into a Nuclepore backing, but a non-homogenous deposit formed. The non-homogeneity was verified by the different results obtained by analyzing replicate targets made from the same solution. The target non-homogeneity is not a major limitation as long as the proton beam is uniformly distributed across the surface of the target. But the major problem which could not be overcome was the process of elemental loss through the adhesion of the mixture to the wall container and to the mortar and pestle. In addition, thin targets could not be manfactured since smaller droplets could not be

effected using the capillary pipette due to the suspension phase of the resultant solution. As a consequence, this method of preparation was discarded.

6.4.1.1.2: Using General Acid Digestion Methods: To prepare thin targets the main effort was then concentrated on the well recognized acid treatment of samples.

The digestion was started with the common wet ashing technique using nitric acid. This is often used since nitric acid acts both as an acid and as oxidizing agent achieving solution by virtue of both properties (Gorsuch, 1970). The earliest use of nitric acid alone for the oxidation of organic matter is the well known method of Carius (1860). It is not clear, in fact, that Carius applied his method to tissue, but he suggested that it would be suitable for protein. This acid is most satisfactory from the viewpoint of volatilization. The normal concentration acid boils at about 120°C, which assists in its removal after oxidation.

The general procedure for treating the sample with this agent is to start oxidation with dilute nitric acid. 2 ml of 25% nitric acid was added to 300 mg of bovine liver powder. Heating was necessary to complete digestion, since at room temperature the dissolving powder of nitric acid is considerably low. For example, it did not dissolve the bovine liver powder even when kept overnight. Acid digestion was commenced on a hot plate at a moderate temperature (80 - 100)°C. After a few minutes of this gentle heating, a further 3 ml of concentrated nitric acid was added, dropwise. After the mixture had started bubbling it was transferred to a hot plate at about 160°. Heating to fume with the addition of a further 3 ml deionized water was continued. A clear solution with a very thick foam-like layer was achieved. On cooling down a cystalline precipitate formed.

The procedure was repeated adding more nitric acid 4 ml instead of 3 ml. When the solution seemed to approach dryness, deionized water was added repeatedly (up to about 2 hours). A clear solution with a thinner layer of foam on the top of it resulted, without any precipitation. Treating this foam as a protein with 2-Mercaptoethanol [HS.CH_2. CH_2OH] of 10% diluted with deionized water was not successful. Accordingly, it was concluded that the foam layer consisted mainly of fat. Among the workers who digested organic tissue with nitric acid and found that the fat would not dissolve are Gorsuch (1959), and Dankworth (1926).

The fat produced in this experiment could be separated entirely from the solution with centrifugation.

In attempting to overcome this problem, the procedure was slightly changed. The experiment was started to degrade the sample with a small amount of sulphuric acid (0.5 ml) added to the homogenized powder-deionized water mixture. Using a gentle heating the mixture was further treated with nitric acid. Charring occurred which could not be returned back to solution form.

Since the material resisted this gentle technique, a more rigorous digestion procedure was employed, namely the standard acid digestion procedure. The mixture of sample and deionized water was heated in a mixture of 1 ml sulphuric acid and 2 ml nitric acid for 2 - 4 hours during which more deionized water was added gradually. The final solution was a clear solution but still with the layer of the foam on the top.

However, the solution of concentrated nitric acid and sulphuric acid has a very low vapour pressure, hence the evaporation from the target backing required an excessive length of time to dry. The sample prepared from this solution dried in three days in a vacuum dessicator. Therefore it may seem that evaporation of the digested sample to dryness and redissolve it in dilute nitric acid before making deposits would be a method to overcome this problem. But unfortunately, sulphuric acid has a very

high boiling point, and evaporation to dryness is not feasible. More-
over there is a great potential for introducing contaminations into the
sample, also the loss of volatile elements in the chemicals processed can
be expected.

Finally, we could conclude that the targets made from any of the
solution prepared with one of the procedures, with undissolved fat, are
not suitable for PIXE.

The alternative acids for digestion of biological material are per-
chloric acid and hydrogen peroxide. These are potentially dangerous and
explosions from heating of these solutions is almost certain unless ex-
treme care is taken, and such explosions can be extremely violent.

Therefore, the digestion procedure utilizing a teflon-lined pressure
bomb was selected (section 6.3.2). Some of the workers in this field,
Campbell (1975), Gallorini et al (1978) have effected digestion through
using this equipment successfully. NBS confirm the virtue of this tech-
nique (private communication). Successful experiments on Atomic Apsorp-
tion Spectroscopy have been performed by a group of workers of this uni-
versity, Barlow (1979), utilizing this decomposition vessel for a variety
of samples.

6.4.1.1.3 Using Teflon Digestion Vessel: The digestion of biologi-
cal material was effected by using a uniseal high pressure decomposition
ion vessel (Uni-Seal Decomposition Vessel Ltd - Haifa, Israel). This
equipment consists of a sealed teflon digestion vessel inside a stainless
steel jacket. It is capable of pressures of 80 atmospheres and tempera-
tures of up to 170°C. The main features of the vessel are illustrated
in Figure 6.1. Under the vigorous conditions of elevated temperature and
pressure, decomposition reactions proceed much more rapidly than with
usual procedures. Since the vessel is sealed, volatile losses should not
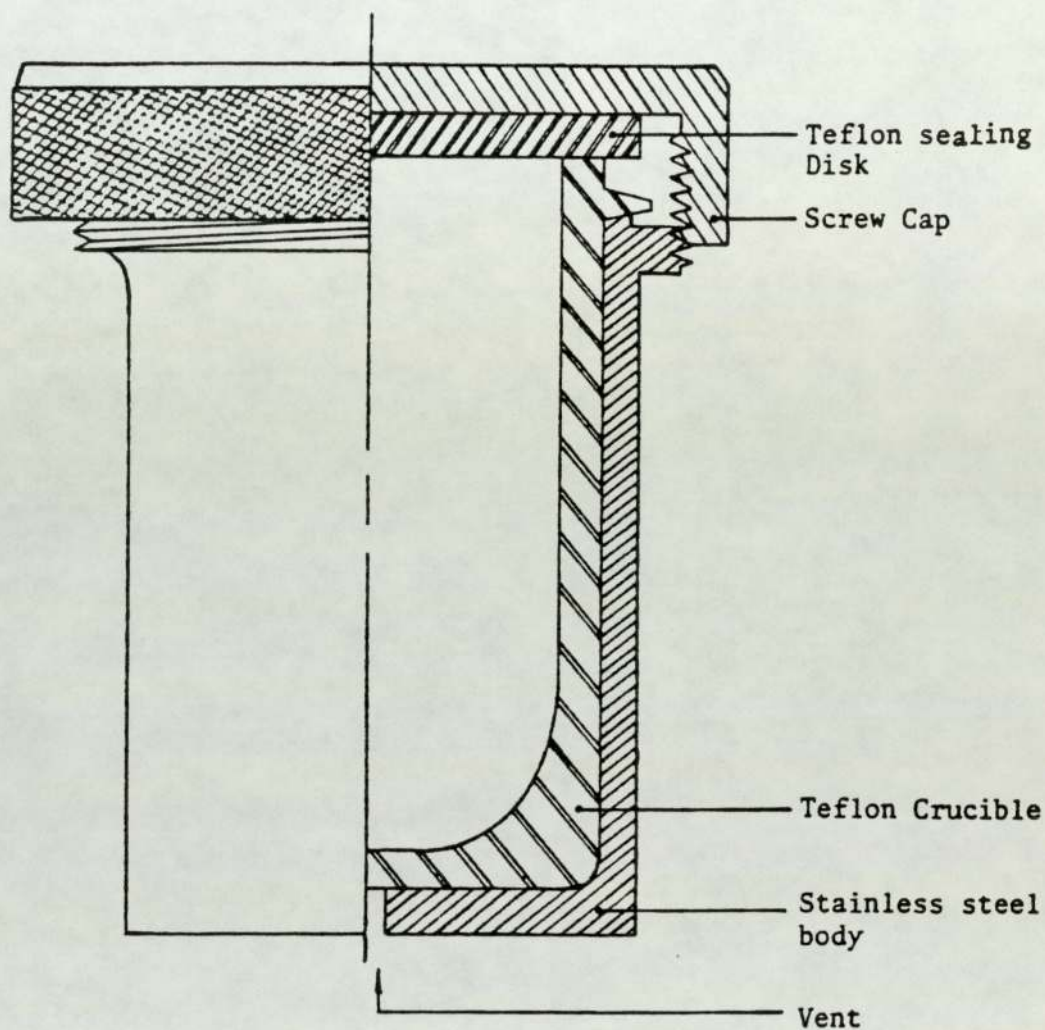
Figure 6.1   The main features of the decomposition vessel

occur during decomposition.

An acid-clean teflon spatula was used to transfer 250 mg bovine liver powder to the teflon vessel, then 2 ml of concentrated nitric acid was added. The teflon vessel was positioned in the stainless steel pressure vessel and the screw cap tightened. The digestion bomb was then heated in a preheated oven at 150° for two hours. After cooling down for at least 1.5 hours, the pressure bomb was opened. The mixture obtained was a pale yellow clear solution. After the solution had been left overnight a small quantitiy of crystal material formed in the solution. A second digestion was therefore carried out, adding a further 1 ml of concentrated nitric acid. The resulting solution was clear and no crystals appeared even after several days.

Two targets were made, one from the digested solution after the first digestion and the other from the solution following the second digestion. 3 µl from each solution was deposited onto a Nuclepore filter to form the target. After the ashed solution had dried the formation of a fine crystalline structure was observed. This may be the result of the formation of insoluble materials or the residue from the inorganic compounds such as silicates which are present in a significant amount in the original biological specimen. The crystals in the first deposit were thicker and more numerous than the crystals in the second deposit. From the view point of quantitative evaluation, crystal formation is a disadvantage as it increases the bremsstrahlung and also results in the absorption of low energy X-rays. Since the second digestion reduced this phenomena, it was thought that performing a third digestion would be useful. This was indeed the case, the size and the number of the crystals were reduced after the third digestion. Figure 6.2 shows photographs of the three deposits after the first, second and the third digestion. The overall digestion procedure is outlined in Figure 6.3. However, one

A
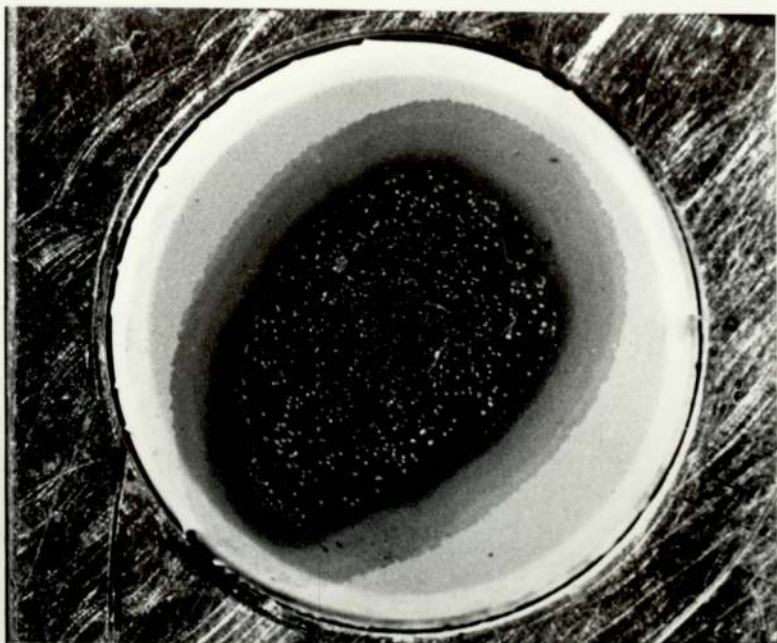
B

C

Figure 6.2 Photographs of a digested bovine liver deposited on a Nuclepore filter; A, B and C are after the first, second and third digestion procedure. This illustrates the active effect of this procedure to eliminate the crystallization phenomena gradually.

WET DIGESTION PROCEDURE

250mg NBS Bovine Liver Powder + 2ml ultra pure nitric acid

Digestion at 150°C for 2 hours in a pressure vessel

cool

Add 1ml HNO_3, digest as above

cool

Add ½ml HNO_3, digest as above

2ml clear digestion solution

Figure 6.3   The outline of wet digestion procedure

should not assume a uniform areal distribution of trace elements in the resulting spot. Beside the crystalline residue, the migration of the elements towards the outer edge of the deposition during the drying process have been observed by Baum et al (1977). Hence, there is a tendancy of the deposit to leave rings rather than a disc on the filter backing. Since this phenomena is ascribed to the air drying of the deposit which takes a long time, rapid freezing of the sample was attempted in an attempt to stop migration of the elements, since the resultant solution was a very strong acidic solution with a freezing point of $-42°$, the deposit froze rapidly at liquid nitrogen and at solid ice (CO_2) temperatures. The frozen deposit was transferred to the evacuated chamber in which the lyophilization takes place. This required (10 - 15) minutes to pump down prior to the sublimation evacuation. This period of time was adequate for the deposit to melt. Titrating of these samples (e.g. adding Na OH) to increase the melting point was avoided to prevent introducing contamination, so freeze drying of these samples could not readily be achieved. This non-uniformity does not cause any shortcomings if the proton beam is distributed uniformly over the target surface.

In addition to the advantages of using a teflon decomposition vessel mentioned above, the number of manipulations during target preparation were kept to a minimum, so contamination was minimized.

In any boiling process, large amounts of material can be lost when drops of solution leave the surface of the sample, this effect of kinetics was eliminated using the sealed vessel. In addition, use of teflon container avoids dissolution of trace metals from the container wall. Hence, we conclude that using teflon bomb for digestion of biological material is by far the most convenient.

All the bovine liver standard targets were made by depositing 3 μl of the digested solution in a well controlled region of the Nuclepore

filter using an Oxford micropipettor. The Nuclepore filters were stretched over a 1.5 cm diameter ring which was clamped to the target holder. The filters were then allowed to air dry in a clean atmosphere inside a dessicator, to prevent dust contamination. A single dust grain of medium size (1 μm) has a weight of about 10^{-12} g (Johansson, 1976); comparing this with trace elements present in ppm ranges show the serious effect of this and how even a short exposure to the atmosphere can cause problems.

Vacuum drying of the deposit was possible when it was required to accelerate the evaporation process.

It was found that the dehydrate deposits attached more rigidly to the Nuclepore than the other backing materials such as Kimfol or Mylar, that were investigated.

Because contamination is so important every effort was made to prevent it, first through the preparation process and then special attention was given to the sample handling prior to irradiation. All glassware was first washed with detergent then twice with diluted nitric acid and rinsed three times with deionized water. Deionized water was always used instead of distilled water, since much smaller concentrations of metal element contamination remain in deionized water (Valkovic 1975). The possibility of contamination from the acid was minimized by using ultra high purity acid (Aristar, BDH, Chemical Ltd, Workshire, England). The level of trace elements are typically given as Fe, 0.01 ppm; Cu, 0.005 ppm; Zn, 0.01 ppm. This represents a very small portion of the concentration of the elements of interest.

Tests were performed to check the reliability of the washing procedure and acid purity for trace element contamination. The acid was stored in all items used prior to target preparation and drops of this were placed on Nuclepore filter and analyzed in the usual way. The

resulting X-ray spectra were similar to that of the blank Nuclepore, in-dicating the contamination was negligible.

Extreme care was taken when handling the solvent, the digested sol-ution or the equipment. Rubber gloves were always worn. The digestion and deposition was carried out in a fume cupboard to exhaust the toxic gases released, and the digestion vessel was opened behind a safety screen.

6.4.1.2 Micro Slices of Tissue: Thin targets of brain tissue were made from frozen tissue samples. The bulk of the tissue was originally placed in a cryostatic microtome, which was kept at - 30°C. At this temp-erature the sliced tissue does not becomes irregular or adhere to the stainless steel blade, although a possibility of loosing a portion while slicing still exists. The slices were cut as 5 microns. Selected sec-tions were removed by cold forceps and placed onto a Nuclepore substrate. It was found that the hydrated tissue dried and formed a sufficiently strong bond with the Nuclepore such that no additional adhesive was re-quired.

Heart muscle tissues were washed with deionized-distilled water and alcohol, then strengthened by embedding with paraffin. The resulting block was sliced with a precision microtome using a stainless steel knife. Thicknesses as low as 5-15 microns were cut and floated in a bath of de-ionized water at 20°C. The Nuclepore was positioned on glass slides, then by dipping the glass slides into the water, and carefully manipula-ting the position and movement in the water, sections were attached onto the Nuclepore backing. The slides with the Nuclepore and tissue sections were then put in an oven of 55° to melt the wax and allow the tissue to become fixed to the Nuclepore filter. These tissues were deparaffinized prior to irradiation utilizing xylene. The Nuclepore with the tissue

section adhering to it was immersed into three different xylene solutions in order to remove the wax completely. The Nuclepore was detached from the glass slides using plastic forceps then mounted on the target frames prior to irradiation. All samples were kept and transferred in a dessicator.

From the view point of contamination the freezing method is more desirable than embedding with a hardening agent, as contamination may be introduced from using the paraffin and xylene. Although it is known that the use of a stainless steel blade introduces some contamination to the sliced tissue, no alternative facility is available with microtome instruments.

6.4.2 Thick Target Preparation: Thick specimens may be made by pelletizing powder or by exposing a thick cut of sample directly to the beam.

6.4.2.1 Thick Pellets: Specimens which can be dried or lyophilized and ground into a fine powder are often suitable for making pellets. Thick pellets were made from bovine liver powder NBS - 1577 as followed.

200 mg of the powder was transferred to the compression chamber of a 1.5 cm diameter stainless steel die. The powder was compressed into a rigid pellet at about 4000 N/cm^2 for about 2 minutes. The pellet was then ejected from the die by applying a steady force on the piston. Pellets with a smooth surface and mechanically strong were produced in this manner, no binder was necessary. Experiments carried out to analyze a set of 8 pellets showed a large level of contamination in all the analyzed pellets. This was ascribed to the stainless stell compression chamber and die. Therefore, both the die and the chamber were covered with a pure aluminium foil and further samples made. No evidence of contamination was observed upon analysis of these samples.

The pellets were mounted by using a small amount of an adhesive to attach them to an aluminium sheet. Aluminium backing was preferred to the usual backing due to its good heat conductivity. To prevent the pellets from absorbing atmospheric moisture and to protect them from contamination, they were stored and transferred in a dessicator containing silica gel prior to irradiation.

The accumulated charge during the irradiation of these pellets causes sparking if it is not conducted away before a large voltage is built up. This results in an intense background. Therefore, the pellets were coated with about 1000 A° of 99.99% pure aluminium to make them conductive. The authors, Walter et al (1974), F. Folkmann et al (1974) and others have found the continuous background radiation to increase considerably when the samples are good insulators. The spectrum of non-conductive pellet compared with that of a coated pellet, presented in Figure 6.4, shows that this phenomenon is observed clearly in this work. Moreover, the sensitivity could be further increased by inserting an absorber infront of the detector. This reduced the low energy X-ray signal in the detector and allowed an increase in proton current. The effect of the 10 μm aluminium absorber on the spectrum is shown in the same Figure.

The aluminium coating is very pure, thus careful pellet making should not add trace impurities. The problem of the impurities in the backing with these targets, is completely removed. In addition, one has a gain in the X-ray counting rate due to an increase in the irradiation mass of the sample.

6.4.2.2 Direct Preparation: Thick sections or thick pieces of bladder and kidney stones were cut directly from the bulk of the stone using a stainless steel blade. These were mounted on an aluminium sheet using glue. The front face of the mounted sample was coated with pure

Top spectrum:

100 x log (counts)

504
441
378
315
252
189
126
63
0

K_α
K_β
Cl
S
Fe_α
Fe_β
Mn
Cu
Zn

30 68 106 144 182 220 258 296 334

Channel Number

Bottom spectrum:

100 x log (counts)

540
472
405
337
270
202
135
67

K_α
K_β
S
P
Fe_α
Fe_β
Cr
Mn
Cu_α
Zn_α
Zn_β
As or Pb

30 68 106 144 182 220 258 296 334

Channel Number
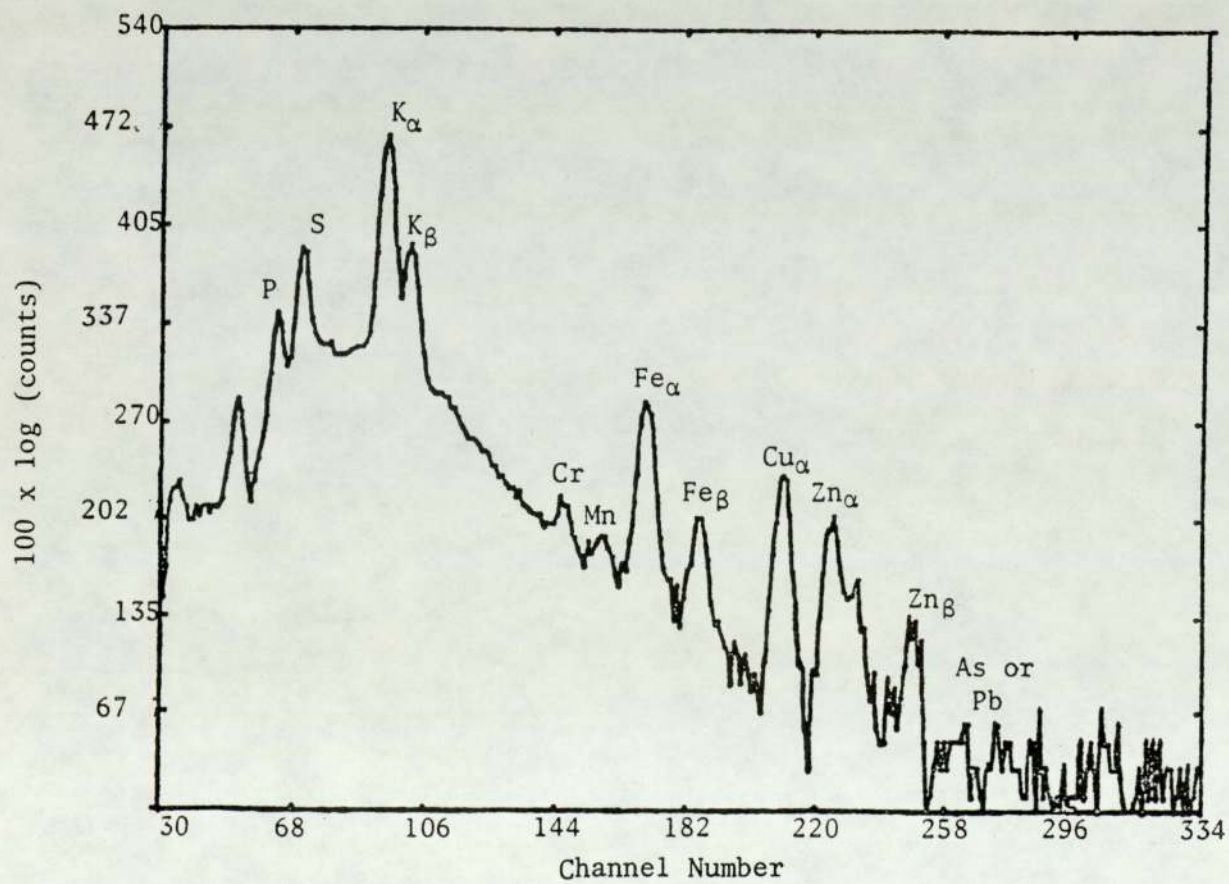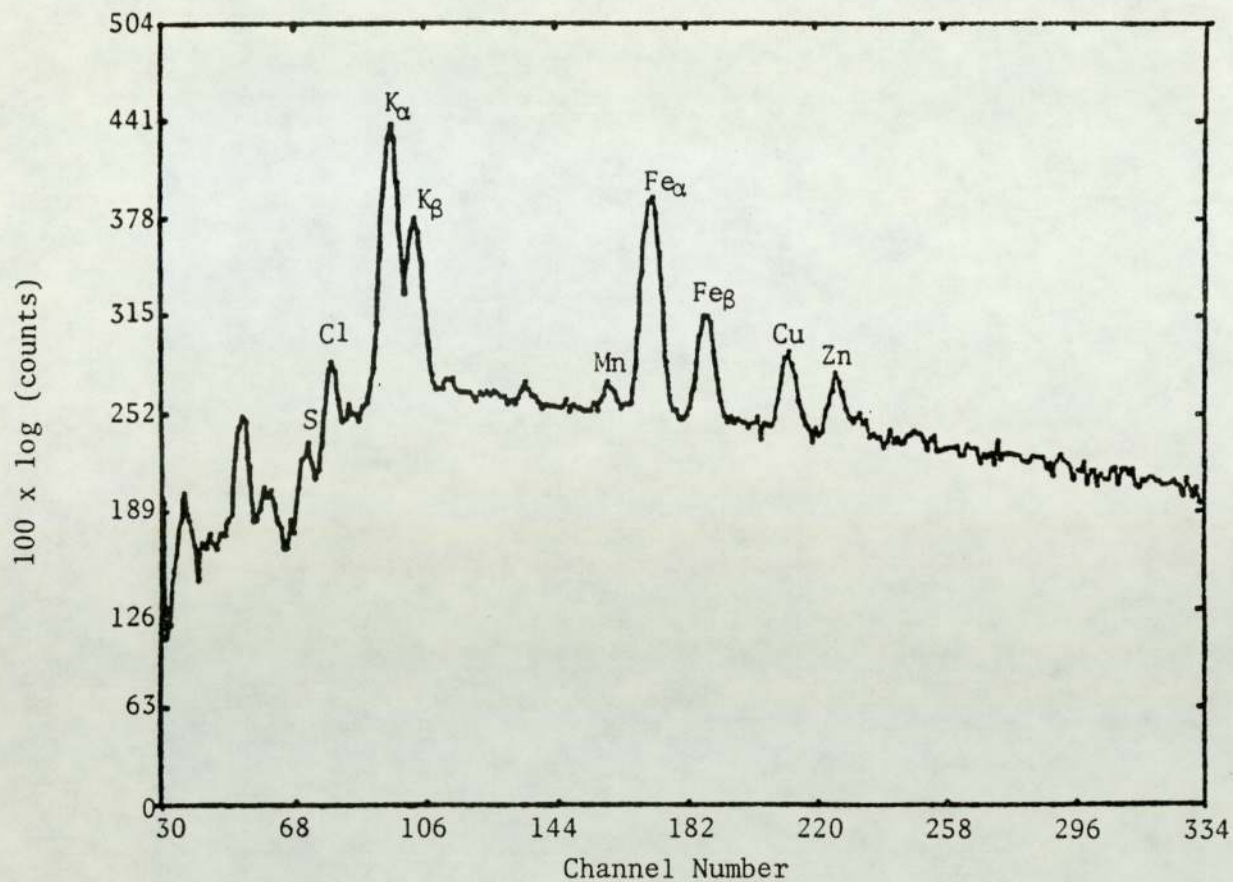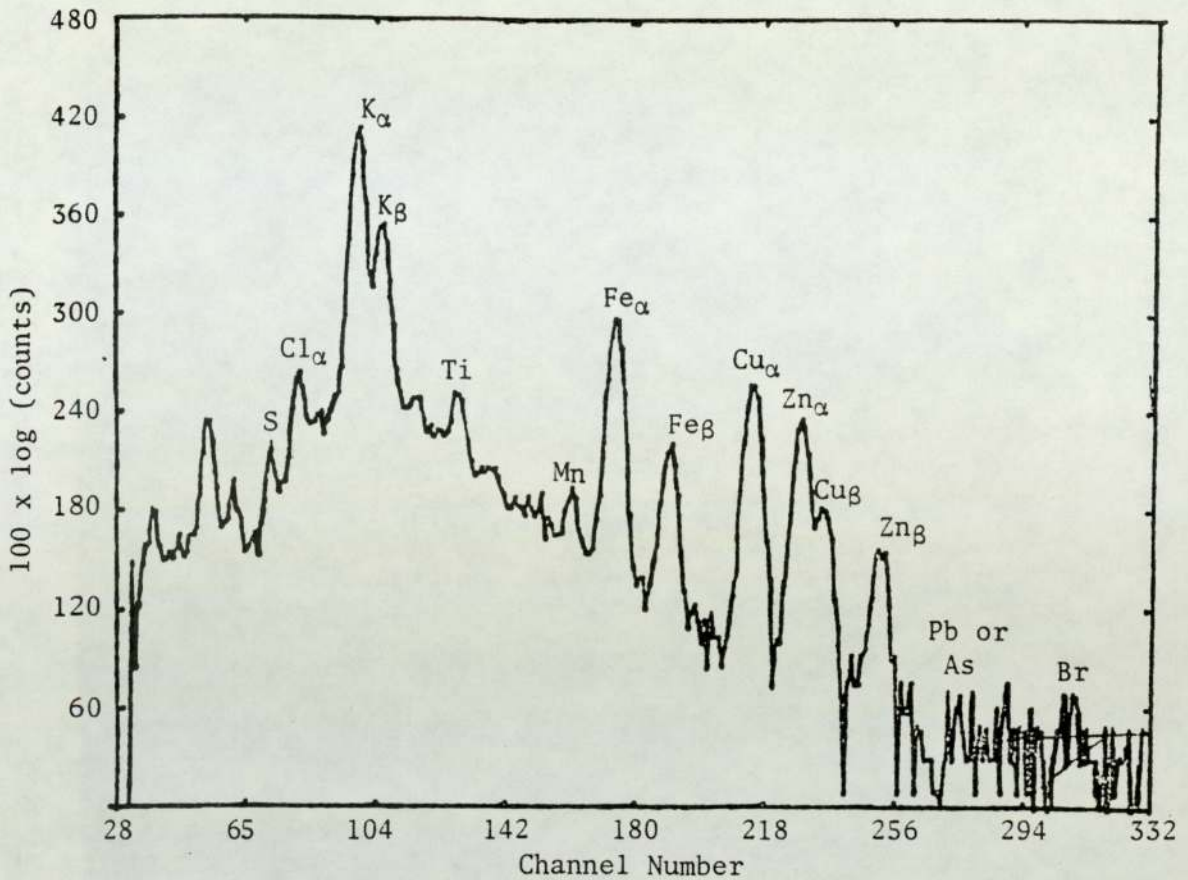
Figure 6.4   A: PIXE spectrum of uncoated pellet illustrating the
                   adverse effect of charge build-up with 10 μm
                   aluminium absorber placed infront of the detector

              B: PIXE spectrum of a conductive pellet coated with
                   aluminium, without any X-ray absorber

              C: PIXE spectrum of the pellet in Figure B with a 10 μm
                   aluminium absorber. Comparison of A and C demonstrates
                   the sensitivity improvement due to conductivity of the
                   pellet. Comparison of B and C illustrates the sensiti-
                   vity improvement achieved by placing an aluminium
                   absorber between the coated pellet and the detector.

aluminium to prevent charge build up. This type of sample preparation is the least demanding in terms of time and also it results in an un-touched surface (except for original sectioning). Sample handling and hence contamination are minimized. However, it should be borne in mind that the direct analysis of thick sections like that of thin sections will not give an average result for the whole organ due to the non-homo-geneous structure of this sample.

CHAPTER SEVEN

SELECTED APPLICATIONS FOR PIXE ANALYSIS

7.1   STUDIES ON HAIR SAMPLES

7.1.1   Introduction

Hair is a biological material that is readily obtained and easily collected without the requirement of special equipment or storage facilities. Large samples are normally available making the task of the analyst easier, moreover it is a stable dry sample which does not deteriorate. Hair is a protein tissue which contains trace elements of comparatively high concentration that reflect the long term biomedical history of the donor. These trace elements once incorporated into the hair are no longer in any dynamic equilibrium with the rest of the body. Thus, they should correlate to a large extent to the whole body content or the content in a specific tissue of the body, at a particular earlier time.

Hilderbrand et al (1974) discuss the question of extrapolating a body mineral history from hair analysis, which could provide information on the time distribution of elemental content as well as total elemental content.

The use of hair analysis as an indicator of body content is however hindered by surface contamination problems. These will be considered later.

In spite of the surface contamination problems, studies on certain elements suggested their possible insensitivity to environmental contaminants. Klevay (1970) reported that Zn concentration in hair is independent of environmental conditions and the majority of zinc in hair is assimilated through the diet, since human nutrition contains large concentrations of zinc. This was further supported by the work of Renshaw

(1972), Hambidge et al (1972), Valkovic (1973), Jolly et al (1974) and F. Khan (1979).

Furthermore, Obrunski et al (1972) observed from neutron activation analysis of different segments of individual human hair that Co, Zn and Hg concentrations were fairly constant in hairs from different parts of the head of an individual. Thus the criteria for characterization of hair may be satisfied in the case of three elements, vis Co, Zn and Hg. However, great variations were observed from hair samples of the population at large.

The usefulness of hair analysis as an index to biological processes within an organism has been demonstrated by the work of several authors.

According to Valkovic (1977) the balance of the ratios of the elements Ca-Mg, Ca-K, Ca-Mn and Ca-Zn govern most of the biological activities of the body, such as nerve cell activities, hormonal excretion, enzyme action, the quality of the sperm, muscular tone, and skeleton structure. Distortion of these ratios can easily be detected with hair analysis.

It is well known that trace element levels in hair during pregnancy deviate significantly from normal values (Valkovic 1973).

Kaptio et al (1974) suggested that alteration in hair elemental composition may serve as a diagnositc aid in cystic fibrosis, celiac disease, intoxication with heavy metals and severe nutritional deficiencies.

Deviations of elemental ratios in hair were shown by Larsen et al (1974) to correlate with arthritic condition in females.

Since hair is porous, fibrous and hygroscopic, various soluble substances along with water or other liquids (sweat, shampoos and cosmetics) including of course the ions of trace element pollutants, can enter hair. Thus, the composition of hair is determined by the entry of substances not only from the blood stream but also from the external surface of hair,

Berg et al (1967) and Steinnes (1975). Consequently, hair analysis can play an important role in monitoring the contamination of human beings with environmental pollutants. Poisoning by heavy metals can be easily detected by their build up in growing hair. Kapito (1967) has shown that the detection of lead in hair provided an additional confirmation to the diagnosis of mild lead poisoning in children. Renshaw (1972) measured the variation in lead concentration along a single hair which was found to increase significantly from the root to the top of the hair which suggests that lead enters the hair by deposition from its surface followed by diffusion into the hair structure.

The results of several experiments, e.g. Yurachek (1969), Gradus (1973) on the composition of normal hair showed that about 27 trace elements ranging in concentration from 0.1 to 1000 ppm are present in normal hair. The term "normal" as applied to hair is a relative one since the trace element concentration varies with geographical location, Mahler (1970), Hammer (1971), El-Dukhakhny (1972), Roberts (1974). This in its turn indicates the importance of environmental effects. Table 7.1 illustrates the various values of different elements specified to characterize normal hair. This shows that normal and accepted laboratory standards are not yet established and indeed may be impossible to establish.

As mentioned earlier, the concentration of trace elements in human hair depends largely on personal covariations. Obrusnki(1972) confirmed that such characterization is of great assistance in forensic investigation. Perkons et al (1966) reported accurate trace element results for hair and suggested that identification of hair samples could be made on the basis of trace element content. Petering et al (1971) reported logarithmic relationships between copper and zinc levels in hair with age.

TABLE 7.1

NORMAL CONCENTRATIONS OF ELEMENTS IN HUMAN HAIR IN ppm

REPORTED BY DIFFERENT AUTHORS

Sample	Mean ± SD or Range (µg/g)				
	Mg	Ca	Cu	Zn	Ref
Human	10-101	188-4900	4-128	9-569	Widdowson (1964)
Female		750-9750	5-70	100-700	Coleman (1967)
Male		750-9750	5-70	100-700	" "
Normal	10-75		9.7-24.2	143-205	Harrison (1969)
Female	105±16		67±12	195±13	Schroeder (1969)
Male	58±11		18±12	165±9	" "
Woman				167	Klevay (1972)
Man				142	" "
Healthy Subject			13±7	195±69	Briggs (1972)
Female			22±18	205±93	" "
Male			16±9	184±66	" "
Female	380±200	620±260	18±5		Othman (1978)
Male	320±200	510±250	18±7		" "
Female	11.2-1412	77-10887	7.7-151	55-905	Imahori (1978)
Male	9.8-405	157-3184	5.4-184	57-734	" "
Female	1.4-3	500-1750	16-150	100-180	Barlow (1980)
Male	1.6-3.6	400-1150	16-140	100-160	" "

7.1.2 PIXE Analysis of Hair

The trace element content of hair is often of special interest because of the above mentioned reasons. PIXE is one of the many different analytical techniques used for studying elemental concentration of hair. A number of analyses of hair samples using PIXE have been reported in the literature, Valkovic (1973, 1977), Cookson et al (1975), Horowitz et al (1975), Chen et al (1981) serve as examples.

Generally, two main approaches have been adopted in hair analysis by PIXE. The first approach is using physical or chemical means to break down the structure of hair samples, in order to provide a homogenized sample. One of the obvious advantages of this method is in determining a reliable average value of a trace element, extracted from rather large quantities of the hair specimen. However, all information relating element concentration with hair structure is lost with homogenized samples.

The alternative approach is the non-destructive analysis of hair. Hair strands are analyzed directly using longitudinal scanning and radial microbeam scanning of hair cross-sections. However, a hair strand of ~ 0.01 mm diameter is a thick sample and difficulties in the interpretation of data arise from the energy loss of the incident particles with penetration depth, X-ray self absorption and a lack of knowledge of the distribution of elements in the sample. In addition, hair from different subjects vary by a factor 5 in linear density. Each X-ray analysis, therefore should be accompanied by an accurate mass determination. The problems associated with the direct analysis of hair by PIXE have been discussed by Whitehead (1979). A mode for calculating correction factors when using PIXE analysis for hair strands is proposed by Montenegro et al (1980).

Furthermore, measurements of the characteristic X-rays produced in the analysis of a surface region of hair or a specific cross-section of

hair under proton bombardment are not necessarily representative of the bulk material. However, the use of proton beam in particular, a highly focused beam to scan the length of a strand of hair, can provide a time record of the body's ingestion or exposure to heavy metals.

Whitehead et al (1979) followed the first approach; for preparing their samples they wet digested hair directly in nitric acid. Chen et al (1981) have ashed hair samples from mentally defective children using a plasma incinerator and dissolved the samples in nitric acid. A comparison of the results obtained from normal and defective children for both Fe content and Cu/Zn ratio were quite different. Baptisa et al (1981) compared the results obtained from analyzing scalp dissolved in nitric acid with those obtained from the direct analysis of the scalp. The two sets of results were of the same magnitude. However, the first method proved to be more convenient.

Khan (1979) analyzed pellets made from pulverized hair for the determination of the chromium concentration for different catagories of people, including a control group and workers in a chromium plant. A high chromium concentration of 60-1000 ppm was found in the hair of adult workers, $\sim$ 10 ppm for children and 70 ppm for housewives and students. Bodart (1978) froze hair samples in liquid nitrogen and then fabricated pellets from the ground material. Following this approach samples from 100 individuals were studied, 50 of which were suspected of having Cr contamination and showed a concentration of 10-970 ppm Cr. The other half were a control group and had 9 ppm or less Cr. Detection of environmental contaminations was confirmed by these studies of Cr concentrations in human hair samples.

Henely (1976) analyzed individual hair roots directly from 23 school children in connection with a nutrition study and found that eight elements determined in hair roots (Si, P, Cl, K, Ca, Zn, Mn and Fe) could be

- 189 -

used in assessing one or more of the nutrition status, i.e. height, weight, haemoglobin, serum iron, etc. Moreover, the study gave further evidence that the trace element content of hair changes as a result of dietary manipulation.

Rendic et al (1976) and Lodi et al (1978) both independently determined elemental concentrations relative to zinc employing the direct irradiation method. It was found by Lodi that higher Pb levels were present in the hair of people living in the capital compared with the levels observed in village subjects. In Rendic's investigations, of the variation of elemental composition along the length of hair strands, elemental to zinc ratio for Pb, Br, Sr and As increased from the roots to the outer end of hair, indicating that elements are pollutants in the subjects environment.

Horowitz et al (1976) have employed a proton microprobe to scan the length of human hair. This method can provide a time record of the body's ingestion or exposure to heavy metals. The hair samples in their experiment were taken from an arsenic inhalation exposure victim. The results for As, Fe and Zn are shown in Figure 7.1, where the pronounced correlation between the As and Zn concentration can be seen, while the Fe concentrations remained constant.

Jolley et al (1974) have used a collimated proton beam to scan hair strands obtained from school children, to study the history of exposure of the donor to toxic trace metals. Scans showed a continual build-up of Pb as a function of distance from the root. The concentration of Zn was found to be constant. The variation of elements along the length of hair with resolution in the millimeter range have been studied by Pearson et al (1971), Renshaw et al (1972) and Valkovic et al (1973); these results show the variation of the relative concentration as a function of the distance from the scalp.
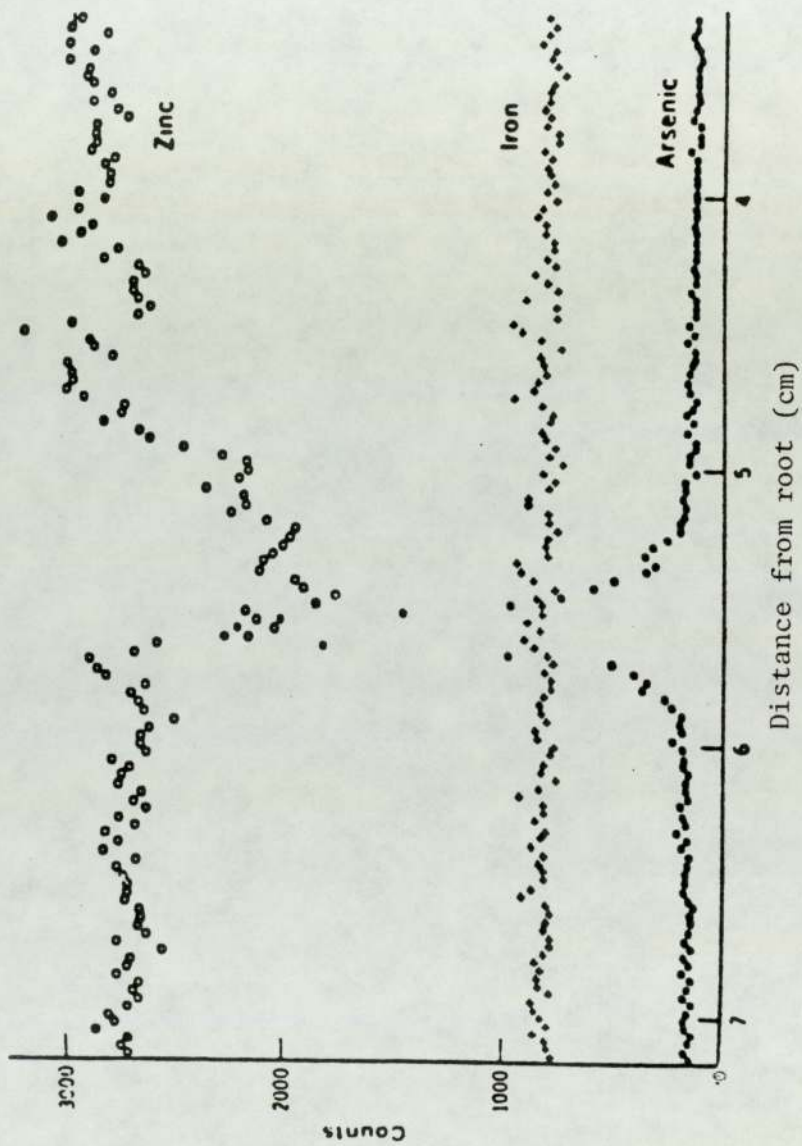
Figure 7.1   Trace element distributions in a single hair strand from a victim of arsenic inhalation. The spacing between successive points represents approximately one day's growth (Horowitz, 1976)

Cookson et al (1975) employing a 4 μm diameter proton beam, measured the radial concentration of different trace elements in a segment of hair which enabled them to differentiate between trace elements of exogeneous and endogeneous nature.

The above study revealed a homogeneous concentration of the trace elements, S, Ca, Zn which are thought to be unaffected by external contaminants.

7.1.3 Experiments on Hair Samples

The purpose of this chapter is illustrative in nature. It is concerned with demonstrating the applicability and capability of the present PIXE system in dealing with a variety of samples. Measurements have been made on a variety of biological samples to evaluate the effectiveness for trace element identification and quantification.

The present analysis on hair samples was initiated as a result of clinical interest in the analysis of hair. The hair samples used in the present work were supplied by Fazackerly General Hospital, Liverpool, England. The hair was taken from the heads of a group of mentally defective females who had resided for a long period of time in the same hospital environment.

Since this group of samples were the first true samples to be analyzed by this system, it was decided in addition to PIXE to analyze the samples by Atomic Absorption Spectroscopy. Hence, a test of the ability to perform quantitative analysis was afforded and the confidence needed to discuss the results could be assured.

It is clear from numerous studies that values for elements investigaed in human hair can be unreliable,Hilderbrand (1974), due to the effect of several variable factors such as hair washing and hair treatments, and the use of wave lotion,laquers and deodorant sprays. To

reduce this problem it is advantageous to control the washing process and
hair treatment of the samples to be analyzed well before cutting. For
this reason the patients, whose hair was to be investigated and inter-
compared in this study, used the same shampoo and their hair had not been
exposed to any treatment. In addition, they were exposed to the same
environmental condition for a long period of time, long enough to assure
that the bunch of the hair studied was grown and treated under these
control conditions. Since washing hair samples before analysis appears
to remove a considerable portion of the true hair mineral, the hair sam-
ples investigated in this study were not washed before digestion and an-
alysis. These samples represent as nearly an ideal sample of control hair
as could reasonably be expected.

About 20-30 g of hair was taken from each patient from different
parts of the head. After a proper mixing, 5 g was taken from each bunch.
Each segment of hair was cut into $\sim$ 3 mm or smaller pieces, using clean
stainless stell scissors and then mixed thoroughly. All the samples from
the six patients were prepared separately using the same ashing procedure.
100 mg of hair was digested using 4 ml nitric acid, following the method
discussed in section 6.4.1.1.3.

As discussed previously, to test the applicability of any technique
its reproducibility has to be verified. Thus, from each of the six dif-
ferent prepared samples, RC, RD, RE, RF, RG, RH, 2 sets of 7 replicate
targets were made by depositing (5-6) μl samples onto both Nuclepore and
Kimfol backings.

TABLE 7.2

PARAMETERS EMPLOYED FOR ANALYSIS OF HAIR SAMPLES

E_p (MeV)	I (nA/cm^2)	Collected charge	Absorber	Time per irradiation	Proton beam area	Chamber Pressure
2.37	80 - 100	25 μC	7 μm Al	20 - 25 min	0.255 cm^2	10^{-5} torr

A great deal of care was taken to ensure that the targets made were thin, while a fair amount of sample was deposited to ensure a moderate count from the trace elements. The spot deposits were made smaller than the beam area to ensure that the entire deposit was irradiated. For irradiation of these hair samples the experimental conditions given in Table 7.2 were employed.

TABLE 7.3

TYPICAL RESULTS OF X-RAY COUNTS FOR PREDOMINANT ELEMENTS

FOR SEVEN TARGETS MADE FROM THE HAIR OF THE SUBJECT RD

Element / Sample	S ($K_\alpha + K_\beta$)	Ca	Fe	Cu	Zn
RD_1	2379	9005	138	301	747
RD_2	2403	11037	198	308	671
RD_3	2225	9877	198	292	704
RD_4	2542	9685	205	257	686
RD_5	2311	9591	173	275	719
RD_6	2280	8654	171	298	670
RD_7	2213	10699	139	254	820
Mean	2336	9755	175	283	717
c.v %	5	9	16	8	7

TABLE 7.4

MEAN VALUES OF X-RAY COUNTS WITH THE ASSOCIATED C.V FOR

DIFFERENT ELEMENTS DETECTED IN THE SIX SAMPLES ANALYZED

Sample / Element	RC Mean	RC C.V %	RD Mean	RD C.V %	RE Mean	RE C.V %	RF Mean	RF C.V %	RG Mean	RG C.V %	RH Mean	RH C.V %
S	2587	9	2336	5	2460	9	1919	14	3032	15	2856	10
Ca	7563	7	9755	9	7765	8	3437	12	7487	12	4149	12
Fe	987	11	175	16	743	9	112	18	207	18	194	16
Cu	304	16	283	8	328	14	90	14	151	7	136	10
Zn	813	10	717	7	862	10	621	13	800	9	736	8

7.1.3.1 Results: Typical results obtained from the seven targets de-
posited onto Kimfol for the patient RD for most of the predominant elements
S, Ca, Fe, Cu and Zn are presented in Table 7.3. This table illustrates
the individual spread of X-ray counts obtained and also gives the mean and
coefficient of variance.

Table 7.4 presents the mean value and relative standard deviation ob-
tained for the same elements for all six patients. The observed variations
within the groups are larger than the computed statistical uncertainty which
is partly determined by the background underlying the characteristic X-ray
peak and partly by the total counts in the peak itself. This is ascribed
to the variation in the samples themselves, such as any gross non-homoge-
neity inaccurate sample size due to pipetting. In addition, the amount of
material impurity present on the target backing, which interferes with the

true spectra of the targets, varies considerably among various targets. Possible errors due to interfering X-rays are discussed later. However, a reasonable reproducibility was obtained as it can be seen in Table 7.4. The only exception is in the case of Fe K_α line where the c.v is occasionally as large as 18%. The S X-ray is severely attenuated by the absorber and target itself before the detector, and its characteristic peak is located on steeply rising background. Thus the uncertainty given is about 50%. We finally approximate the overall reproducibility for one standard deviation from the mean to be about 7 - 18% depending on the element.

Figures 7.2 through to 7.7 show the pulse height spectra from the PIXE analysis of six different specimens, each taken from an individual hair sample (i.e. RC, RD, RE, RF, RG and RH). Peaks corresponding to between eight and thirteen different elements, ranging from P(Z=14) to Pb (Z=82), were identified in these spectra. The energies of the X-rays detected vary from about 2 keV to 17 keV. It should be noted that the vertical scale of spectra is logarithmic and therefore visually enhances regions of low counts as well as the size of the background contribution relative to the peak amplitude. The number of counts associated with each specified peak was integrated after subtraction of the associated continuum background as described earlier.

Most of the trace elements impurities found in the backing material appear in the integrated spectra and in certain cases of low concentration such as Fe account for 30% of the observed signal. Therefore, the amount of impurity in the backing material was carefully determined from a group of ten backings (see section 5.2.4) and the mean values of these impurities were subtracted from the corresponding peaks in the target spectra. The net X-ray counts were then converted into absolute abundance using the following relation:

Figures 7.2 through to 7.7

Typical pulse height spectra from the analysis
of six targets each made from the wet digestion
solution of one of the six hair samples studied
i.e. RC, RD, RE, RF, RG and RH respectively
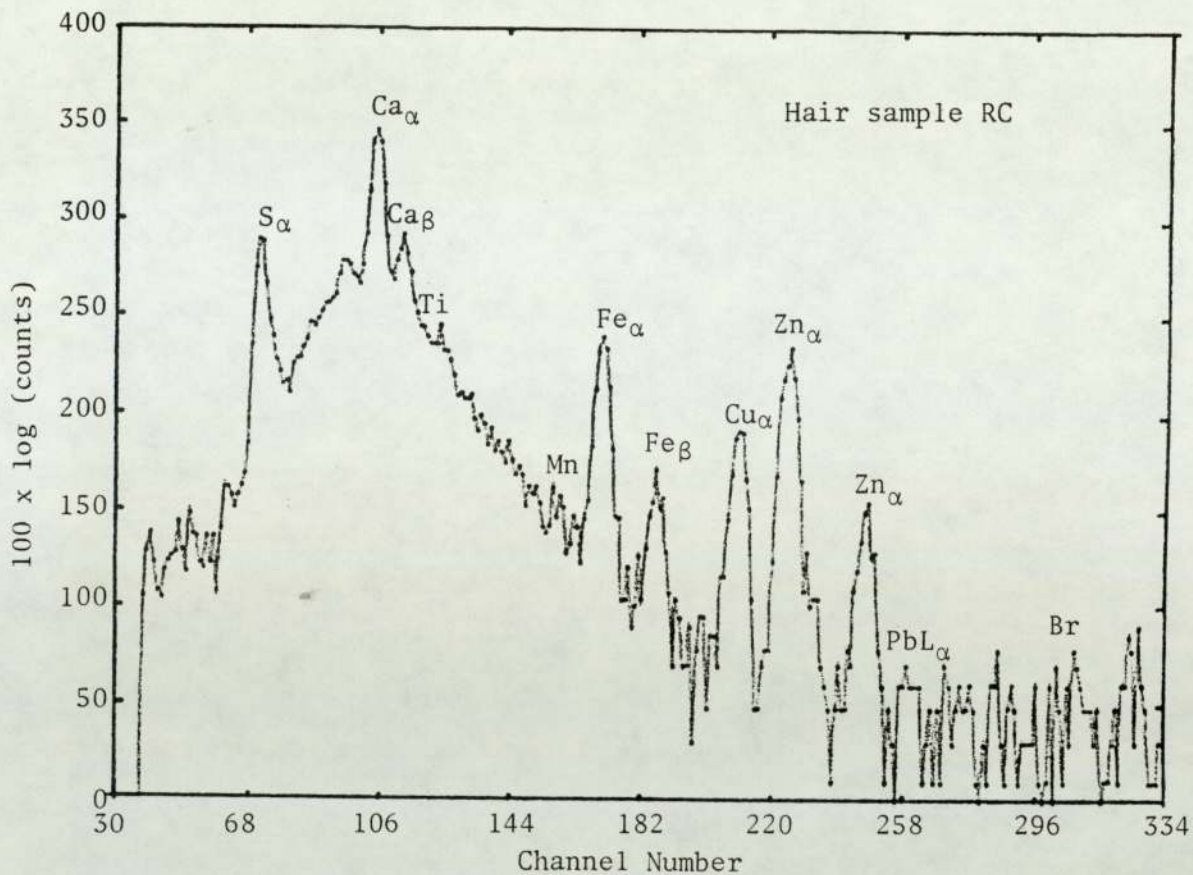
Figure 7.2
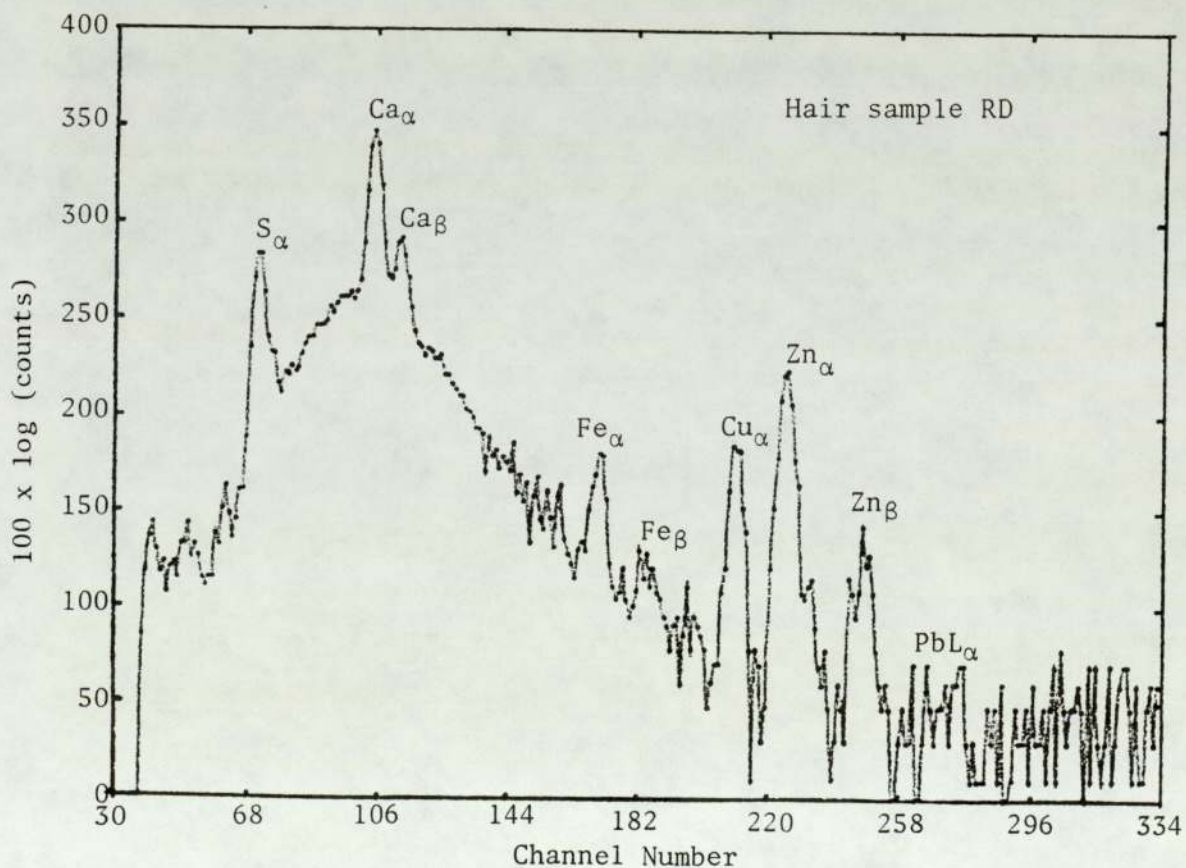
Figure 7.3
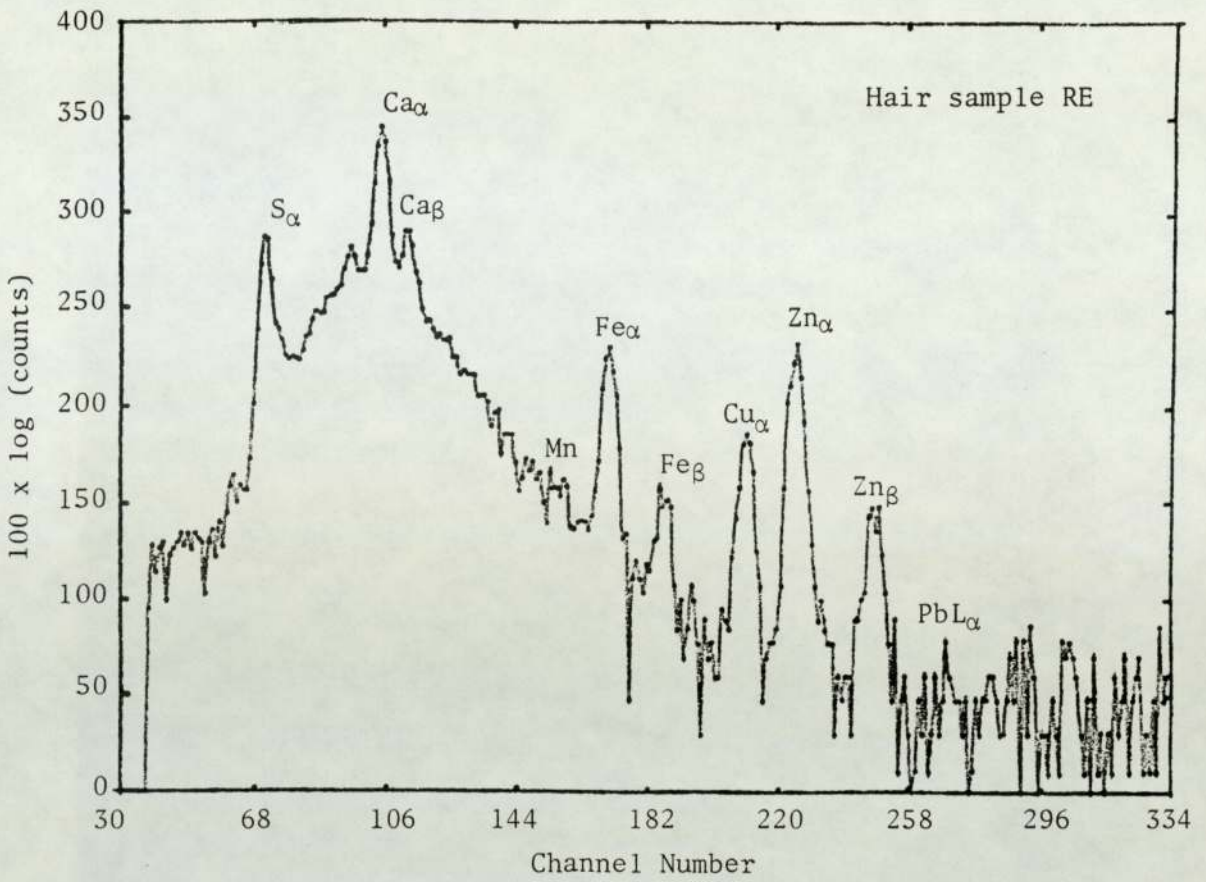
Figure 7.4

Figure 7.5

- 199 -
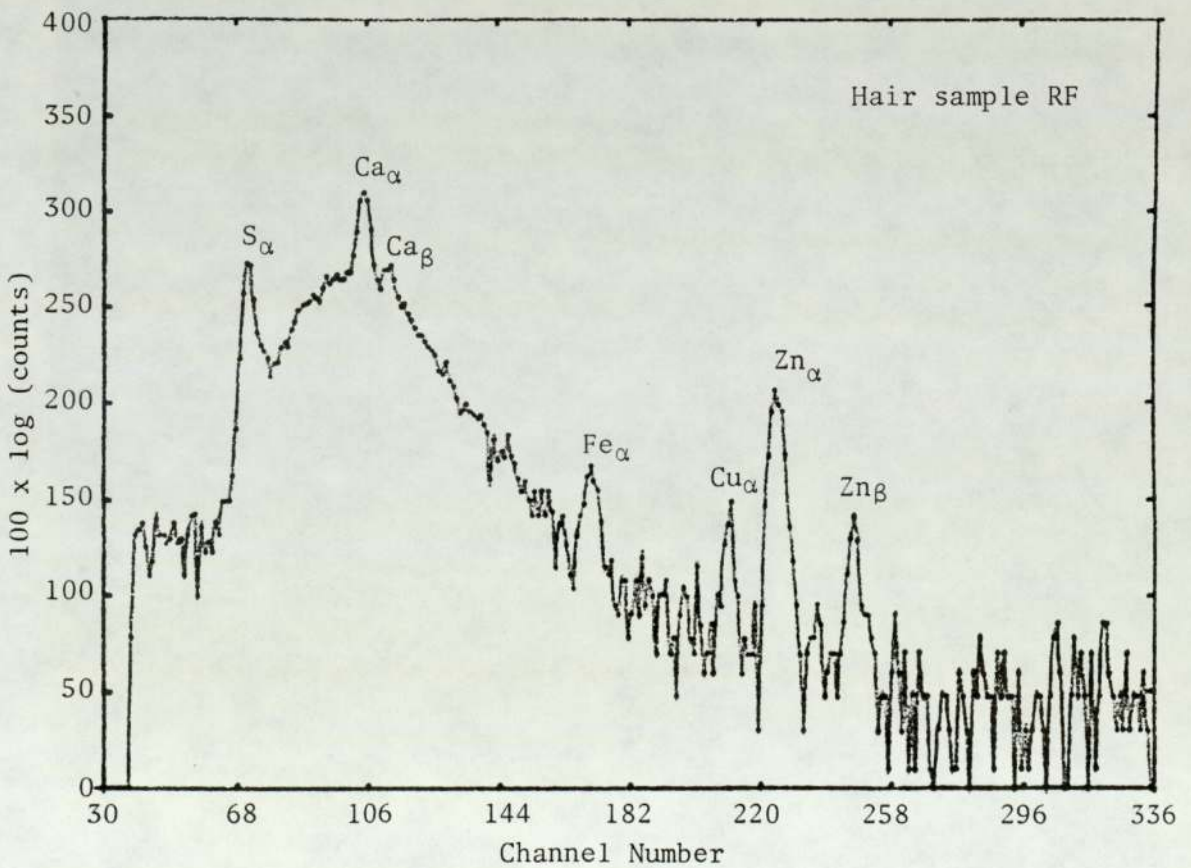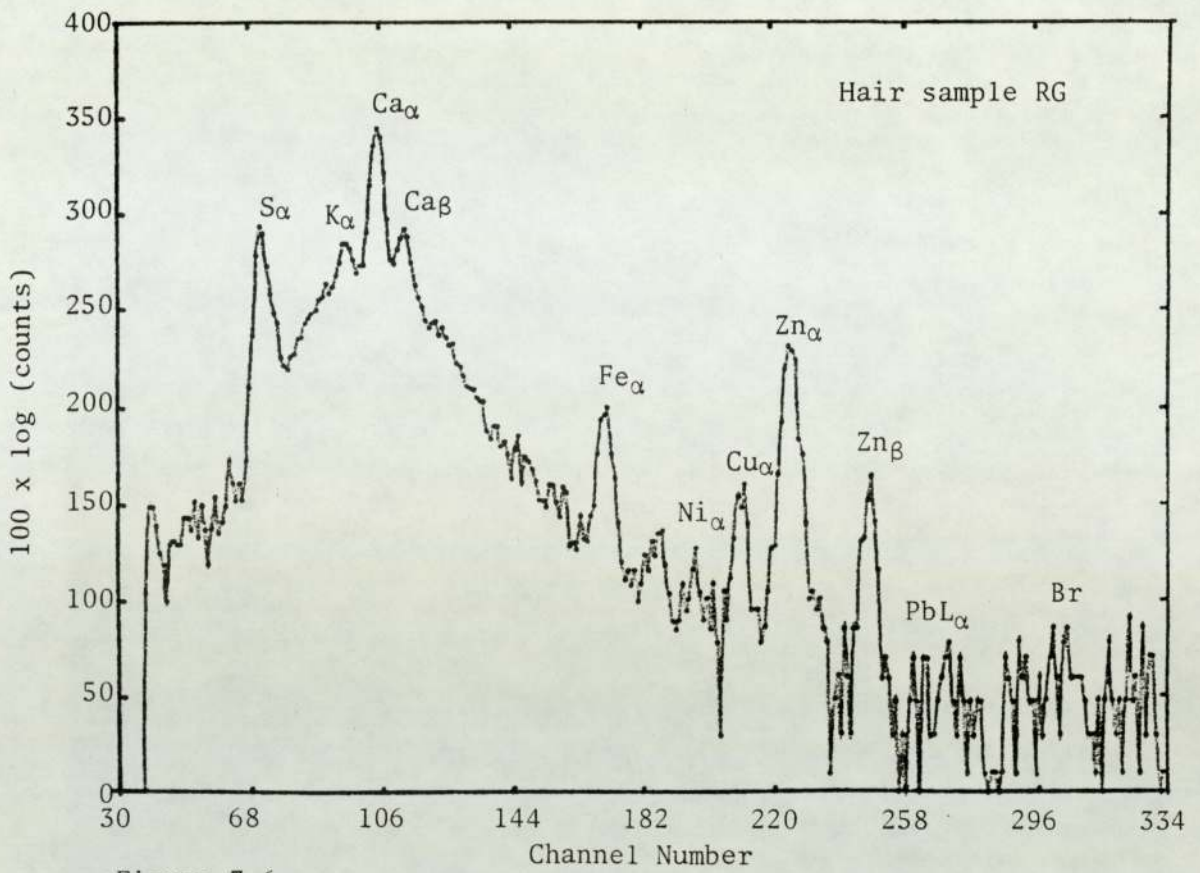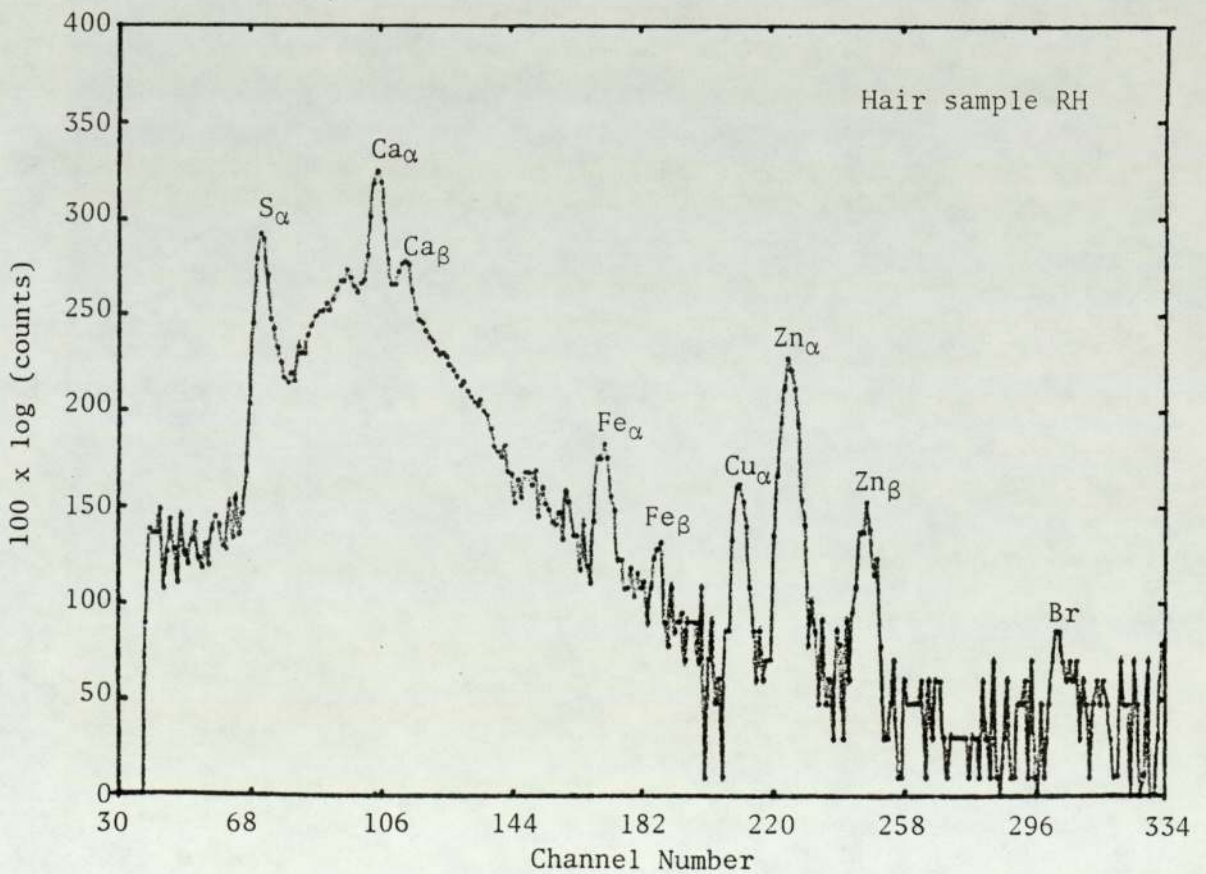
Figure 7.6

Figure 7.7
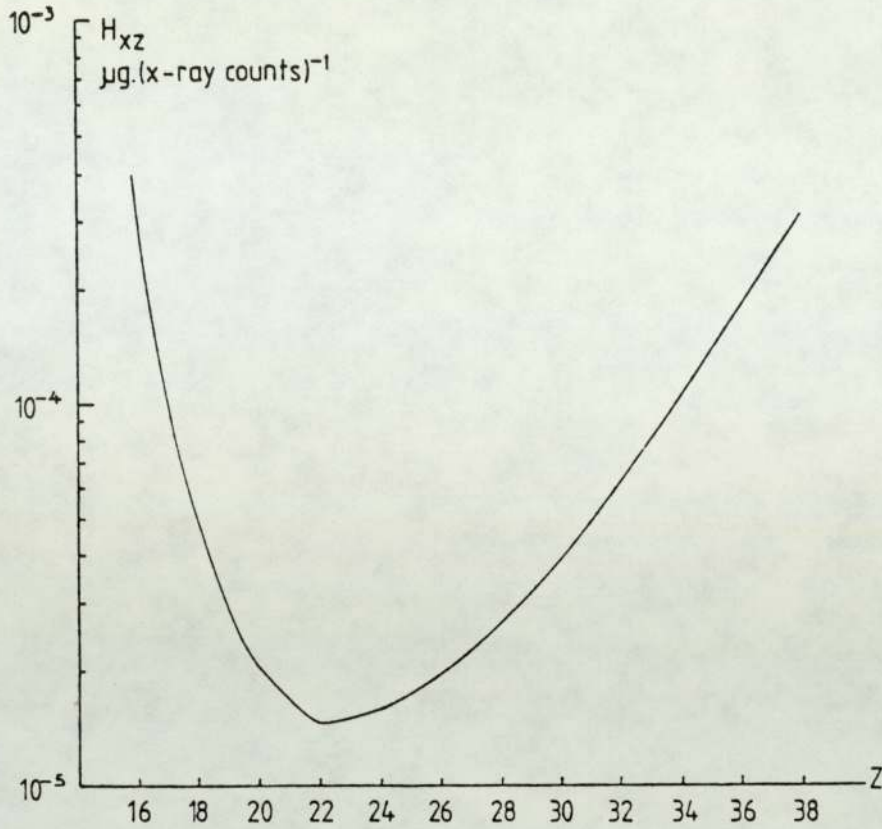
Figure 7.8   A plot of H_{xz} values vs Z.
This is associated with this particular
experimental conditions with the exist-
ence of 7 μm aluminium absorber infront
of the detector

Absolute mass (μg) = H_{xz} x (X-ray yield/25 μC protons)

$$M_{sm} = (\frac{N_x}{N_p}) \times \frac{1}{C_{Al}} \times \frac{1}{F_{xz}} \times dS_b$$

$$= N_x \times [\frac{dS_B}{N_p \ C_{Al} \ F_{xz}}]$$

$$M_{sm} = N_x \times H_{xz}$$

where $$H_{xz} = \frac{dS_b}{N_p \ C_{Al} \ F_{xz}}$$

and all the symbols and subscripts are as defined previously.

For this particular experimental situation H_{xz} was experimentally

determined for different elements and plotted against Z, as shown in Figure 7.8. Thus the mass M_{sm} was then determined directly by multiplying N_X by the corresponding H_{XZ} value from the graph, which is a smoothly varying function of Z. The concentration of the element of interest was found from dividing by the dry mass of hair deposited on the backings. The mean concentration of all detected elements obtained are tabulated with the associated absolute error in Table 7.5 through to 7.10. Also included are the AAS results, which are discussed later.

It should be noted that the results presented in these Tables on S, Ca, Zn, Cu, Fe were obtained as an average from the measurement derived from seven targets made from the hair of one person. In an attempt to find out whether other trace elements other than those mentioned were present and to improve the data for those already observed, the series of 7 single spectra from each sample were added together in order to increase the sensitivity. The new trace elements which were detected in the composite or sum spectra were K, Ti, Cr, Mn, Ni, Se, Br, Pb and Mo. The peaks of most of these elements were hardly discernible above the background in the individual spectra. Other elements such as Ni and Mn could not be observed in any individual spectra.

It was found that Fe, Cu, Zn were present in relatively large amounts in all the six hair samples, while strong Ca and S peaks were also observed. Small amount of Mn, Ni and Br were determined in all the cases, Pb and Cr were detected in half of the samples. But Se was seen in the hair sample of two of the patients, while a very small amount of Mo was found in just one of the samples and a relatively large amount of K was detected in one of the other samples. A fair amount of P was also detected in hair samples of one of the subjects. The amount of S detected in all the analyzed samples from the six patients tended to remain constant.

TABLE 7.5

MEASURED ELEMENTAL ABUNDANCES IN ppm

DRY WEIGHT BASIS IN HAIR SAMPLE RC

Element	AAS The range (µg/g)	PIXE conc.(µg/g) ± abs.err.
S		3198 ± 1535
K		-
Ca	627 - 607	683 ± 89
Ti		10.4 ± 1.7
Cr	< 0.75	2.1 ± 0.74
Mn	0.7 - 0.3	3 ± 0.73
Fe	2.5 - 2.4	86 ± 8
Ni		2.1 ± 0.51
Cu	39.2 - 35.7	44 ± 4.7
Zn	113 - 112	146.2 ± 13.6
Se		8.78 ± 3.9
Br		7.37 ± 2.16
Pb	< 2.0	13.5 ± 2

TABLE 7.6

MEASURED ELEMENTAL ABUNDANCES IN ppm

DRY WEIGHT BASIS IN HAIR SAMPLE RD

Element	AAS The range (µg/g)	PIXE conc.(µg/g) ± abs.err.
S		3130 ± 1532
K		-
Ca	943 - 994	955 ± 127
Ti		-
Cr	< 0.75	5.8 ± 0.96
Mn	0.68 - 0.70	2.4 ± 0.81
Fe	2.5 - 2.3	16.5 ± 2.7
Ni		2.9 ± 0.59
Cu	42.7 - 42.6	44.8 ± 4.88
Zn	113 - 117	138 ± 12.9
Se		-
Br		8.4 ± 2.34
Pb	< 2.0	10 ± 1.1

TABLE 7.7

MEASURED ELEMENTAL ABUNDANCES IN ppm

DRY WEIGHT BASIS IN HAIR SAMPLE RE

Element	AAS The range (µg/g)	PIXE conc.(µg/g) ± abs.err.
S		2887 ± 1409
K		-
Ca	543 - 579	667 ± 87
Ti		-
Cr	< 0.75	-
Mn	0.25 - 0.32	1.6 ± 0.64
Fe	3.9 - 3.1	61.6 ± 6.0
Ni		1.40 ± 0.46
Cu	31 - 29	45.20 ± 4.78
Zn	150 - 149	145.80 ± 13.47
Se		0.6 ± 0.2
Br		11.3 ± 2.3
Pb	< 2.0	2 ± 0.3

TABLE 7.8

MEASURED ELEMENTAL ABUNDANCES IN ppm

DRY WEIGHT BASIS IN HAIR SAMPLE RF

Element	AAS The range (µg/g)	PIXE conc.(µg/g) ± abs.err.
S		2520 ± 1231
K		-
Ca	377 - 389	330.6 ± 43
Ti		-
Cr	< 0.75	-
Mn	< 0.1 - 0.2	2.23 ± 0.34
Fe	2.4 - 2.2	10.4 ± 2.37
Ni		1.5 ± 0.5
Cu	14.5 - 14.6	13.8 ± 2.4
Zn	108 - 111	115 ± 11
Se		-
Br		9.94 ± 2.38
Pb	< 2.0	-
Mo		-

TABLE 7.9

MEASURED ELEMENTAL ABUNDANCES IN ppm

DRY WEIGHT BASIS IN HAIR SAMPLE RG

Element	AAS The range (µg/g)	PIXE conc.(µg/g) ± abs.err.
S		3998 ± 1951
K		76.8 ± 19.8
Ca	741 - 721	722.8 ± 95
Ti		-
Cr	< 0.75	1.86 ± 0.80
Mn	0.8 - 0.4	3.50 ± 1.78
Fe	3.9 - 4.1	19.3 ± 3.0
Ni	-	1.67 ± 53
Cu	27.6 - 25	23.1 ± 3.12
Zn	129 - 131	152 ± 14
Se		-
Br		11 ± 2.44
Pb	< 2.0	-

TABLE 7.10

MEASURED ELEMENTAL ABUNDANCES IN ppm

DRY WEIGHT BASIS IN HAIR SAMPLE RH

Element	AAS The range (µg/g)	PIXE conc.(µg/g) ± abs.err.
S		3711 ± 1811
K		-
Ca	398 - 407	404 ± 53.7
Ti		6.9 ± 1.67
Cr	< 0.75	-
Mn	0.2 - 0.1	2.08 ± 0.77
Fe	2.2 - 2.3	18.8 ± 3.03
Ni		1.87 ± 0.55
Cu	19.5 - 23.6	22 ± 3.03
Zn	117 - 115	146.7 ± 13.7
Se		-
Br		12.2 ± 1.9
Pb	< 2.0	-

Note: - sign indicates that the element was not detected

The general trend of the abundances of these elements in hair of these six patients are shown in Figures 7.9 through to 7.14.

An important indication that we were effectively dealing with thin targets, where there is no significant matrix effect due to thickness or non-uniformities in thickness, is the consistency of the observed Ca/Zn and S/Zn ratios in the replicate targets. The mean values of Ca/Zn and standard deviations for the 7 targets for each sample were satisfactory

Both Ca/Zn and S/ Zn show a great deal of sensitivity to thickness due to the large target absorption coefficient for S and Ca X-rays. Moreover, the agreement between these results with those of the established method as it will be discussed later, is another confirmation that the targets are thin.

The results obtained for elemental levels in the hair samples are compared with the normal levels reported by Barlow (1980) which are shown in Table 7.11. Some of the values shown in this Table have already been presented in Table 7.1. Inspection of this Table clearly indicates that the data obtained by Barlow are in reasonable agreement with the published results of other authors. It should be noted that the data of Widowson (1964), Coleman (1967) and Imahor (1978) show large deviations from the general trends.

The results obtained for Mn, Zn and Pb are in agreement with the normal values for all the hair samples studied. The values for Fe are in agreement except for the two samples RC and RE which are higher than the normal level. Ca values for RH and RF are lower than the expected, however a good agreement was obtained for the rest of the samples for this element. A good degree of agreement for Cu was obtained, the only exception to this was RF which is slightly lower than the normal value.

The medical interpretation of the data obtained in this study is currently being studied by the medical group which supplied the hair samples and initiated this work.

- 206 -

Figures 7.9 through to 7.14

    General trend of the abundances of different
    elements detected in the six hair samples
    analyzed, RC, RD, RE, RF, RG and RH
    respectively.
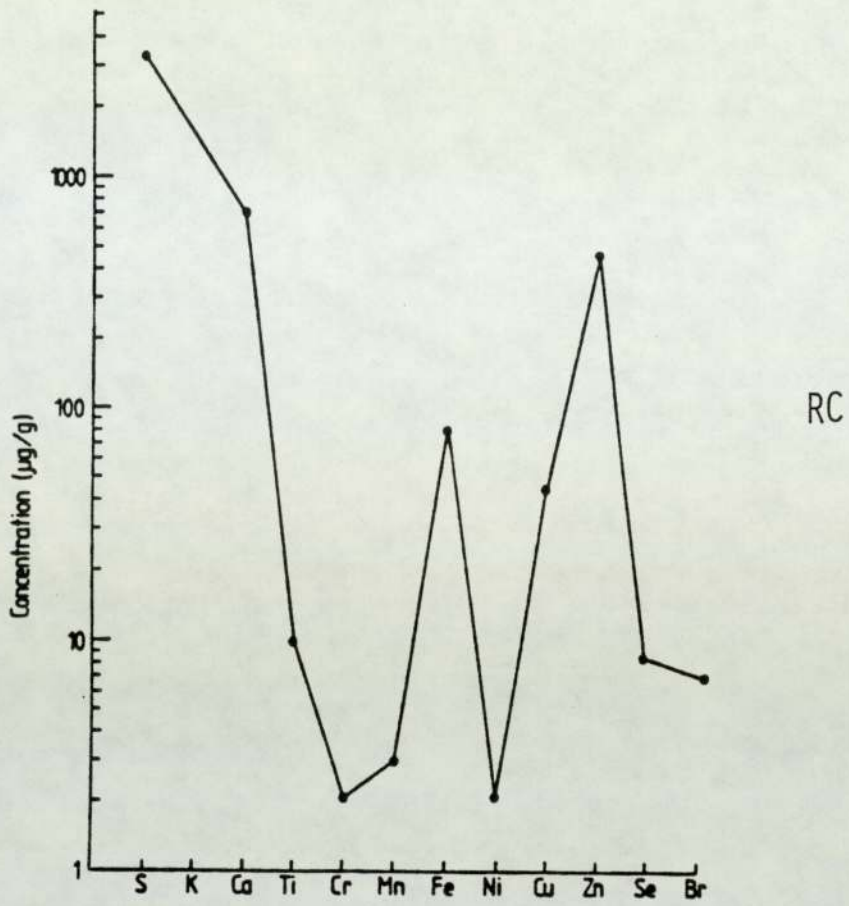
Figure 7.9
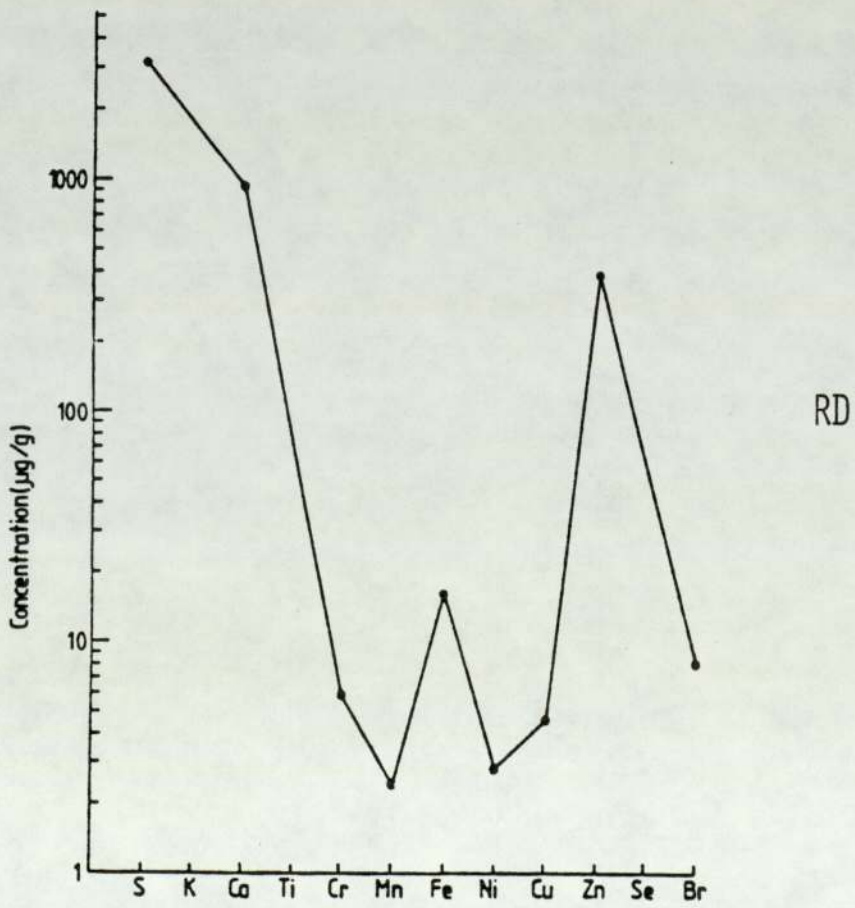
Figure 7.10
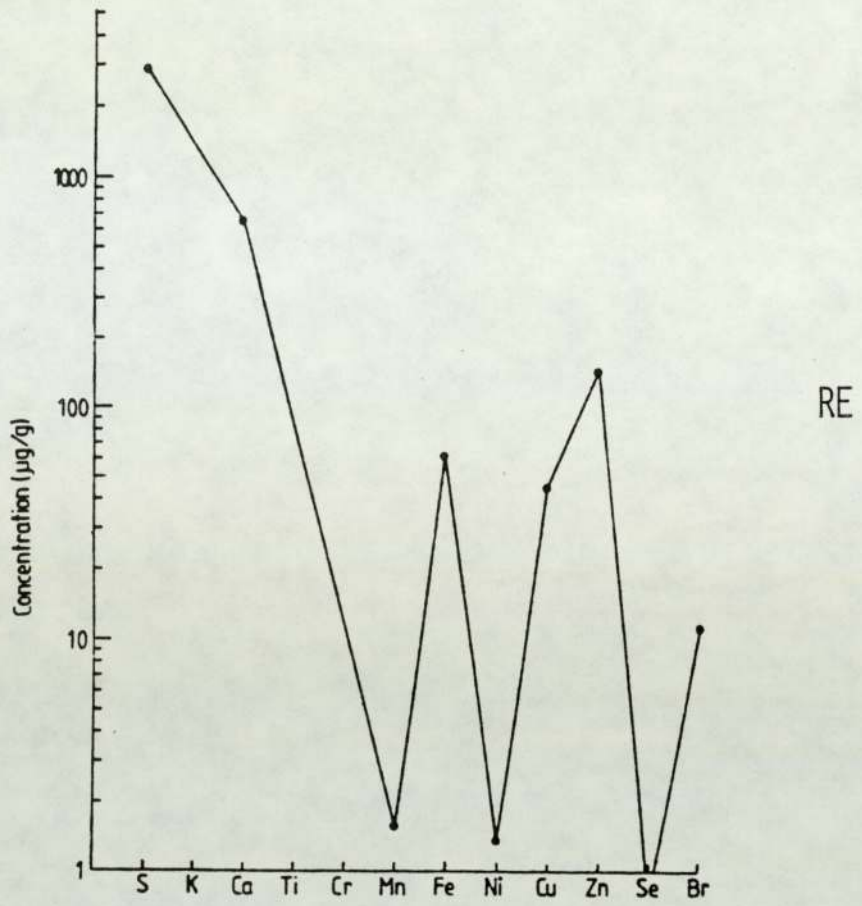
Figure 7.11
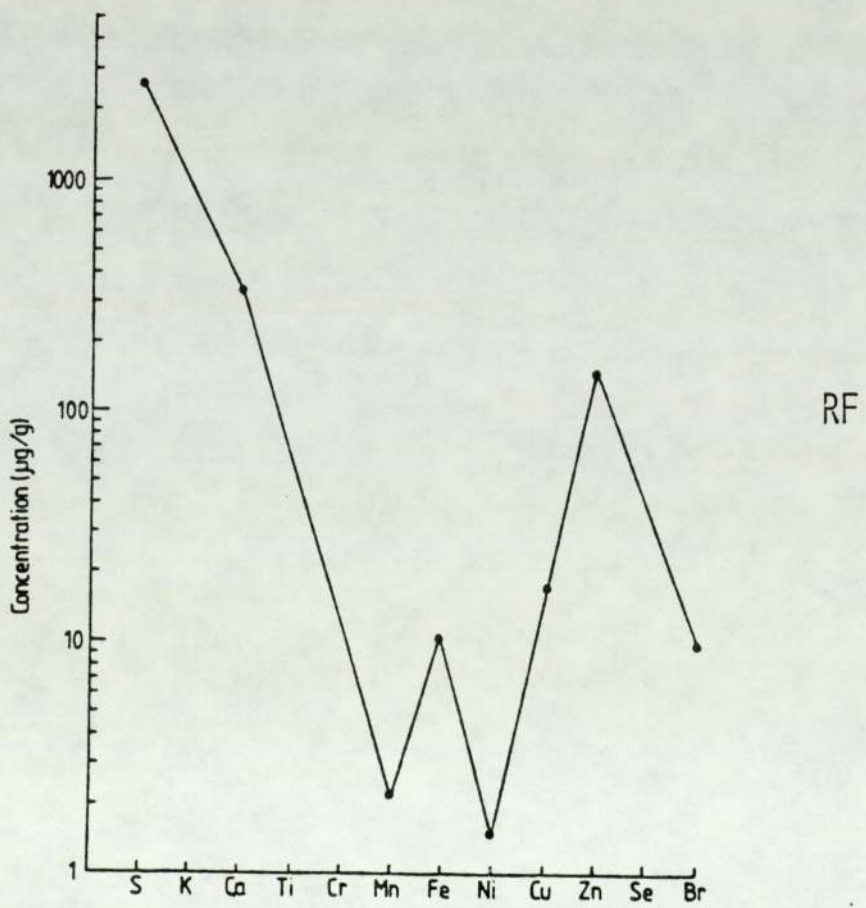
Figure 7.12
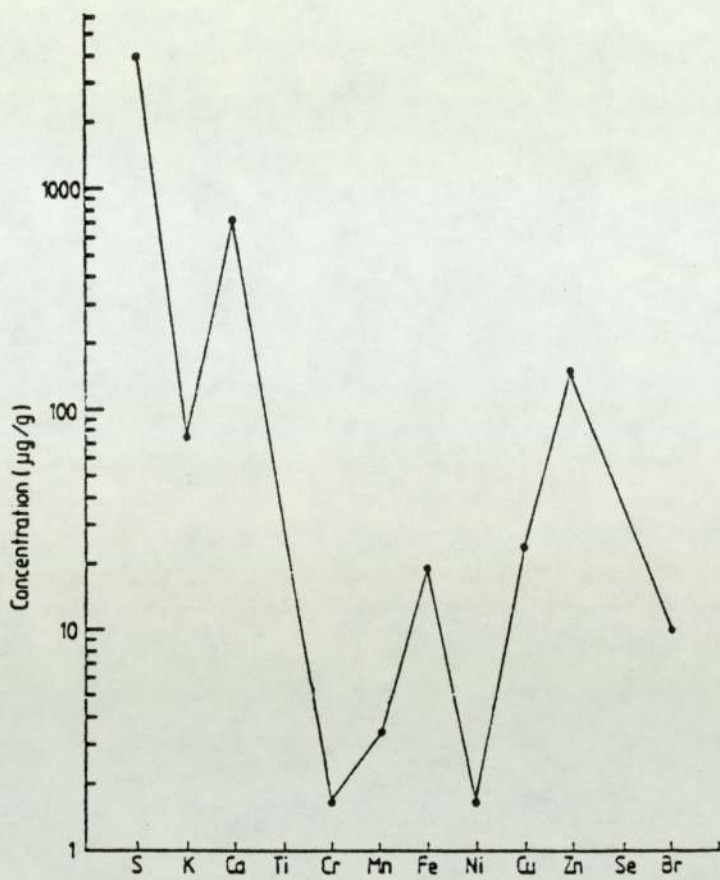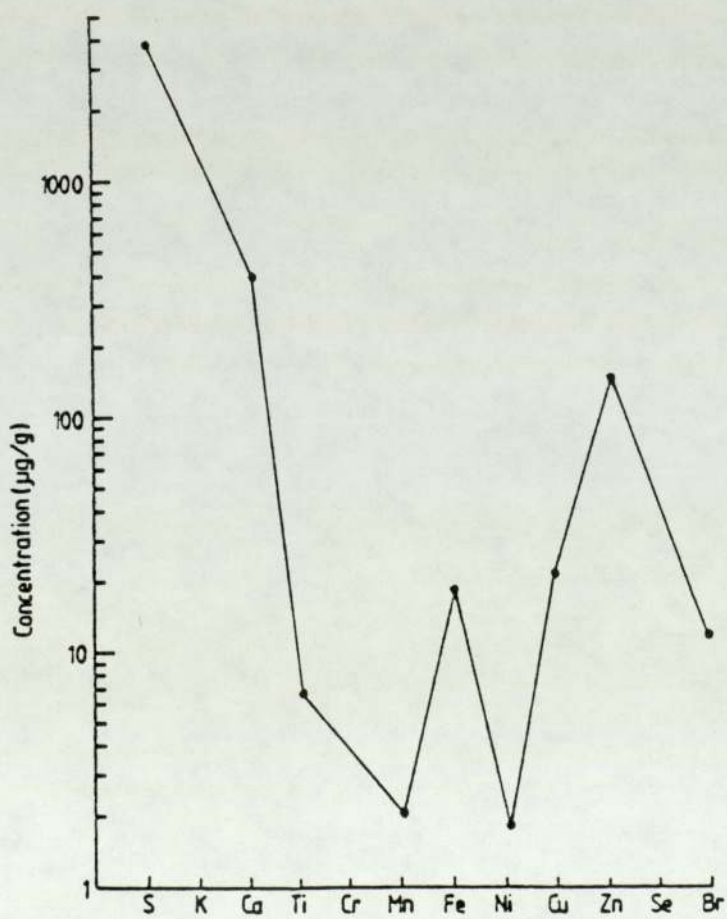
Figure 7.13

Figure 7.14

TABLE 7.11

HAIR METAL ANALYSIS RESULTS FOR FEMALE CONTROL SUBJECTS IN μg/g

Manganese	Cadmium	Iron	Lead	Copper	Magnesium	Zinc	Calcium
4.80	2.40	47.0	48.0	96	120	280	4000
4.40	2.20	38.0	44.0	88	110	260	3500
4.00	2.00	35.0	40.0	80	100	240	3000
3.60	1.80	32.0	36.0	72	90	220	2500
3.20	1.60	29.0	32.0	64	80	200	2000
2.80	1.40	26.0	28.0	56	70	180	1750
2.40	1.20	23.0	24.0	48	60	160	1500
2.00	1.00	20.0	20.0	40	50	140	1250
1.60	0.80	17.0	16.0	32	40	120	1000
1.20	0.60	14.0	12.0	24	30	100	750
0.80	0.40	11.0	8.0	16	20	80	500
0.40	0.20	8.0	4.0	8	10	60	250
0.0	0.0	5.0	0.0	0	0	40	200

Aluminium —————— (Control 15.5 μg/g)

Chromium -------- (Control < 0.75 μg/g)

Female Control

- 211 -

7.1.3.2 Comparison of Results: The elemental concentrations obtained by PIXE for these hair samples were compared with the results obtained by the Environmental Health Department of Aston University. They prepared the hair samples following a slightly different procedure than that followed by the present work, using the mixture of sulphuric and nitric acid for digestion utilizing hot plates, and then analyzing them using Atomic Absorption Spectrometry, AAS. The results of this analysis are listed with those of PIXE in Tables 7.5 through to 7.10. The elements Al and Mg which are usually expected to be present in hair samples could not be determined by the PIXE technique, because the energiesof the X-rays for these elements were too low to be detected by the Si(Li) detector employed. The elements Ni and Se can be determined by PIXE and not easily by AAS.

Although comparison of PIXE and AAS results involved comparison of sample preparation methods as well as analytical methods, the agreement between the results obtained from the two methods is fairly good. This is particularly true for all the elements present in hair in concentration of more than a few ppm. The only exception to this was Fe in which the AAS results are systematically lower than those of PIXE. A similar disagreement was observed when AAS and PIXE results for analyzing NBS bovine liver were compared with the certified value of NBS. A good agreement was obtained between PIXE with that of NBS while Fe determined value by AAS was about 30% lower than that of NBS. However, the degree of agreement is quite encouraging as our expected systematic error is about (10-15)% for intermediate Z elements and considering that the levels involved are of the order of ppm and different preparation procedures were followed. However, it should be noticed that the sample size used by PIXE is very small, especially compared to the amount of sample used by AAS.

In summary, the PIXE technique combined with the convenient sample preparation method followed has proven its powerful capabilities for
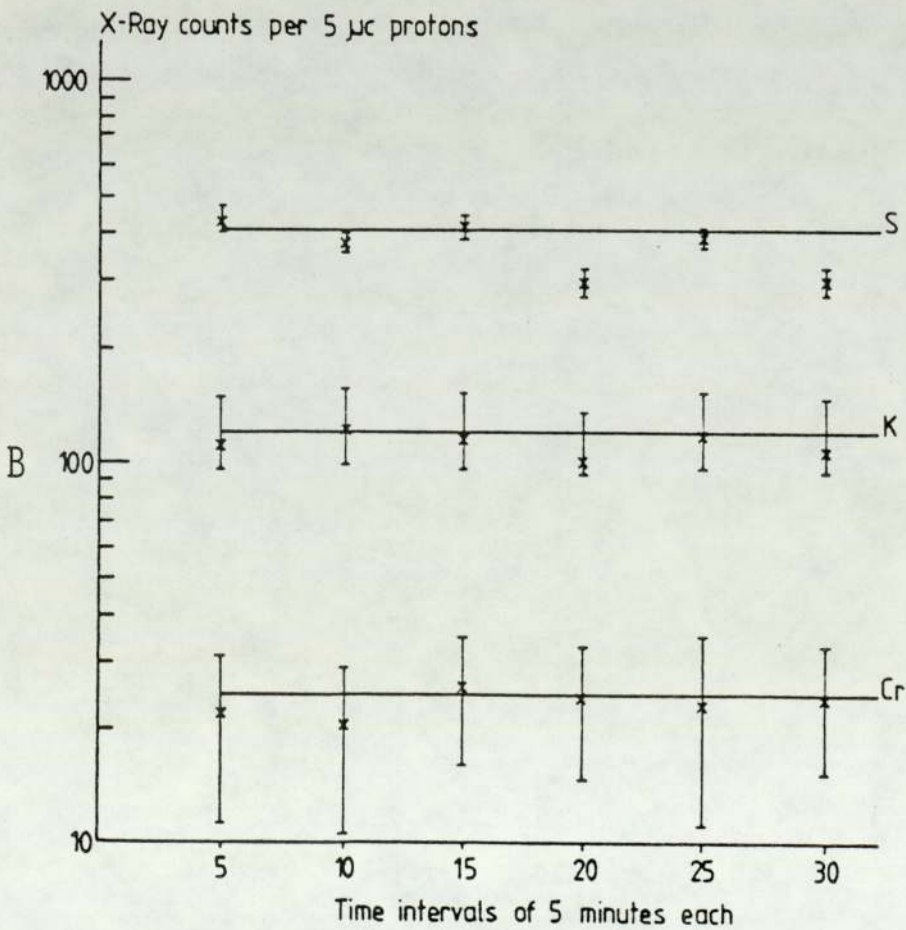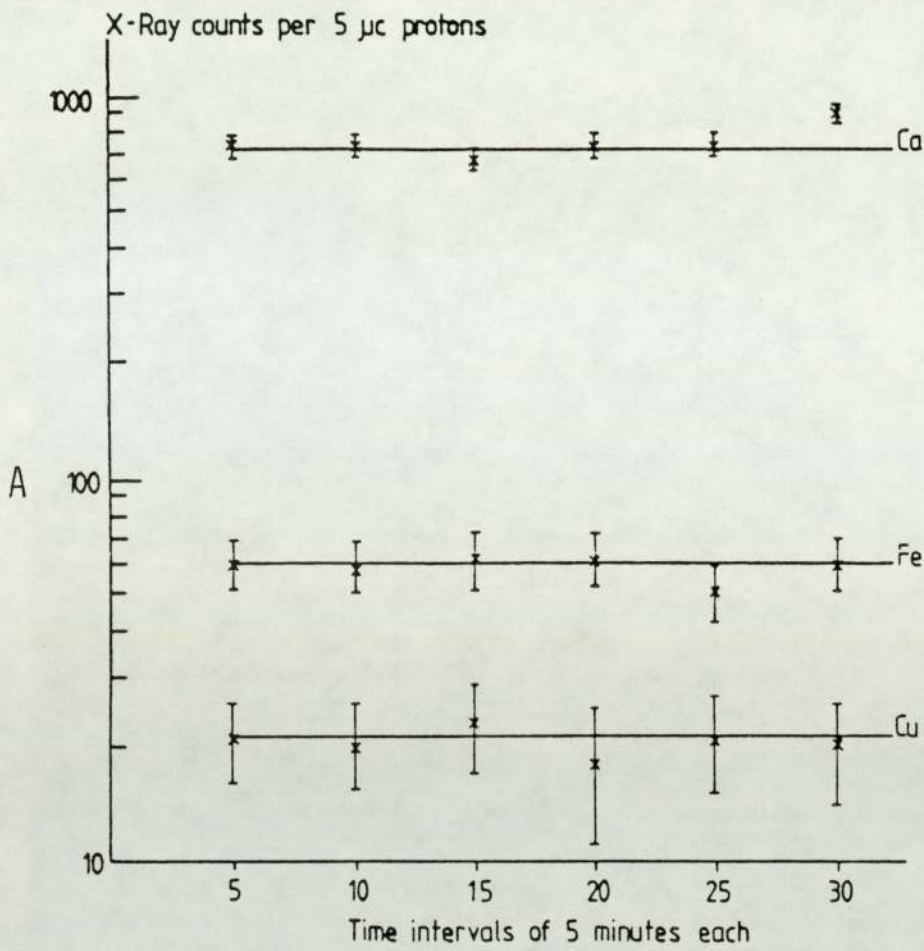
monitoring elemental abundances and interelement relationship in hair samples. This work demonstrates that it is possible to detect nearly all the elements present in hair in the range 15 < Z < 42 plus Pb.

The method which requires that samples be in an aqueous solution to form thin targets has obvious advantages. The variation of results obtained from replicate targets analyzed illustrated the high reproducibility of both, the preparation method and analytical technique.

7.1.3.3 Volatilization Studies:

A possible source of error in PIXE analysis is the loss of volatile elements. The losses may occur because of excessive sample heating or because of the requirement that the sample has to be placed in vacuum.

Results of beam heating volatility tests on biological samples have been reported by several authors. Campbell et al (1974, 1975) investigated volatility losses in wet-digested samples of liver and kidney deposited on thin carbon backings, no sample losses were observed in their experiment employing 0.5 μA. However Valkovic et al (1975) found slight losses of K and Br from samples of blood serum deposited on Formvar backing when irradiated with 150 nA of protons. Alexander et al (1974) in their analysis of fish samples found that Cu level showed some degradation with increasing beam levels. These results suggest that volatilization losses for thin targets are insignificant. However, a beam heating test was thought to be imperative for each analysis, to determine if any elements were being lost during the irradiation.

Six successive runs were made on one of the hair targets to measure the X-ray intensity for each element in the spectra as a function of time, using 25 nA proton beam equivalent to current density of about 100 nA/cm^2 for irradiation. After each irradiation, the spectrum was recorded and the analyzer memory cleared before accumulating the next spectrum.

X-Ray counts per 5 μc protons

A

Ca
Fe
Cu

Time intervals of 5 minutes each

X-Ray counts per 5 μc protons

B

S
K
Cr

Time intervals of 5 minutes each

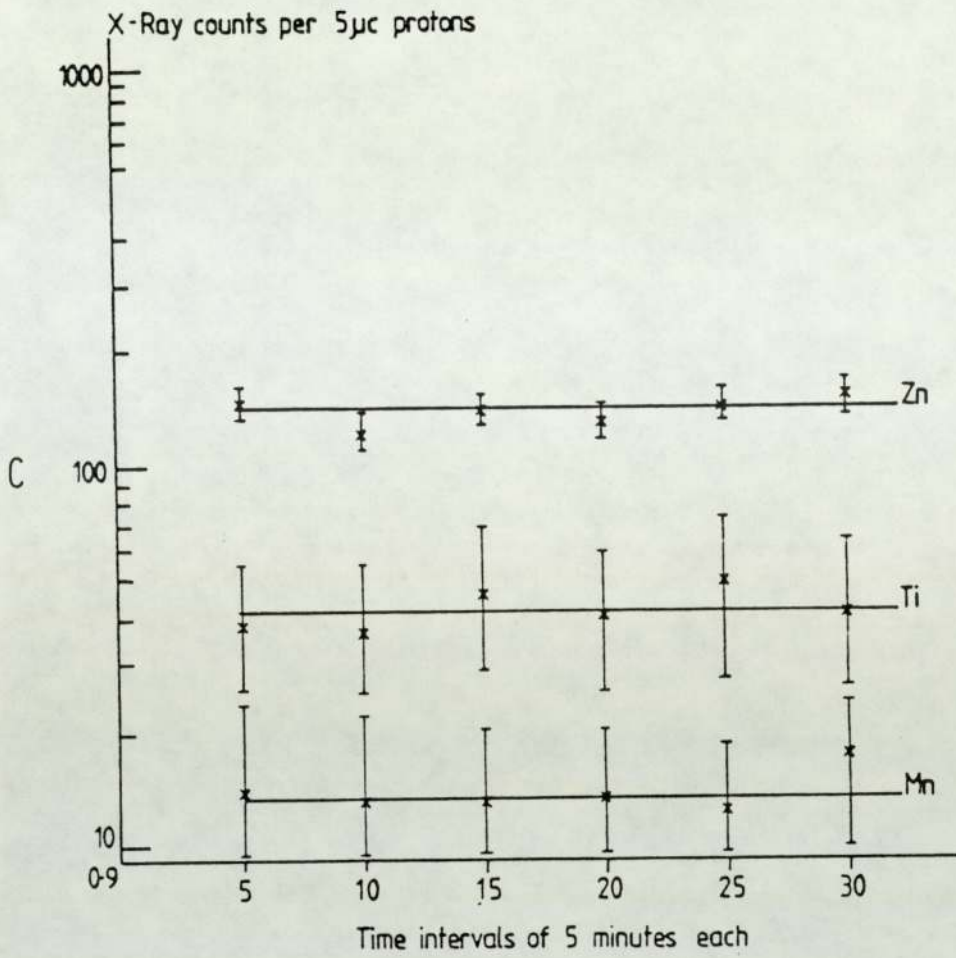Figure 7.15   Results of volatilization study on wet
               digested hair sample for 2.37 MeV pro-
               ton irradiation, a beam current of
               25 nA and beam area of 0.255 cm^2

- 215 -

The beam was allowed to remain on the target between periods of data accumulation for duration of about 5 minutes. The X-ray intensities of each element, normalized to equal integrated charge were then plotted versus elapsed time, Figure 7.15. The error bars are relatively large in some cases because the accumulated charge was only 5 μC and the quantity of detected element was close to the detectable limit of the system;in addition the associated peak was located on top of a large background.

If an element is being lost as the target is heated, the X-ray intensity should decrease as the irradiation time increases. However, as it is seen in Figure 7.15, there is no downward trend and within experimental error, the data points lie on a line horizontal to the X-axis. This indicates that during the run there was no loss of material from the deposit, although there could be losses when the sample is first introduced into the vacuum.

7.1.3.4 Spectral Analysis and Interferences: The energies of elements of interest in hair samples and in most other biological samples lie below 20 keV where the K X-rays of elements with Z < 40 and L X-rays of heavier elements are observed.

The method of proton excitation employed results in a system having a good sensitivity for K_α X-rays for the elements from about P(Z = 15) to Cd(Z = 48); for heavier elements the L X-rays are more strongly excited. Nevertheless, the limited resolution power of Si(Li) detector makes line interference unavoidable. The mostly common interference encountered is that between K_α of element Z and K_β of element Z-1. For the present system, this usually occurs for Z values up to 35. As the L X-rays are about 7 - 10 times lower in energy than the K X-rays from the same element, thus the L X-ray peak of a heavy element may coincide with K X-ray of light element. Figure 7.16 presented by Deconnink (1975) shows an X-ray spectrum where possible interference for most of the elements are summarized.

- 216 -
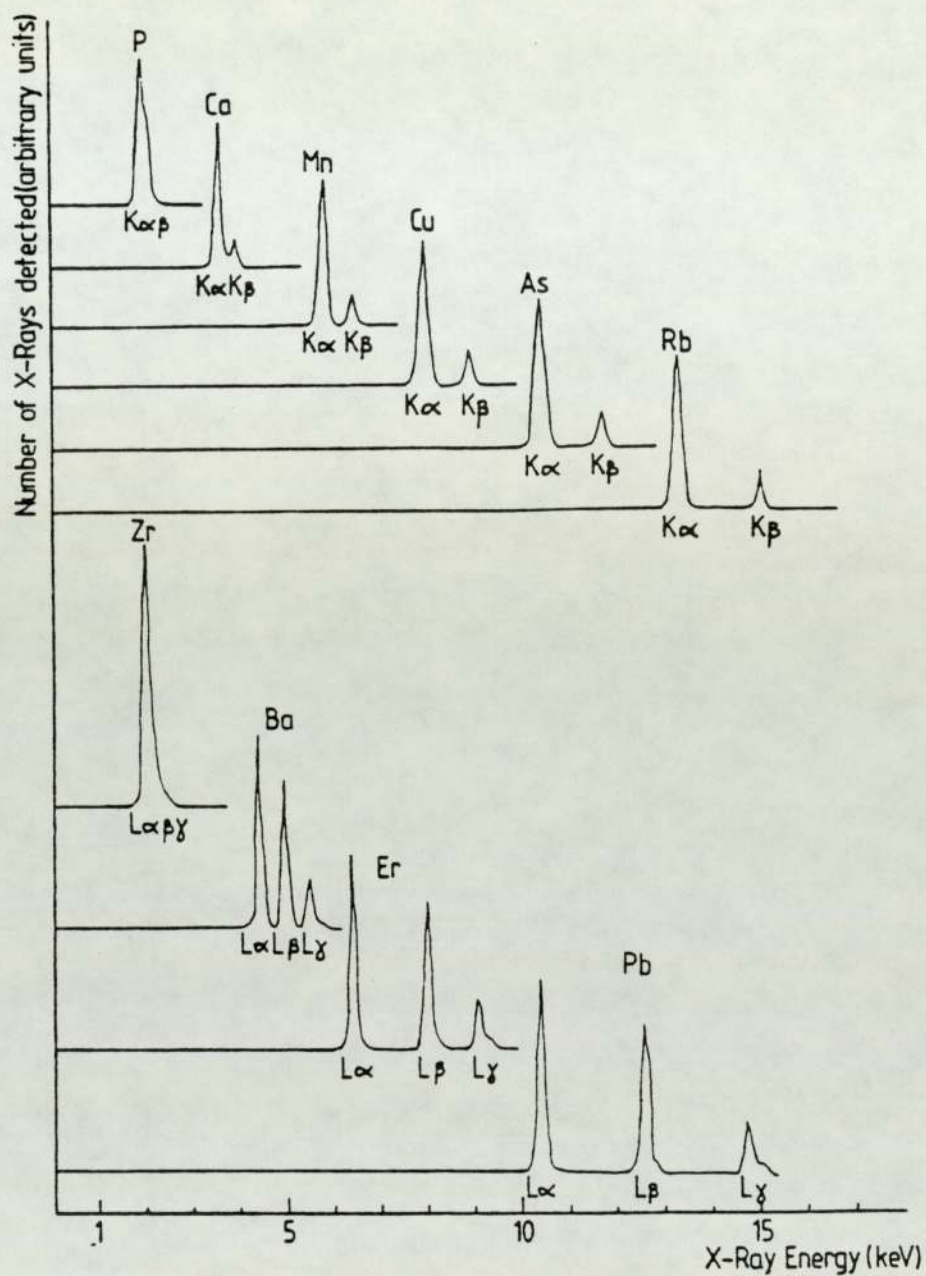
Figure 7..16   Exploded view of an X-ray spectrum showing
                the overlapping of K-lines from light ele-
                ments with L-lines from heavy elements when
                detected with a standard Si(Li) detector
                (from Deconnink, 1975)

The energy difference between K_α and K_β X-ray lines decreases at low Z and the absolute detector resolution does not permit separation of these lines, thus they appear as doublet of $K_{\alpha+\beta}$. The experimental K_β/K_α ratios extracted from the standard foils (section 3.4.2.1) were used to separate the K_α intensities. In hair sample analysis not more than 10 - 15 elements were detected so interference problems between X-ray lines from different elements were rather limited and are considered below:

Phosphorus: $K_{\alpha+\beta}$ X-ray of P is equal to 2.02 keV. The resolution of the detector exployed at this energy is equal to 112 eV at this energy. Thus, any X-ray energy between 1.908 keV and 2.13 keV will overlap with P peak. The L_α X-ray of Zr and Nb lies within this range, but these elements were not observed in the hair sample.

Sulphur: Elements which have X-rays in the energy region from 2.193 keV to 2.43 keV can overlap the 2.31 keV $K_{\alpha+\beta}$ X-ray of sulphur. The L_α X-rays of Mo and L_β X-ray of Nb and Mo can overlap this region. None of these elements were observed in hair samples except Mo, which was detected only in one of the hair samples and in a negligible amount compared to the large quantity of sulphur.

Potassium: Potassium K_α X-ray has an energy of 3.31 keV   adjacent to an intense Ca peak. This element detected in one of the hair samples in the concentration of 76 μg/g which is fairly high allowing the peak area to be determined easily. The potassium K_α X-ray overlaps with any X-ray in the energy 3.178 to 3.442 keV. Elements with L X-rays in this energy range, namely Cd, In and Sn were not detected in these samples.

Calcium: Calcium's K_α X-ray at 3.69 keV will overlap on X-ray in the energy range of 3.553 to 3.827 keV. No elements were observed in this analysis which cause interference in this range, except when K is observed. The K K_α/K_β ratio is required in extracting from the Ca peak area since the K K_β X-ray underlies the Ca peak.

Chromium and titanium: There were no heavy elements observed in hair samples to overlap with K X-ray of chromium and titanium.

Manganese, iron and cobalt: An X-ray in the energy region 6.245 to 6.575 keV will overlap with Fe K_α X-ray of 6.41 keV. The Mn K_β of 6.49 overlaps with Fe K_α. Since Mn occurred in a very small amount (2-3) ppm, this would not cause a significant uncertainty in spectra analysis. Co K_α of energy 6.93 keV overlaps with Fe K_β of energy 7.05. This makes determination of Co very difficult, particularly if a small quantity was present.

Copper: The only possible interference for copper K_α X-ray at 8.05 keV is Ni K_β X-ray. The correction for this is unnecessary since the amount of Ni detected was very small.

Zinc: To overlap with the K_α X-rays of Zn at 8.638 keV X-rays must have an energy between 8.35 and 8.92 keV. This energy range includes Cu K_β X-rays and L X-rays of the heavy elements which were not usually detected.

In the current work, the Cu-Zn interference was found to be significant. Since the Cu K_α was interference free corrections were made using the known Cu K_β/K_α ratio.

Arsenic, lead, selenium and bromine: Arsenic K_α X-ray of energy 10.53 keV is completely unresolved with lead L_α X-ray of energy 10.55 keV. Because the concentrations of these elements are very low, this overlap is a serious interference. From L_β/L_α ratio, Pb L_α X-ray yield can be determined from known Pb L_β X-ray yield. But Pb L_β at 12.6 keV occur together with Se K_β X-ray. Using K_β/K_α ratio, Se K_β X-ray yield can be determined from Se K_α X-ray yield. No interference occurs with Se K_α X-ray. Thus Se K_β was determined and subtracted from the total yield at 12.6 keV to find Pb L_β yield. Following this Pb L_α could be determined. To determine the As X-ray yield, the Pb L_α X-ray yield was subtracted from the total. The bromine K_α X-ray at 11.91 keV overlaps with As K_β. Thus, it has to be corrected for, if As is detected.

7.2   OTHER APPLICATIONS OF PIXE

Interest in trace elements, especially in biomedical fields and environmental systems is steadily increasing; this is partly due to the fact that these trace elements play an important role in human life.

If the effect of trace elements on health are to be accurately understood, it is necessary that their concentration shall be determined.

In this section we will demonstrate the applicability of PIXE for trace element analysis of a variety of samples.   It should be noted that some of the applications described concern only initial observations of a long term cooperative research programme being conducted by academic and medical authorities.

PIXE has already been applied for the determination of trace elemental concentrations in a number of biological tissues as reported in the literature Campbell (1974), Valkovic (1977), Willis (1977).

The analyses in this study have been performed on a human heart muscle and brain tissues; kidney, bladder and gall bladder stones.

7.2.1   Heart Muscle Tissue

Despite extensive research work on establishing laboratory data on trace element level of different organs and tissues including the previous work of Tipton   (1963) , it seems that data on "normal individuals" are still scanty. Consequently, a programme was initiated to establish normal concentration of trace elements in the hearts of humans who had died due to causes unrelated to their hearts. The short time available for this particular work only allowed preliminary observations to be made. However, the homogeneity level of trace element distribution throughout heart muscle was investigated.

The levels of homogeneity are different for different organs and tissues; and the homogeneity problem is directly related to the nature of

primary organ material. Inhomogeneity of these samples is the major problem with this particular analytical procedure employing untreated sections of the organ. In addition, the level of homogeneity has not been reported in literature for each individual organ, heart muscle being one of them.

An investigation was performed on a block of heart provided by Fazackarly District General Hospital, Liverpool. This investigation was conducted by studying 36 different sections from a block of paraffin embedded heart muscle and analyzing different positions on the same section then comparing the elemental abundances and elemental ratios obtained from these measurements. This approach permitted evaluation of the elemental content of the tissue via averaging out the results of the measurements made on the whole sections analyzed.

The work was initiated with 5 micron microtome section of the heart. A description of the procedure adopted in target preparation is provided in section 6.3.1.2. The irradiation was performed with 20-25 nA, 2.37 MeV protons, the measured X-ray yield was averaged out from 0.255 cm^2 area. The results obtained from analyzing six different sections indicated significant variations of trace elements existing among different sections. The experiment was repeated for the same beam area with another six samples of 10 μm thickness. Different results were obtained, but the range of variation was less than that observed with the previous set of samples. The rest of the experiment was carried out with tissues of 15 μm thickness, hoping that the combination of the operated beam area with this thickness would probably average out results representing a more homogeneous trace elements distributions. But the results obtained still gave a wide statistical variation. Since the fluctuation in the results was not attributed to experimental error, it apparently reflected true individual differences. Thus it was determined that there is a noticeable variation in elemental abundances for sections of muscle tissue

TABLE 7.12

INTENSITY RATIOS OF SOME DETECTED ELEMENTS

IN DIFFERENT THICKNESS TISSUES OF HEART MUSCLE

	5 μm		10 μm		15 μm	
	Fe/Zn	Cu/Zn	Fe/Zn	Cu/Zn	Fe/Zn	Cu/Zn
1	10.20	1.07	2.1	0.64	5.13	0.78
2	10.00	1.14	5.5	0.84	4.46	0.75
3	14.60	1.83	9.8	0.60	4.50	0.76
4	17.00	2.50	9.5	0.86	5.40	1.00
5	9.85	1.10	8.7	1.05	3.97	0.80
6	9.20	2.03	7.2	0.70	6.70	0.80

TABLE 7.13

MEASURED ELEMENTAL ABUNDANCES IN HEART TISSUE

IN ppm WET WEIGHT BASIS STUDIED, COMPARED

WITH THAT OF STANDARD MAN

Element	Present Work (μg/g)	Standard Man μg/g
P	791.7 ± 387	1760
S	1065.9 ± 511	-
Cl	737 ± 192	-
K	204 ± 51	2530
Ca	771.8 ± 102	48.4
Cr	7.9 ± 1.2	1.5
Mn	2.27 ± 0.66	0.253
Fe	92.2 ± 8.3	55
Cu	35 ± 3.8	3.85
Zn	41.8 ± 3.33	30.8
Ni	0.75 ± 0.48	< 5
Br	2.32 ± 0.9	-
Vn	2.58 ± 1.01	< 1
Ti	4 ± 0.9	< 5

Note: (-) indicates   elements which are not reported

taken from different regions of the same block. A photograph of 5 micron thick heart tissue shown in Figure 7.17 illustrates the non-homogeneity of this section which could be seen by naked eyes.

The reproducibility of some of the elemental ratios such as Fe/Zn, Cu/Zn was better with the thickest sections. A typical example of these ratios is given in Table 7.12. A PIXE spectrum from heart muscle tissue section of 15 μm is presented in Figure 7.18 illustrating the peak and background magnitude associated with the elements detected. Peaks corresponds to 14 different elements were identified in such spectra.

In determining trace element content of these tissues, concentration measurements were performed considering yield as the weighed average of the total analysis of all the sections and via the following relation:

$$M_{sm} = M_{st} \times \frac{y_{sm}}{y_{st}} \times \frac{dS_{sm}}{dS_{st}} \qquad \ldots \ldots (2$$

$$= \frac{1}{(F_{xz})_{st}} \times y_{sm} \times dS_{sm}$$

since concentration of any specific element is given as:

$$conc = \frac{M_{sm}}{M_{total}}$$

$$M_{total} = \text{the total sample mass}$$

$$conc. = \frac{y_{sm}}{(F_{xz})_{st} \times (\rho t)_{sm}}$$

As mentioned previously, the thickness of the samples ranged from (5-15) microns, equivalent to mass thickness of (0.5-1.5) mg/cm^2 of wet tissue. These sections are considered thin according to thin target criteria, Campbell (1975), thus no corrections were required due to X-ray absorption effect and/or proton energy loss which is the primary

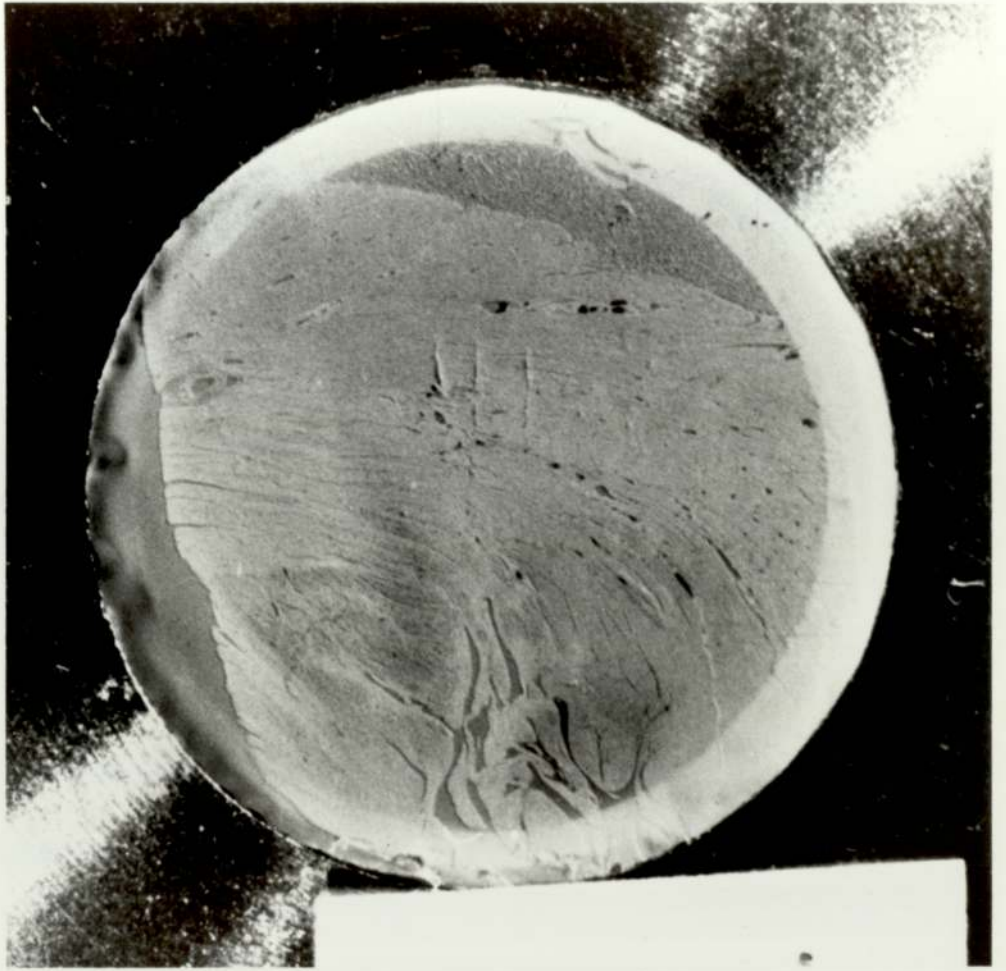Figure 7.17   A photograph of 5 micron thick heart tissue, illustrates the nonhomogenity of this section which could be readily observed.
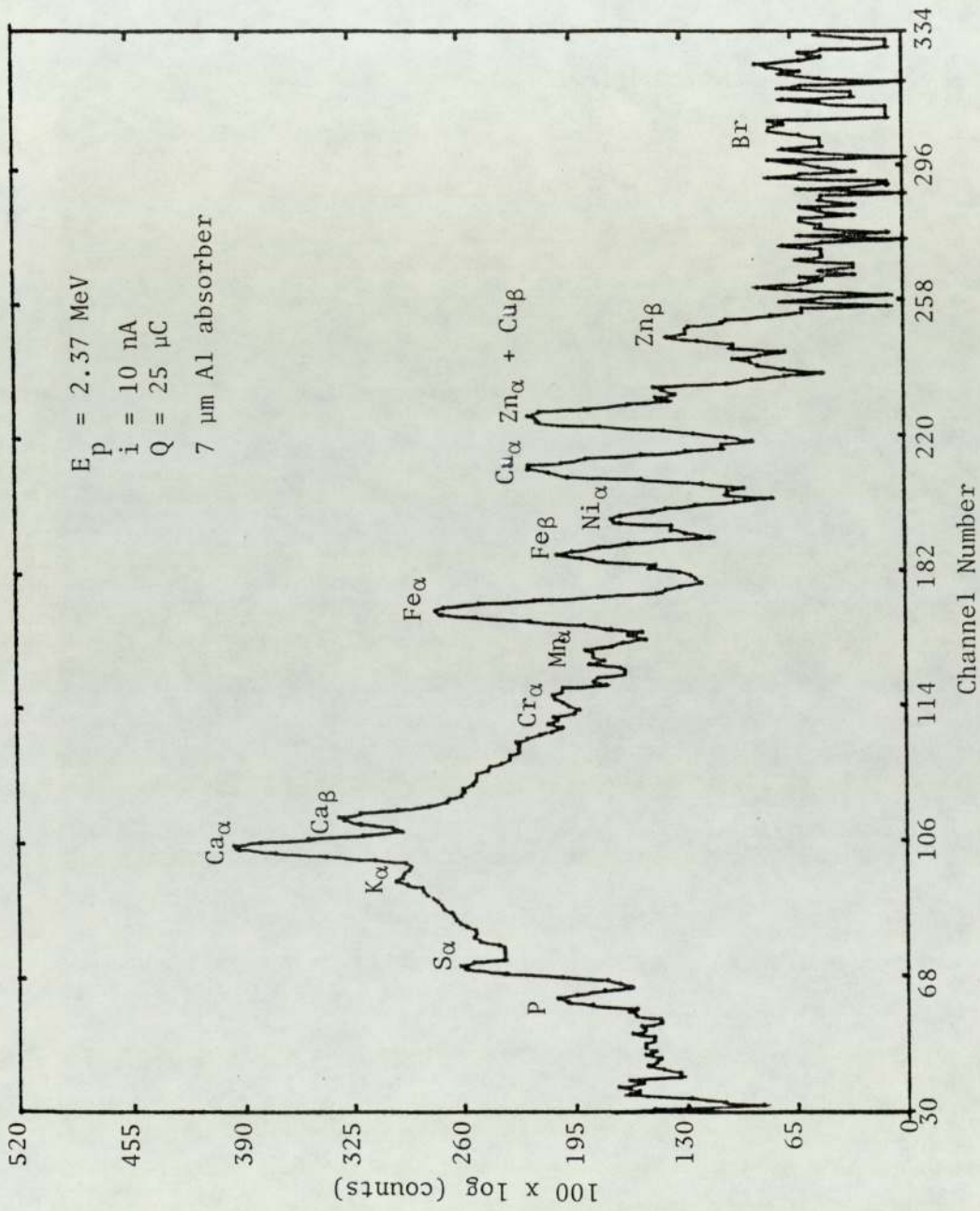
Figure 7.18   PIXE spectrum from analysis of a 15 µm thick section of
human heart tissue, with an irradiated area of 0.255 cm²

- 225 -

advantage of using thin tissue sections. It is estimated that the amount of tissue analyzed by a beam of 0.255 cm^2 area on 15 μm thick slice is only about 0.01 mg of wet tissue. This emphasizes the concern about obtaining representative results from such small quantity. On the other hand, the need for clean thin backing for such small samples is imperative. One is however concerned about the possibility of sample contamination from the paraffin and from the microtome blade as well as trace impurities in the target backing since each microtome slice was mounted on a backing of a Nuclepore and the trace element impurities present in the backing interfere with the elements present in the tissue. The estimated mean concentrations of elements which were observed in a set of Nuclepore backing were subtracted from the spectra analyzed.

It was found that Fe, Cu, Zn, Cl, Ca were present in relatively large amounts and almost in every section analyzed. K and S were observed in 95% of the measurements made while P was absent in more than 20% of the tissues, and Ni was rarely detected. V , Ti, Mn, Br concentrations were evaluated from a composition spectrum obtained by adding up from 4 up to 11 single spectra. The detection of Br in some of the samples is an indication that no volatilization took place due to beam heating.

It is worth noting that apart from complexities introduced by some inter-element interference which were treated as discussed previously, the other phenomena such as Si escape peaks, pile up peak and low energy tailing were not of concern in this analysis.

The experimental results obtained for trace element content of the block of heart are listed in Table 7.13 with the published data on typical elemental concentration in wet heart specimen from standard man given by Tipton (1963). The results however cannot be meaningfully compared since further work is required to draw a firm conclusion concerning the sample representative and to better understand the variations observed.

Should the results obtained from analyzing mass sections represent

the trace elment content of the whole block clearly in that case the
trace element content determined differ than that of standard man and
except potassium the rest of the trace element are systematically higher.
The measurements made evaluate the effectiveness of the system for the
identification of trace elements in similar samples. The detection of
the major elements, P, S, Cl, K and Ca; the predominant trace elements
Mn, Fe, Cu and the toxic elements As, Pb and inessential Br, present no
particular problem. Analyses of adjacent areas of the same tissue
sections revealed large inhomogeneities suggesting that the tissue
sections cannot be considered representative of the entire specimen.
A large number of samples must therefore be analyzed if the results are
to be meaningful.

7.2.2 Brain Tissue

Since the analysis of trace elements in brain tissue may be of med-
ical interest like almost all other tissues, PIXE has been applied to
the analysis of brain microtome sliced tissue. A block brain was put in
liquid nitrogen temperature and was divided into slices of 5 μm. Six
slices were randomly selected to be analyzed in an identical experimental
condition to that of heart muscle. The PIXE spectrum from a brain tissue
using the 7 μm aluminium absorber is shown in Figure 7.19. It was nec-
essary to employ an absorber to reduce the very intense low energy X-
rays, (e.g. K). The large absorption of the low energy X-rays enabled
higher beam currents to be used. Consequently, the efficiency for
heavier elements was maximized.

The procedure discussed in the previous section was applied to de-
termine the concentration of the trace elements detected in these samples.
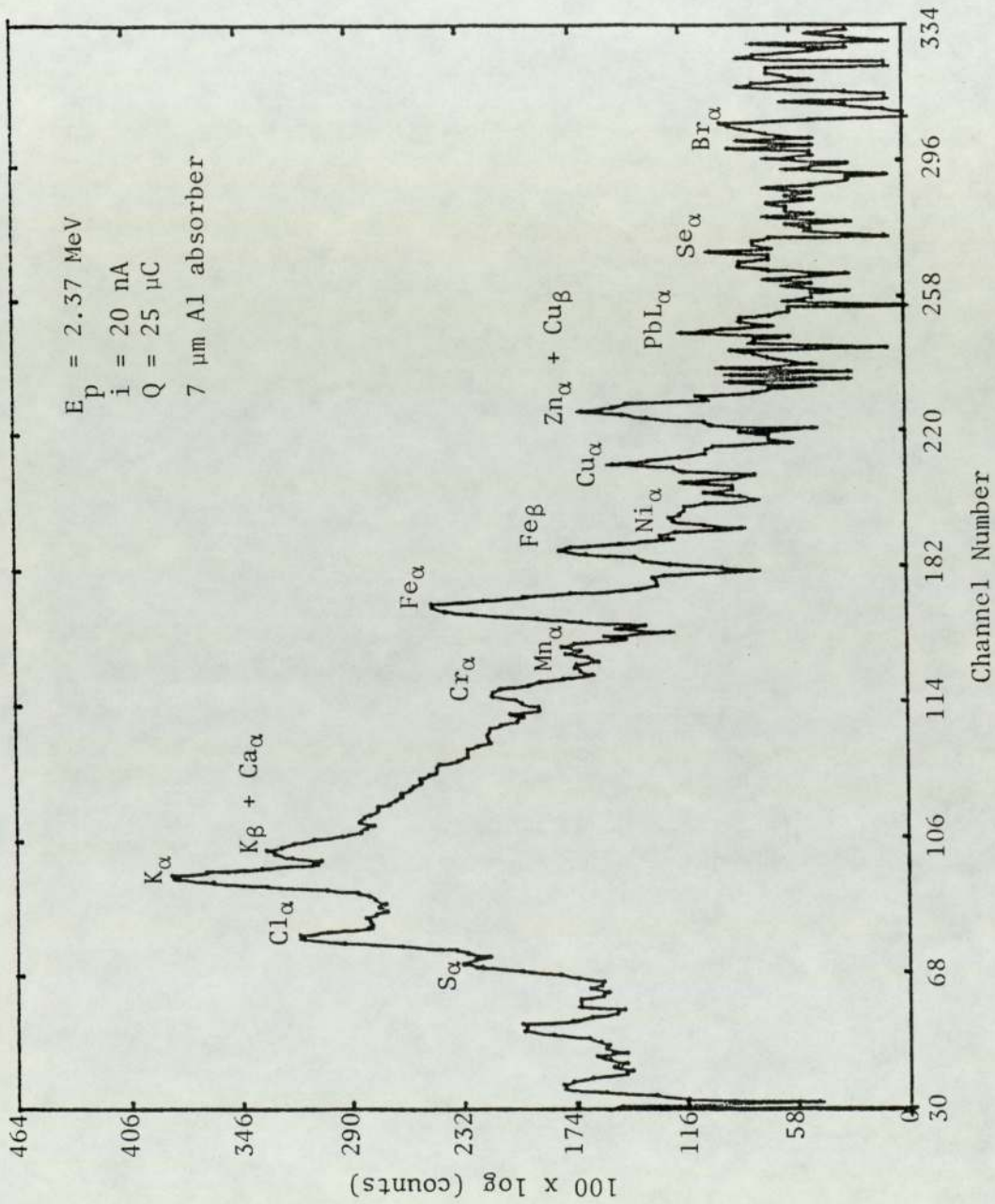The results obtained for these wet tissue with that of standard man given

Figure 7.19   PIXE spectrum from analysis of a 5 μm slice of human
brain tissue with an irradiated area of 0.255 cm²

by Tipton are presented in Table 7.14. As it could be seen the agreement of some experimental values with the published data of standard man is reasonably good in view of small quantities analyzed.

Although the study is not yet completed, the agreement obtained between the six sections of brain tissue suggest that the sections are more representative than the heart tissues. However, it may be stated that most of the elements are not homogeneously distributed among the individual sections of this group of samples. The target fluctuations observed in Cl which was from (4179 - 16889) counts for 25 μC, while Zn was the most stable element observed and the variation was between (130 - 165) counts per 25 μC.

TABLE 7.14

MEASURED ELEMENTAL ABUNDANCES IN ppm WET

WEIGHT BASIS IN BRAIN TISSUE STUDIED

COMPARED WITH THAT OF STANDARD MAN

Element	Present Work μg/g	Tipton μg/g
Al		22
S	800 ± 392	-
Cl	1786 ± 478	-
K	2631 ± 489	3230
Ca	177 ± 36.5	100
Vn	6.7 ± 1.9	< 1
Cr	4.2 ± 0.5	0.2
Mn	5.2 ± 1.5	0.34
Fe	51.5 ± 4.6	57
Ni	1.5 ± 0.96	< 5
Cu	6.96 ± 1.38	6.3
Zn	24.74 ± 3.5	14

We conclude, therefore, that a single section is not truly representative of the whole specimen.

Almost all the elements observed in heart tissue were seen in brain also, in addition there was positive evidence for presence of Hg in the composite spectra of the six brain tissues.

7.2.3 Analysis of Biliary and Urinary Calculi

Biliary calculi are concretions which occur in the gall bladder and urinary calculi are formed in the bladder, kidney or ureter.

In general, calculi are found to consist of varying proportions of several components, and the stones are grouped under the heading of their major constituents, i.e.

1. Uric acid; 2. Urates; 3. Oxalates; 4. Phosphate; 5. Others - cystine, xanthim and unknown.

Many theories have been propounded to explain the mechanism of stone formation and growth, Robertson (1976). However, none have satisfactorily accounted for all aspects of the problem. One of the main problems has been in determining when the stone formation takes place, whether the nucleation is essentially homogeneous (i.e. takes place spontaneously from higher saturated urine) or whether it is heterogeneous (i.e. is initiated by some other agent such as trace elements). The present day theory is the latter.

The problem of stone formation, however, is not entirely solved by the spontaneous passage or removal of the stone, as the abnormalities that caused its formation may remain. Because of the frequent occurence of biliary and urinary stone formation and the resultant morbidity, more information regarding the pathogenesis of the diseases is urgently required.

It is accepted generally that the study of stone composition and

- 230 -

structure is of prime importance from the therapeutic and prophylactic view point (Panel Discussion on Urolithiasis, 1954). Reliable analytical information is fundamental for a survey of the actiology of stone formation and is absolutely necessary for planning medical regimes, Beisher (1955). The foremost authorities on stone analysis (Panel Discussion on Analytical Methods and Structure Study of Calculi, 1972) have agreed upon the important criteria for work in this field.

"A sensitive, accurate, rapid, non-destructive and inexpensive method of stone analysis which will be powerful enough to deal with small stones of mixed composition as well as studying different zones independently, are the optimum requirements".

Numerous methods have been employed to determine stones composition including flame spectrometry, Hodgkinson et al (1968), Optical crystallography, Cifuentes-Dellatte et al (1972) and Hesse et al (1981), X-ray diffraction, Sutor et al (1968, 1969) and Hicking et al (1981). Infrared spectroscopy, Zarembski (1972) and Hicking (1981) and Electron microscopy, Cijentes et al (1967) and McConvielle (1979). It is clear from these studies that there is no one method of analysis capable of answering all the questions.

However, we have found experimentally in this work that PIXE fulfils almost all the analytical requirements, in particular regarding trace elements.

Experiments on trace element analysis have been carried out on different stones using proton induced X-ray emission (Taylor et al 1981), Present work. One of the most obvious advantageous of using PIXE is the limit of detection. Detection limits are of the order of a part per million and such low levels of trace elements have been undetectable by previous methods of stone analysis.

Cross-sections of stones were usually used and particular attention was given to the central or nuclear regions of the stone. Calculi sections

were coated with a thin layer of aluminium (approximately 1000 A°) prior to the PIXE analyses to eliminate background due to the non-conductivity of the stones. Qualitative analysis was performed to determine the elements present in about 10 different stones.

An interesting illustration of the PIXE analysis is shown here, where a so-called "pure" uric acid calculus supplied by University College, London, was found to contain trace amount of sulphur, chlorine, potassium, iron, copper and zinc (Figures 7 - 20) in the nuclear or the central region of the stone. However, the PIXE spectra of the interior regions of the stone clearly revealed additional elements such as titanium and calcium (Figure 7.21). A similar uric acid stone supplied for analysis by the Leeds Royal Infirmary was found to contain sulphur, chlorine, calcium, titanium, iron, nickel and copper in the nucleus (Figure 7.22). Additional elements cadmium, zinc , selenium and bromine were found in the interior regions(Figure 7.23). However, the presence of sulphur was not observed in this region while it was detected in the nucleus region. The detected silver peak was due to conductive paint applied to the stone edges prior to analysis.

"Ordinary" chemical analysis, together with auto-radiographic and X-ray micro-analysis on both of these stones revealed no unexpected trace elements, Taylor (1981).

Since trace elements are obviously excluded from "ordinary" chemical analysis, the PIXE technique is particularly useful in their determination especially in the region of the nucleus.

Considerable trace element variation across stone sections was observed as seen by the spectra of the two calculi presented for illustration here. There was also a considerable variation in the proportion of the elements found, for example, the main peaks were not always the same. In the first stone, (Figure 7.20), the major element at the centre was found to

Figure 7.20   PIXE spectrum from analysis of a thick section of "pure" uric acid (bladder stone), nucleus region, with an irradiated area of 0.255 cm^2

Figure 7.21   PIXE spectrum from analysis of the same section of stone, obtained from irradiation of the interior region of it with the same irrdiated area
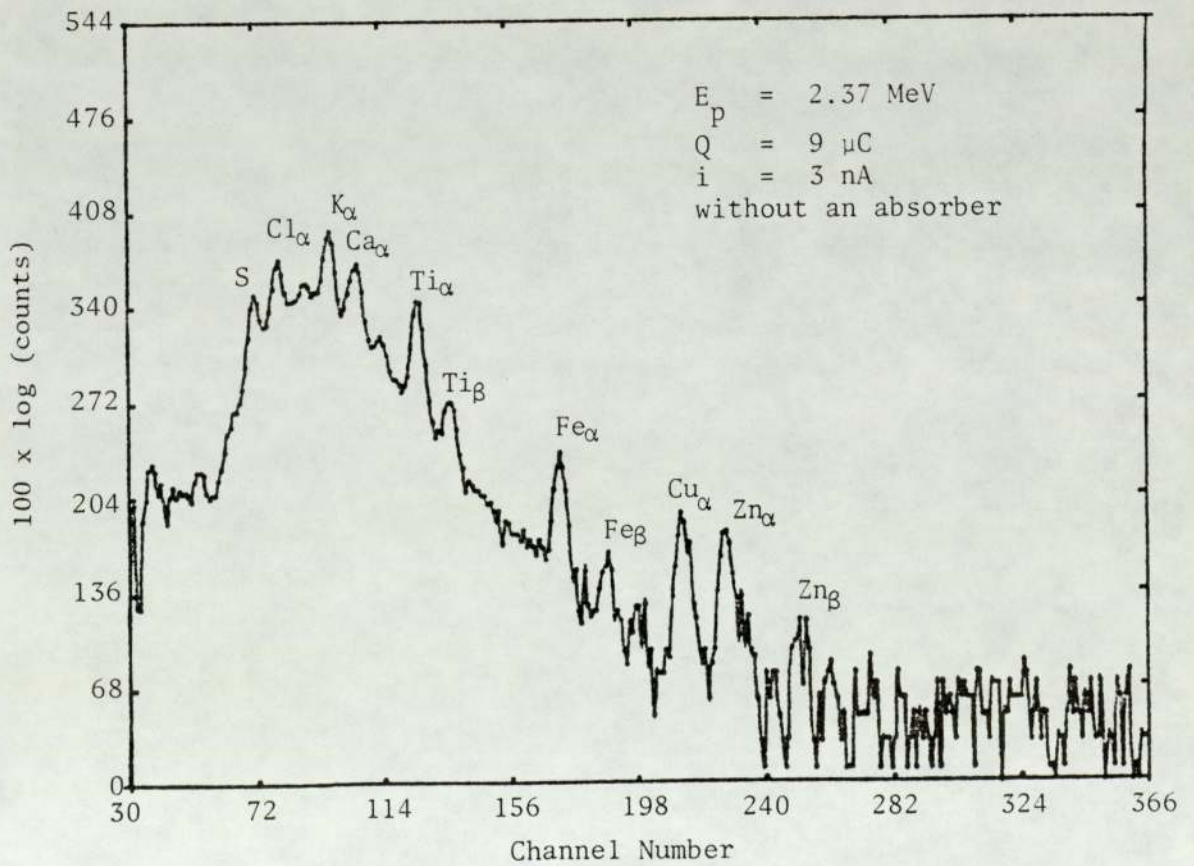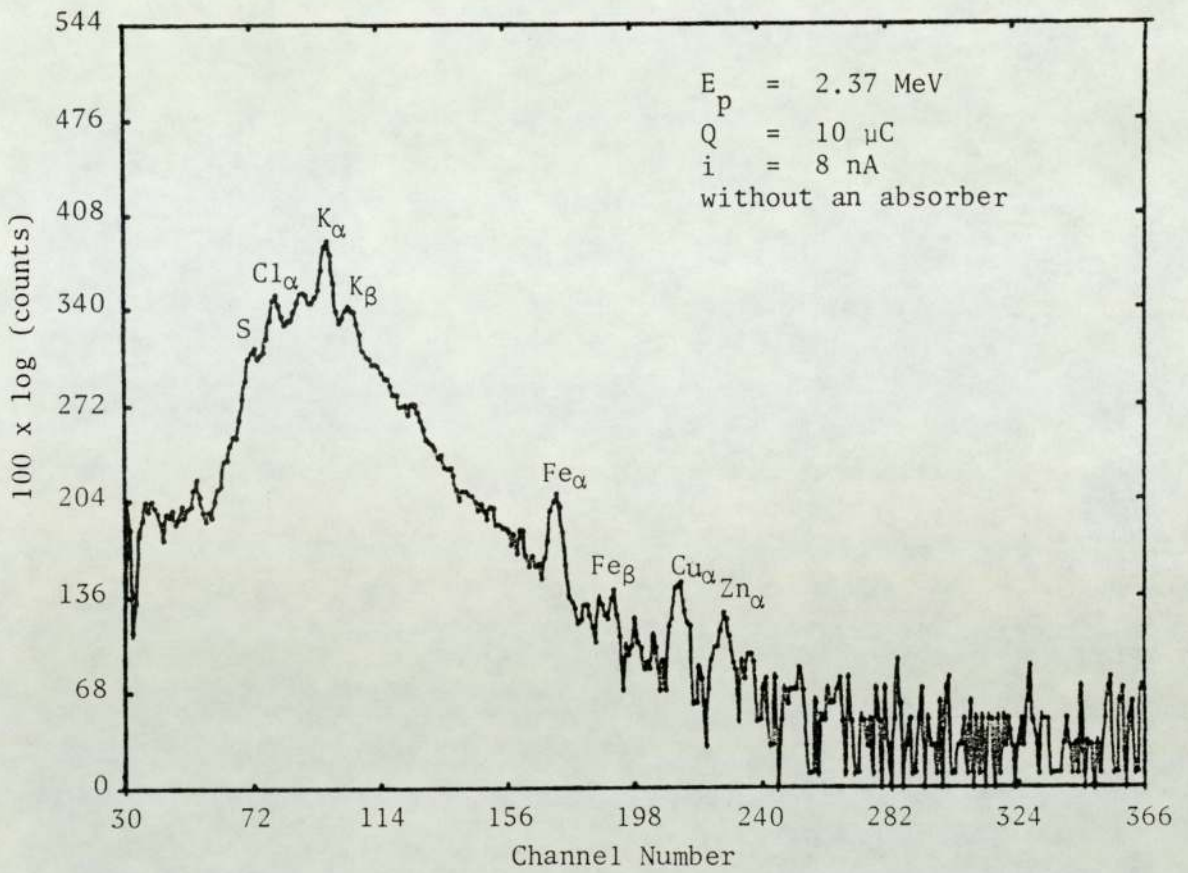
Figure 7.22   PIXE spectrum from the analysis of a thick
                section of uric acid and stone (kidney
                stone), the nucleus region was irradiated
                and a 10 μm absorber was employed.

Figure 7.23   PIXE spectrum from the analysis of the same
                stone, as shown in the above Figure, employ-
                ing the same absorber, whereas the irradia-
                tion zone was the interior region
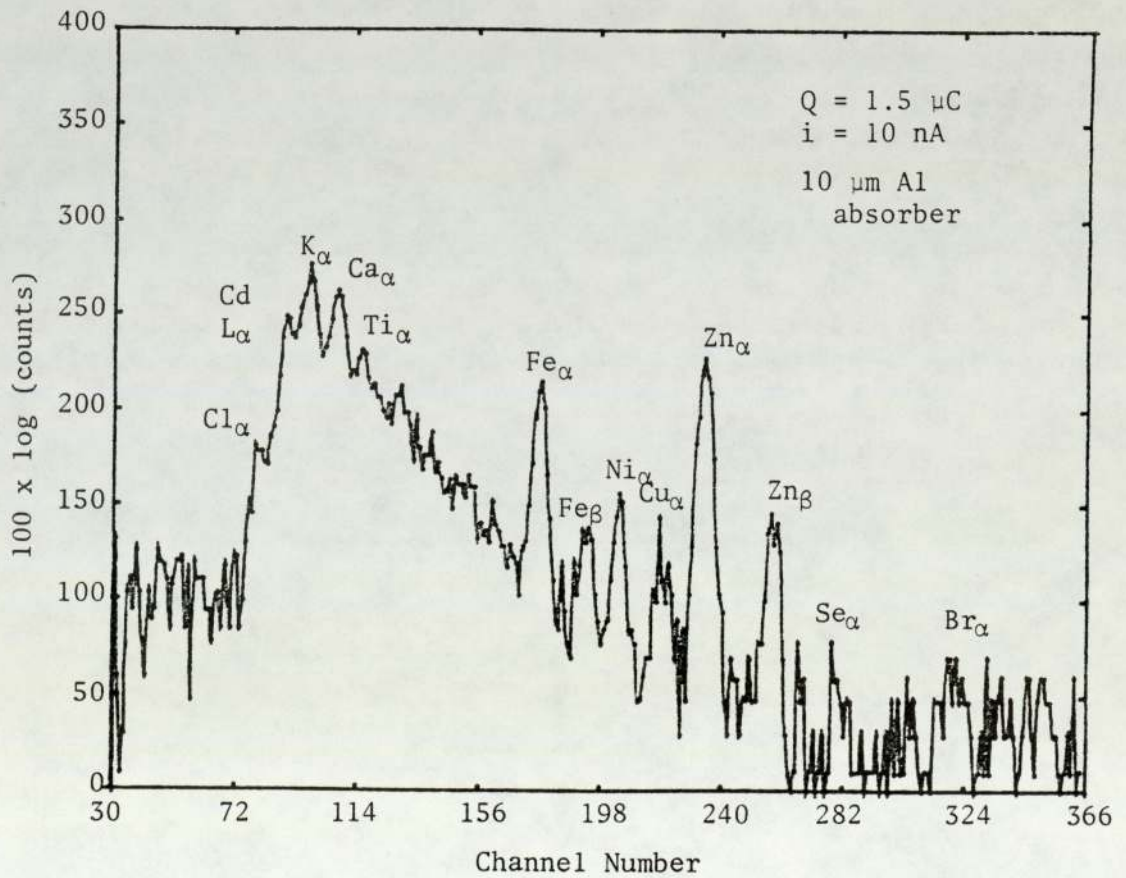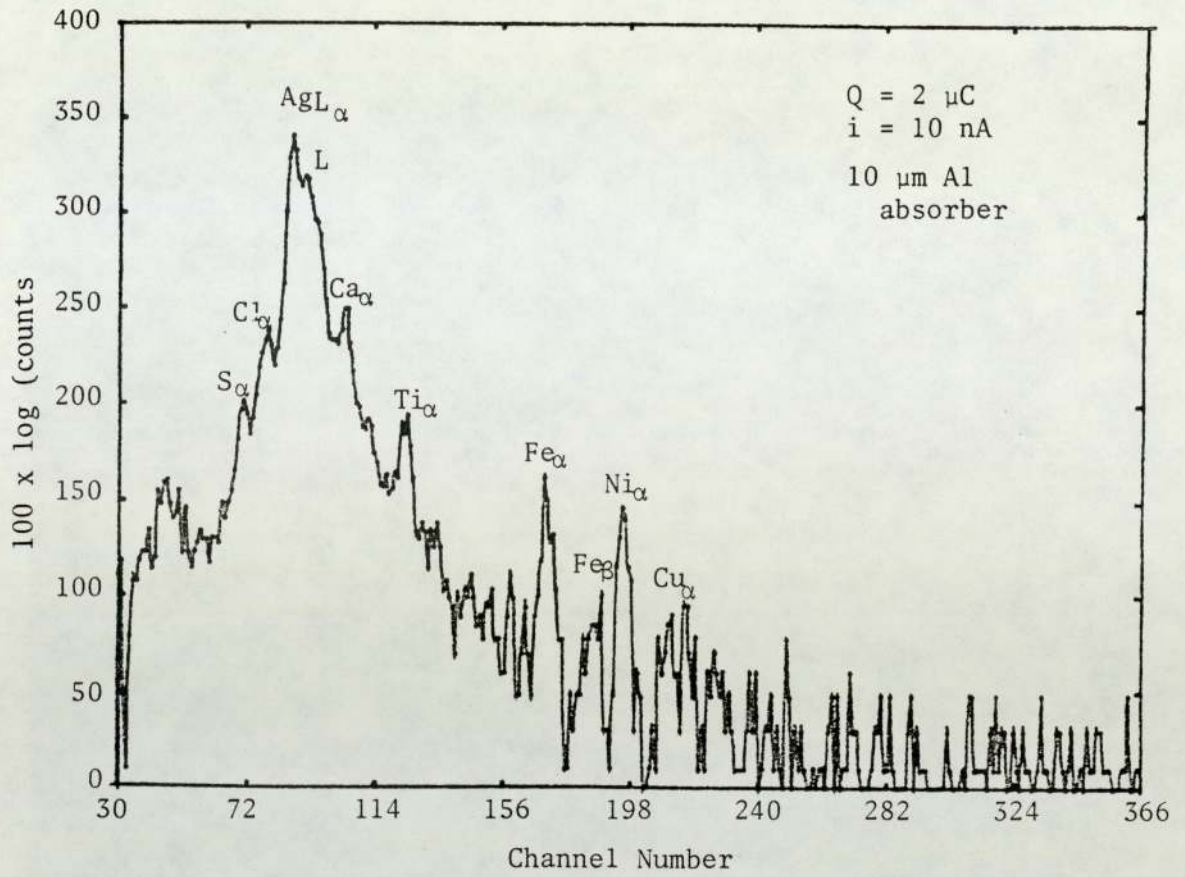
be potassium whereas the spectra from the interior of the stone showed calcium to be predominant also. The proportion of chlorine and sulphur present in this stone was also greater at the interior region.

The absence of zinc in the nucleus region of the second stone, Figure 7.22 was interesting. The variations of the rest of the elements in different zone of this stone are discussed above.

A noticeable difference observed between the elements detected in the exterior (shell) and the interior regions of one of the other stones as its shown in Figures 7.24 and 7.25 respectively. The elements manganese, nickel and copper were indeed detected in the interior regions while they were absent in the exterior regions of the stone. Arsenic and/or lead were just detectable only in exterior regions of the stone.

The examples shown above are typical and are presented as an illustration of the advantage of this sensitive technique. Interpretation of the results is open to discussion. The differences in composition between the nucleus region and the interior could reflect changes in trace elements of the urine at the time of stone formation, however, the presence of a greater number of trace elements in the centre is of particular interest and merits further studies.

Finally, we conclude that the ease and rapidity with which PIXE data was generated for these stones make PIXE a very suitable technique for rapid scanning of samples, particularly when quantitative data is not required.

Figure 7.24   PIXE spectrum of gall stone obtained from the
               irradiation of the exterior region with an
               irradiation area of 0.255 cm^2, and an X-ray
               absorption filter of 15 μm Al

Figure 7.25   PIXE spectrum of the same gall stone obtained
               from the irradiation of interior region with
               exactly the same experimental condition
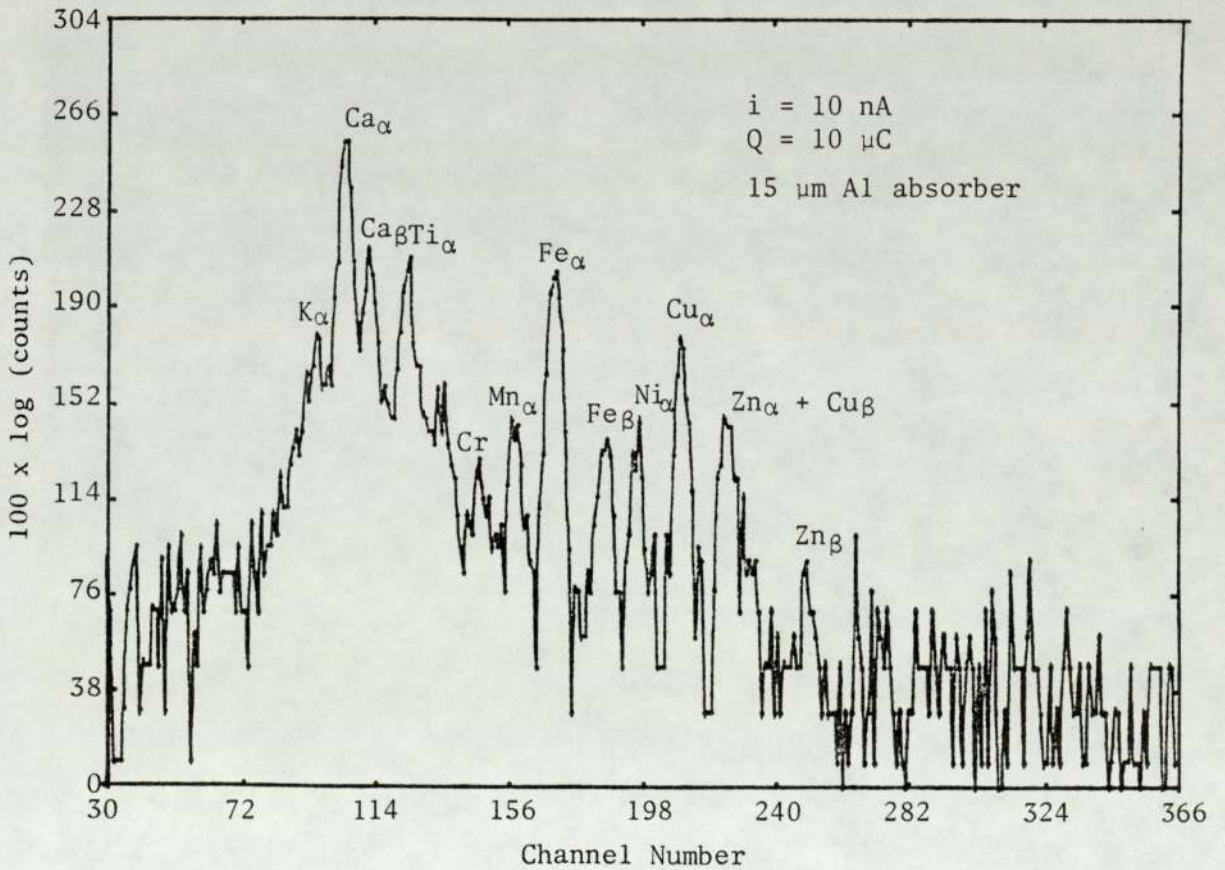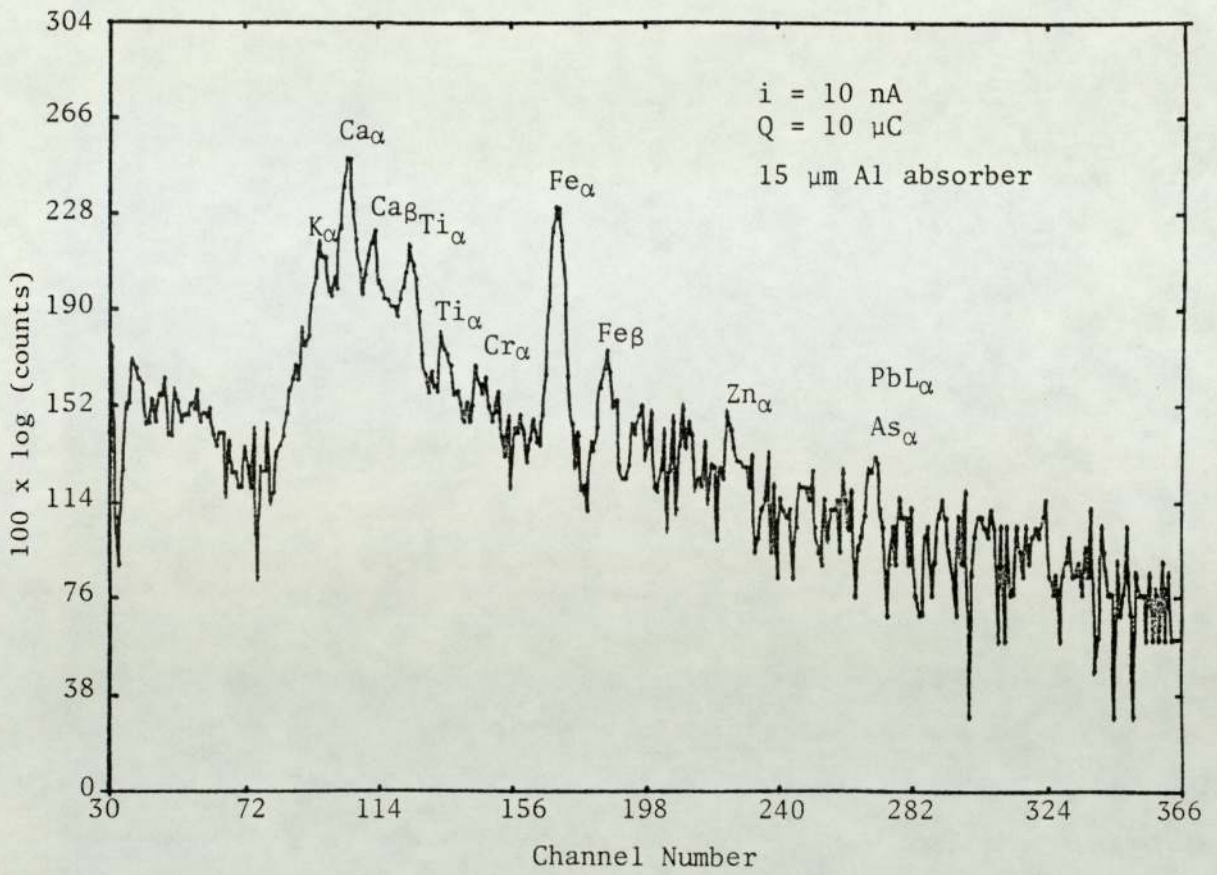
CHAPTER EIGHT

CONCLUSIONS

During the last decade, PIXE analysis has been shown to be a power-
ful analytical technique, with PIXE research workers making remarkable
progress in demonstrating its versatility and usefulness in many different
application areas. The optimization of experimental parameters which has
been investigated in detail in this study is in general agreement with
the results of other recent studies. The present work has demonstrated
that the reproducibility and accuracy required for reliable analytical
work can be achieved with PIXE, but requires considerable experimental
expertise. The quantitative results obtained for primary and secondary
standards indicate that the system as developed is of sufficient accuracy
and precision to meet the needs of different biomedical studies where sig-
nificant changes in elemental concentration are being observed. In this
respect it is competitive with other more established analytical methods.

Generally, the major feature of the PIXE technique lies in its capa-
bility of multi-elemental analysis, in which typically 10-20 elements in
a given sample can be determined simultaneously. Moreover, the method is
reasonably sensitive. The investigation made on minimum detectable con-
centration shows that the MDL of about 0.1-1 ppm can be readily obtained
with acceptable accuracy, employing thin targets. Due to the very small
sample size analyzed the minimum detectable amounts, in terms of absolute
abundance, were found to be at the ng level or lower. PIXE analysis is
relatively fast requiring short irradiation times; typically 5-20 minutes
were required in the present work for analyzing biomedical samples with
acceptable statistical accuracy. In general, it is a non-destructive
technique. Sample preparation in many cases is minimal while in others
it requires a considerable amount of experimental effort. The optimization

of the sample preparation technique for a variety of samples has been a particular feature of the present work. Triple digestion with nitric acid utilizing a sealed teflon digestion vessel, was found to digest a variety of biological samples effectively, from which suitable homogeneous samples were successfully prepared. The integrity of this method was experimentally verified by the analysis both of the NBS bovine liver standard and the real samples of hair, which produced acceptable results. The most reliable quantitative results are obtained by PIXE when thin samples are used, while quantitative analysis of thick targets is complicated by matrix effects. The resulting detection limits are also somewhat poorer than for thin targets. Volatile compounds in both types of sample may be lost due to the vacuum environment or the irradiation of the sample.

Moreover, representative sampling of non-homogeneous samples is of considerable importance in PIXE analysis as revealed by the study of heart and brain tissues. In a single irradiation only a small non-representative quantity of sample is irradiated unless a preconcentration technique is used. To achieve representative results many targets of the same unconcentrated sample must be analyzed, which requires considerable time.

For samples yielding complicated X-ray spectra elemental interference can limit the sensitivity and impair the accuracy and precision of the results. This problem can be reduced by further improvement in the resolution of energy dispersive Si(Li) detectors or occasionally with selected filters.

The need for a well-equipped accelerator facility is an added disadvantage to the general application of the PIXE technique for trace element analysis.

The development undertaken in the present work has resulted in a PIXE system which was found to be very acceptable for the analysis of a

limited number of samples. However, further modification to the system will eliminate some of the existing limitations and lead to an improved analytical capability. For the rapid analysis of large numbers of samples the most significant advance that can be made is the automation of the irradiation facility with increased sample capacity. Arising out of this, work has already commenced on a multi-sample facility capable of handling 80 samples. This will be incorporated in a new vacuum chamber with its own pumps and cold trap. A facility will be included for mounting the detector either at 90° or 135° to the incoming beam. The solid angle will be increased by reducing target-to-detector distance, resulting in a higher X-ray count rate and a consequent reduction in analysis time. The facility to position the detector in a backward angle of 135° will allow the anisotropic distribution of electron bremsstrahlung to be exploited with advantage. According to Chu et al (1977) and Kaji et al (1977) a reduction by factor of nearly two in this source of background is possible by moving the detector from 90° to a backward angle of 135°.

For certain multi-elemental samples consisting of a high proportion of low Z elements, several absorbers of different thicknesses have to be used for optimizing the efficiency for a selected region of interest in a single target. Thus the sample must be analyzed several times using a different filter each time. Alternatively, a filter which has a small hole in the centre (Cahill, 1965) can be used. This permits only a fraction of the intense low energy X-rays to pass unattenuated into the detector and achieves essentially the same results obtained by using multiple absorbers but in a single irradiation.

The use of pulsed proton beam triggered by a signal from the X-ray preamplifier provides significant advantages over continuous beam excitation and removes some of the limitation experienced in the present work regarding the count rate effects. Consequently, work has been initiated to build an on-demand beam pulsing

system for the PIXE analysis line. This technique will reduce target damage and give better sensitivity due to improved performance at high count rates.

The combination of PIXE with proton scattering can also be utilized for biomedical sample analysis. The elastically scattered protons detected with a solid state detector at an appropriate angle, can be utilized to find the accurate thickness of biomedical targets analyzed.

The development of microbeams where ions are focused to a beam diametre of the order of 10 μm or less, offer a powerful method for using PIXE as a tool for scanning surfaces for their elemental microstruture, as reported recently in the literature.

LIST OF REFERENCES

Ahlberg M., "Simple Depth Profile Determination by Proton-Induced X-ray
      Emission" Nulcear Instruments and Methods 131(1973) pp 381-384

Ahlberg M., Akselsson R., "Proton-Induced X-ray Emission in the Trace
      Analysis of Human Tooth Enamel and Dentine" International Journal
      of Applied Radiation and Isotopes, 27(1976) pp 279-290

Alder K., Bohr A., Huss T., Mottleson B. and Winther A., "A Study of
      Nuclear Structure by Electromagnetic Excitation with Accelerated
      Ions" Review Modern Physics 28(1956) pp 432-542

Alexander M.E., Biegert E.K., Jones J.K., Thurston R.C., Valkovic V.,
      Wheeler R.M., Wingate C.A. and Zabel R., "Trace Element Analysis
      of Seawater and Fish Samples by Proton Induced X-ray Emission
      Spectrometry" International Journal of Applied Radiation and Iso-
      topes 25(1974) pp 229-235

Anderson H.H. and Zieglar J.F., "Hydrogen Stopping Powers and Ranges in
      all Elements" The Stopping Power and Ranges of Ions in Matter,
      Vol.3, Pergamon Press, New York (1977)

Baeri P., Rimini E., Pluglisi O., Pignataro S., "Analytical Potentiality
      of PIXE" La Chimica El'' industria 60 no.6 (1978) pp 510-515

Bambynek W., Grasemann B., Fink R.W., Freund H.H., Mark H., Swift C.D.,
      Price R.E., Venugopala R., "X-ray Fluorescence Yield, Auger and
      Coster-Kronig Probabilities" Review Modern Physics, 44(1972)
      pp 716-813

Bang J., Hansteen J.M. kgl. Dansk. Videnskab. Selskab. Mat. -Fys. Medd
      31(1959) No.13

Baptista G.B.,Montenegro E.C., Paschoa A.C., Barrosleite C.V., "Analysis
      of Trace Elements in Human Hair by PIXE" Nuclear Instruments and
      Methods 181(1981) pp 263-267

Barfoot K.M., PhD Thesis "Central Bureau for Nuclear Measurement, Geel (1980)

Barlow P., Private Communication (1979)

Barlow P., PhD Thesis, Leeds University (1980),

Barrette M., Lamoreux G., Lebel E., Lecomte R., Paradise P. and Monaro S.,
      "Trace Element Analysis of Freeze-dried Blood Serum by Proton and
      Alpha-Induced X-rays" Nuclear Instruments and Methods, 134(1976)
      pp 186-196

Baum R.M., Willis R.D., Walter R.L.,Gutknecht W.F., Stiles A.R., (X-ray Fluorescence of Environmental Samples) ed. T.G. Dzubay, 1977 Pub Ann. Arbot. Science Publication, pp 165-173

Bearse R.C., Close D.A., Malanify J.J. and Umbarger C.J., "Production of K_α and L_α X-rays by Protons of 1 - 3.7 MeV" Physics Review A7(1973) pp 1269-1272

Bearse R.C., Close D.A., Malanify J.J. and Umbarger C.J., "Elemental Analysis of Whole Blood Using Proton-Induced X-ray Emission" Analytical Chemistry 46, no.4(1974), pp 499-503

Bearse R.C., Burns C.E., Close D.A. and Malanify J.J., "Elemental Variations in Whole Blood Following Gamma Radiation Injury of Mice", Nuclear Instruments and Methods, 142(1977), pp 143-150

Berg V.D., DE Bruin M., Houthman J.P.W., "Sorption Behaviour of Trace Elements in Human Hair" Nuclear Activation Techniques in the life science, IAEA, Vienna (1967), pp 661

Bernas B., "A New Method for Decomposition and Comprehensive Analysis of Silicate by Atomic Absorption Spectrometry" Analytical Chemistry 40 no.11 (1968) pp 1682-1686

Besenbacher F., Anderson J.U. and Bonderup E., "Straggling in energy loss of energetic hydrogen and helium ions" Nuclear Instruments and Methods 168(1980) pp 1-15

Birks L.S., Seebold R.E., Batt A.P., "Excitation of Characteristic X-rays by Protons, Electrons and Primary X-rays" Journal of Applied Physics 35(1964) pp 2578-2581

Birks L.S. and Gilfrich, "X-ray Spectrometry" Analytical Chemistry 48 (1976) pp 273R-281R

Bisher D.H., "Analysis of Renal Calculi by I.R. Spectrometry" Journal of Urology 73(1955) pp 4

Bodart, Report of the Coordinate Research Meeting on Nuclear Based Methods for the Analysis of Pollutants in Human Hair, CEN-Saclay (IAEA, Vienna, 1978)

Bowen H.J., Trace Elements in Biochemistry, Academic Press, New York (1966)

Briggs M.H., Briggs M. and Wakatama A., "Trace Substances in Human Hair" Experientia 28(1972) pp 406-407

Cahill T.A., Flocchini R.C., Feeney P.J. and Shadon D.J., "Comparison of Equal-Velocity Ion Beams for Elemental Analysis by Ion Excited X-ray Emission" Nuclear Instruments and Methods 120(1974) pp 193-195

Cahill T.A., "Ion Excited X-ray Analysis of Environmental Sample" New Uses of Ion Accelerators ed. J.F. Ziegler (Plenum, New York, 1975) pp 1-71

Campbell J.L., Herman A.W., McNelles L.A., Orr B.H. and Willoughby R.A., "Some Biomedical Applications of Charged Particle Induced X-ray Fluorescence Analysis" Advances in X-ray Analysis 17(1974) pp 457-466

Campbell J.L., Orr B.H., Herman A.W., McNelles L.A., Thomson J.A. Cook W.B., "Trace Element Analysis of Fluids by Proton Induced X-ray Fluorescence Spectrometry" Analytical Chemistry 47 no 9(1975) pp 1542-1553

Campbell J.L., "Specimen Preparation in PIXE Analysis" Nuclear Instruments and Methods, 142(1977) pp 263-273

Campbell J.L., "Progress in Biological Applications of PIXE" IEEE Transactions on Nuclear Science, NS-26 no.1 (1979) pp 1363-1367

Campbell J.L., Russell S.B., Faiq S., Schutte C.W., Ollerhead R.W. and Gingerich R.R., "Optimisation of PIXE Sensitivity for Biomedical Applications" Nuclear Instruments and Methods, 181(1981), pp 285-292

Carius L., Annela, 116(1860) pp 1, and 136(1865) pp 129

Chen J.X., Guo Y.Z., Li H.K., Ren C.G., Tang G.H., Wand X.D. Yang F.C. and Yao H.Y., "Trace Element Analysis of Human Hair by PIXE" Nuclear Instruments and Methods 181(1981), pp 269-273

Chipperfield B., Chipperfield J.R., Bower N.R., "Silicon and Aluminium in Hearth Deaths" The Lancet 2(1977) pp 755-756

Cifuentes-Dellatte, L., Hildago A., Bellanto J., Santos M., "Interpretation de Imagenes Cristaline de Calculas Can Microscopic de Polarization Espectroscopia Infra-Raja" Proceedings of Renal Stone Research Symposium" Madrid (1972)

Cijentes L., Catalina F., Garcia J., "Electron Microscopy and X-ray Diffraction of Precipitated Urinary Calcium phosphates" British Journal of Urology 39(1967) pp 450-455

Chu C.T., Navarrete V.R. Kaji H., Izawa G., Shiokawa, Ishiik, Marita S., Tawara H., "A Study on Proton Induced X-ray Analysis and its Application to Environmental Samples" Journal of Radioanalytical Chemistry, Vol.36(1977) pp 195-207

Coleman R.F. et al "The Determination of Trace Elements in Human Hair by Neutron Activation and Application to Forensic Science" AWRE Report no. 0-86/66, 1967

Cookson J.A. and Pilling F.D., "Trace Element Distribution Across the Diameter of Human Hair" Physics Medical and Biology 20 no.6 (1975) pp 1015-1020

Cooper J.A., "Comparison of Particle and Photon Excited X-ray Fluorescence Applied to Trace Element Measurements of Environmental Samples" Nuclear Instruments and Methods 106 (1973) pp 525-538

Crumpton D. and Khan Md.R., "Proton Induced X-ray Emission Analysis' Critical Review in Analytical Chemistry, Vol.2, Issue 2(1981) pp 103; Vol.2, Issue 3 (1981), pp 161

Currie L.A., "Limits for Quantitative Detection and Quantitative Determination" Analytical Chemistry 40 no.3(1968), pp 586-593

Currie L.A., "Detection and Quantitation in X-ray Fluorescence Spectrometry" X-ray Fluorescence Analysis of Environmental Samples ed. T.G. Dznbay (1978), Pub. ann arbor, Science

Dankworth P.W. and Ude W. Ach, Archiv Der Pharmazie und Berichte der Dutschen, 264(1926), pp 712

Deconnink G., Demortier G., Bodart F., "Application of X-ray Production by Charged Particles to Elemental Analysis" Atomic Energy Review 13, no.2 (1975) pp 367-412

Deconnink G., "Trace Element Analysis in Liquids by Proton Induced X-ray Emission" Nuclear Instruments and Methods 142(1977) pp 275-284

Dzubay T.D., Lamothe P.J. and Yasuda H., "Polymar Films as Calibration Standards for X-ray Fluorescence Analysis" Advances in X-ray Analysis 20 (1978) pp 411-421

El-Dakhakhnya and El-Sadik, "Lead in Hair Among Exposed Workers" American Industrial Hygenic Association Journal 33(1972) pp 31-34

Flocchini R.G., Feeney P.J., Sommerville R.J., Cahill T.A., "Sensitivity
    Versus Target Backing for Elemental Analysis by Alpha Excited X-ray
    Emission" Nuclear Instruments and Methods 100(1972) pp 397-402

Folkmann F., Graade C., Huss T. and Kemp K., "Proton Induced X-ray Emis-
    sion as a Tool for Trace Element Analysis" Nuclear Instruments and
    Methods 116(1974a) pp 487-499

Folkmann F., Barggren J. and Kjeldgaard A., "Sensitivity in Trace Element
    Analysis by P, α and ^{16}O Induced X-rays" Nuclear Instruments and
    methods 119(1974b) pp 117-123

Folkmann F., "Analytical Use of Ion-Induced X-rays" Journal of Physics
    E: Scientific Instruments 8(1975) pp 429-444

Folkmann F., Material Characterization Using Ion Beam, ed. A. Cachard and
    J.P. Thomas (Plenum, New York, 1977)

Freedman, Trace Element Geochemistry in Health and Disease, (Geological
    Society of America, 1975)

Frieden F., "The Chemical Elements of Life" Scientific American 227(1972
    pp 52-57

Garcia J.D., "Inner-Shell Ionization by Proton Impact" Physics Review
    A1(1970a) pp 280-285

Garcia J.D., "X-ray Production Cross-Section" Physics Review A1(1970)
    pp 1402-1403

Garcia J.D., Fortner R.J. and Kavanagh T.M., "Inner-Shell Vacancy Prod-
    uction in Ion-Atom Collision" Review Modern Physics 45(1973)
    pp 111-177

Gilfrich J.V., Burkhalter P.G. and Birks L.S., "X-ray Spectrometry for
    Particulate Air Pollution - A Quantitative Comparison of Techniques"
    Analytical Chemistry, 45 no.12(1973) pp 2002-2009

Gorden B.M. and Kraner H.W., "On the Development of a System for Trace
    Element Analysis in the Environment by Charged Particle X-ray
    Fluorescence" Journal of Radioanalytical Chemistry 12(1972) pp 181-
    188

Gorsuch T.T., "Radiochemical Investigation on the Recovery for Analysis of
    Trace Element in Organic and Biological Materials" Analyst, 84(1959)
    pp 135-173

Gorsuch T.T., "The Destruction of Organic Matter", Pergamon Press, Oxford (1970)

Goulding F.S. and Jaklevic J.M., "Photon-Excited Energy Dispersive X-ray Fluorescence Analysis for Trace Elements" Annual Review of Nuclear Science 23(1973) pp 45-74

Goulding F.S. and Jaklevic J.M., "XRF Analysis Some Sensitivity Comparison between Charged Particle and Photons Excitation" Nuclear Instruments and Methods 142(1977) pp 323-332

Gradus A.J. "Factors affecting the Trace-Metal Content of Human Hair" Radioanal Chemistry 15(1973) pp 229-243

Guffey J.A. and Van Rinsvelt H.A., "Comparison of the Elemental Composition of Normal and Diseased Human Tissues by PIXE Analysis" Nuclear Instruments and Methods 149(1978) pp 489-494

Hambidge K.M. and Baum J.D., "Hair Chromium Concentration of Human Newborn and Changes During Infancy" American Journal Clinical Nutrition 25(1972) pp 376-379

Hammer D.I. Finklea J.F., Hendricks R.H. and Sly C.H.,"Hair Trace Metal Levels and Environmental Exposure" American Journal Epidermid 93 (1971) pp 84-92

Hansteen J.M. and Mosebekk O.P., "Atomic Coulomb Excitation by Heavy Charged Particles" Nuclear Physics, A201(1973) pp 541-560

Hensteen J.M., Advances in Atomic and Molecular Physics, eds. D.R. Bates and B. Bederson (Academic, New York, 1975) vol.11 pp 299

Hasselmann, Koenig W., Richter F.W., Steiner U., Wätjen U., Bode J, Chr, and Ohta W., "Application of PIXE to Trace Element Analysis in Biological Tissues" Nuclear Instruments and Methods 142(1977) pp 163-169

Harrison W.W., Yurachek Y.P. and Benson C.A., "The Determination of Trace Elements in Human Hair by Atomic Absorption Spectroscopy" Clinica Chimica Acta 23(1969) pp 83-91

Henley E.C., Thesis, Florida State University (1976)

Herman A.W., McNelles L.A. and Campbell J.L., "Target Backing for Charged Particle Induced X-ray Fluorescence Analysis" Nuclear Instruments and Methods 109(1973a) pp 429-437

Herman A.W., McNelles L.A. and Campbell J.L., "Choice of Physical Para-
   meters in Charged Particle Induced X-ray Fluorescence Analysis"
   International Journal of Applied Radiation and Isotopes 24(1973b)
   pp 677-688

Hesse A., Hicking W. and Vahlensieck W., Investigation for Characterizing
   Single Crystal Phase in Urinary Stones by Means of an Arrangement
   of Light Microscope in Combination with Scanning, Urolithiasis
   pp 1009-1013, ed. Smith, Robertson and Finalyson, Pub. Plenum(1981)

Hicking W., Hesse A. and Vahlensieck., Comparison of X-ray Diffraction,
   I.R. Spectroscopy and Polarizing Microscopic Careshell Analysis,
   Urolithiasis pp 985-993 ed. Smith, Robertson and Finalyson, Pub.
   Plenum (1981)

Hilderbrand D.C. and White D.H., "Trace Element Analysis in Hair; An
   Evaluation" Clinical Chemistry 20/2(1974) pp 148-151

Hodgkinson A, Peacock M. and Nicholson M., "Quantitative Analysis of
   Calcium Containing Urinary Calculi" Proceeding of the Renal Stone
   Research Symposium, Leeds, (1968)

Horowitz P., Aronsson M., Grodzins L., Lodd W., Ruan J., Merrian G. and
   Lechene C., "Elemental Analysis of Biological Specimen in Air with
   a Proton Microprobe" Science 194(1976) pp 1162-1165

Imahori et al "A Study on Trace Elements in the Hair of Some Local Japa-
   nese Population" Part 1, Inhabitants of the Tokyo Metropolitan
   Area. The IAEA Symposium on Nuclear Activation Techniques in the
   Life Science, Vienna, (1978) SM-227/16

Ishii K., Morita S., Tawara H., Chu T.C., Kaji H. and Shiokawa T.,
   "Quantitative Trace Element Analysis by Proton Induced X-rays"
   Nuclear Instruments and Methods 126(1975) pp 75-80

Ishii K., Kamuya M., Sera K., Morita S. and Tawara H., "Directional Ani-
   sotroby of Secondary-Electron Bremsstrahlung Induced by Proton
   Bombardment of Thin Solid Targets" Physics Review A15(1977) pp 2126-
   2129

Jacklevic J.M. and Goulding F.C., "Detection of Low Energy X-ray with
   Si(Li) Detectors, IEEE Transaction Nuclear Science Ns-18(1971)
   pp187-189

Johansson T.B., Akselsson R.K. and Johansson S.A.E., "X-ray Analysis
   Elemental Trace Analysis at the 10^{-12}g level" Nuclear Instruments
   and Methods 84(1970) pp 141-143

Johansson T.B., Akselsson R.K. and Johansson S.A.E., "Proton Induced X-ray Emission Spectroscopy in Elemental Trace Analysis" Advances in X-ray Analysis 15(1972) pp 372-377

Johansson T.B., Van Grieken R.E., Nelson J.W. and Winchester J.W., "Elemental Trace Analysis of Small Samples by Proton Induced X-ray Emission" Analytical Chemistry 47 no.6 (1975) pp 855-859

Johansson S.A.E. and Johansson T.B., "Analytical Application of Particle Induced X-ray Emission" Nuclear Instruments and Methods 137(1976) pp 473-516

Johansson S.A.E., "Proton Induced X-ray Emission" Proceedings of the 1st International Conference on PIXE and its applications, Lund, Sweden, August 1976. Published in Nuclear Instruments and Methods, 142(1977)

Johansson S.A.E., "Proton Induced X-ray Emission and its Analytical Applications" Proceeding of the 2nd International Conference on PIXE and its Applications, Lund, Sweden, June 1980, Published in Nuclear Instruments and Methods 181(1981)

Johansson G.I., Pallon J., Malmqvist K.G. and Akselsson K.R., "Calibration and Long-Term Stability of PIXE Set-Up" Nuclear Instruments and Methods, 181(1981) pp 81-88

Jolly, R.K., Randers-Pherson G., Gupta S.K., Buckle D.C. and Aceto H.Jr. Process of 3rd Conference on Application of Small Accelerators, (Texas) Vol.1(1974) pp 203-208

Jolly R.K., Khan J.R., Buckle D.C., Rander-Pherson G., Teoh W., and Aceto H., "Target Chamber for PIXE Analysis Using Microamp Beams of 4 MeV Protons" Nuclear Instruments and Methods 151(1978) pp 183-188

Jundt F.C., Purser K.H., Kubo H. and Schenk E.A., "Proton Induced X-ray Analysis of Trace Element in Tissue Section" The Journal of Histochemistry and Cytochemistry 22 no.1 (1974) pp 1-6

Kaji M., Shiokawa T., Ishii K., Morita S., Kamiyo M., Sera K., Tawara H., "Application of Proton-Induced X-ray Emission to Quantitative Trace Element Analysis" Nuclear Instruments and Methods 142(1977) pp 21-26

Kapito L.E., Byers R.F. and Schwchman H., "Lead in Hair of Children with Chronic Lead Poisoning" New England Journal of Medicine 976(1967) pp 949-953

Kapito L.E. and Schwachman H., In the First Human Hair Symposium, ed. A.C. Brown, Hedcom Press (1974) pp 83-90

Katsanos A. and Hodjiantonious A., "Sensitivity of the External Beam
    PIXE Elemental Analysis Method" Nuclear Instruments and Methods
    149(1978) pp 469-473

Kemp K., Palmgren Jensen F., Tscherning Moller J. and Gyrd-Hanson N.,
    "Multi-element Analysis of Biological Tissue by Proton Induced
    X-ray Emission Spectroscopy" Physics Medical and Biology 20 no.5
    (1975) pp 834-838

Khaliquzzaman M., Zaman M.B. and Khan A.H., "Trace Element Analysis in
    Biological Materials by External Beam PIXE" Nuclear Instruments and
    Methods 181(1981) pp 209-215

Khan A.H., Khaliquzzaman M., Husan M. and Abdulla M., "Elemental Analysis
    of Liquids by External Beam PIXE down to ppb Level" Nuclear Instru-
    ments and Methods 165(1979) pp 253-259

Khan F., PhD Thesis, University of Birmingham (1979)

Khan J.M., Potter D.L. and Worley R.D., "Proposed Method for Microgram
    Surface Density Measurement by Observation of Proton-Produced X-rays"
    Journal of Applied Physics 37(1966) pp 564-567

Khan M.D. PhD Thesis, Aston University of Birmingham (1975)

Khan M.D., Sattar A., Crumpton D., "The response of Si(Li) Detector System
    to Microphonic" Nuclear Instruments and Methods 160(1979) pp 127-129

Khan O.R., MPhil Thesis, Aston University of Birmingham (1979)

Khandelwale G.S., Choi B.H. and Merzbacher E., "Atomic Data 1(1969) pp 103;
    Choi B.H., Merzbacher E. and Khandelwal, Atomic Data 5(1973) pp 291

Kivitz H., DeRooij F. and Wijnhoven G.,"A Fast Method for PIXE and XRF
    Target Preparation of Aqueous Samples" Nuclear Instruments and
    Methods, 164(1979) pp 225-229

Kivitz H., PhD Thesis, Eindhoven University of Technology Holland (1980)

Klevay M., "Hair as a Biopsy Material" American Journal of Clinical
    Nutrition 23(1970) pp 1194-1202

Klevay M., "Hair as a Biopsy Material" American Journal of Clinical
    Nutrition 25(1972) pp 263-264

Krause M.O., "Atomic Radiative and Radiationless Yields for K and L Shell" Journal of Physical and Chemical Reference Data 8(1979) pp 307-322

Kubo H., "Reproducibility of Proton-Induced Elemental Analysis in Biological Tissue Sections" Nuclear Instruments and Methods 121(1974) pp 541-545

Kubo H., Hashimato S., Akira A., Chiba R. and Yokota H., "Simultaneous Determinations of Fe, Cu, Zn and Br Concentrations in Human Tissue Sections" Medical Physics 3 no.4 (1976) pp 204-209

La Fleur P.D., "Biological Matrix Standard Reference Materials for Trace Element Determinations" Journal of Radioanalytical Chemistry 19 (1974) pp 277-232

Larsen W.B., Lord R.S., Miller J.J., "Cellular Chemical Analysis of Hair; Preliminary Report" Journal of American Osteopathic Association 74(1974) pp 131/101-136/106

Lear R.D., Van Rinsvelt H.A. and Adams W.R., "An Investigation of the Correlation Between Human Disease and Trace Element Levels by Proton-Induced X-ray Emission Analysis" Advances in X-ray Analysis 19 (1976) pp 521-532

Lear R.D., Van Rinsvelt H.A., Adams W.R., "Proton Induced X-ray Emission Analysis of Human Autopsy Tissues" Advances in X-ray Analysis 20 (1977) pp 403-410

Legge G.J.F. and Mazzolini A.P., "Elemental Microanalysis of Biological and Medical Specimens with a Scanning Proton Microprobe" Nuclear Instruments and Methods 168(1980) pp 563-569

Lodi et al, Report of the Coordinated Research Meeting on Nuclear based Methods for the Analysis of Pollutants in Human Hair, CEN - Saclay (IAEA, Vienna, 1978)

Madison D.H. and Merzbacher E., Atomic Inner-Shell Processes, ed. B. Crasemann (Academic, New York, 1975) Vol.1, pp 1

Mahler D.J., Scott A.F., Walsh J.R. and Haynie C., "A Study of Trace Metals in Fingernails and Hair Using Neutron Activation Analysis" Journal of Nuclear and Medical II (1970) pp 739-742

Maenhaut W., Rinsvelt H.A. and Cafmeyer J., "Particle-Induced X-ray Emission (PIXE) Analysis of Biological Material:Precision Accuracy and Application to Cancer Tissue" Nuclear Instruments and Methods 168(1980) pp 557-562

Mangelsson N.F., Hill M.W., Nielson K.K. and Ryder J.F., "Proton Induced
     X-ray Emission Analysis of Biological Samples: Some Approaches and
     Applications" Nuclear Instruments and Methods 142(1977) pp 133-142

Mangelsson N.F., Private Communication (1980)

Marion J.B. and Zimmerman B.A., "Multiple Scattering of Charged Particles"
     Nuclear Instruments and Methods 51(1967) pp 93-101

Marion J.B. and Young F.C., Nuclear Reactor Analysis, North-Holland
     Publishing Company (1968)

McConivelle B.E., Ultrastructural Analysis of Biliary Calculi Microbeam
     Analysis, ed. D.E. Newbury San Fransisco Press (1979) pp 80-81

Merzbacher E. and Lewis H.W., Handbuch der Physik, ed. S. Flugge; Springer
     Verlage, Berlin 34 (1958) pp166

Middleton G., "The Preparation of Biological Material for the Determina-
     tion of Trace Metals; Part 1. A critical Review of Existing Pro-
     cedure" Analyst 78(1953) pp 532-542

Middleton G. and Stuckey R.E., "The Preparation of Biological Material
     for the Determination of Trace Metals" Analyst 79(1954) pp 138-142

Mitchell I.V. and Zeigler J.F., "Ion Induced X-rays" Advances in X-rays
     Analysis 17 no.213 (1975) pp 311-484

Mitchell I.V., Barfoot K.M. and Poli De "Particle Induced X-ray Emission
     Analysis Application to Analytical Problems" Internal Report/CBNM/
     AS/53/79

Mitchell I.V., Private Communication, 1980

Mommsen H., Bauer K.G. and Faziy Q., "Sensitivity of High Energy PIXE
     Bulk Analysis" Nuclear Instruments and Methods 157(1978) pp 305-309

Montenegro E.C., Baptista G.B., De Castro Faria L.V. and Paschoa A.S.
     "Correction Factor for Hair Analysis by PIXE" Nuclear Instruments
     and Methods 168(1980) pp 479-483

Moret H. and Louwerix E., Vacuum Microbalance Techniques, Plenum Press
     5(1966) pp 59-75

Moriya Y., Ato Y. and Oawa S.M., "Sensitivity in Light Element Analysis by 2 MeV and 150 keV Proton and Photon Induced X-rays" Nuclear Instruments and Methods 150(1978) pp 523-528

Morrison G.H., Trace Analysis (Interscience, New York, 1965)

Mott, N.F., Massey S.N., "The Theory of Atomic Collisions, Oxford U.P., London, 3rd Edition (1965) pp 338

Musket R.G., "Detection of Proton-Induced Boron X-ray with a Si(Li) Detector", Nuclear Instruments and Methods 117(1974) pp 385-389

Navarrete V.R., Izawa G., Shiokawa T., Kamiya M., Morita S., "The Quantitative Analysis of Bowen's Kale by PIXE Using the International Standard" Radiochem Radioanal. Letters 36(2-3) (1978a) pp 151-158

Navarrete V.R., Izawa G., Shiolawa T., "Direct Multi-Element Analysis of Self-Supporting Targets of Some Biological Standard Reference Materials and Others by PIXE" Japanies Journal of Applied Physics 17 (1978b) pp 422-424

Nielson K.K., PhD Thesis, Birgham Young University (1975)

Nielson K.K., Hill M.W. and Mangelson N.F., "Calibration and Correction Methods for Quantitative Proton-Induced X-ray Emission Analysis of Autopsy Tissue" Advances in X-ray Analysis 19(1976a)pp 511-519

Nielson K.K., Hill M.W., Mangelson N.F. and Nelson F.W., "Elemental Analysis of Obsidian Artifacts by Proton Particle Induced X-ray Emission 48 no.13 (1976b) pp 1947-1950

Obrusnik I., Gisloson J., McMillian D.M., Auria J.D. and Pate B.D., "The Variation of Trace Element Concentration in Single Human Head Hairs" Journal of Forensic Science 17(1972) pp 426-439

Othman J., Spyrou N.M., "Elemental Concentrations in Hair and Nail from a Selected Population Group in the Machakos District of Kenyea" The IAEA Symposium on Nuclear Technique in the Life Science, Vienna, (1978) SM-227/33

Pallon J. and Malmqvist K.G., "Evaluation of Low Temperature Ashing of Biological Materials as a Preconcentration Method for PIXE analysis" Nuclear Instruments and Methods 181(1981) pp 71-75

Panel Discussion on Urolithiasis, Urological Survey 4(1954) pp 2-65

Panel Discussion on Analytical Methods and Structure Study of Calculi, Symposium Para La Investigation de Lalithiasis Renal, Madrid (1972)

Pearson E.F. and Pounds C.A., "A Close Involving the Administration of Known Amount of Arsenic and its Analysis in Hair" Journal of Forensic Science and Society 11(1971) pp 229-234

Perkons A.K. and Jervis R.E., "Trace Element in Human Hair Head" Journal of Forensic Science 11 no.1 (1966) pp 50-63

Perry S.K. and Brady F.P., "A Comparative Study of Alpha and X-ray Induced X-ray Emission for Elemental Analysis" Nuclear Instruments and Methods 108(1973) pp 389-402

Petering H.G., Yeagear D.W. and Witherup S.O., "Trace Metal Content of Hair" Archievs of Environmental Health 23(1971) pp 202-207

Prasad A.S., Trace Elements Analysis (Academic Press, New York, 1976, Vol. 1 and Vol.2)

Raith B., Roth M., Collner K., Gonsior B., Ostermann H. and Uhlhorn C.D., "Trace Element Analysis by Ion Induced X-ray Emission Spectroscopy" Nuclear Instruments and Methods 142(1977) pp 39-44

Renan M.J.,"Optimization of Trace Analysis by PIXE Angular Dependence of the Background Continuum" X-ray Spectrometry 9 no.2 (1980) pp 90-94

Rendic D., Holjevic S., Valkovic V., Zabel T. and Phillips G.G., "Trace Element Concentrations in Human Hair Measured by Proton Induced X-ray Emission" Journal Investigative Dermatol 60(1976) pp 371-375

Renshaw G.D., Pounds C.A., Pearson E.F., "Variation in Lead Concentration Along Single Hair as Measured by Non-Flame Atomic Absorption Spectroscopy" Nature 238(1972) pp 162-163

Roberts T.M., Hutchinson T.C., Paciga, Chattopadyah A., Jervis R.E. and Vanloon J., "Lead Contamination Around Secondary Smelters; Estimation of Dispersal and Accumulation by Humans" Science 186(1974) pp 1120-1122

Robertson W.G., Urolithiasis Research, New York, Plenum (1976) pp 5-25

Rudolph H., Kliwer J.K., Kraushaar J.J., Ristinen R.A. and Smythe W.R., "Trace Analysis by Proton and X-ray Induced Characteristic X-rays" Analysis Instrumentation 10(1972) 151

Russell S.B., Private Communication (1981)

Schroeder H.A., and Nason A.P., "Trace Metals in Human Hair" Journal
of Investigative Dermatology 53(1969) pp 71-78

Schroeder H.A. and Nason A.P., "Trace Element in Clinical Chemistry"
Clinical Chemistry 17(1971) pp 461-474

Schutte K.H., The Biology of Trace Elements, ed. J.B. Tippincott, phela-
delphia (1964) pp 5

Scofield J.H., "Exchange corrections of K X-ray emission rates" Physics
Review, A9 no.3(1974) 1041

Sharon L., PhD Thesis, University of Kentucky (1977)

Simms P.C. and Rickey F.A., "The Multi-elemental Analysis of Drinking
Water Using Proton-Induced X-ray Emission" International Report,
Purude University, West Lafayette Ind., EPA-600/1-78-058 (1978)

Spahn G. and Groeneveld K.O., "Angular Straggling of Heavy and Light Ions
in Thin Solid Foils" Nuclear Instruments and Methods 123(1975)
pp 425-429

Steinnes E., "Uptake of Trace Elements in Human Hair by Anion Exchange"
International Journal of Applied Radiation Isotopes, 26 no.10 (1975)
pp 595-599

Stiles A.R., Dzbay T.G., Baum B.M., Walter R.L., Willis R.D., Moore L.J.,
Garner, E.L., Gramlich J.W., Machlan L.A., U.S., Dept. of Commerce
NBS "Calibration of an Energy Dispersive X-ray Fluorescence Spect-
rometer" Advances in X-ray Analysis 20(1976) pp 473-486

Storm E. and Israel, "Photon Cross-sections from 1 keV to 100 MeV for
Elements Z = 1 to Z = 100" Nuclear Data Tables A7(1970) pp 565-681

Stranshiskii A.G., Khomyakov C.K., Skakun N.A., Serykh N.V., Klyucharer
A.P. and Sevenn N.F., "Elemental Analysis of Biological Specimens
from the Characteristic X-radiation Excited by the P otons" Biofi-
zika 4(1975) pp 621-623

Sutor D.J. and Scheidt, "Identification Standards for Human Urinary Cal-
culi Components Using Crystallographic Methods" British Journal of
Urology 40(1968) pp 22-28

Sutor D.J. and Wooley S., "Composition of Urinary Calculi by X-ray Dif-
fraction, Collected Data from Various Localities" British Journal
of Urology 41(1969) pp 397-400

Tawara H., Ishii K., Marita S., "Bremsstrahlung Induced by Proton and Helium-3 Ion Impact" Nuclear Instruments and Methods 132(1976) pp 503-505

Taylor B.E., Private Communication, (1981)

Taylor B.E., Saied S.O., British Journal of Urology, in press

Tipton I.H. and Cook M.J., "Trace Element in Human Tissue" Part II: Health Physics, 9(1963) pp 103-145

Tschalar C., "Straggling Distribution of Large Energy Losses" Nuclear Instruments and Methods 61(1968a) pp 141-156

Tschalar C., "Straggling Distribution of Extremely Large Energy Losses" Nuclear Instruments and Methods 64(1968b) pp 234-234

Umbarger C.J., Bearse R.C., Close D.A. and Malanify, "Sensitivity and Detectability Limit for Elemental Analysis by Proton Induced X-ray Fluorescence with a 3 MeV Van De Graft" Advances in X-ray Analysis 16(1973) pp 102-110

Underwood E.J., Trace Elements in Human and Animal Nutrition, Academic Press, New York (1971)

Valkovic V., X-ray Emission Spectroscopy, Part I and II Contemp Physics 14 no.5(1973) pp 415-462

Valkovic V., Miljanic D., Wheeler R.M., Liebert R.B., Zabel T., Phillips G.C., "Variation in Trace Metal Concentrations Along a Single Hair as Measured by Proton-Induced X-ray Emission Photometry, Natur 243 (1973) pp 543-544

Valkovic V., Liebert R.B., Zabel T., Larson H.T., Millanic D., Wheeler R.M. and Philips G.C., "Trace Element Analysis Using Proton Induced X-ray Emission Spectroscopy" Nuclear Instruments and Methods 114(1974) pp 573-579

Valkovic V., Trace Element Analysis, (Taylor and Francis Ltd, London, 1975)

Valkovic V., "Proton-Induced X-ray Emission: Applications in Medicine" Nuclear Instruments and Methods 142(1977) pp 151-158

Walter R.L., Willis R.D., Gutknecht W.F. and Joyce J.M., "Analysis of Biological Clinical and Environmental Samples Using Proton Induced X-ray Emission" Analytical Chemistry 46 no.7(1974) pp 843-855

Walter R.L., Willis R.D., Gutknecht W.F., Shaw R.W., "The Application of Proton-Induced X-ray Emission to Bioenvironmental Analysis" Nuclear Instruments and Methods 142(1977) pp 181-197

Watson R.L.. Sjurseth J.R. and Howard R.W., "An Investigation of the Analytical Capabilities of X-ray Emission Induced by High Energy Alpha Particles" Nuclear Instruments and Methods 93(1971) pp 69-76

Watson R.L., McNeal C.J. and Jenson F.E., "Application of Heavy Charged Particles Induced X-ray Emission to the Trace Elements Analysis of Human Tissue and Blood Serum" Advances in X-ray Analysis 18(1975) pp 288-298

Wheeler R.M., Liebert R.B., Zabel T., Chaturvedi R.P., Valkovic V., Phillips G.C., Ong P.S., Chen E.L. and Hrgoveic M., "Techniques for Trace Element Analysis: X-ray Fluorescence, X-ray Excitation with Photons and Flame Atomic Absorption" Medical Physics, 1 no.2 1974 pp 68-71

Whitehead N.E., Report of IAEA, Advisory Group Meeting on "Accelerator Based Techniques for the Analysis of Pollutants in Man" Vienna (1978)

Whitehead N.E. "Methods of Hair Analysis by (PIXE) Spectrometry Nuclear Instruments and Methods 164(1979) pp 381-388

Whitton J.L., "Change in Stoichiometry of Thin Films of Polladium Chloride During Ion Beam Analysis" Nuclear Instruments and Methods 149(1978) pp 743-747

Widdowson E.M. and Dickerson J.W.T., "Chemical Composition of the Body in Mineral Metabolism, 2 Part A, C.L. Comar and F. Bronner eds. Academic Press, New York (1964) pp 119

Willis R.D., PhD Thesis, Duke University, 1977

Willis R.D., Walter R.D., Show R.W. and Gutknecht W.F., "Proton Induced X-ray Emission Analysis of Thick and Thin Targets" Nuclear Instruments and Methods 142(1977) pp 67-77

Woldseth R., X-ray Energy Spectrometry, Published by Kevex Corporation, Burlington, California (1973)

Yuarchek J.P., Clemena and Harrison W.W., "Analysis of Human Hair by Spark Source Mass Spectrometry" Analytical Chemistry 41(1969) pp 1666-1668

Zaldins C.S., "A Method for Energy-loss and Range Calculations Based on Empirical Approximations" Nuclear Instruments and Methods 120(1974) pp 125-129

Zambola R.R., PhD Thesis, University of Kensas, 1978

Zarembski P.M. and Grieve J., "Infra-red Spectroscopy in the Clinical Analysis of Renal Stone Research Symposium, Madrid (1972)

Zulliger and Aitken W., "Fano Factor and Fallacy" IEEE Transaction Nuclear Science, NS-17 no.3 (1970) pp 187-193